Terms and Conditions of Use of Digitised Theses from Trinity College Library Dublin

Copyright statement

All material supplied by Trinity College Library is protected by copyright (under the Copyright and Related Rights Act, 2000 as amended) and other relevant Intellectual Property Rights. By accessing and using a Digitised Thesis from Trinity College Library you acknowledge that all Intellectual Property Rights in any Works supplied are the sole and exclusive property of the copyright and/or other IPR holder. Specific copyright holders may not be explicitly identified. Use of materials from other sources within a thesis should not be construed as a claim over them.

A non-exclusive, non-transferable licence is hereby granted to those using or reproducing, in whole or in part, the material for valid purposes, providing the copyright owners are acknowledged using the normal conventions. Where specific permission to use material is required, this is identified and such permission must be sought from the copyright holder or agency cited.

Liability statement

By using a Digitised Thesis, I accept that Trinity College Dublin bears no legal responsibility for the accuracy, legality or comprehensiveness of materials contained within the thesis, and that Trinity College Dublin accepts no liability for indirect, consequential, or incidental, damages or losses arising from use of the thesis for whatever reason. Information located in a thesis may be subject to specific use constraints, details of which may not be explicitly described. It is the responsibility of potential and actual users to be aware of such constraints and to abide by them. By making use of material from a digitised thesis, you accept these copyright and disclaimer provisions. Where it is brought to the attention of Trinity College Library that there may be a breach of copyright or other restraint, it is the policy to withdraw or take down access to a thesis while the issue is being resolved.

Access Agreement

By using a Digitised Thesis from Trinity College Library you are bound by the following Terms & Conditions. Please read them carefully.

I have read and I understand the following statement: All material supplied via a Digitised Thesis from Trinity College Library is protected by copyright and other intellectual property rights, and duplication or sale of all or part of any of a thesis is not permitted, except that material may be duplicated by you for your research use or for educational purposes in electronic or print form providing the copyright owners are acknowledged using the normal conventions. You must obtain permission for any other use. Electronic or print copies may not be offered, whether for sale or otherwise to anyone. This copy has been supplied on the understanding that it is copyright material and that no quotation from the thesis may be published without proper acknowledgement.

Hybrid Organic-Inorganic Polyoxometalates: Synthesis and characterisation of organoarsonate and organophosphonate functionalised polyoxovanadate clusters

John Michael Breen

A thesis submitted to the University of Dublin for the degree of

Doctor of Philosophy

School of Chemistry

University of Dublin

2010

Declaration

This thesis has not been submitted as an exercise for a degree at any other University. Except where otherwise indicated, the work described herein has been carried out by the author alone.

I agree that the library of the University of Dublin may at their discretion lend or copy the thesis upon request.

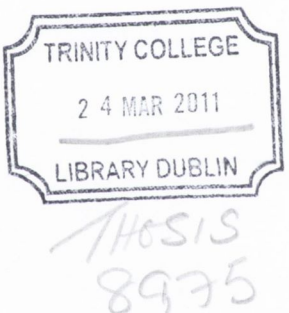

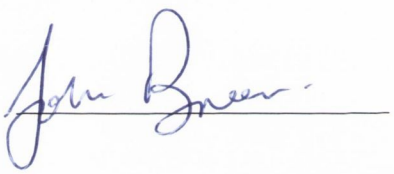

John Breen

For my parents Michael and Marie, and for my support team Michael, Martin, Catherine and Donall

"A tidy laboratory means a lazy chemist"

Jöns Jacob Berzelius (1779-1848)

Table of Contents

Acknowledgements

First and foremost, I would like to thank my supervisor Dr Wolfgang Schmitt for his patience, encouragement, and above all, his infectious enthusiasm in chemistry.

I would like to gratefully acknowledge that the magnetic susceptibility measurements were recorded and modeled by Dr. Rodolphe Clèrac using a Quantum Design SQUID magnetometer MPMS-XL housed at the Centre de Recherche Paul Pascal and that the preliminary anti-cancer studiesn were carried out in collaboration with Prof Clive William's group (Elaine Kennedy, Dr Suzanne Cloonan and Trevor Price) of the biochemistry department, Trinity College Dublin.

I would also formally like to thank all the technical staff that has assisted me throughout my time here in Trinity College, Dr Tom Mc Cabe, Dr Martin Feeney, Dr John O'Brien, Dr Manuel Rüther, Brendan Barry and all of the Cocker lab staff. I wish to offer a special thanks to Fred, Dorothy, Glen and Peggy who have not only assisted me with technical support throughout the years but have advised me with their years of wisdom throughout the challenging times within my research.

At the heart of all great research is a great research group. I would like to thank the oldest to the youngest research members of the Schmitt group for all their help and advice: Camelia Onet, Bartosz Marzec, Anne-Marie O Toole, Gerard Tobin, Lukas Reck, Giuseppe la Spina, David Walsh, Ian Mc Keogh and Lei Zhang.

I would sincerely like to thank Carmel Breen and Ian Mc Keogh for reading and suggesting corrections for my thesis.

I would like to thank SFI and the Trinity Postgraduate scheme for their financial support.

I would like to thank all of my friends for their words of encouragement, years of good advice and for being inspirational when I struggled, I would particularly like to thank a few of my friends (Paul Hamm (**2**), Joyce Leader (**3**), Leonard Leader (**4**), Frank Leader (**4**), Jonathan Russell (**5**), Brian Deighan (**6**), Brian Fitzgerald (**7**), Aine O Reilly (**8**), Caoimhe Bennis (**9**), Sebastian Vencken (**10**), James Rooney (**11**), Paul Dhillon (**12**), James O Brien (**13**), Shane Huston (**14**) and Paul Tighe (**15**)) for their input. Within this thesis, I dedicated their names to naming each of the respective compounds.

Finally, I would like to thank my family for all their support, my parents Michael and Marie, my siblings Michael, Martin, Catherine and Donall.

Summary

This thesis presents a significant contribution of research to the field of hybrid inorganic-organic polyoxometalates. Herein the functionalisation of polyoxovanadate clusters with aryl arsonates and aryl phosphonates is described and the structural and physiochemical properties of the product materials are discussed. Chapter 1 introduces the reader to the field of research, highlights recent significant achievements and puts accomplishments into a broader context.

Chapter 2 discusses the isolation of four novel mixed–valent pentanuclear clusters stabilised by aryl arsonate ligands. The mixed-valent pentanuclear vanadium $\{V_5O_9\}^{3+}$ unit was stabilised by the following arsonate ligands: (4-aminophenyl)arsonic acid , (4-carboxylphenyl)arsonic acid, (4-hydroxyphenyl)arsonic acid and (3-acetamido-4-hydroxyphenyl)arsonic acid to give the respective complexes: $Na_5[V_5O_9(O_3AsC_6H_4\text{-}4\text{-}NH_2)_4]\cdot 20.5H_2O\cdot 3DMF$ (**1**), $Na_9[V_5O_9(O_3AsC_6H_4\text{-}4\text{-}COO)_4]\cdot 6DMF\cdot 27H_2O$ (**2**), $Na_5[V_5O_9(O_3AsC_6H_4\text{-}4\text{-}OH)_4]\cdot 17.5H_2O\cdot 5DMF$ (**3**) and $Na_5[V_5O_9(O_3AsC_6H_4\text{-}3\text{-}NHCOCH_3\text{-}4\text{-}OH)_4]\cdot 19H_2O\cdot 3DMF$ (**4**).

Within Chapter 3, it is reported that pH variations and increased metal:ligand ratios lead to the synthesis and structural characterisation of four nano-sized cluster cages which are contained in the following compounds: $Na_4[V_{12}O_{14}(OH)_4(H_2O)_4(O_3AsC_6H_4\text{-}4\text{-}NH_2)_{10}]\cdot 3DMF\cdot 16H_2O$ (**5**), $Na_4H_2[V_{14}O_{22}(OH)_4(H_2O)_2(O_3PC_6H_4\text{-}4\text{-}NH_2)_8]\cdot 7DMF\cdot 12H_2O$ (**6**), $Na_4H_2[Cl_2{\subset}V_{14}O_{14}(OH)_8(O_3AsC_6H_4\text{-}4\text{-}NH_2)_{10}]\cdot 6DMF\cdot 15H_2O$ (**7**) and $Na_2H_6[V_{16}O_{24}(OH)_8(O_3AsC_6H_4\text{-}4\text{-}NH_2)_8]\cdot 6DMF\cdot 13H_2O$ (**8**).

Chapter 4 discusses the formation, the structures and the characterisation of three caged mixed-valent structures stabilised by aryl diphosphonate ligands: $Na_8H_2[(H_2O)_2{\subset}V_{10}O_{18}$

$(O_3PC_6H_4\text{-}4\text{-}PO_3)_4]\cdot 34H_2O$ (**9**), $Na_8H_2[(H_2O)_2{\subset}V_{10}O_{18}(O_3PC_{10}H_6\text{-}4\text{-}PO_3)_4]\cdot 44H_2O$ (**10**), and $Na_8H_2[(DMF)_2{\subset}V_{10}O_{18}(O_3PC_{12}H_8\text{-}4\text{-}PO_3)_4]\cdot 30H_2O$ (**11**).

Potency studies were undertaken for **9** and **11**. These indicate that the compounds have low toxicity against cells derived from K562: chronic myelogenous leukaemia cancer cell lines, A549: lung carcinoma cancer cell lines and mutu-I: Burkitt's lymphoma cancer cell lines.

The magnetic susceptibility was measured and modelled for compounds **1**, **5**, **9** and **11**. Ferromagnetic interactions within the pentanuclear units in **9** and **11** stabilise S=2 ground states. Comparable pentanuclear subunits in the arsonate-stabilised compounds **1** and **5** reveal anti-ferromagnetic interactions with the bridging dinuclear moieties. Tentatively, a magneto-structural correlation graph has been plotted of the magnetic exchange constant, *J*, as a function of the V-O-V angle.

Chapter 5 reports the synthesis and characterisation of self-assembled condensed hybrid cluster cores at lower pH values. Two condensed polyoxovanadate cores stabilised by (4-aminophenyl)arsonic acid were isolated, $NaH_4[V_{10}O_{18}(O_3AsC_6H_4\text{-}4\text{-}NH_2)_7(DMF)_2]\cdot 5H_2O \cdot 7DMF$ (**12**) and $Na_6[V_{13}O_{31}(O_3AsC_6H_4\text{-}4\text{-}NH_2)_3]\cdot 7H_2O\cdot 8DMF$ (**13**). A cubane structural motif in $H_2Na_2[(V^{IV}O)_4(OH)_4\ (O_3PC_{10}H_7)_4]\cdot 3DMF\cdot 12H_2O$ (**14**), was stabilised using (1-naphthalene)phosphonic acid. The solvothermal synthesis of functionalised polyoxovanadates was also investigated resulting in the isolation of $H_4[(VO)_{12}(OH)_{12}(O_3PC_{10}H_7)_8]\cdot 13H_2O \cdot 6DMF$ (**15**). In some cases, ligand decomposition was observed and in one case we were able to isolate the decomposition product, $H_4[V_{12}As_8O_{40}(H_2O)]$.

Chapter 6 provides a description of the materials and methods used as well as the experimental details for the synthesis of the compounds described herein.

Abbreviations

MOFs	Metal Organic Frameworks
3-D	Three dimensional (structures)
DMF	Dimethylformamide
CHN	Carbon-Hydrogen-Nitrogen analysis
TGA	Thermogravimetric analysis
IR	Infrared spectroscopy
UV-vis	Ultraviolet-visible spectroscopy
BVSA/BVS	Bond Valence Sum Analysis
O.S.	Oxidation State
M/Z	mass/charge ratio (mass spectrometry)
TOF-MS	Time of Flight Mass Spectrometry
MALDI	Matrix Assisted Laser Desorption/Ionisation
DTA	Differential Thermal Analysis
ν	symmetric stretch (IR)
ν_{as}	asymmetric stretch (IR)
IVCT	Intervalence Charge Transfer

Chapter One

Introduction

1.1 Polyoxometalate definition and history

Polyoxometalates clusters can generally be described as anionic clusters built from early transition metal ions in their highest oxidation state (typically Mo, W and V) linked by bridging oxo-ligands. The history of polyoxometalates originates with the synthesis of the first heteropoly acid, ammonium 12-molybdophosphate in 1826 by Berzelius.[1] However, it was not until the discovery of the tungstosilicic acids and their salts by Galisard de Marignac in 1864 that the analytical composition of the 12:1 heteropoly acid species was precisely determined.[2]

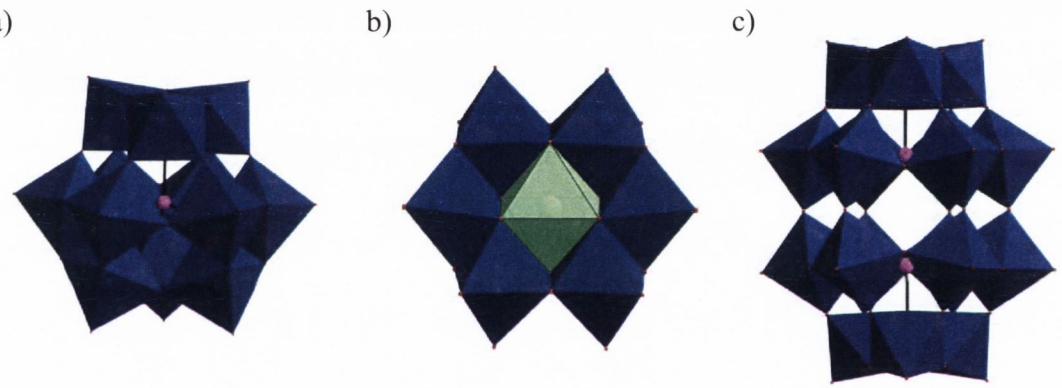

Figure 1.1 – (a) α-Keggin structure: $[PMo_{12}O_{40}]^{3-}$. (b) Evans-Anderson structure: $[H_7CrMo_6O_{24}]^{2-}$. (c) Wells-Dawson structure: $[P_2W_{18}O_{62}]^{8-}$. Colour Code: Mo blue, Cr green, P pink, O red; polyhedral representations.

The first attempts to explain the structure of 12:1 heteropoly species were made by Werner in 1907 based on his new ideas of coordination chemistry. Later Pauling proposed that the structure could consist of a 12:1 complex in which the twelve $\{MO_6\}$ units were arranged surrounding a central AO_4 tetrahedron (A = suitable heteroatom such as P, As, Si *etc*).[3] The structure that Pauling elaborated upon was revealed to be incorrect because he did not consider the possibility of edge-sharing $\{MO_6\}$ octahedra. The correct structure of this heterpolyanionic cluster was determined when J. F. Keggin identified the structure utilising X-ray powder diffraction (Fig. 1.1a).[4] The Keggin structure consists of a heteroatom binding

to four oxygen atoms to form a tetrahedron; this tetrahedron is located centrally in the cluster. The tetrahedron is surrounded by twelve octahedral $\{MO_6\}$ units which share common edges within three characteristics $\{Mo_3O_{13}\}$ units. The development of X-ray crystallography was to play a critical role in the confirmation of this structure. This analytical technique was also crucial for the discovery of many other subtypes of polyoxometalates such as Evans – Anderson and Wells – Dawson structures (Fig. 1.1).[4] It was realised that many different structural isomers exist for these previously mentioned structures. Baker and Figgis were able to demonstrate this for the Keggin structure in 1970 when they showed that different rotational orientations of the $\{Mo_3O_{13}\}$ units connected to the central heteroatom of the Keggin structure can lead to the stabilisation of five different structural isomers (α, β, γ, δ and ε).[5]

In addition to the isomeric forms of the Keggin structure, it was found that one, two or three of the $\{MO_6\}$ units could be removed resulting in species which are known as lacunary derivates. These lacunary systems could be achieved by treating the Keggin structure with a strong base or by careful control of the pH and stoichiometry during the synthesis. Upon removal of the $\{MO_6\}$ unit, the resulting 'missing octahedron' provides an ideal binding site to functionalise these clusters with geometrical compatible transition metal ions which in turn can be functionalised with a wide variety of external coordinating ligands. This synthetic approach for functionalisation, however, is not applicable to all Keggin isomers, as not all Keggin lacunary structures are kinetically or thermodynamically stable. Lacunary structures and the functionalisation of such polyoxometalates will be further discussed in section 1.3.

Polyoxometalates can be sub divided in isopolyoxometalates or heteropolyoxometalates. Isopolyoxometalates exclusively consist of early transition metal and oxygen atoms while heteropolyoxometalates contains heteroatoms preferentially located in the centre of metal oxide cluster and usually display tetrahedral or octahedral coordination geometry. The

Keggin and Wells-Dawson structures are the most prominent examples of heteropolyoxometalates.

Due to the wide variety of polyoxometalates constantly being generated, a strict and inclusive definition of what constitutes a polyoxometalate cluster is constantly evolving; however there are some characteristic features of this class of compound. Polyoxometalates are generally composed of $\{MO_4\}$, $\{MO_5\}$ or $\{MO_6\}$ metal-oxo building units or a combination of these units. These basic building blocks can be combined to form a variety of clusters depending on the connectivity modes. The connectivity of these metal oxide building units is predominantly characterised by edge-sharing or corner-sharing interactions. The metal oxide building blocks are composed of early transition metal ions that polarise terminal oxo ligands efficiently. This normally results in clusters where the metal-oxygen bonds point radially outwards. These short M=O bonds possess stabilising $d\pi$-$p\pi$ contributions that protect the polyoxometalate cluster from decomposition but this bond also hampers the functionalisation of these clusters and limits the formation of often desired hybrid organic-inorganic materials. Alternatively, it could be considered that the M=O bond blocks one coordinating site of the building units ($\{MO_4\}$, $\{MO_5\}$, $\{MO_6\}$) when they undergo condensation reactions. The effect of this blocked coordination site might explain why this class of compound is capable of forming large 0-dimensional systems.

In recent years there has been great interest in polyoxometalate research, with the advent of large, highly symmetrical polyoxometalates such as wheel shaped molybdenum blue anions and spherical Keplerates reported by Müller *et al.*[6] These clusters are the result of linking repeating sub-units of molybdenum oxide through condensation reactions. These condensation reactions lead to giant, nano-sized polyoxomolybdates whose structures are dependent on the formation of particular building units as defined by the experimental procedure.[7] Spherical polyoxometalate clusters similar to those shown in Fig. 1.2 can serve

as molecular containers containing functional sites that can be exploited for molecular recognition utilising supramolecular chemistry approaches.[8] One of the largest spherical polyoxometalate clusters containing 368 molybdenum atoms was reported in 2002.[9]

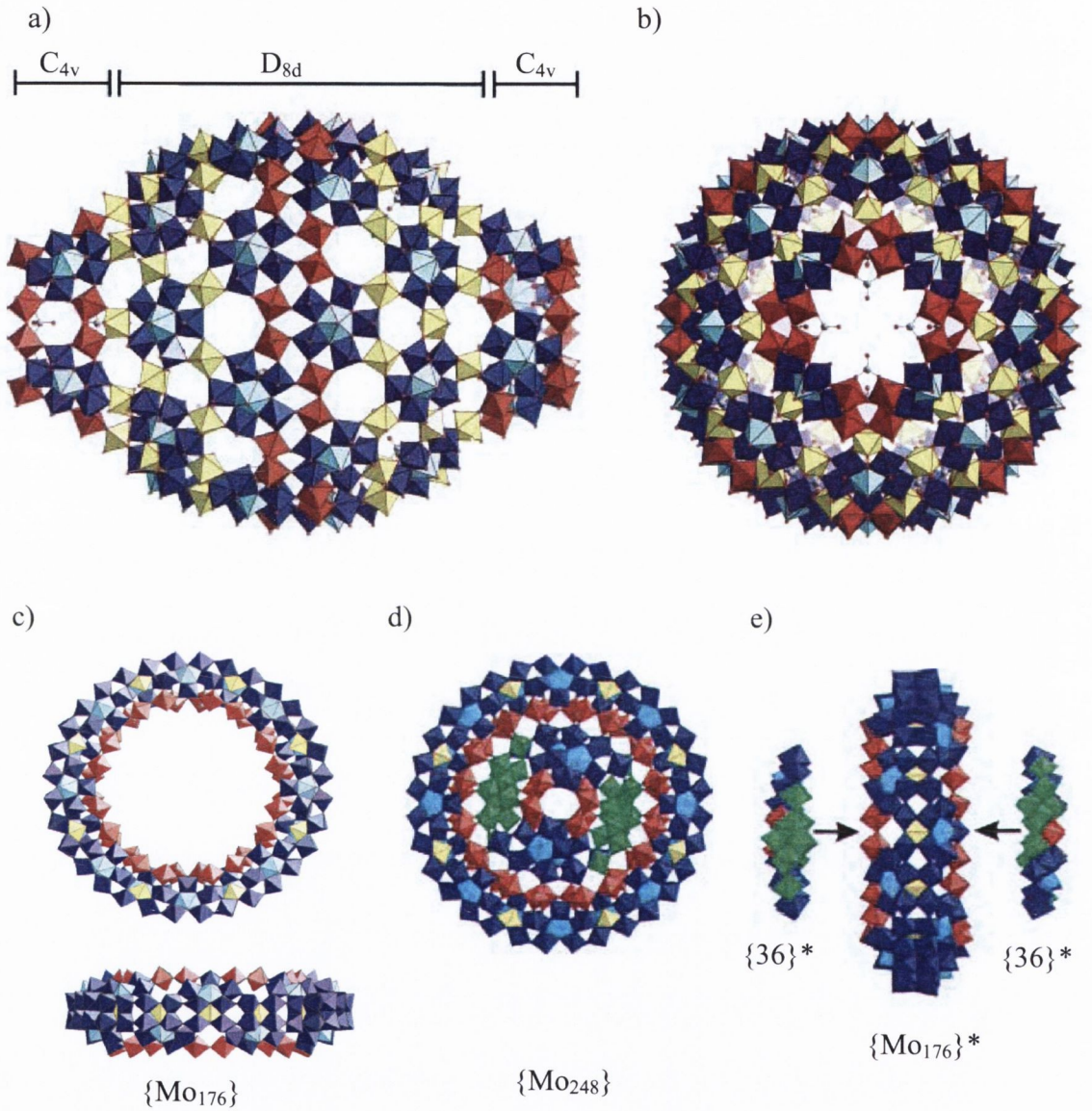

Figure 1.2 – (a) A polyhedral representation of the giant anionic polyoxometalate cluster of $[H_{16}Mo_{368}O_{1032}(H_2O)_{240}(SO_4)_{48}]^{48-}$ with the observed symmetry fragments of $\{Mo_{288}\}$ (D_{8d}) and $\{Mo_{40}\}$ (C_{4v}). (b) A perspective view of the pore at either end of the giant $\{Mo_{368}\}$ cluster.[9] (c) An example of a nano-sized metal oxide $[(MoO_3)_{176}(H_2O)_{80}]^{32-}$ ring.[10] (d) A large spherical-shaped $[\{Mo_2^{VI}O_5(H_2O)_2\}_{16}\{Mo_8^{VI/V}O_{26}(\mu_3\text{-}O)_2H(H_2O)_3Mo^{VI/V}\}_{16}\{Mo_{36}^{VI/V}O_{96}(H_2O)_{24}\}_2]^{16-}$ cluster.[11] (e) The formal addition of two $\{Mo_{36}\}$* units to the inner surface of the $\{Mo_{176}\}$* wheel leads to the formation of the $\{Mo_{248}\}$ cluster. Polyhedral represented building units $\{Mo_1\}$ yellow, $\{Mo_2\}$ red, $\{Mo_8\}$ blue with blue-turquoise pentagonal bipyramids, $\{Mo_8\}$' green.

The $[H_{16}Mo_{368}O_{1032}(H_2O)_{240}(SO_4)_{48}]^{48-}$ cluster anion has an approximate D_4 symmetry and consists of a central $\{Mo_{288}\}$ ball-shaped fragment with D_{8d} symmetry ($\{Mo_{288}\} \equiv \{Mo_{288}O_{784}(H_2O)_{192}(SO_4)_{32}\}$) and two $\{Mo_{40}\}$ capping fragments ($\{Mo_{40}\} \equiv \{Mo_{40}O_{124}(H_2O)_{24}(SO_4)_8\}$) with C_{4v} symmetry. It has a cavity of approximately 2.5 x 4.0 nm which encapsulates *ca.* 400 water molecules.

The wheel-shaped $\{Mo_{176}\}$ cluster reported in 1998, has an inner diameter of 2.3 nm (Fig. 1.2c)[10] and can also be considered to be a building unit for a closed shell $\{Mo_{248}\}$[11] cluster (Fig. 1.2d) where the $\{Mo_{176}\}$ ring unit is capped by two $\{Mo_{36}\}$ fragments (Fig. 1.2e). These clusters can be considered as molecular nanoparticles of molybdenum oxide and therefore the properties of these clusters are of significant interest due to their potential industrial applications. The application of polyoxometalates as catalysts will be discussed in more detail in section 1.5.

1.2 Structures of polyoxovanadates

1.2.1 Polyoxovanadates

In this thesis, I intend to explore the formation of novel vanadium oxide clusters stabilised by organic functionalities. Vanadium oxides represent a large subclass of polyoxometalate clusters. Some examples of purely inorganic polyoxovanadates can be seen in Fig. 1.3.[12] The building units of these clusters include $\{VO_4\}$, $\{VO_5\}$ and $\{VO_6\}$ polyhedra. Their tendency to polymerise and to form shell or cage structures allows for a wide range of polyoxovanadate clusters to be formed.[13] Purely inorganic polyoxovanadate clusters that have been synthesised range from small oligomeric structures to clusters with nano-sized entities. Examples include $[V_3O_9]^{3-}$, $[V_4O_{12}]^{4-}$, $[V_5O_{14}]^{5-}$, $[V_{10}O_{26}]^{4-}$, $[V_{10}O_{30}]^{11-}$, $[V_{12}O_{30}]^{4-}$,

$[V_{13}O_{34}]^{3-}$, $[V_{14}O_{36}]^{4-}$, $[V_{15}O_{36}]^{5-}$, $[V_{15}O_{42}]^{9-}$, $[V_{16}O_{38}]^{3-}$, $[V_{16}O_{38}]^{7-}$, $[V_{16}O_{38}]^{12-}$, $[V_{17}O_{42}]^{4-}$, $[V_{18}O_{42}]^{12-}$, $[V_{18}O_{46}]^{5-}$, $[V_{19}O_{49}]^{9-}$, $[V_{22}O_{54}]^{6-}$ and $[V_{34}O_{82}]^{10-}$ anions.[14]

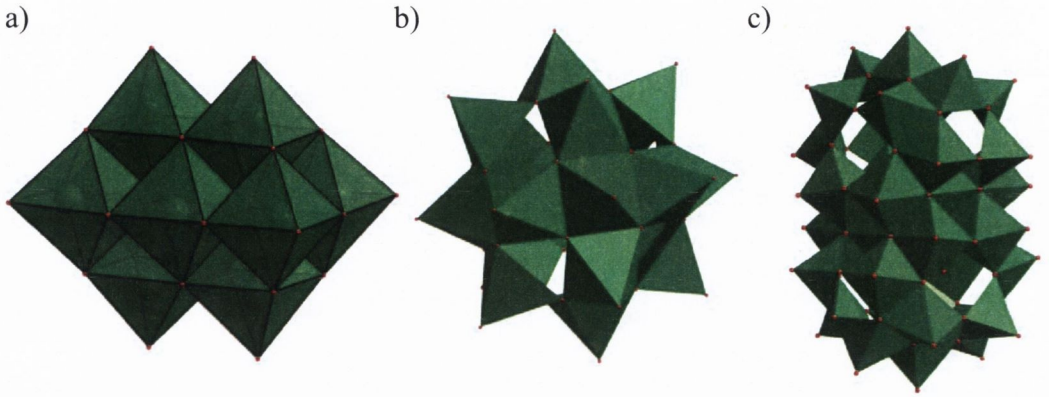

Figure 1.3 – (a) A polyhedral representation of an anionic decavanadate $[V_{10}O_{28}]^{6-}$ cluster. (b) A cavitand polyoxovanadate $[V_{18}O_{42}(X)]^{9-}$ cluster[15]. (c) A 'cluster within a cluster'- $[V_{34}O_{82}]^{10-}$ [14] (X = halide excluding F^-); Polyhedral representations $\{VO_n\}$ green.

The type and composition of the resultant polyoxovanadate clusters can be influenced by the synthetic conditions. For instance it is well established that reducing conditions influence the condensation process and consequently the cluster type. Common reducing agents affect the reduction of vanadium(V) ions to oxidation state (IV). Another important structure-directing effect in the synthesis of polyoxovanadate clusters can be attributed to templating agents present in solution.

1.2.2 The template effect in the synthesis of polyoxovanadate clusters of different shapes and sizes

Templating agents that have been used to influence the shape and size of the resultant polyoxovanadate cluster shells include but are not limited to anions such as N_3^-, NO_3^-,ClO_4^-, Br^-, Cl^-,I^-, F^-, SO_4^{2-}, PO_4^{3-} and VO_4^{3-} ions. In addition, cationic species and H_2O are known to have structure-directing effects during the polyoxovanadate formation. The geometric and

electronic features associated with the V=O moiety are also regarded to have a significant influence on polyoxovanadate phases that evolve during condensation reactions (self-templating effect). Anionic template agents can be subdivided into two classes: templating agents with weak interactions with the cluster shell and templating agents that strongly interact with vanadium ions and the cluster shell. It has been demonstrated that if the type of interaction is weak between the central nucleophilic anion or molecule (Cl^-, Br^-, I^-, H_2O, N_3^-, NO_3^-, ClO_4^-, V=O group, SO_4^{2-}) and the electrophilic V^{n+} centre, then the square pyramidal coordinated vanadium ions are linked to form a cavitand cluster.[15] Alternatively, when the anion carries a sufficiently high charge, (PO_4^{3-}, VO_4^{3-}) strong templating interactions promote the formation of building blocks that contain vanadium ions with predominately octahedral coordination environments.[16] In the latter case, template ions become an integral part of the cluster and are bonded to the vanadium centres of the cluster shell through strong coordination bonds.

Examples of different templated polyoxovanadates can be found in Fig. 1.4: Fig. 1.4a displays the polyoxovanadate cluster $[H_4V_{18}O_{42}(X)]^{9-}$ assembled in the presence of a weakly interacting halide template[17], where (X = Cl^-, Br^-, I^-). Fig. 1.4b highlights the polyoxovanadate cluster $[H_9V_{18}O_{46}VO_4]^{8-}$ assembled around a strongly interacting VO_4^{3-} template[18] which becomes an integral part of the cluster shell through coordinative bonding. Fig. 1.4c displays a cyclic $[Ni_4V_{10}O_{30}(OH)_2(H_2O)_2]^{4-}$ polyoxovanadate incorporating a cationic $\{Ni_4O_{16}\}$ transition metal template.[19] Fig. 1.4d shows the V_2O_5 structure that can be considered as a self-templated structure whereby the V=O bonds stabilise an undulated layered arrangement.[13, 16] The classification of templates can be substantiated by examining cluster topologies and the bond lengths between templates and cluster atoms. $[H_4V_{18}O_{42}(X)]^{9-}$ clusters are templated by spherical halide atoms with the resulting cage structure having approximately D_{4d} symmetry[17] (Fig. 1.3b, Fig. 1.4a). The effective inner cavity of the

clusters display radii of 375 pm (mean value from V-atoms to the centre) and can encapsulate Cl^-, Br^- and I^- ions (covalent radii ranging between 181 pm to 220 pm).[16] Although there are large distances between the central halide ions and the vanadium atoms in these species, there are very weak coordination bonds which are decisive for the stability and the formation of the cluster compound.

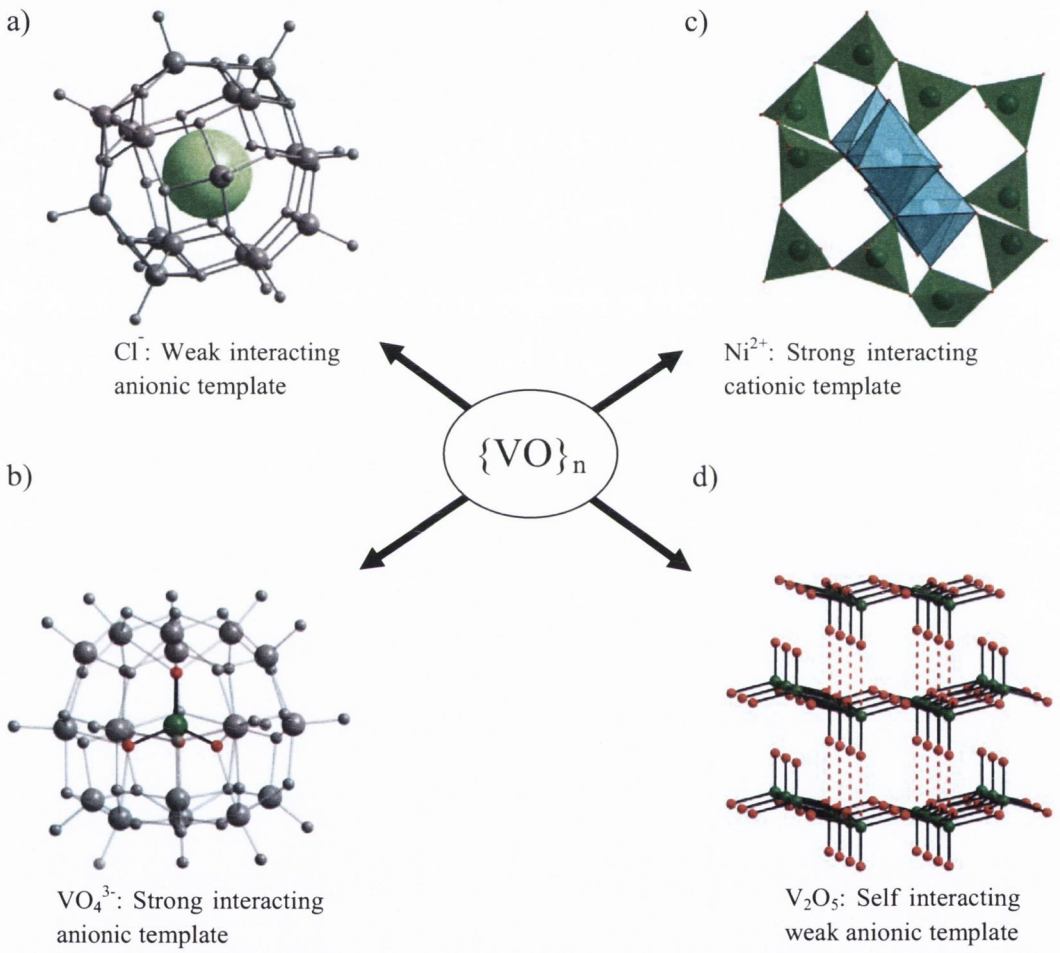

Figure 1.4 – The crystal structures of polyoxovanadate clusters stabilised by different templates; (a) $[H_4V_{18}O_{42}(X)]^{9-}$,[17] (b) $[H_9V_{18}O_{46}VO_4]^{8-}$,[18] (c) $[Ni_4V_{10}O_{30}(OH)_2(H_2O)_2]^{4-}$ [19] and (d) $[V_2O_5]_n$. [13, 16] Polyoxovanadate *exo* skeleton shell gray, Vanadium green, oxygen red. Polyhedral representations: $\{VO_5\}$ green, $\{NiO_6\}$ light blue. Red dash lines represent weak V=O to V=O interaction.

The shape and size of the templating agent can be critical for the formation of different polyoxovanadate clusters. It can be shown that if Cl^- and SO_4^{2-} are used under comparable

reaction conditions, the resulting polyoxovanadate clusters $[V_{18}O_{42}(Cl)]^{13-}$ and $[V_{18}O_{42}(SO_4)]^{8-}$ reveal symmetry and topologies that are related to the structure of the anionic templating agent (Fig. 1.5).

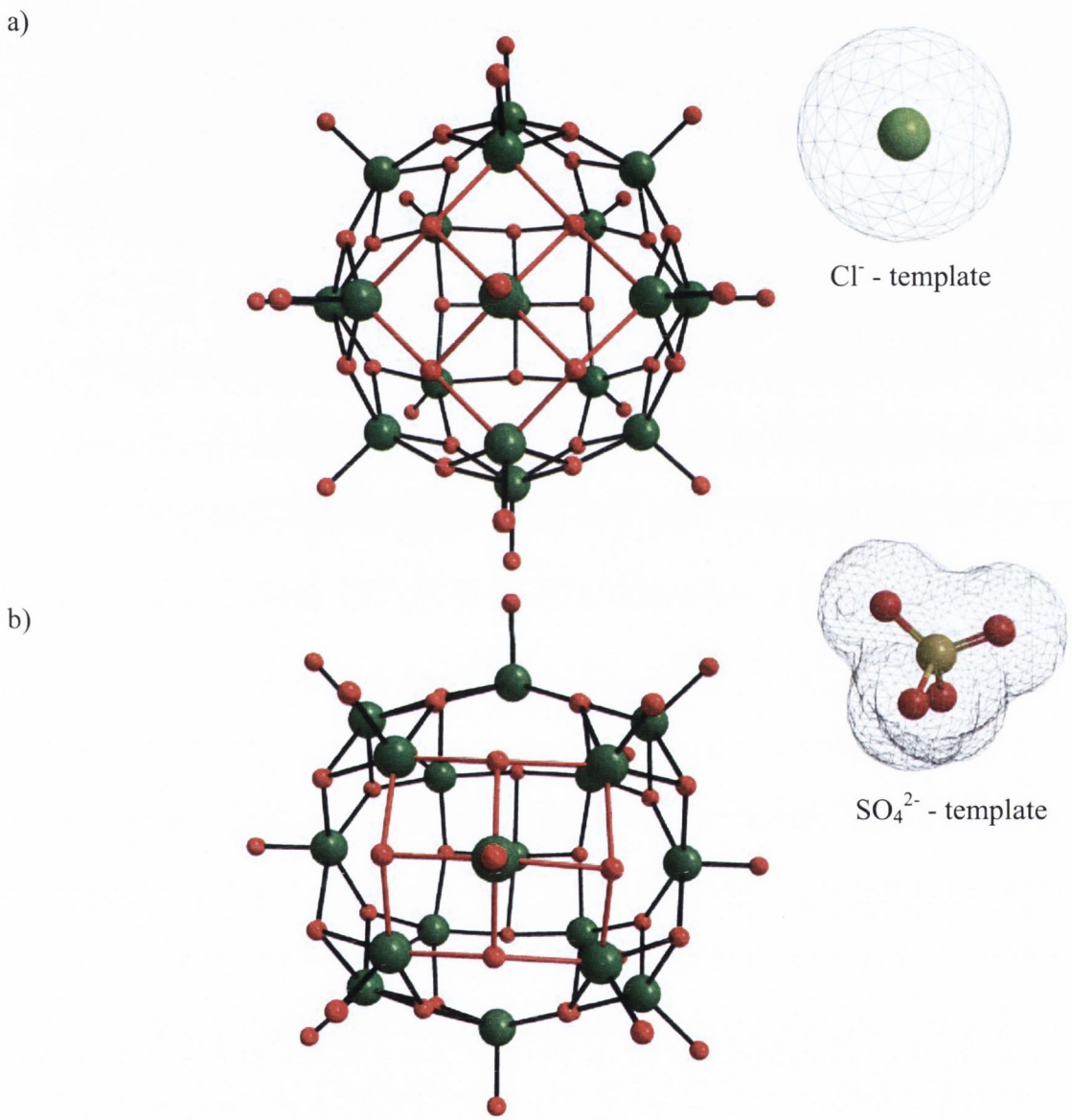

Figure 1.5 – A perspective view of the ball and stick representations of two structurally related polyoxovanadate structures. (a) The pentanuclear vanadium $\{V_5O_9\}$ substructures are at 45° to each other in $[V_{18}O_{42}(Cl)]^{13-}$ (D_{4d}). (b) In $[V_{18}O_{42}(SO_4)]^{8-}$ (T_d), the pentanuclear $\{V_5O_9\}$ units are aligned due to the different template effect of the sulphate anion.[15] Red bonds highlight the pentanuclear $\{V_5O_9\}$ unit on one face for comparison. The template ions shown on the right have been modelled showing their solvent accessible surface areas. Colour code: V green, Cl light green, S golden-brown, O red.

The cluster shell of $[V_{18}O_{42}(Cl)]^{13-}$ (Fig. 1.5a) can formally be converted into the cluster shell of $[V_{18}O_{42}(SO_4)]^{8-}$ by the rotation of one of its pentanuclear $\{V_5O_9\}$ sub-units by 45°.[17] This phenomenon, described as induced self-organisation has lead to the characterisation of a series of structurally related clusters that from in the presence of different sized and shaped templates. If a more linear type of template anion is used, *e.g.* an azide anion, the polyoxovanadate $[V_{18}O_{44}(N_3)]^{7-}$ can be isolated[15] where pentanuclear sub-units $\{V_5O_9\}$ are mirror images of each other resulting in an structural arrangement that is similar to the $[V_{18}O_{42}(SO_4)]^{8-}$ cluster (Fig. 1.5b). However, the use of the azide template results in a cluster with an oblong shape and incorporates two additional oxygen donor atoms in the shell structure. Utilising perchlorate as the template anion leads to a cluster which has a similar tetrahedral symmetry to the structure obtained when the sulphate anions are employed. However, the perchlorate ion which weakly interacts with the host shell templates a larger cluster with the formula $[V_{22}O_{54}(ClO_4)]^{6-}$.[15]

The weak interaction between a cavitand cluster and its guest are comparable to interlayer $\{V{=}O....V{=}O\}$ interactions in the V_2O_5 (Fig. 1.4d). However, while in V_2O_5, the self-templating effect predetermines an undulated layered structure; spherical anionic templating agents often affect the formation of curved building units to produce spherical clusters. A common prerequisite for a weakly interacting template is that the template agent has a relative low nucleophilicity and low bascity, a feature which is agreement with the frequently observed encapsulation of Br^-, Cl^-, I^-, ClO_4^- or NO_3^- ions.[15]

When the anionic template carries a sufficiently high charge, the interaction between the template and cluster ions is strong. PO_4^{3-}, VO_4^{3-} are examples of strongly interacting templates. The structures of a large proportion of the classical heteropolyoxometalates are based on such templates. The Keggin structure, the Wells-Dawson structure and the Evans-Anderson structure are prominent examples that incorporate strongly interacting templates

containing group 14 or 15 elements. The small F^- ions usually do not reside in the cavity of polyoxovanadate clusters. It has been demonstrated that the F^- ion strongly interacts with the vanadium metal centres to induce condensed structures of octahedral building blocks. In this respect, it behaves similar to phosphoric acid templates.[20]

The tendency of polyoxovanadates to encapsulate species of different sizes is associated with the preferred linking motifs of tetragonal $\{VO_5\}$ pyramids to condense into convex sub-units; this can be explained in analogue to the *trans* effect with respect to the V=O bond.[21] Polyoxomolybdates and polyoxotungstates prefer octahedral $\{MO_6\}$ structural motifs and weakly coordinating template ions contained within hollow spheres are rarely observed.

1.3 Functionalisation of polyoxometalates

Methodologies to functionalise polyoxometalates are wide ranging and many different research groups have provided a substantial base of literature for the functionalisation of polyoxometalates. The majority of the functionalisation approaches can be grouped into one of the following categories:

1.3.1 Counter-ion exchange for the functionalisation of polyoxometalates

One functionalisation method involves exchanging the counter-ions of a polyoxometalate cluster with organic counter-ions in order to gain advantageous properties from the resultant hybrid materials. Such hybrid materials may exhibit an increased solubility in common solvents. Common organic cationic counter-ions used in conjunction with anionic polyoxometalates are quaternary ammonium salts.[22] These quaternary ammonium salts can be synthesised to include a tailored functional group depending on the desired application.

Examples of polyoxometalates functionalised by quaternary ammonium ions comprise of the inclusion of photo-active chromophores for photocatalysis, the inclusion of long alkyl chains to aid self-assembly processes or the use of organic amine groups to attach the salt to a metal surface for corrosion inhibition.[22] Corrosion resistant coatings using polyoxometalates are well established industrial applications of these functionalised materials; often a synergistic effect between the properties of polyoxometalates and the ammonium counter-ions is observed. In the case of corrosion inhibition, the organic amines offer a cathodic protection of the metal surface whilst the polyoxometalates inhibit oxidation. Polyoxometalate functionalised by quaternary ammonium ions are used as dyes, pigments and inks. Furthermore, these hybrid materials have found use in membrane sensors such as gas sensors, solid-state electrochromic devices and electrochemical fuel cells. Further industrial applications of these hybrid polyoxometalates have been reviewed by Katsoulis *et al.*[22]

1.3.2 Oxo ligand exchange to incorporate organic moieties

Synthetic approaches to incorporate organic moieties into polyoxometalates include the preparation of imido, diazenido, organosilyl, and alkoxo derivatives. Their preparation has been an active research field over the last two decades and a huge range of compounds have been reported. Most of these compounds tend to be more sensitive to decomposition on exposure to air or moisture than traditional polyoxometalates with Keggin or Wells-Dawson structure that contain solely terminal oxo ligands. Research in the functionalisation of the polyoxometalates through covalent grafting of organic moieties allows the redox and acid–base properties of functionalised polyoxometalates to be tuned. Most of the resulting functionalised polyoxometalates find potential applications in catalysis and material science.

Covalent grafting approaches to introduce organic moieties into polyoxometalates have been reviewed by Proust *et al.*, in 1998[23] and more recently again in 2008.[24]

1.3.3 Functionalisation through the incorporation of main-group and transition metals in polyoxometalate clusters

Over the past several decades, many research groups have explored the incorporation of main group elements into polyoxovanadate clusters.[20] These different research groups have mainly focused on the functionalisation of the spherical $[V_{18}O_{42}]^{12-}$ cluster and the use of these functionalised clusters as building blocks for open-framework materials. Such efforts resulted in a large number of vanadoarsenate, vandoantimonate, vandogermanate and vanadosilicate clusters that have been synthesised and characterised. The vanadoarsenates $[As_{2n}V_{18-n}O_{42}(G)]^{2n-12}$ (G = H_2O, Cl^-, SO_4^{2-} or NO_3^-) in particular are of interest as they display interesting electronic and magnetic properties or host-guest interactions. Examples of these vanadoarsenates in which a water molecule is located at the centre of these clusters have been detailed in Table 1.1.

Table 1.1 – Vanadoarsenate clusters $[As_{2n}V_{18-n}O_{42}]^{2n-12}$		
$[As_4V_{16}O_{42}(H_2O)]^{8-}$	n=2	Guo-Yu Yang *et al.* 2008[25]
$[As_6V_{15}O_{42}(H_2O)]^{6-}$	n=3	Müller *et al.* 1998[26]
$[As_8V_{14}O_{42}(H_2O)_{0.5}]^{4-}$	n=4	Jacobson *et al.* 1991[27]

The $[As_4V_{16}O_{42}(H_2O)]^{8-}$ vanadoarsenate cluster can be derived from a $[V_{18}O_{42}H_9(VO_4)]^{6-}$ (Fig. 1.4b) rhombicuboactahedron-type cluster by omitting the central vanadium atom and replacing two square pyramidal $\{VO_5\}$ ions with two $[As_2O_5]^{4-}$ groups. Further replacement

of two square pyramids $\{VO_5\}$ ions of polyoxoanion $[As_4V_{16}O_{42}(H_2O)]^{8-}$ with two $[As_2O_5]^{4-}$ groups results in the formation of the polyoxoanionic $[As_8V_{14}O_{42}(H_2O)_{0.5}]^{4-}$ cluster (Fig. 1.6b). These vanadoarsenate clusters have also been extensively investigated as building blocks for robust three dimensional frameworks when can be linked through transition metal units (Fig. 1.6c).[28]

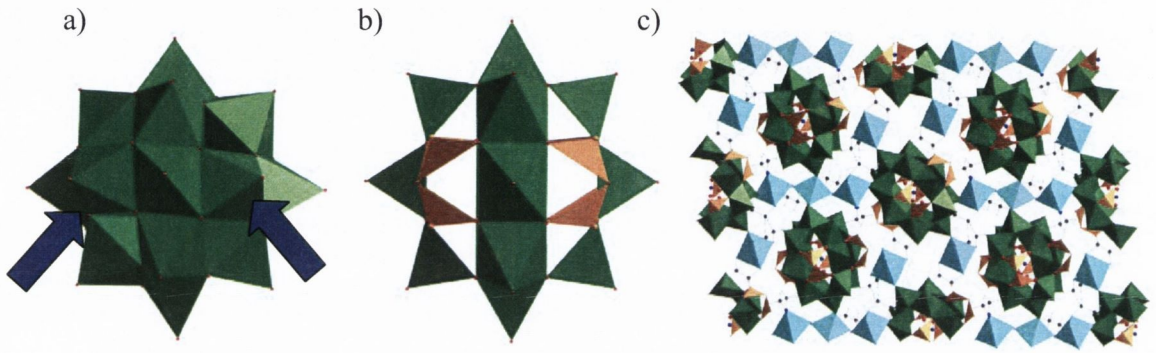

Figure 1.6 – (a) Functionalisation of the anionic $[V_{18}O_{42}H_9(VO_4)]^{6-}$ [18] cluster through the replacement of the vanadium$\{VO_5\}$ square pyramids with $\{As_2O_5\}$ (blue arrows). (b) The resulting vanadoarsenate cluster $[As_8V_{14}O_{42}(H_2O)_{0.5}]^{4-}$ [27] where four $\{As_2O_5\}$ units replace four vanadium $\{VO_5\}$ units. (c) $[\{Ni(en)_2\}_4(4,4'\text{-bipy})_4\{Ni(H_2O)_2\}]_2[As_8V_{14}O_{42}(NO_3)]_4 \cdot 16H_2O$, is one of the many examples of 3-D networks utilising an polyoxovanadoarsenate as a building block in combination with a transition metal.[28] Polyhedral representations: $\{VO_n\}$ green, $\{AsO_3\}$ orange, $\{NiO_6\}$ blue; Oxygen red.

The incorporation of a transition metal into the lacunary sites of a polyoxometalate cluster has been a long established research area and due to the large volume of research material, the functionalisation of polyoxometalates by transition metals will not be discussed in detail within this thesis except to highlight some examples.[29] The incorporation of catalytically active transition metals into the shell of a polyoxometalate cluster provides an approach to generate unique advantageous properties. An example of such a catalyst is achieved by the incorporation of a vanadate ion in a heteropolytungstate cluster by Hill *et al.* He reports the selective delignification/bleaching of wood fibres for the production of cellulose (paper) using a two step oxidation process using this catalyst.[30] Recently, Cronin *et al.* have reported

a large number of polyoxometalate clusters that have been functionalised with transition metals, lanthanide metals or main group elements leading to many diverse and interesting structural cluster motifs.[31] Some general examples of such structures include the anionic clusters of $[KFe_{12}(OH)_{18}(\alpha\text{-}1,2,3\text{-}P_2W_{15}O_{56})_4]^{29-}$, $[(Mo_{128}Eu_4O_{388}H_{10}(H_2O)_{81})_2]^{20-}$, $[(M_2P_2W_{16}O_{60})_3]^{24-}$ M = Co, Mn, Fe, $[(Ni_2P_2W_{16}O_{60})_3]^{30-}$, $[W_{72}Mn_{12}O_{268}Ge_7]^{40-}$ and $[H_6W_{63}Se_6O_{221}]^{24-}$.[32]

1.3.4 The incorporation of organoarsonate and organophosphonate ligands in the structural shell of functionalised polyoxovanadates

The functionalisation of polyoxometalates through the incorporation of organoarsonate and organophosphonate groups has been established for sometime but has not been advanced to the same extent as most of the previously mentioned functionalisation techniques. Phosphonate ligands show versatility in the preparation of structurally unique clusters and extended compounds in which the metal centres of the hybrid clusters can be fully oxidised, reduced or exist in a mixed-valent oxidation state. Hybrid polyoxometalates containing organophosphonate ligands or organoarsonate ligands can be categorised depending on their dimensionality: 0-D molecular coordination compounds, 1-D linear chains, 2-D layered compounds and 3-D networks. The unusual absorptive and catalytic properties for layered hybrid phosphonate materials have lead to the development of these materials as catalysts and ion exchangers.[20, 33]

-Phosphonate functionalised polyoxovanadates

Recently there has been a revived interest in nano-sized phosphonate stabilised vanadium complexes with a view to the synthesis and design of inorganic materials of specific size,

conformation and properties for potential application in electronics, catalysis and medicine.[13] The desire to synthesise large spherical or discrete bowl-shaped metal-oxo clusters using organic ligands is motivated by the interesting host-guest and encapsulation properties of these compounds.[13] Their physical properties make them promising materials for electronic devices and recently it has been demonstrated, that ligand-stabilised species can self assemble into potential components for molecular nanodevices. This approach has been referred to by Cronin *et al.* as the "bottom-up" route in the synthesis of nano-scale polyoxometalate molecular devices.[29, 34]

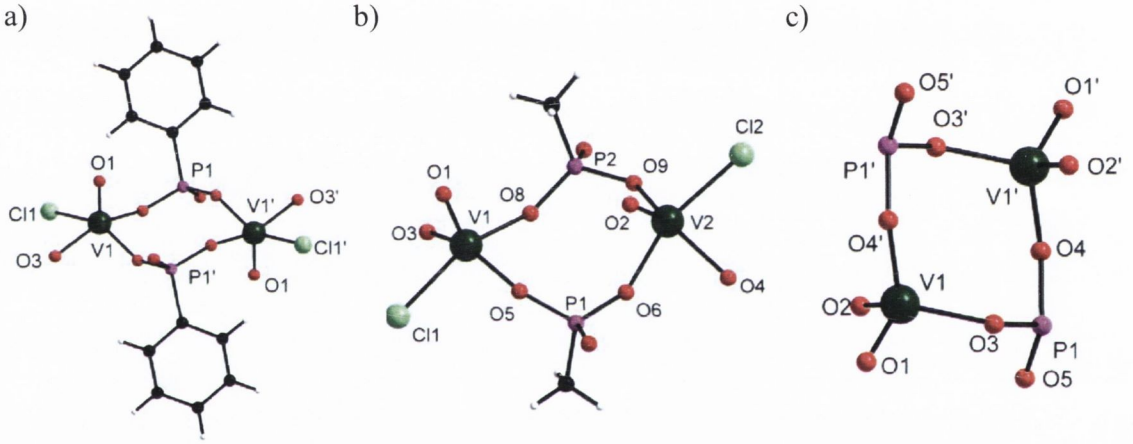

Figure 1.7 – Ball and stick representations of dinuclear vanadium complexes that contain two bridging organophosphonate ligands.[37] (a) $[V_2O_2Cl_2(PhPO_3H)_2(H_2O)_2]$ (b) $[(VO)_2O_2Cl_2(t\text{-}C_4H_9PO_3H_2)]^{2-}$ (c) $[V_2O_4(CH_3C_6H_4CH_2PO_3)_2]^{2-}$ (organic moiety deleted for clarity). Colour code: V dark green, Cl light green, P purple, O red, C black, H white.

The structural motifs observed in dinuclear phosphonate-stabilised species can be considered as building blocks of larger polyoxovanadate clusters.[35] Three representative dinuclear vanadium complexes that contain μ-O, O' bridging organophosphonates are shown in Fig. 1.7. $[V_2O_2Cl_2(PhPO_3H)_2(H_2O)_2]$ and $[(VO)_2O_2Cl_2(t\text{-}C_4H_9PO_3H_2)]^{2-}$ contains vanadium ions in the oxidation state +IV.[35, 36] In $[V_2O_2Cl_2(PhPO_3H)_2(H_2O)_2]$ the two terminal oxo ligands of the two vanadium ions are arranged in an *anti*-position whilst in $[(VO)_2O_2Cl_2(t\text{-}C_4H_9PO_3H_2)]^{2-}$ the terminal oxo ligands adopt *syn*-positions. To prepare these complexes large bulky $(PPh_4)^+$ counter-ions were used to prevent the condensation of the dinuclear complexes into larger

oligomers or clusters. The oxidised analogue of $[V_2O_2Cl_2(PhPO_3H)_2(H_2O)_2]$ has also been prepared.[35] The oxidised compound, $[V_2O_4(CH_3C_6H_4CH_2PO_3)_2]^{2-}$, shown in Fig. 1.7c represents a rare example of a complex in which the V^V ions are tetrahedrally coordinated and have two *cis* coordinating terminal oxo ligands. The isolation of these dinuclear species has consecutively lead to the synthesis of many structural motifs depending on the reaction conditions.

As can be seen from the reaction profiles in Fig. 1.8,[37] the introduction of water and/or oxygen leads to the isolation of a much larger molecular species or the formation of condensed layered vanadium phosphonates.

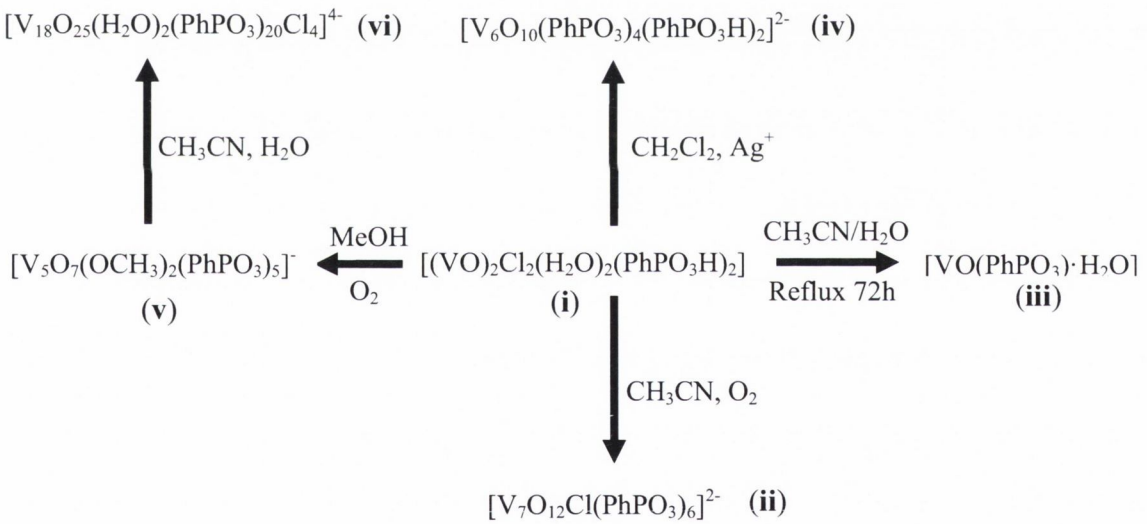

Figure 1.8 – Reaction profile using the dinuclear species as a precursor for condensation into larger oligomers, clusters and inorganic solids.[37] (i) $[(VO)_2Cl_2(H_2O)_2(PhPO_3H)_2]$; (ii) $[V_7O_{12}Cl(PhPO_3)_6]^{2-}$; (iii) $[VO(PhPO_3)\cdot H_2O]$; (iv) $[V_6O_{10}(PhPO_3)_4(PhPO_3H)_2]^{2-}$; (v) $[V_5O_7(OCH_3)_2(PhPO_3)_5]^-$ and (vi) $[V_{18}O_{25}(H_2O)_2(PhPO_3)_{20}Cl_4]^{4-}$.

The cluster $[V_{18}O_{25}(H_2O)_2(PhPO_3)_{20}Cl_4]^{4-}$ is suggested to be a 'cluster of clusters' demonstrating that the small oligomers can be linked into cluster of nanometre dimensions by comparatively rational synthetic routes.[12] In this thesis, we will examine whether similar

building units can be isolated in aqueous solution and whether these building units can be used to produce larger oligomers similar to that observed in the reaction profile of Fig. 1.8.

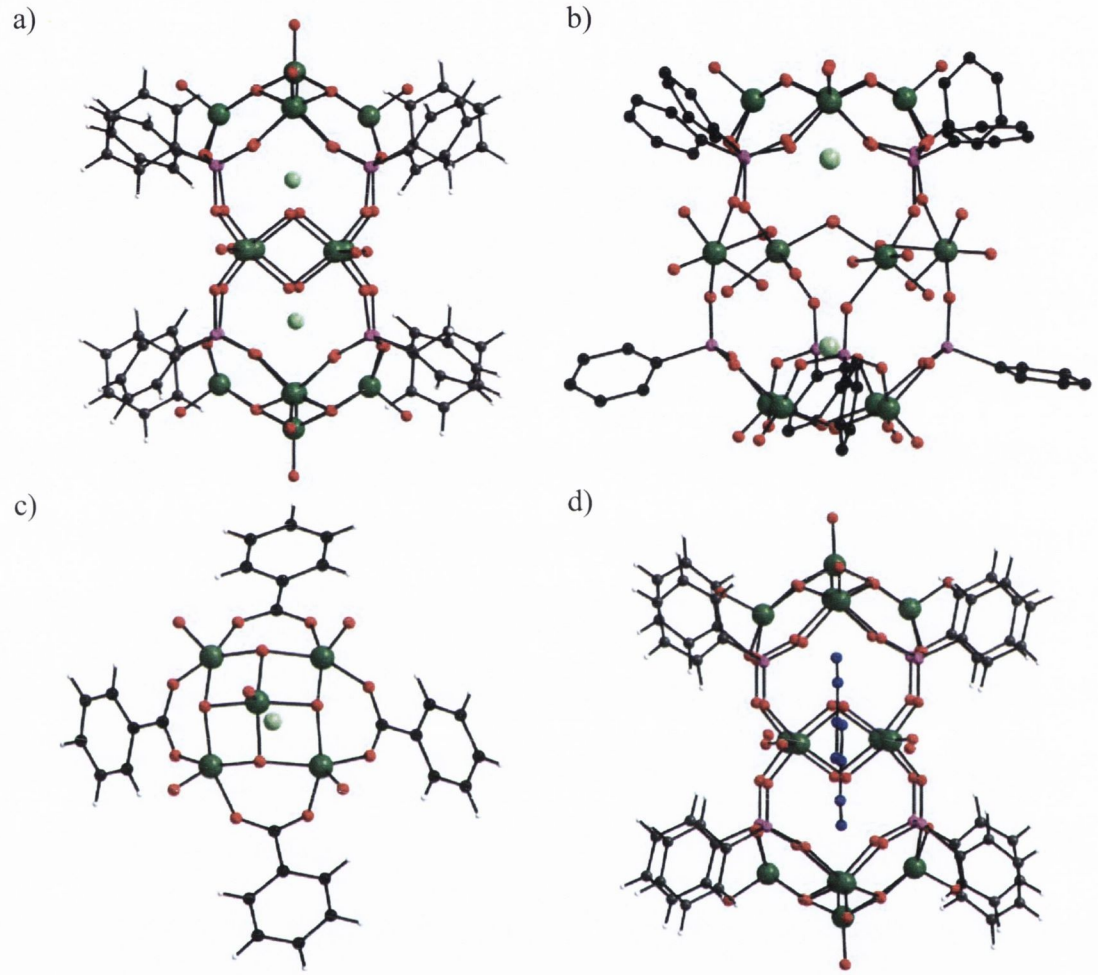

Figure 1.9 – Ball and stick representations of four related functionalised polyoxovanadate clusters: (a) $[Cl_2 \subset V_{14}O_{22}(OH)_4(H_2O)(O_3PPh)_8]^{6-}$,[38] (b) $[Cl_2 \subset (V_{12}O_{20})(H_2O)_{12}(PhPO_3)_8]$,[39] (c) $[Cl \subset V_5O_9(O_2CPh)_4]^{2-}$ [41] and (d) $[(N_3)_2 \subset V_{14}O_{22}(OH)_4(H_2O)(O_3PPh)_8]^{6-}$.[42] Colour Code: V green, Cl light green, P purple, O red, N blue, C black, H white.

A second synthetic approach to prepare nano-sized clusters of phosphonate functionalised polyoxovanadates involves the self-assembly of phosphonate ligands and vanadate salts under reducing conditions in aqueous solutions. Müller *et al.* reported the synthesis of $[V_{14}O_{22}(OH)_4(H_2O)(O_3PPh)_8]^{6-}$.[38] This cluster that provides a nanometre-sized cavity for the inclusion of anions and cations is shown in Fig. 1.9. The cluster consists of two mixed-valent pentanuclear $\{V_5O_9\}^{3+}$ sub-units, each with a localised central V(V) site which are bridged

intramolecularly by two binuclear $\{V_2^{IV}O_2(OH)_2(H_2O)(O_3PPh)_4\}$ moieties. These fragments condense to form a cage structure with a cavity enclosing two NH_4Cl units. The choice of solvent can be hugely influential on the condensation process as seen in Fig. 1.8.

Clearfield *et al.* recently reported the non-aqueous synthesis of a related mixed-valent dodecanuclear vanadium cluster $[Cl_2\subset(V_{12}O_{20})(H_2O)_{12}(PhPO_3)_8]$ encapsulating two chloride anions (see Fig. 1.9b).[39] Clearfield's structure could be described as two cationic $\{V_4O_8\}^{4+}$ caps which are symmetrically bridged though four $PhPO_3^{2-}$ tetrahedra to a central grid of four $\{V^{IV}O(H_2O)_3\}^{2+}$ units.[40] The cluster is therefore charge neutral and the charge of the two chloride ions that reside in the cavity of cluster is balanced by two external triethylammonium cations. It is noteworthy that the $\{V_4O_8\}^{4+}$ units in $[Cl_2\subset(V_{12}O_{20})(H_2O)_{12}(PhPO_3)_8]$ (Fig. 1.9b) are topologically related to the $\{V_5O_9\}^{3+}$ sub-units observed in $[V_{14}O_{22}(OH)_4(H_2O)(O_3PPh)_8]^{6-}$ (Fig. 1.9a) and $[H_4V_{18}O_{42}X]^{9-}$ (Fig. 1.5) by removal of the central $\{V^VO_3\}^{3+}$ and flattening of the $\{V_4O_4\}^{4+}$ motif. This observation reveals the structural relationship between this series of clusters. $[V_{14}O_{22}(OH)_4(H_2O)(O_3PPh)_8]^{6-}$ (Fig. 1.9a) can be formally constructed from $[Cl_2\subset (V_{12}O_{20})(H_2O)_{12}(PhPO_3)_8]$ (Fig. 1.9b) by the reduction of the V^V centres, capping of each $\{V_4O_8\}^{4+}$ structural motif by a $\{V^VO_3\}^{3+}$ group, and pair-wise condensation of the four $\{VO(H_2O)_3\}^{2+}$ units to give two bridging $\{V_2O_2(OH)_2(H_2O)\}^{2+}$ groups. The redox related structural transformations of the $\{V_5O_9\}^{3+}$ and $\{V_4O_8\}^{4+}$ units have been further investigated and resulted in the synthesis of a tetranuclear and a mixed-valent pentanuclear vanadium carboxylate complex (Fig. 1.9c).[41]

Most of the complexes that we have discussed contain chloride ions in the centre of their concave building units strongly suggesting that these ions act as templates during their formation. However, the templating mechanism remains somehow obscure considering the

fact that the same $[V_{14}O_{22}(OH)_4(H_2O)(O_3PPh)_8]^{6-}$ structure can be obtained using different anionic or neutral templates including azide anions or acetonitrile molecules (Fig. 1.9d).[42] Charge compensation, steric and geometrical effects may also contribute to the assembly processes of these hybrid polyoxovanadate clusters.[37]

Investigations into the solvothermal synthesis of hybrid polyoxovanadates has also been carried out in the last decade with numerous novel compounds being reported[20, 43] (Fig. 1.10a).

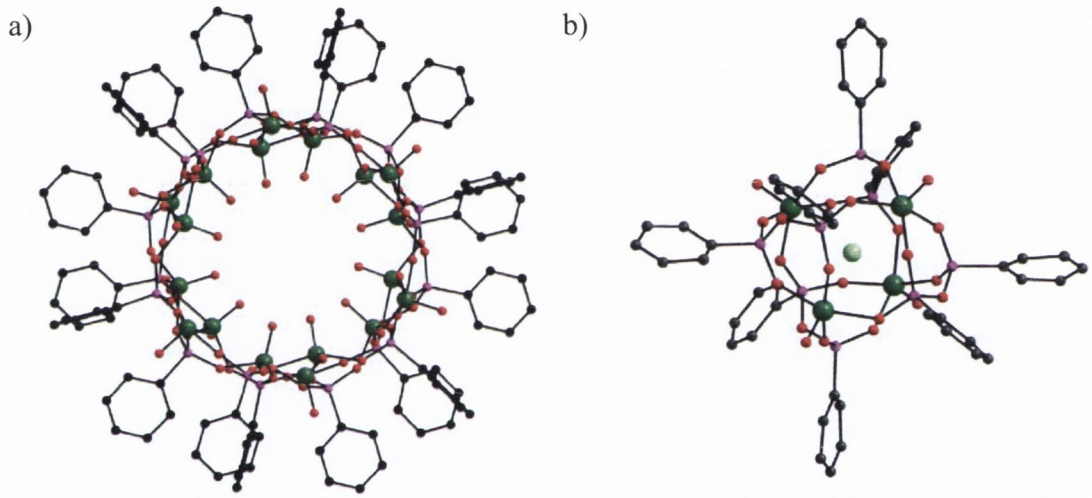

Figure 1.10 – The crystal structures of solvothermally synthesised polyoxovanadate solids. (a) A functionalised polyoxovanadate $[(V_3O_4)(H_2O)(PhPO_3)_3]^{n-}$ tubular structure as viewed in the crystallographic *c*-axis.[44] (b) A pyrophosphonate functionalised polyoxovanadate enclosing a chloride anion.[45] Colour code: V green, Cl light green, P purple, O red, C black.

In particular, Zubieta *et al.* reported the synthesis of a fascinating tubular organophosphonate structure.[44] The structure shown in Fig. 1.10a consists of $[(V_3O_4)(H_2O)(PhPO_3)_3]^{n-}{}_n$ tubes running parallel to the crystallographic *c*-axis. The phenyl groups of the organic ligands extend outwards from the periphery of the tubes, while the vanadyl oxo groups are directed both to the interior and the exterior of the resulting cavity. Solvothermal reaction conditions can also lead to metal mediated, thermally induced condensation reactions that involve the *in situ* fusion of phosphonic acids into pyrophosphonate ligands which allows the self-assembly of novel clusters.

An example of this is the solvothermal synthesis of $[(VO)_4(PhP(O)_2OP(O)_2Ph)_4Cl]^-$ in which the cluster shell is constructed from vanadium centred square pyramids and the fused pyrophosphonate tetrahedra which enclose a chloride anion (Fig. 1.10b).[45]

-Arsonate functionalised polyoxovanadates

The introduction of purely inorganic arsenate ions, AsO_4^{3-} which are geometrically similar to the square pentanuclear $\{VO_4\}$ units has been previously discussed in section 1.3.3. The geometry and bonding requirements of an organoarsonate moiety are comparable to those of an arsenate anion and therefore their mutual substitution during synthesis could provide a promising approach for the preparation of functionalised polyoxovanadates. The synthetic procedures for the functionalisation of polyoxovanadate clusters using organoarsonates are comparable to those generating organophosphonate stabilised oxovanadates. However, there are some subtle differences that influence the product formation and to date the numbers of organoarsonate stabilised polyoxovanadate structures reported are far lower than those of the phosphonate functionalised clusters.

Bond valence sum analysis shows that the typical lengths of the As^V-O and the V^V-O single bonds are almost identical.[46] However, the P^V-O bond is 0.15Å shorter than the As^V-O bond and therefore the arsonate functionality is favourably suited for incorporation in a polyoxovanadate cluster without major change to the overall structural arrangement of the cluster. Reported aryl arsonate functionalised polyoxovanadates include the anionic clusters $[V_{10}O_{24}(O_3AsC_6H_4\text{-}4\text{-}NH_2)_3]^{4-}$,[47] $[H_2(V_6O_{10}(O_3AsPh)_6)]^{2-}$,[47] $[2CH_3OH\subset V_{12}O_{14}(OH)_4(PhAsO_3)_{10}]^{4-}$ [46] and $[2H_2O\subset V_{12}O_{12}(OH)_2(H_2O)_2(PhAsO_3)_{10}(PhAsO_3H)_4]^{2-}$.[46]

$[V_{10}O_{24}(O_3AsC_6H_4\text{-}4\text{-}NH_2)_3]^{4-}$ (Fig. 1.11a) and $[H_2(V_6O_{10}(O_3AsPh)_6)]^{2-}$ were synthesised by refluxing an inorganic decavanadate cluster $[V_{10}O_{28}]^{4-}$ in methanol with (4-aminophenyl)arsonic acid and phenylarsonic acid, respectively. It is reported that the two

geometrically different clusters are isolated due to the minor changes of the organic ligand structure. Both, $[2CH_3OH \subset V_{12}O_{14}(OH)_4(PhAsO_3)_{10}]^{4-}$ (Fig 1.11b) and $[2H_2O \subset V_{12}O_{12}(OH)_2(H_2O)_2(PhAsO_3)_{10}(PhAsO_3H)_4]^{2-}$ were synthesised under solvothermal reaction conditions.[46] Similarly to the phosphonate ligand systems, pyroarsonate-containing vanadates can also be *in situ* synthesised as a result of metal mediated, thermally induced condensation reactions.[48]

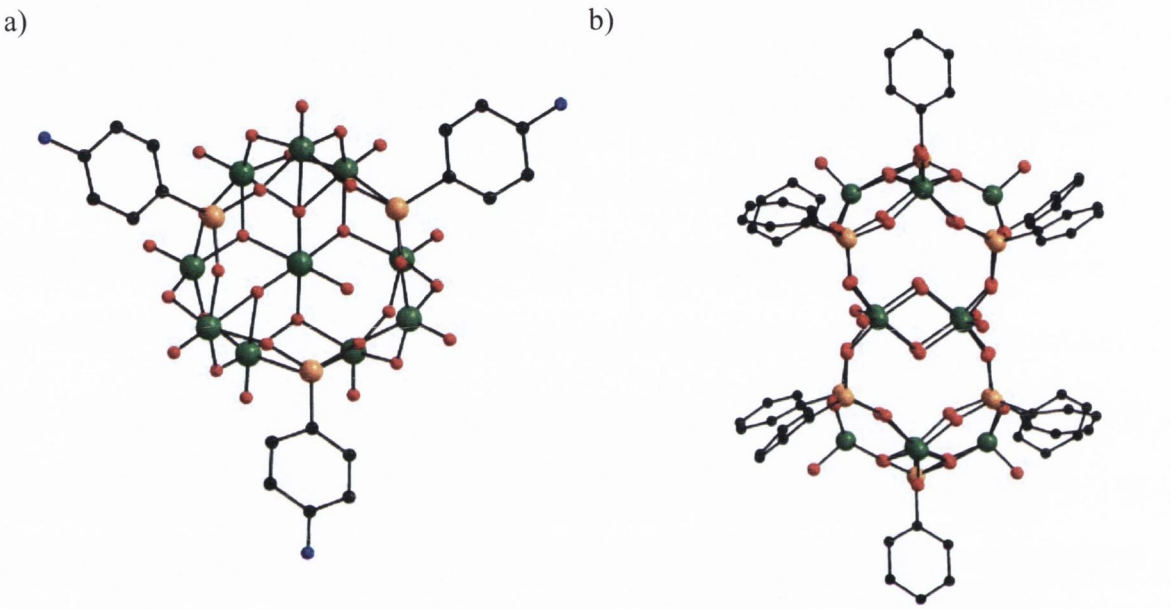

Figure 1.11 – Two organoarsonate functionalised polyoxovanadates. (a) $[V_{10}O_{24}(O_3AsC_6H_4\text{-}4\text{-}NH_2)_3]^{4-}$.[47] (b) $[V_{12}O_{14}(OH)_4(PhAsO_3)_{10}]^{4-}$.[46] Colour code: V green, As orange, O red, N blue, C black.

1.4 Metal organic frameworks (MOFs) – Functionalised polyoxometalates as potential building units

It is worth noting that in 2001, Stein *et al.* synthesised a series of organoarsonate functionalised polyoxomolybdate clusters with the concept that the functionalised polyoxomolybdate clusters could be used as building blocks for constructing a predictable open framework coordination network.

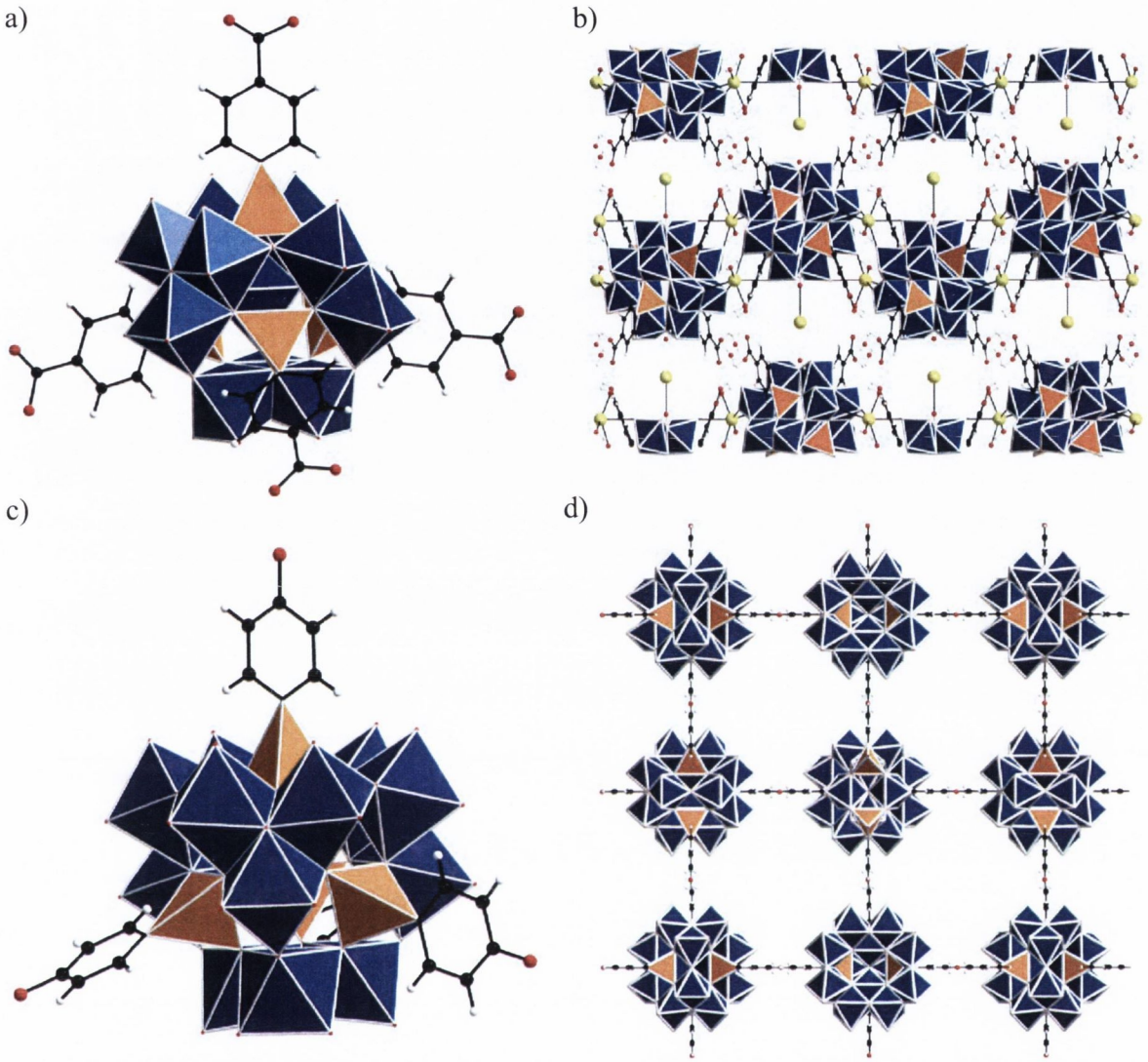

Figure 1.12 –Polyhedral representations of two organoarsonate functionalised polyoxomolybdate clusters.[49] (a) The (4-carboxylphenyl)arsonate functionalised polyoxomolybdate, $[Mo_{12}O_{43}(O_3AsC_6H_4COOH)_4]^{4-}$. (b) The packing arrangement of the clusters of (a) in the crystal structure as viewed in the crystallographic *a*-axis. (c) The (4-hydroxylphenyl)arsonate functionalised polyoxomolybdate, $[Mo_{12}O_{43}(O_3AsC_6H_4OH)_4]^{4-}$. (d) The packing arrangement of the clusters of (c) in the crystal structure as viewed in the crystallographic *c*-axis. Colour code: Mo blue, As orange, O red, C black, H white.

Stein proposed that by "*employing well-defined clusters, with a set number of bonding sites and with directionality to the bonding interactions, as building blocks, it could be possible to predetermine with more accuracy the final connectivity and architecture of the crystalline material*". Utilising previously synthesised polyoxomolybdate building blocks ($[Mo_{12}O_{43}(O_3AsR)_4]^{4-}$ where R = CH_3, C_2H_4OH, Ph, $C_6H_4NH_3^+$, C_6H_4CN, C_6H_4OH,

C_6H_4COOH), Stein intended to use the functionalising arsonate ligands to influence both the connectivity and the formation of new polyoxometalate frameworks.

Two examples of building blocks and their respective packing arrangements in their crystal structure have been shown in Fig. 1.12. The functionalised polyoxomolybdate building blocks, $[Mo_{12}O_{43}(O_3AsC_6H_4COOH)_4]^{4-}$ and $[Mo_{12}O_{43}(O_3AsC_6H_4OH)_4]^{4-}$, consist of four units of three edge sharing $\{MoO_6\}$ octahedra which are bridged by four organoarsonate tetrahedra.[51] These organoarsonate tetrahedra are arranged around the functionalised molybdate cluster in a tetrahedral fashion (Fig. 1.12a and 1.12c). The overall crystal structure including the $[Mo_{12}O_{43}(O_3AsC_6H_4COOH)_4]^{4-}$ building unit can be described as two independent, interpenetrating 3D frameworks containing hydrogen-bonded 2D sheets held together along the third axis by {O-Na-O} linkages leading to a closely packed structure. In contrast, the overall crystal structure of the (4-hydroxyphenyl)arsonate $[Mo_{12}O_{43}(O_3AsC_6H_4OH)_4]^{4-}$ building units can be described as an open-framework structure in which solvent filled channels run parallel to the crystallographic *c*-axis (Fig. 1.12d). Finally, it is important to note that the synthesis of these latter discussed structures was achieved by the addition of transition metal salts: aqueous copper sulphate was added to $[Mo_{12}O_{43}(O_3AsC_6H_4COOH)_4]^{4-}$ to generate the closely packed framework and aqueous iron nitrate was added to $[Mo_{12}O_{43}(O_3AsC_6H_4OH)_4]^{4-}$ in a DMSO/water solution to produce the open-framework structure. However, neither of the transition metals was present in the final product. Ideally, the construction of functionalised polyoxometalates with stronger interactions between the clusters such as coordination bonds or covalent bonds will lead to more robust 3-D frameworks. However, the difficulty to predict the favourable linkages of the building blocks and the consequences of these linkages on the overall connectivity in the crystal structure meant that Stein was unable to produce significant numbers of 'rational' network structures. Possible and difficult to predict linkages that can prevail include

interactions between the terminal oxo ligands of the clusters and the counter-ions/transition metals, interactions between terminal oxo ligands and the functionalising organic groups and interactions between the functionalised organic groups themselves. Additionally, if the bonding interactions are weak and dynamic (*i.e.* hydrogen bonding) then small changes in the synthetic technique (use of different solvents or counter-ions) can lead to differently ordered crystalline products as reported by Stein *et al.*[49]

Prior to Stein's work, a class of hybrid materials classified as metal-organic frameworks were proposed by Hoskins and Robson in 1989.[50] Later, Yaghi *et al.* successfully developed a conceptual approach that requires the use of secondary building units to direct the assembly of ordered frameworks.[51] By systematically varying and functionalising the pore matrices of the framework, it is possible to produce some of the most efficient gas storage metal-organic frameworks.[52] However, Yaghi states that "*specific future challenges include the ability to design sophisticated molecular building blocks that would act as carriers of structural and functional information to be expressed in a target material*".[51] The desirability of such target materials would be large pore size, high apparent surface area, selective uptake of small molecules, and optical responses to the inclusion of guests. In order to produce a robust porous material, one must consider the construction of a molecular scaffold by connecting inorganic clusters through rigid organic linkers. These 'building blocks' will predetermine a geometrically well defined structure. It is the connectivity of the building unit that determines the topologies of the resultant hybrid material and therefore its properties. Yaghi's reticular synthetic concept allows the rationalisation of the formation and structure of the hybrid organic-inorganic material. It derives metal-organic frameworks from their parent classical inorganic structure types in which bonds and polyhedrons are augmented by rigid linkers and organic/inorganic SBUs.[51] Fig. 1.13 shows a cubic primitive network whose topology can be related to the ReO_3 structure. The tetranuclear subunits in $[Zn_4(\mu_4\text{-}O)(BDA)_4]$ can be

envisaged as octahedral SBUs and are linked through rigid benzene dicarboxylic acid ligands into an augmented ReO_3 network.[52] In these structures, extension of the ligand system provides a facile approach to increase pore size and surface area. The expansion of a given topology using a modular set of ligands is usually described as isoreticular expansion.

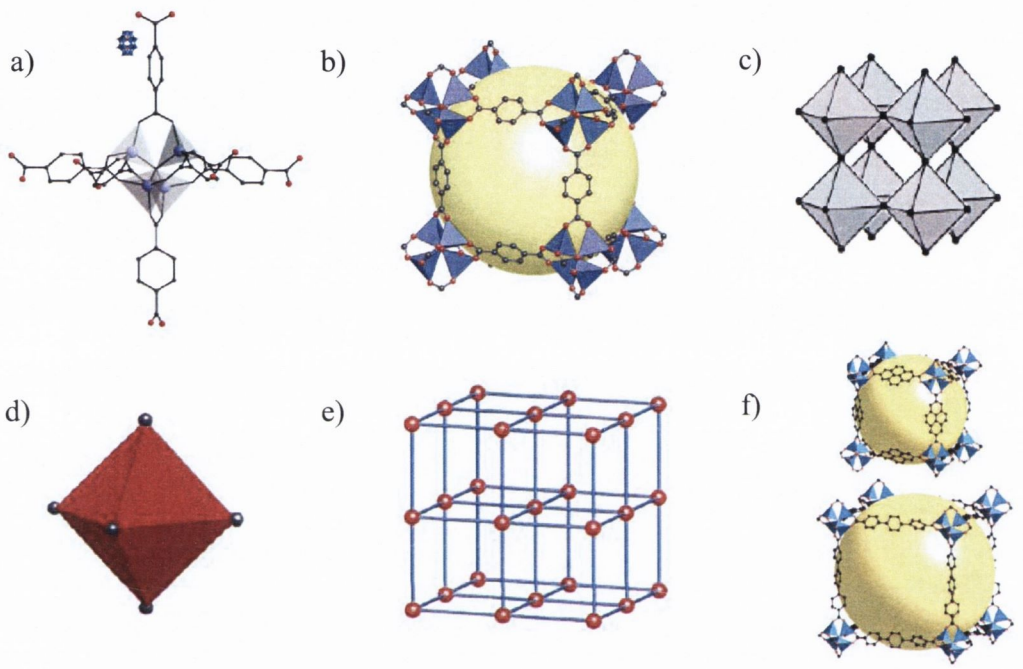

Figure 1.13 – Representation of the reticular synthesis concept which can be applied to prepare metal-organic frameworks.[51] (a - b) Linkage of tetranuclear zinc complexes $[Zn_4(\mu_4\text{-}O)(BDA)_4]$ into a metal organic framework. (c) ReO_3 topology. (d) Representation of the octahedral $\{Zn_4OCO_2\}$ SBU in this structure. (e) Topology of the structure (primitive cubic net) shown as ball and stick model. (f) Augmentation of this topology by using extended ligands (isoreticular expansion).

Yaghi *et al.* have argued that although there are numerous different topologies in existence, there seems to be only a small number of simple, high symmetry structures that would be predicted to form most commonly.[51] The suitability of the building unit will rely both on the rigidity and directionality of the bonding which must be reliably maintained during the assembly process. However, even if the predetermined structure is formed, one must be aware that there is a possibility of catenation, where two or more identical frameworks are inter-grown leading to interpenetration and interweaving which occurs at the expense of pore

volume and surface area. It is surprising that the vast number of existing polyoxometalate clusters with physiochemical properties allowing their use in catalysis and gas sorption have not yet been systematically exploited as building blocks for MOFs.

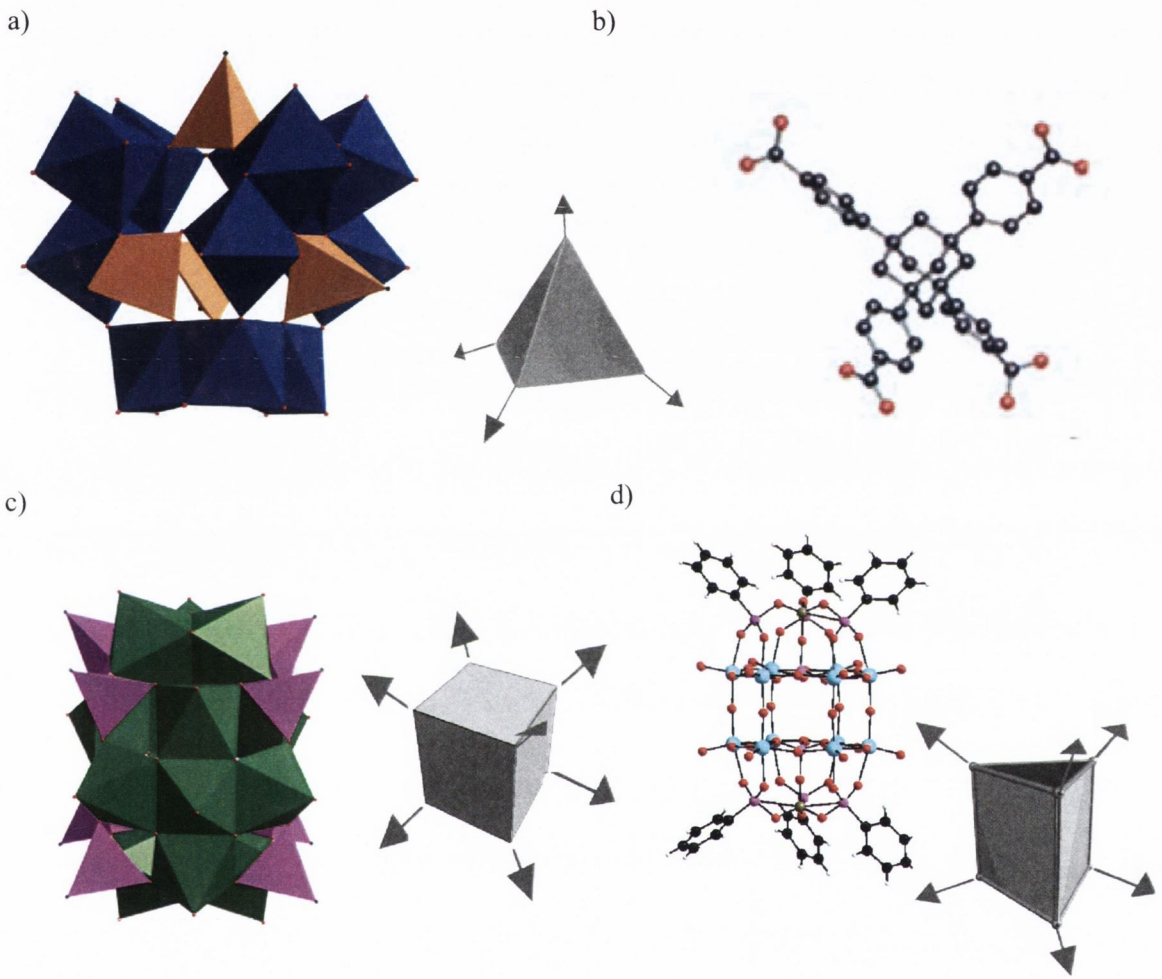

Figure 1.14 – Potential polyoxometalate building blocks. (a) The functionalised polymolybdate $[Mo_{12}O_{43}(O_3AsC_6H_4COOH)_4]^{4-}$ representing a tetrahedral secondary building unit (SBU) [51] could be compared to the already established tetrahedral SBUs. (b) An example of an organic tetrahedral SBU, adamantine-1,3,5,7-tetracarboxylate.[52] (c - d) The proposed functionalisation of the previously synthesised polyoxovanadate $[Cl_2V_{14}O_{22}(OH)_4(H_2O)(O_3PPH)_8]^{6-}$ cluster and polyoxomolybdate - $[Mo_5{}^{V}Mo_7{}^{VI}O_{30}(BPO_4)_2(O_3PPh)_6]^{5-}$ cluster[38] could lead to the potential isolation of new POM - MOFs. Topologies of the predicted SBUs have been highlighted in grey framework with arrows indicating the theoretical points of connectivity. Colour code: Mo cyan, V green, P purple, O red, C black, H white.

Following the combination of Stein's ideas and Yaghi's reticular synthesis concept, we could envisage an SBU approach that takes advantage of polyoxometalate clusters which are

stabilised by organic ligands and whose coordination sites point into distinct directions of space (see Fig. 1.14). One could expect that the assembly of these building blocks into networks preferentially results in a limited number of default topologies which are determined by the geometries of the SBUs used and which are often related to an inorganic structure type. The use of tetrahedral SBUs, for instance should preferentially result in networks related to the diamond, $SrAl^{2-}$ or $CaGa_2O^{4-}$ structure whilst the combination of tetrahedral and square planar SBUs could lead to an augmented PtS topology. The rigid ligands could be systemically extended resulting in further augmentation of a new topology. This reticular synthesis concept for functionalised polyoxometalates could yield compounds that exhibit unprecedented surface areas, are thermally stable and readily accommodate guests. The high surface area hybrid polyoxometalate frameworks would provide additional functionalities from the organic components within the highly ordered and amendable cavities that will allow for shape- and size-selectivity; characteristics that could be exploited for catalytic acid-base and redox processes.

1.5 Polyoxometalates as catalysts

Many industrially driven research activities aim to exploit polyoxometalates as acids and redox catalysts (Table 1.2).[53] The role of polyoxometalates as heterogeneous catalysts has previously been reviewed by Misono *et al.*,[54] and the role of polyoxometalates as a homogeneous catalyst has been reviewed by Hill *et al.*[55] Polyoxometalates, both solid and in solution, are amongst the strongest mineral acids often exhibiting acid strengths higher than those of H_2SO_4 and $HClO_4$. At present, about 180 important industrial processes use solid acids.

Examples of reactions in which polyoxometalates are applied as catalysts include dehydration of alcohols, cracking and alkylation of hydrocarbons and electrophilic addition of alcohols to olefins.[56] However, a significant number of acid-catalysed reactions, such as esterifications, hydrations, hydrolysis and Friedel-Crafts reactions still use conventional Lewis and Brønsted acids. These processes are typically associated with problems with respect to toxicity, corrosion, catalyst waste, or difficulty in separation and recovery of the catalysts. In particular, solid acids that operate at low temperature in aqueous solutions are for environmental reasons desirable materials for industrial applications.

Table 1.2 – Commercialised products that utilise polyoxometalates as catalysts[56]

Production	Scale (kt/n)	Year of introduction	Catalyst	Place
2-Propanol	50	1972	$H_4SiW_{12}O_{40}$	Tokuyama Soda
Methacrylic acid	220	1982	Mo-V-POM	Mitsubishi
Tert-butyl alcohol	5.6	1984	$H_3PMo_{12}O_{40}$	Asahi Kasei
Butyl ketone-2	40	1985	$H_3PMo_{12}O_{40}$	Dehigary
Poly(trimethylene carbonate)	40	1987	$H_3PW_{12}O_{40}$	Asahi Kasei
Acetic acid	2-3	1997	Pd(Te)-$SiW_{12}O_{40}$	Showa Denkn (Oita)
Ethyl acetate	10	1997	Pd(Te)-$SiW_{12}O_{40}$	Showa Denkn (Oita)
2,6-di-tert-butyl-*p*-methyl phenol	1-2	1996	$H_3PMo_{12}O_{40}$	Jilin, Liaoning, Hebei

In contrast to many solid acids which often lose their activities in aqueous solutions, polyoxometalates can show promising turnover numbers of reactions in which H_2O participates *i.e* esterification, transesterifications, hydrolyses and hydrations.[57] Polyoxometalates have received considerable attention as catalysts and precursors for oxide-based selective oxidations.[58] Research activities include the investigation of catalytic oxygen transfer reactions in heterogeneous and homogenous phases to provide alternatives to stoichiometric oxidations.[59, 60]

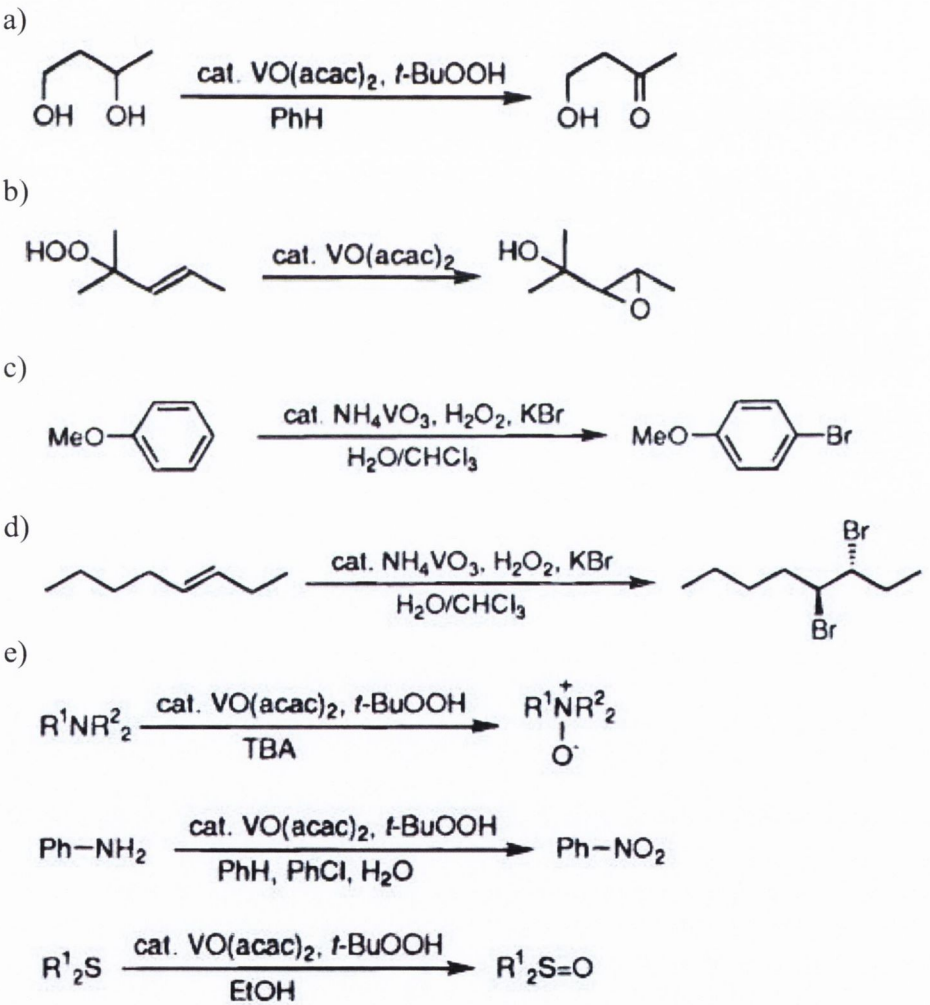

Figure 1.15 – Some examples of catalytic reactions utilising the $VO(acac)_2$ or NH_4VO_3:[57] (a) dehydrogenation, (b) oxygenation, (c) & (d) bromoperoxidase mimic (e) oxidation of heteroatoms.

Selective catalytic oxidation reactions are amongst the most important industrial processes.

Of particular interest are selective oxidations of aldehydes and alcohols, oxidative dehydrogenations of alkenes, selective epoxidations, ammoxidations or metathesis reactions of alkenes (Fig. 1.15).[56] Important prerequisites for applicable technologies are stable catalysts that minimise the waste product of the applied oxidant in combination with high product selectivity and reaction rates at ambient temperature.[60, 61]

1.6 Molecular entities – Supramolecular host-guest chemistry

The assembly of metal–ligand mediated molecular capsules comprises one of the most vibrant areas of chemistry. A key issue for the formation of such metallosupramolecular entities is the identification of pre-organised, kinetically stable building blocks that provide ligand-accessible coordination sites to direct assembly into the desired molecules.

Depending on their dimension and composition, the cavities in molecular capsules can provide unique chemical environments serving, for instance, as reaction vessels or supramolecular containers. There are many examples in which polyoxometalate clusters can be identified as supramolecular cages/hosts for guest compounds. Müller *et al.* has established a wide base of research on large polyoxometalates cluster cages that can capture, retain and release guest molecules.[62] An example of a supramolecular host-guest interaction within a polyoxometalate is provided by the inclusion of a rather large zinc porphyrin guest within a $\{Mo_{176}\}$ ring cavity which was demonstrated by Aida *et al.* (Fig. 1.16a).[63]

The first soluble oxide inclusion compound, $[(C_6H_5)_4P]_4[CH_3CN{\subset}V_{12}O_{32}]\cdot 3CH_3CN\cdot 4H_2O$, was reported by Yaghi *et al.* in 1989 (Fig. 1.16b).[64] This polyoxovanadate cluster contains a weakly coordinating acetonitrile solvent molecule. The N donor of the acetonitrile molecule forms only weak bonds to the vanadium ions in the cluster in the range of 3.238 Å to 3.747 Å. However, upon dissolving the compound in acetonitrile, the acetonitrile guests remain

largely associated with the polyoxovanadate host as confirmed by NMR experiments. The methyl ^{1}H NMR signals of the bound acetonitrile molecules are shifted downfield (δ = 2.38 ppm) compared to the solvent acetonitrile molecules (δ = 2.08 ppm). These host-guest interactions were subsequently theoretically modelled by Bénard *et al.* who confirmed that the permanent dipole moment on the acetonitrile molecules interacts with an opposite dipolar field generated inside the cavity resulting in an interaction energy of -14.4 kcal·mol^{-1}.[65]

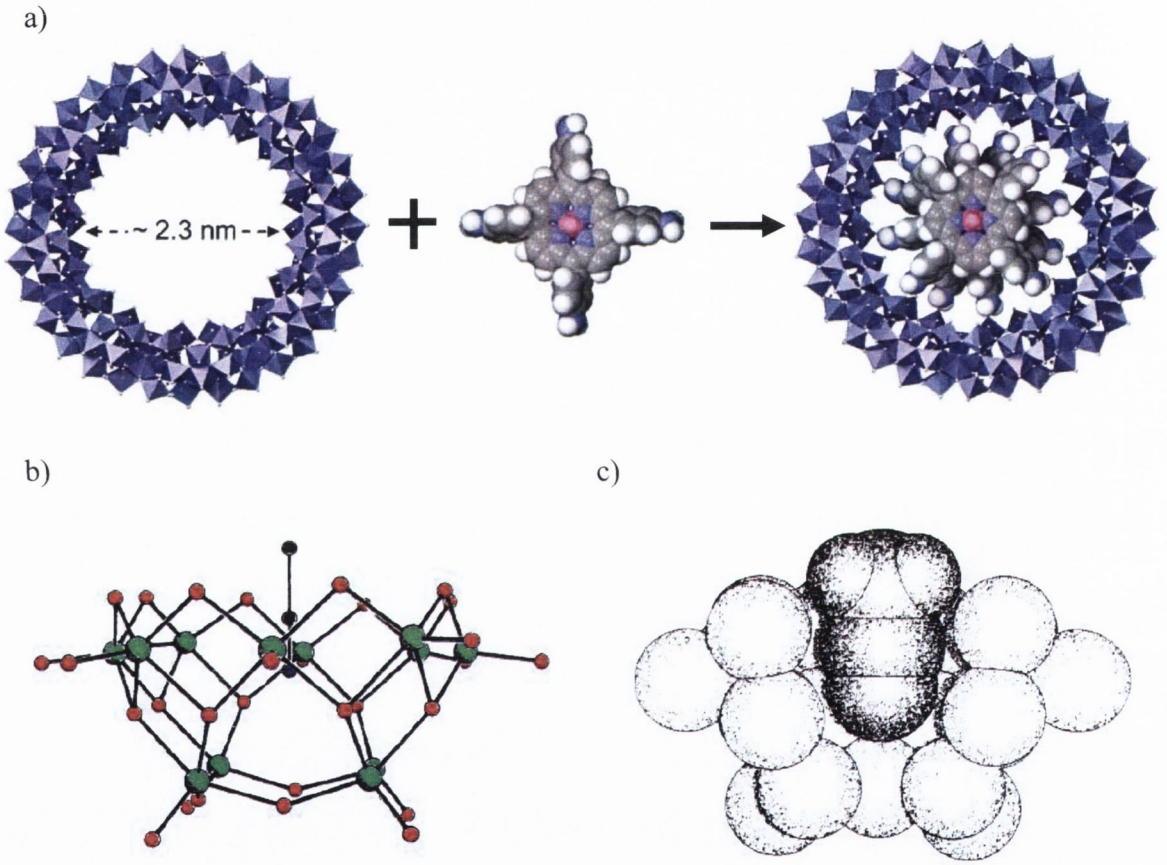

Figure 1.16 – (a) Schematic representation of the incorporation of zinc 5,10,15,20-tetrakis(4-aminophenyl)porphyrin within the cavity of a {Mo_{176}} wheel-type cluster (polyhedral representation)(Zn: pink, N: blue, C: grey, H: white).[63] (b) Perspective plot of the non-hydrogen atoms for the $[CH_3CN{\subset}V_{12}O_{32}]^{4-}$ anion as observed in $[(C_6H_5)_4P]_4[CH_3CN{\subset}V_{12}O_{32}]\cdot 3CH_3CN\cdot 4H_2O$.[64] Colour code: V green, O red, N blue and C black. (c) A space filling representation highlighting the host-guest interaction between the weakly coordinating acetonitrile molecules and the $[V_{12}O_{32}]^{4-}$ host.

A more recent theoretical study by Su *et al.* in 2010 underlines that the incorporation of different guest anions, *e.g.* Cl^-, Br^-, I^-, NO_3^- within the bowl shaped hybrid polyoxovanadate cluster, $[V_5O_9(O_2CPh)_4]^{2-}$ (Fig. 1.9c), can influence its redox properties. The study

demonstrated that generally host-guest interactions afford the redox potentials of the involved V atoms to shift to negative values when compared to the V redox potentials of the isolated hosts. Thus the shift in redox potentials could be exploited for ion recognition.[66]

1.7 Magnetic properties of polyoxometalates

Following the establishment by Müller *et al.* that giant polyoxometalates clusters could be synthesised, a substantial effort was undertaken to understand the magnetic attributes of these clusters and develop new related giant molecular clusters with advantageous magnetic properties.

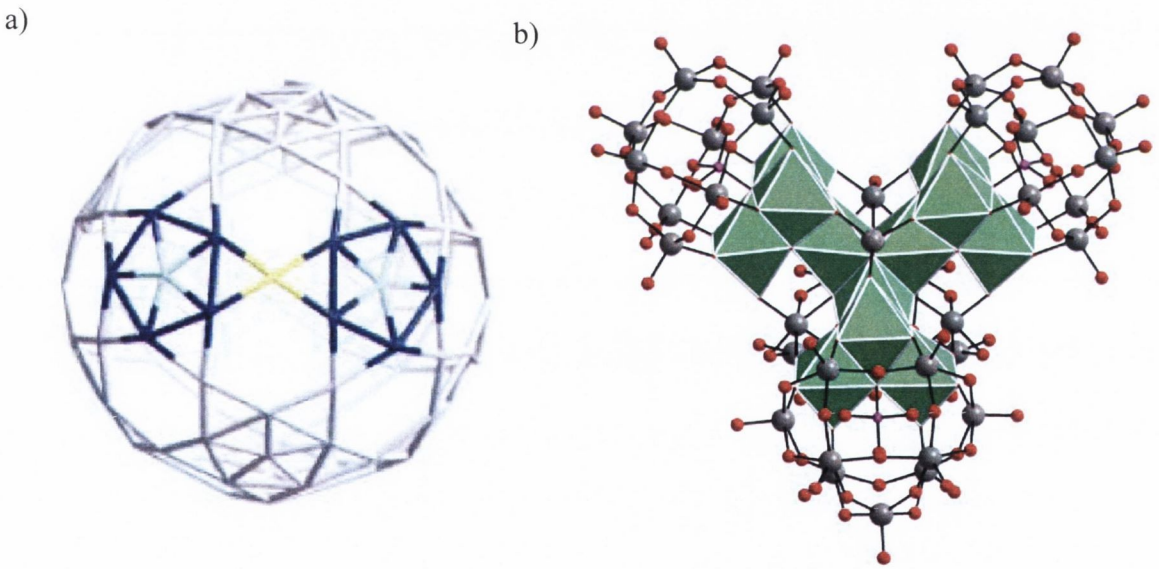

Figure 1.17 – (a) A wire frame representation of the $\{Mo_{72}Fe_{30}\}$ polyoxometalate cluster highlighting the Fe^{III} magnetic centres (yellow) which are isolated and connected the molybdate sub-units (blue).[67,69] (b) A $\{Ni_{12}\}$ cluster stabilised by three polyoxotungstate ligands to give the anionic $[Ni_{12}(OH)_9\text{-}WO_4(W_7O_{26}(OH))(PW_9O_{34})_3]^{25-}$ cluster.[70] Colour code: W grey, Mo blue, Fe yellow, Ni green, O red.

A review by Gatteschi *et al.* summarises the commonly observed magnetic characteristics in these giant polyoxometalate clusters.[67] There have been several investigations into the incorporation of paramagnetic centres into polyoxometalate clusters in order to synthesise

tailor-made magnets. For instance, 30 iron(III) metal centres were incorporated into a large polyoxometalate clusters resulting in a compound with the formula $[Mo_{72}Fe_{30}(Mo_2O_7(H_2O))_2(Mo_2O_8H_2(H_2O))\text{-}(CH_3COO)_{12}(H_2O)_{91}]\cdot 150H_2O$ (Fig. 1.17a).[68] The iron ions are embedded within the diamagnetic polyoxomolybdate framework of the molecule and are approximately equally spaced apart (*ca.* 6.4 Å). There is a general anti-ferromagnetic exchange interaction between the iron centres between 300 and 30 K. At low temperature (65 mK), the iron centres within these polyoxomolybdate clusters experience spin frustration and a low energy magnetic excitation spectrum was recorded using low temperature inelastic neutron scattering studies to confirm this behaviour.[69]

However, tailor-made magnets require a high degree of control over the size of the cluster, the arrangement of the magnetic centres, the spin topology and the magnetic anisotropy, all of which is still difficult to achieve. A feature of polyoxometalates is that they are used as ligands to stabilise transition metal clusters in which the metal centres are strongly magnetically coupled. An example of such a system includes the stabilisation of a $\{Ni_{12}\}$ cluster (Fig. 1.17b) by three magnetically silent polyoxotungstate ligands, $[Ni_{12}(OH)_9WO_4(W_7O_{26}(OH))(PW_9O_{34})_3]^{25-}$.[70] Magnetic investigation of this compound indicates the presence of dominantly ferromagnetic interactions within the $\{Ni_{12}\}$ core. The χT product reaches a maximum of 23.2 cm^3 K mol^{-1} at 8.0 K. The magnetic interactions between the Ni(II) metal centres could not be modelled due to the low symmetry of the cluster and the large amount of different intra-complex magnetic interactions.

Polyoxovanadates represent an important sub-class of magnetic polyoxometalates. Magnetic polyoxovanadates contain predominantly V(IV) metal centres. The oxovanadium(IV) subunits within these clusters commonly occur as O-bridged dimers and exhibit strong anti-ferromagnetic interactions between the metal centres. Several large polyoxovanadate clusters such as $[V^{IV}_{15}As_6O_{42}(H_2O)]^{6-}$ and $[V^{IV}_{18}O_{42}]^{12-}$ have received attention in literature due to

their interesting magnetic properties.[71, 72] The anionic cluster $[V^{IV}_{15}As_6O_{42}(H_2O)]^{6-}$(Fig. 1.18) contains fifteen paramagnetic vanadium atoms which are organised into three distinct layers. The spin centres within the two hexagon units are anti-ferromagnetically coupled. They represent anti-ferromagnetic layers that sandwich a spin frustrated triangular unit (Fig. 1.18b). It should be noted that the spins within the triangle are weakly coupled to those in the hexagonal units. This $\{V_{15}\}$ cluster can be considered as a simple model of a magnetic multilayer structure.[73]

Müller *et al.* and Plass *et al.* have correlated some structural features of the often occurring oxovanadium dimers to the observed magnetic behaviour.[72, 74] Nevertheless, a detailed magneto-structural correlation is yet to be reported. However, it is apparent that both the metal-metal distance and the angle at the bridging oxygen atom play an important role.[75]

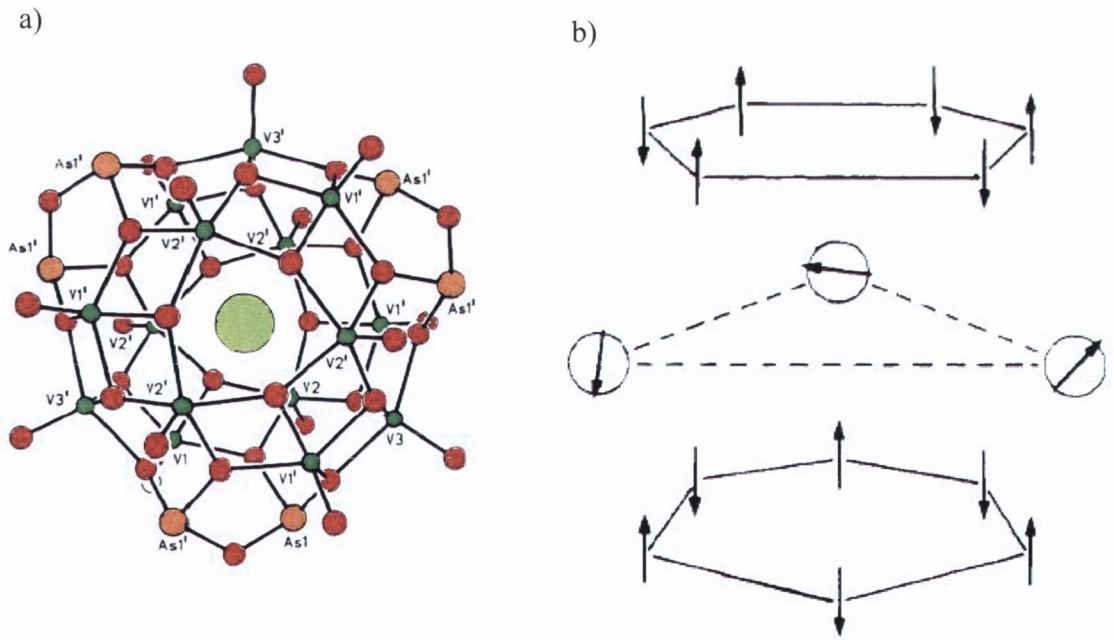

Figure 1.18 – (a) A ball and stick representation of the anionic cluster within $K_5[V^{IV}_{15}As_6O_{42}(H_2O)]\cdot 8H_2O$ - $\{V_{15}\}$.[73] (b) A pictorial representation of the preferred spin orientations on the magnetic planes of $\{V_{15}\}$. Colour code: V dark green, Cl light green, As orange,

Recently, Winpenny *et al.* have investigated the synthesis of V^{III} and V^{IV} phosphonate-stabilised clusters to further develop synthetic approaches or single-molecule magnets.[76]

Christou *et al.* have reported a tetranuclear vanadium(III) complex, $[V_4O_2(O_2CPh)_7(bpy)_2](ClO_4)$, which displays single molecular magnetic characteristics.[77] This compound stabilises an S = 3 ground state and the compound has an anisotropy parameter of D = -1.5 cm^{-1} which confirms that this compound can be classified as a single molecule magnet.

1.8 Medicinal properties of polyoxometalates

Comprehensive accounts on the anti-tumour, anti-viral and anti-bacterial activities of polyoxometalates have been reported by Yamase[78] and Hasenknopf.[79] The significant therapeutically activity of polyoxometalates was first noticed in the 1970s with the discovery that $[SiW_{12}O_{40}]^{4-}$, $[Na(SbW_7O_{24})_3(SbO_7)_2]^{18-}$ and $[(AsW_9O_{33})_4(WO_2)_4]^{28-}$ exhibit activity against various non-retro RNA and DNA viruses *in vitro* and *in vivo*. These polyoxometalates also inhibit RNA-dependent DNA polymerases of retroviruses and show some antiviral activity against the human immunodeficiency virus (HIV). Although these compounds were further tested in two independent human clinical trials, these clusters were found to be too toxic.

Many different roles have been established for vanadium compounds in biological systems but they do not have a significant role in human physiology. In human biochemistry in particular, Evangelou has reviewed the role of vanadium compounds in the treatment of cancer.[80] Vanadium compounds are known to cause DNA cleavage, activation of xenobiotic enzymes, *in vivo* production of free radicals, inhibition of protein tyrosine phosphatases and/or the activation of protein tyrosine kinases. Oxovanadium(IV) and oxovanadium(V) compounds have been shown to have potency as an inhibitor of phosphoryl transfer enzymes. These enzymes transfer phosphate groups from phosphorylated tyrosine residues on proteins

within the body. Additionally, simple oxovanadates have demonstrated promising results as a new potential treatment drug for *diabetes mellitus* in humans.[81] As previously discussed, these compounds show catalytic activity in oxidation and oxygen transfer reactions (see section 1.5) and a similar effect is found for oxovanadium compounds in biological studies. The mechanism through which vanadate compounds act have been extensively investigated[82] but the full mode of action is still not fully understood. It has also been shown that sodium vanadate(V) induces reactive oxygen species in pulmonary lung tissue leading to the transactivation of protein 53 (p53).[83] P53 is a transcription factor that regulates the cell cycle and hence functions as a tumour suppressor. Vanadyl(IV) sulphate was reported to differentially damage DNA in human lymphocytes and HeLa cells.[84] It should be noted that the genotoxicity of the vanadate was increased with the presence of vitamin C. Vitamin C is known for its antioxidative properties and it has been proposed that the vitamin could be interacting with the vanadyl salts and contribute to the oxidative damage to DNA through the production of hydroxyl and lipid alkoxyl radicals.[84] It has also been shown that vanadate salts have a biphasic effect on DNA synthesis. At low concentration, vanadate compounds promote proliferation and differentiation of the cells while at high concentrations, the opposite effect is observed and cell colony formation is inhibited. Finally, vanadate compounds have been found to have a time-dependant response. Short term exposure to vanadate compounds (1-2 days) has lead to an increase in cell numbers while longer exposure to 50μM of vanadate has lead to massive apoptosis of mammary epithelial cells.[84] Sodium vanadate(V) and vanadium(IV) sulphate have been tested in human clinical trials. It was reported that these compounds were well tolerated by patients and that side effects were uncommon, with any such reported side effects primarily related to anomalies in the gastrointestinal tract.[84] The application and potential use of polyoxovanadates and other

vanadium containing compounds has yet to be fully researched for their viability as effective drugs.

1.9 Present study

Early transition metal ions polarise terminal O^{2-} ligands efficiently often resulting in purely 'inorganic' polyoxometalate clusters as described in previous sections of this introduction. Many advanced developments of polyoxometalate containing materials are hindered by the limited availability of functionalised polyoxometalates that contain organic molecules directly incorporated into the cluster shell. Organic ligands with tetrahedral binding sites which display geometrical and electronic similarities to metal-oxygen units in polyoxometalates appear to be good candidates for functionalisation purposes. Organic phosphonates and arsonates fulfil these criteria and our research aims to investigate how these can be rationally exploited to create functionalised polyoxovanadates. One objective is the synthesis and isolation of novel ligand stabilised polyoxovanadate capsular entities incorporating organoarsonate or organophosphonate ligands.

The synthesis of hybrid polyoxovanadate clusters with rigid organophosphonate and organoarsonate ligands that point in defined directions of space might link the clusters into open frameworks that are highly desired for catalysis, gas sorption and separation studies.

In order to produce these hybrid materials, we propose to synthesise a variety of organoarsonate and organophosphonate ligands as well as obtain commercially available organoarsonate ligands. As a short term objective, we intend to investigate the ligands shown in Fig. 1.19 under reducing conditions in the presence of vanadate salts in an aqueous containing solution. Our chosen synthetic approach will involve the partial reduction of vanadate(V) salts in the presence of these organic ligands using appropriate reducing agents.

The synthesis of novel functionalised clusters will be dependent on the careful control of the ligand:metal ratio, the amount and nature of reducing agent used, the template effect of any anionic species present in solution as well as the pH of the reaction mixture.

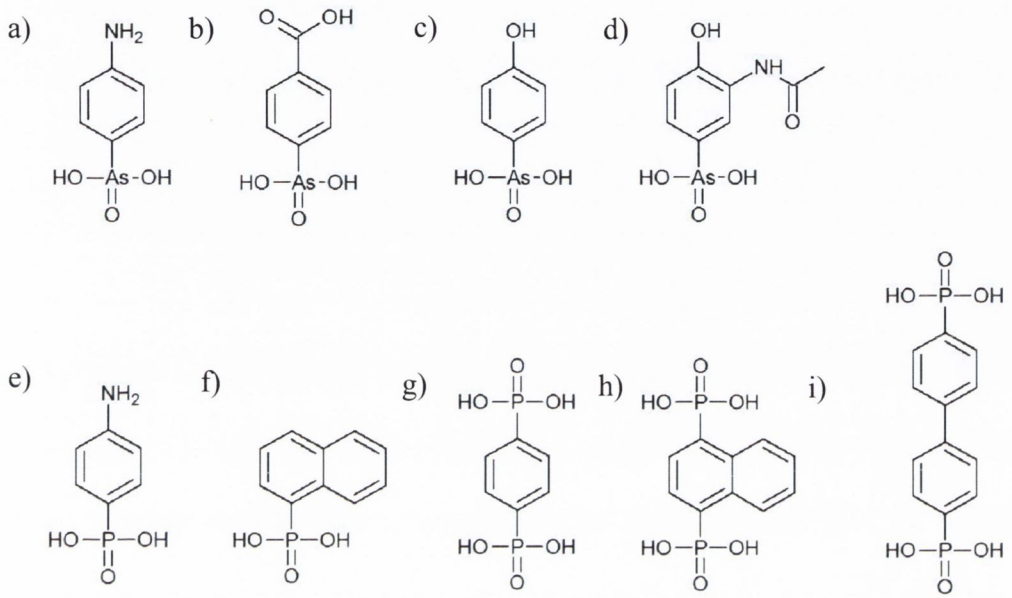

Figure 1.19 – Proposed functionalising organoarsonate and organophosphonate ligands. The organoarsonate ligands can be synthesised by the Bart reaction and the organophosphonate ligands can be synthesised by the modified Michaelis-Arbusov reaction. (a) (4-aminophenyl)arsonic acid (*p*-arsanilic acid), (b) (4-carboxyphenyl)arsonic acid (4-arsonobenzoic acid), (c) (4-hydroxyphenyl)arsonic acid, (d) (3-acetamido-4-hydroxyphenyl)arsonic acid (acetarsone), (e) (4-aminophenyl)phosphonic acid, (f) (1-naphthalene)phosphonic acid, (g) (1,4-benzene)bisphosphonic acid, (h) (1,4-naphthalene)bisphosphonic acid and (i) ([1,1'-biphenyl]-4,4'-diyl)bisphosphonic acid.

In order to accomplish our objectives, we initially set out to obtain the following:

- To synthesise aromatic arsonate and phosphonate ligands
- To investigate the synthesis of novel organoarsonate and organophosphonate stabilised polyoxovanadate clusters
- To augment or enlarge any novel hybrid clusters in order to increase the enclosed cavity

- To use the functionalising ligands to control the self-assembly of the clusters into open framework structures

- To structurally characterise all novel compounds through single crystal X-ray diffraction

- To characterise the physical properties and other attributes of the materials

- To monitor the formation of these compounds *via* spectroscopic methods and investigate the stability of these compounds in solution

Long term objectives:

- To understand the structure directing influences of the functionalised clusters so that the ligands can be used either in an intra-molecular connectivity mode to construct capsular entities or an inter-molecular connectivity mode between clusters in an iso-recticular approach to synthesising new materials

- To investigate the magnetic properties of the relevant compounds with particular emphasis on the magneto structural correlation of different types of polyoxovanadates stabilised by organic moieties

Chapter Two

Pentanuclear aryl arsonate functionalised vanadium complexes

2.1 Introduction

The functionalisation of polyoxovanadates using group 5 elements has seen a wide range of compounds being discovered. Resulting purely inorganic heteropolyoxovanadates that incorporate arsenate and arsenite ions display a diversity of structure types which nowadays are being increasingly used as starting materials in hydrothermal synthesis in order to construct 3-D networks.[28] However, there are a limited number of polyoxovanadate clusters reported which are stabilised by organoarsonates.[46,47] New functionalisation approaches and careful control of the assembly process can give rise to the formation of new compounds which might result in the discovery of new MOFs, cages, hybrid capsules or other supramolecular compounds.

In this chapter, we describe the isolation of novel mixed-valent pentanuclear polyoxovanadates stabilised by aromatic organoarsonate ligands. We demonstrate that the nature and stability of the mixed-valent pentanuclear core structure which is present in all of the isolated compounds, tolerates the incorporation of aromatic organoarsonate ligands with a variety of *para* positioned secondary functional groups. These secondary functional groups direct the assembly of the packing arrangement of the complexes in the crystal structure.

2.1.1 Aromatic arsonate ligands

Aromatic arsonic acid ligands with varying functional groups in the *para* position to the arsonic acid groups were used to prepare a series of functionalised clusters. (3-acetamido-4-hydroxyphenyl)arsonic acid (acetarsone), (4-hydroxyphenyl)arsonic acid and (4-aminophenyl)arsonic acid (*p*-arsanilic acid) are commercially available. (4-carboxylphenyl)arsonic acid (4-arsonobenzoic acid) was prepared by the Bart reaction

according a literature procedure.[85] The Bart reaction involves the addition of an aqueous alkaline solution of sodium arsenate to the diazonium salt of the pre-requisite amine (Fig. 2.1). The reaction requires a copper(II) catalyst and gives the maximum yield when buffered with sodium carbonate. Historically, the first method for preparing aromatic arsonates was the Bechamp reaction which involves heating aromatic amines, phenols or phenyl ethers with arsonic acid under reflux for several hours.[85, 86] However, the yield for this reaction is usually quite poor (< 25%).

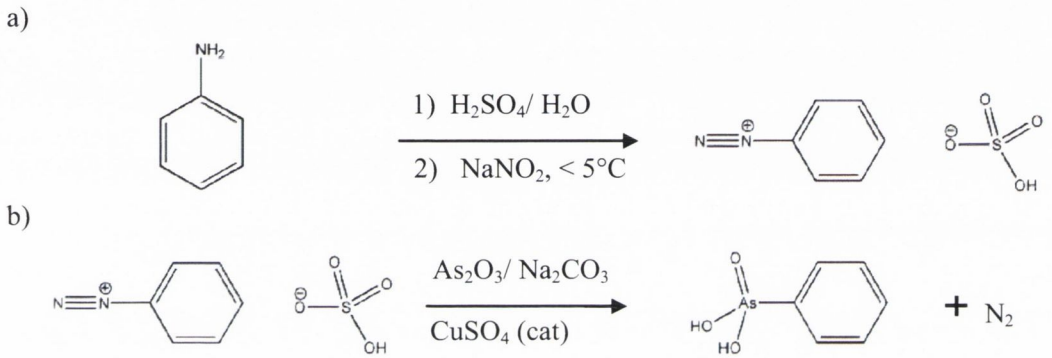

Figure 2.1 – A general reaction schematic of the Bart reaction.[85] (a) Initially the diazonium salt is prepared when the sodium nitrite is added to the acidified amine at 5°C. This freshly prepared diazonium salt is then added with stirring to the alkaline arsonate solution. (b) Nitrogen gas evolves upon formation of the product. Sodium sulphate and carbon dioxide are also produced as by-products of this particular reaction.

Aryl arsonates have a reasonable thermal stability and are expected to be stable in the presence of air, moisture or heat under normal synthetic conditions. This is an important factor when considering organoarsonate ligands as appropriate starting materials for coordination complexes including supramolecular cage structures and MOFs. Differential Thermal Analysis (DTA) in air results generally reveal exothermic decomposition processes above 300 °C where aryl arsonates undergo oxidative degradation.[85] This decomposition temperature, which is common to other aromatic classes of ligands will limit the thermal

stability of any product and might limit applications in certain areas, e.g. heterogeneous catalysis.

2.2 Synthesis of a mixed-valent vanadium(V^{IV}/V^{V}) pentanuclear complex incorporating (4-aminophenyl)arsonic acid

2.2.1 The synthesis of $Na_5[V_5O_9(O_3AsC_6H_4\text{-}4\text{-}NH_2)_4]\cdot 20.5H_2O\cdot 3DMF$ (1)

Compound **1**, $Na_5[V_5O_9(O_3AsC_6H_4\text{-}4\text{-}NH_2)_4]\cdot 20.5H_2O\cdot 3DMF$ is the product of the self-assembly of (4-aminophenyl)arsonic acid, sodium azide and sodium metavanadate under partially reducing conditions in a water/DMF solution. Sodium azide is thought to act as a templating agent as discussed in the chapter 1, 1.2.2. The self-assembly process is initiated with the addition of the reducing agent, hydrazine hydrate, at neutral pH which instigates a colour change from bright yellow to a dark green solution and an accompanying increase in pH. The pH of the solution was monitored and was re-adjusted to a neutral pH with hydrochloric acid after the addition of the reducing agent. Green plate-shaped crystals of **1** formed from the reaction mixture after two days. The resulting crystals were characterised by single crystal X-ray diffraction, CHN analysis, thermogravimetric analysis (TGA), infrared spectroscopy (IR), ultraviolet-visible (UV-vis) spectroscopy and mass spectrometry.

2.2.2 Solid state characterisation: The structural characterisation of $Na_5[V_5O_9(O_3AsC_6H_4\text{-}4\text{-}NH_2)_4]\cdot 20.5H_2O\cdot 3DMF$ (1)

The cluster crystallises in the triclinic space group, *P*-1. The polyoxovanadate core in **1** consists of five vanadium atoms that are surrounded by O-donors in a square pyramidal

coordination mode (Fig. 2.2). The base of the central pyramid shares common edges with its four surrounding $\{V^{IV}O_5\}$ polyhedra to give the typical convex mixed-valent $\{V^{V}O(\mu_3\text{-}O)_4V^{IV}{}_4O_{12}\}$ unit.

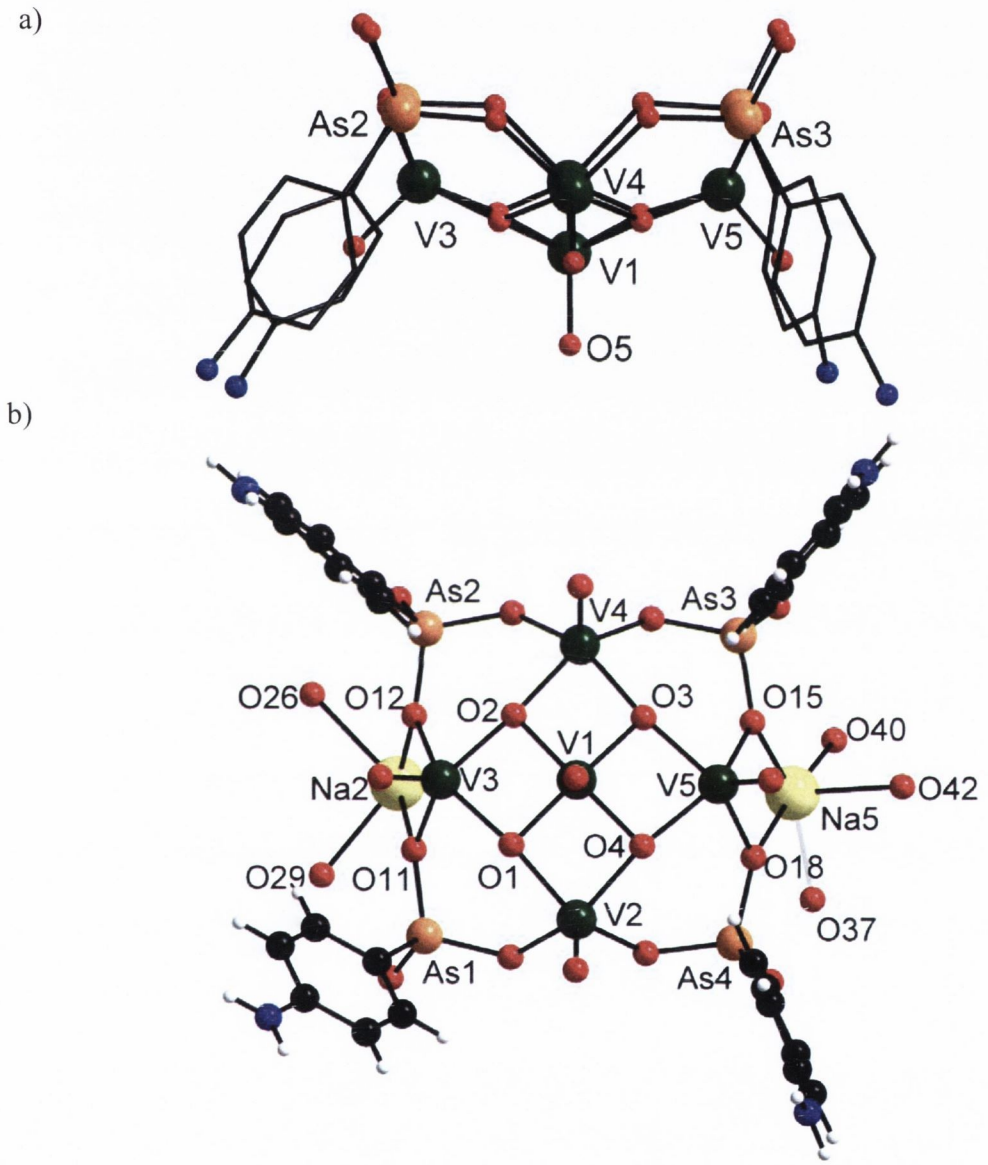

Figure 2.2 – (a) A ball and stick representation of the anionic $[V_5O_9(O_3AsC_6H_4\text{-}4\text{-}NH_2)_4]^{5-}$ cluster as viewed in the direction of the crystallographic *a*-axis. (b) A plan view of the anionic cluster with two coordinating sodium counter-ions which bind to the rim of the complex as viewed along the crystallographic *c*-axis. (Colour code: V green, As orange, Na yellow, O red, N blue, C black, H white.

The remaining two O donors in the base of each $\{V^{IV}O_5\}$ square pyramid are provided by

four (4-aminophenyl)arsonate ligands each bridging between two V atoms in an O,O'-*syn, syn* coordination mode.

The V-O bond lengths are indicative of the oxidation state of the V centres. Using bond valence sum analysis (BVSA – see appendix 1), the oxidation state of V(1) was calculated to be oxidation state +V (Table 2.1). The bond lengths between V(1) and the μ_3-O^{2-} ligands O(1), O(2), O(3), O(4) vary between 1.871(2) – 1.879(2) Å and the terminal V(1)=O_{term} bond is 1.602(1) Å long. The peripheral vanadium ions V(2), V(3), V(4) and V(5) are calculated to be in oxidation state +IV (Table 2.1) which correlates to a lengthening of the bond distances of these metal centres to the μ_3-O^{2-} oxygen donors. These V-O distances range between 1.952(2) – 1.973(2) Å. The bond distances between these V centres and the ligand O donors of the organic ligands vary between 1.956(2) – 1.976(3) Å whilst all terminal V=O bond distances are almost identical and vary between 1.601(2) – 1.606(2) Å.

Table 2.1 – Bond sum valence analysis for **1**

V & O sites	Bond Valence Sum (BVS)	Assigned Oxidation State
V(1)	5.019	+5
V(2)	4.125	+4
V(3)	4.064	+4
V(4)	4.067	+4
V(5)	4.101	+4
μ_3-O (1) (2) (3) (4)	2.031-2.092	-2
μ-O (9) (11) (12) (13) (15) (16) (18) (19)	1.761-1.842	-2
$O_{terminal}$ (5)(6)(7)(8)(32)	1.618-1.722	-2

The polyoxovanadate cluster carries an overall charge of –5 which is compensated by five sodium counter-ions. All of these counter-ions are partially hydrated and display highly distorted octahedral coordination spheres.

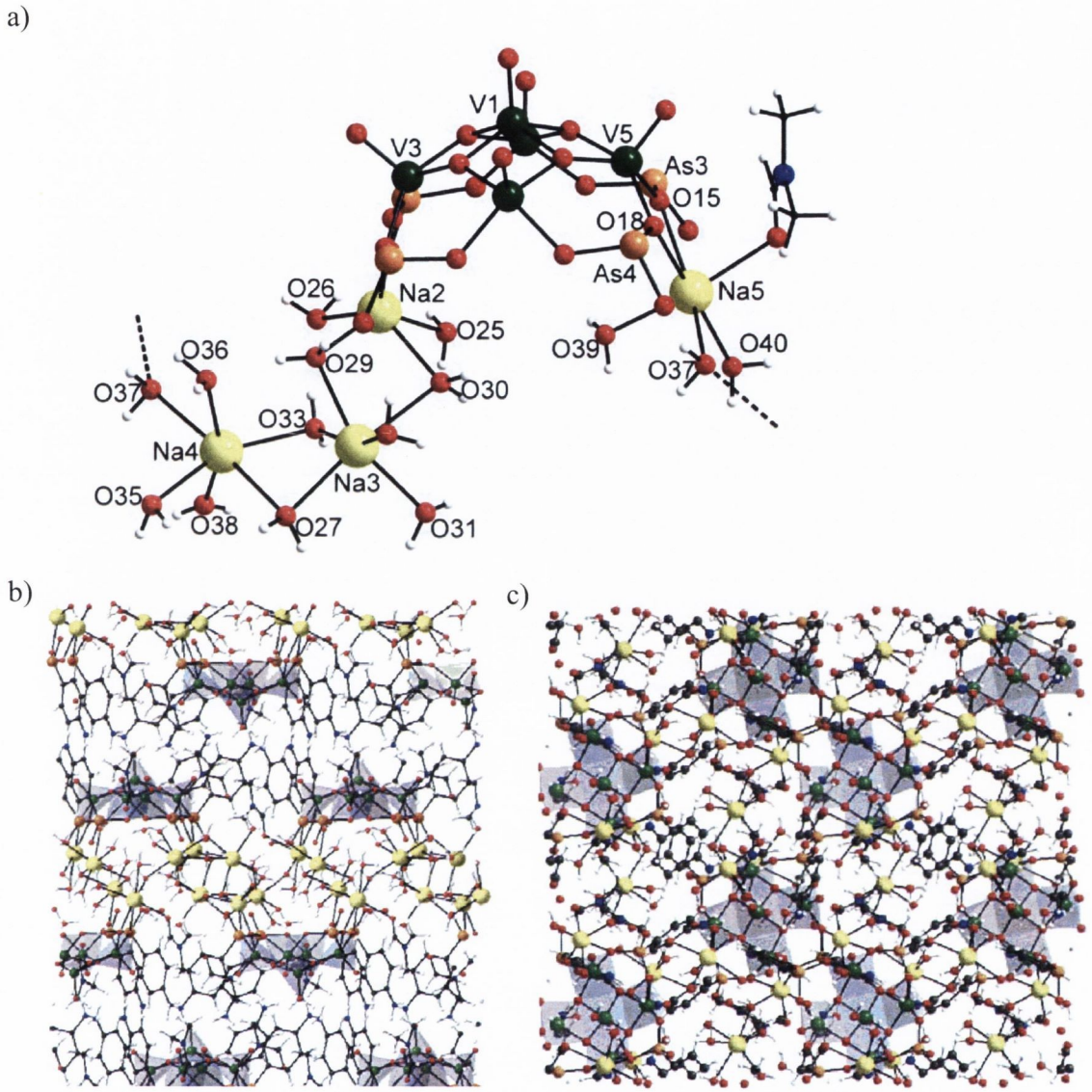

Figure 2.3 – (a) The anionic cluster core with four of the charge balancing sodium ions. The fifth isolated solvated sodium ion, the aromatic rings and the non-bridging oxygen of the arsonate ligand have been removed for clarity. The dashed line represents the polymeric structure involving sodium ions. (b) The packing diagram of **1** with a view in the direction of the crystallographic *a*-axis. (c) A polyhedral representation of the mixed-valent pentanuclear units as viewed in the direction of the crystallographic *c*-axis; the vanadium pentanuclear core are represent by vanadium polyhedra. Colour code: V green, Na yellow, As orange, O red, N blue, C black, H white.

Two of these sodium counter-ions, Na(2) and Na(5) coordinate to opposite sides of the rim of the complex through the arsonate donor atoms O(11), O(12), O(15) and O(18) (Fig. 2.2b). These arsonate functionalities provide bi-dentate binding sites for the sodium ions. Na(2) further connects through two H_2O molecules to Na(3) which itself links to Na(4) through two further H_2O molecules. The resulting distorted octahedra share common edges. Na(5), whose

coordination sphere comprises of a DMF molecule binds through a bridging H_2O molecule to Na(4) and symmetry equivalents (Fig. 2.3a). This bridging motif results in a 1-D chain structure of sodium ions that connect the vanadium complexes and these chains are aligned parallel to crystallographic *a*-axis. An additional sodium Na(1) counter-ion is fully hydrated and is disordered over two positions. It is not connected to the 1-D chain assembly. Within the crystal structure, the solvated sodium ions link the clusters forming areas with demarked hydrophilic boundaries (Fig. 2.3b). The sodium counter-ions are located in the *ab* plane of the crystal structure as shown in Fig. 2.3c. The intermolecular distances of the N atoms of the amine groups to the terminal V=O oxygen atoms range between 3.125(2) to 3.292(4) Å and are in agreement with weak H-bonds.[87]

2.2.3 Further solid state characterisation of 1: Thermogravimetric analysis and Infrared spectroscopy

- Infrared spectroscopy

Before the crystal structure of **1** was determined by X-ray diffraction, the compound was characterised by infrared spectroscopy (Fig. 2.4). To identify new compounds, infrared spectroscopy proved to be a powerful tool in distinguishing unfunctionalised purely inorganic polyoxovanadate clusters from functionalised clusters. The preparation method for **1** was found to be sensitive to the pH range in which the reaction was carried out. A subtle difference in the pH can lead to the formation of the $[V_{18}O_{42}]^{9-}$ cluster which has previously been reported in the literature.[72]

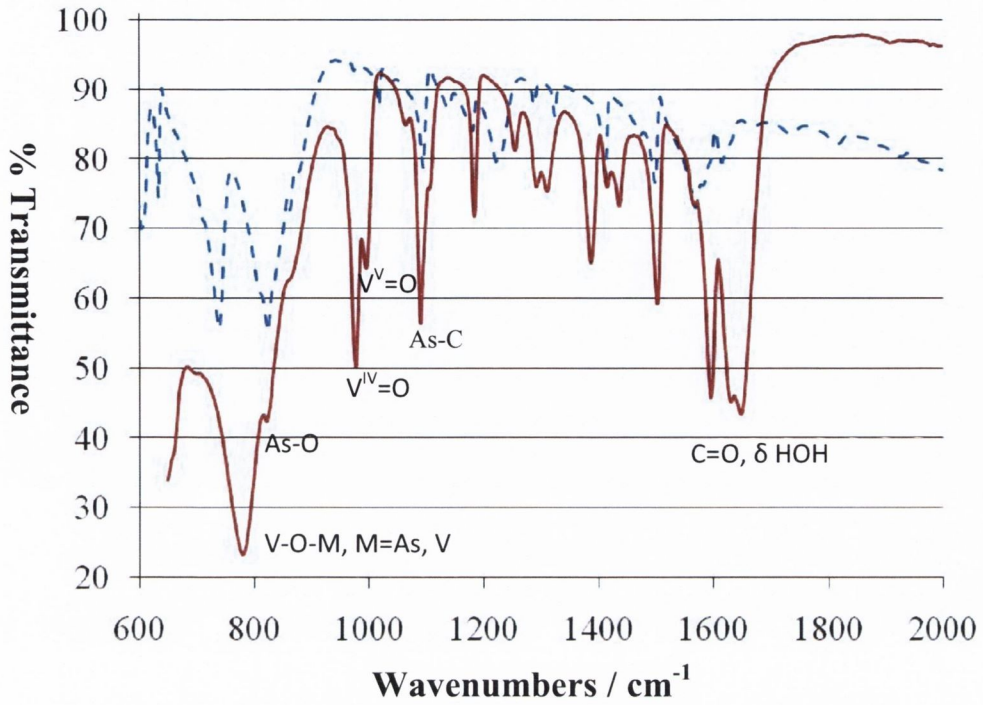

Figure 2.4 –Infrared spectroscopy of **1** (red solid line) compared with the (4-aminophenyl)arsonic ligand (blue dashed line); a complete IR spectrum of **1** can found in the appendix 2.

Observation of characteristic ligand stretches allowed us to identify the functionalised product. Such characteristic stretches of the organoarsonate ligands include signals at 1090 cm^{-1} (m, ν, As-C) and 824 cm^{-1} (s, ν, As-O).[46, 47] Other stretches that were observed appear at 1650 cm^{-1}, 1630 cm^{-1} (s, ν, C=O {DMF}; δ, HOH {H_2O}), 1504 cm^{-1} (m, ν, C=C), 1313 cm^{-1} (w-m, ν, C-N) and 782 cm^{-1} (s, ν, V-O-V/V-O-As). Stretches relating to (ν NH_2) and (ν_{as} NH_2) of the aromatic ligand were not located as they were predicted to reside in the same region as the strong O-H stretches due to water molecules of crystallisation. Stretches for V=O terminal oxygen bonds appeared for **1** at 998 cm^{-1} and 977 cm^{-1} respectively and correspond with those reported in literature for similar compounds.[88, 89]

-Thermogravimetric analysis

The stability of freshly prepared crystals of **1** was investigated by thermogravimetric analysis in a temperature range of 30 – 900°C in air (Fig. 2.5). A broad step between *ca.* 30 °C and

315 °C (17.7%) corresponds to the loss of constitution water and DMF solvent molecules. Total oxidation of the organic ligand starting at *ca.* 314 °C destroys the cluster in **1**. An oxidation at this temperature is in agreement with reported oxidative degradations of organoarsonate ligands.[85] A further thermogravimetric step between *ca.* 390 °C and 545 °C is expected to result in an oxide formation.

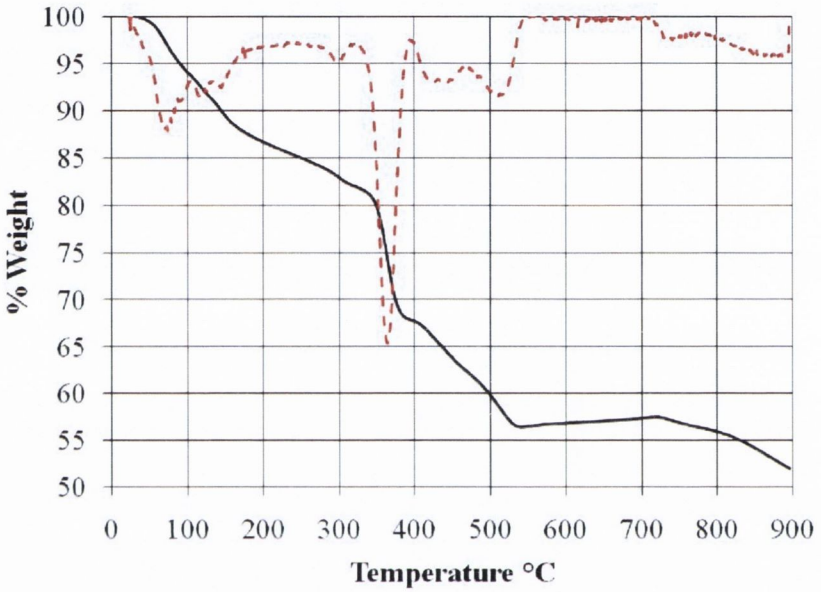

Figure 2.5 – The solid state characterisation of **1**: thermogravimetric analysis carried out under in air. The derivative of the TGA curve was calculated and the derivative curve is represented as a red dashed line.

2.2.4 Solution characterisation of 1: Mass spectrometry, NMR and UV-vis spectroscopy

-Mass spectrometry

Compound **1** was found to dissolve and be stable in polar solvents such as DMSO or DMF. A solution of **1** was prepared in DMSO and the sample was analysed using time of flight mass spectrometry in the negative mode (ES-MS). The mass spectrum recorded for **1** (see Fig. 2.6a and appendix 2) contains a wide spread of defragmentation peaks as well as peaks matching

to the molecular mass of the compound. A molecular weight signal m/z = 1262.4670 was modelled to correspond to the negatively ionised cluster in **1,** (appendix 2). The highest intensity peak measured corresponds to the arsonate ligand, which has a molecular mass of 216.9596 g mol^{-1} (M^-, m/z = 215.9632).

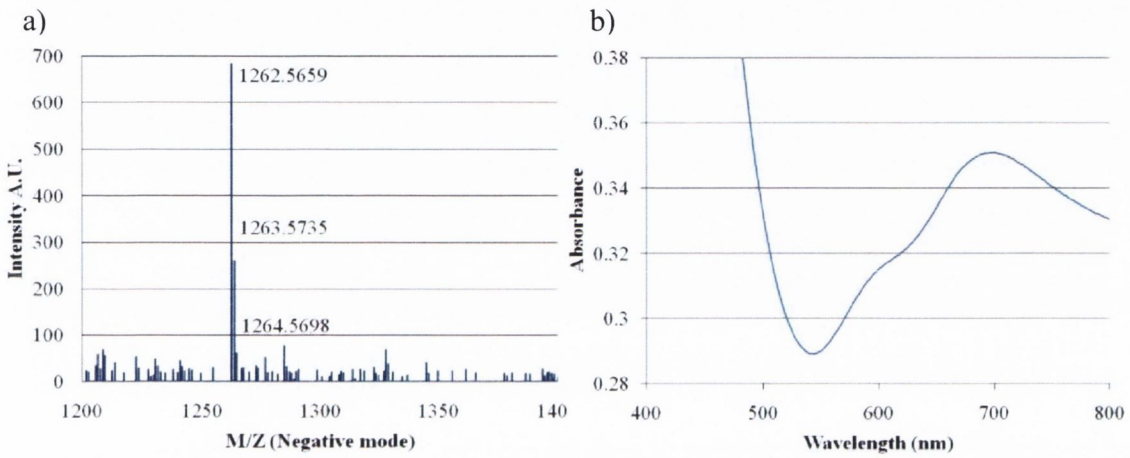

Figure 2.6 – The characterisation of **1** in solution. (a) Mass spectrum of **1** in DMSO utilising TOF-MS spectrometry. Complete mass spectra (see appendix 2). (b) The UV-vis spectrum of a 1 mM solution of **1** in DMSO.

-NMR

The spectrum of **1** in deuterated DMSO is in agreement with the crystallographically determined structure. However, **1** degrades within a few days, liberating free ligand. The spectrum for **1** exhibits resonance shifts at 9.99 ppm (br, 8H), 7.19 ppm (s, 8H) and 5.49 ppm (s, 8H) with an integration of the peaks corresponding to a 1:1:1 ratio (see appendix 2 for NMR spectrum of **1**). Two of the most upfield peaks were assigned to the protons on the aromatic rings of the ligand of the complex. The broad downfield peak was assigned to the protons of the amines. This broad downfield peak is also observed for the free ligand in DMSO. The broadening of the peaks in the NMR spectrum of **1** is a result of the paramagnetic vanadium(IV) ions.

-UV-vis spectroscopy

A solution of **1** was prepared in DMSO and the UV-vis spectrum was measured (Fig. 2.6b). An absorption at 395 nm is observed and is due to a intensive charge transfer in the near UV region ($\pi(O) - d(V)$). [46] A much weaker broad absorbance due to the d-d transitions is observed at 701 nm (ε = 577.3 $L.mol^{-1}cm^{-1}$) with a small shoulder at 600 nm (ε = 518.8 $L.mol^{-1}cm^{-1}$) due to an intervalence charge transfer.[38,42]

Table 2.2 – Crystal data and structure refinement for **1**.

Identification code	Compound **1**	
Empirical formula	$C_{33}\ H_{86}\ As_4\ N_7\ Na_5\ O_{44.50}\ V_5$	
Formula weight	1962.42 g mol^{-1}	
Temperature	150(2) K	
Wavelength	0.71073 Å	
Crystal system	Triclinic	
Space group	*P* -1	
Unit cell dimensions	a = 13.9310(16) Å	α = 82.657(2)°.
	b = 15.1369(17) Å	β = 78.338(2)°.
	c = 17.502(2) Å	γ = 88.612(2)°.
Volume	3584.8(7) $Å^3$	
Z	2	
Density (calculated)	1.818 Mg/m^3	
Absorption coefficient	2.593 mm^{-1}	
F(000)	1982	
Crystal size	0.1 x 0.1 x 0.2 mm^3	
Theta range for data collection	1.20 to 28.32°.	
Index ranges	-18<=h<=18, -20<=k<=20, -23<=l<=23	
Reflections collected	50501	
Independent reflections	17776 [R(int) = 0.0776]	
Completeness to theta = 28.32°	99.6 %	
Refinement method	Full-matrix least-squares on F^2	
Data / restraints / parameters	17776 / 57 / 1026	
Goodness-of-fit on F^2	0.807	
Final R indices [I>2sigma(I)]	R_1 = 0.0339, wR_2 = 0.0887	
R indices (all data)	R_1 = 0.0421, wR_2 = 0.0959	
Largest diff. peak and hole	2.280 and -0.891 e.$Å^{-3}$	

2.3 Synthesis of a mixed-valent vanadium(V^{IV}/V^{V}) pentanuclear complex incorporating (4-carboxylphenyl)arsonic acid

2.3.1 The synthesis of $Na_9[V_5O_9(O_3AsC_6H_4\text{-}4\text{-}COO)_4]\cdot 6DMF\cdot 27H_2O$ (2)

The mixed-valent pentanuclear structure of $Na_9[V_5O_9(O_3AsC_6H_4\text{-}4\text{-}COO)_4]\cdot 6DMF\cdot 27H_2O$ (**2**) was synthesised using the same experimental procedure that led to the formation of **1** (Fig. 2.7). However the ligand, (4-aminophenyl)arsonic acid, was replaced by the corresponding molar equivalents of (4-carboxylphenyl)arsonic acid (Fig. 1.19) during the synthesis. Hydrazine monohydrate was again used as the reducing agent and the pH was adjusted to pH 7.3 using concentrated hydrochloric acid. After several days, dark green block crystals were collected and the structure was determined using single crystal X-ray diffraction.

2.3.2 The structural characterisation of $Na_9[V_5O_9(O_3AsC_6H_4\text{-}4\text{-}COO)_4]\cdot 6DMF\cdot 27H_2O$ (2)

The structure solves in the monoclinic space group, $P2_1/c$. The pentanuclear mixed-valent cluster core in **2** is very similar to that in **1**. Again the typical convex mixed-valent $\{V^{V}O(\mu_3\text{-}O)_4V^{IV}{}_4O_{12}\}$ unit is observed with each of the four fully deprotonated (4-carboxylphenyl)arsonic acid ligands bridging between two V atoms in an O,O'-*syn, syn* coordination mode. The inclusion of a carboxylic acid functionality does not hamper the self-assembly of this arsonate-vanadium hybrid core structure. The central V(1) is in oxidation state +5 as calculated using BVSA (Table 2.3) and the bond lengths between the V(1) ion and

the μ_3-O^{2-} ligands O(1), O(2), O(3), O(4) vary between 1.867(1) –1.883(1) Å and the terminal V(1)=O_{term} bond is 1.633(1) Å long.

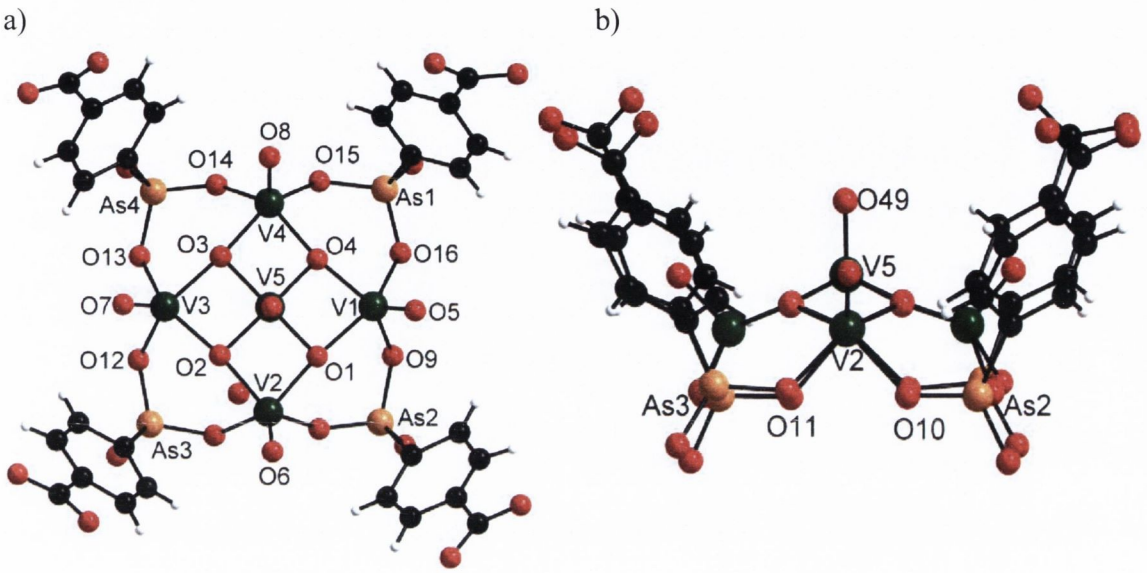

Figure 2.7 – (a) A ball and stick representation of the anionic core $[V_5O_9(O_3AsC_6H_4\text{-}4\text{-}COO)_4]^{9-}$ viewed along the crystallographic *c*-axis. (b) A side on view of the anionic core as viewed along the crystallographic *b*-axis. Colour code: V green, As orange, O red, N blue, C black, H white.

The peripheral vanadium ions V(2), V(3), V(4) and V(5) are again found to be in oxidation state +IV. Their V-O distances range between from 1.941(1) to 2.001(1) Å and are again slightly longer when compared to those in **1**. The bond distances between these V centres and the arsonate O-donors vary between 1.958(1) – 1.990(1) Å; the terminal V=O bond distances are shorter varying between 1.608(1) – 1.615(1) Å when compared with **1**.

Table 2.3 – Bond sum valence analysis for **2**

V site	BVS	Assigned O.S.
V(1)	5.089	+5
V(2)	4.022	+4
V(3)	4.030	+4
V(4)	4.032	+4
V(5)	4.069	+4

The deprotonation of the carboxylic acid functionality at the crystallising pH value infers an extra –4 charge on the cluster in **2**. The resulting overall –9 charge is compensated by nine solvated sodium ions. These solvated sodium ions form a layer between the anionic clusters to give a lamellar structure in which undulated organic and inorganic areas are separated when viewed in the direction of the crystallographic *a*-axis (Fig. 2.8b).

As discussed in section 2.2.2, the rim of the pentanuclear core offers bi-dentate binding sites for the sodium counter-ions. In **2**, all four of these binding sites are occupied by sodium ions.

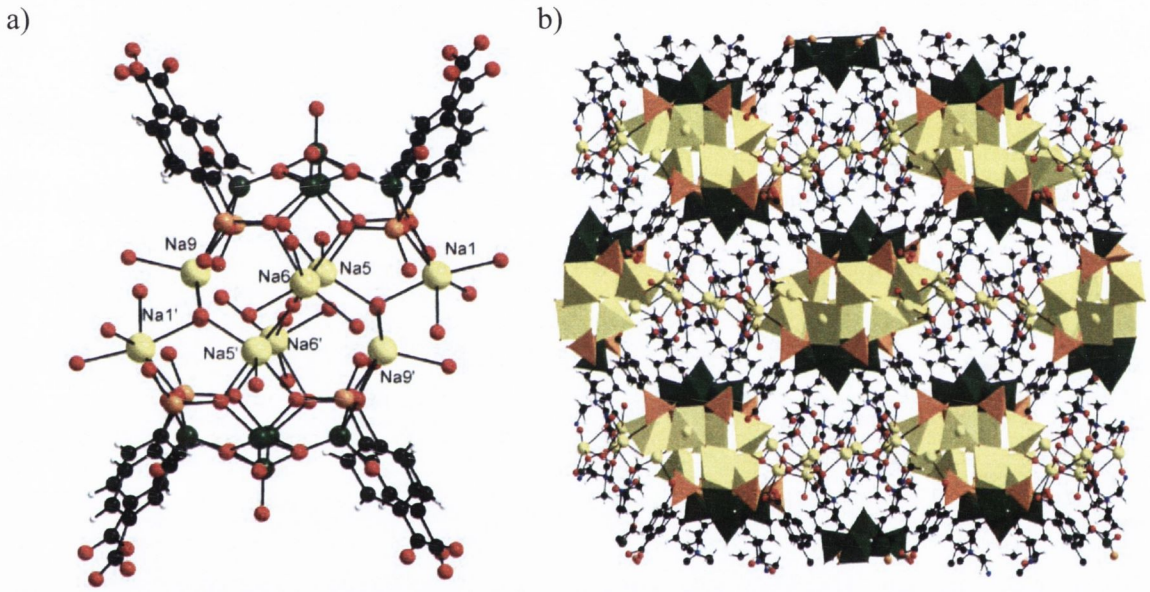

Figure 2.8 – (a) A ball and stick representation of two anionic clusters of **2** showing the coordinated sodium counter-ions sandwiched between these two pentanuclear core structures. (b) A polyhedral representation of these cores when viewed in the direction of the crystallographic *a*-axis Colour code: V green, Na yellow, As orange, O red, N blue, C black, H white.

An inversion centre generates four symmetric equivalent neighbour sodium ions that bind to the latter sodium ions through μ_3-bridging water molecules and bind to the rim of a symmetrically equivalent pentanuclear core. Eight sodium ions make up a small layer that is sandwiched between two pentanuclear clusters (Fig. 2.8a). The remaining sodium ions are further linked through to these sodium ions, bridged by the carboxylate functional groups, DMF and water molecules. The DMF molecules bind to the sodium ions so that undulated,

inorganic-organic layers result and these layers are arranged parallel to the *ab* plane. The carboxylate functionalities of the organic ligands straddle the organic layers and connect the hydrophilic areas, which contain the sodium and vanadium ions.

2.3.3 Further solid state characterisation of 2: Thermogravimetric analysis and Infrared spectroscopy

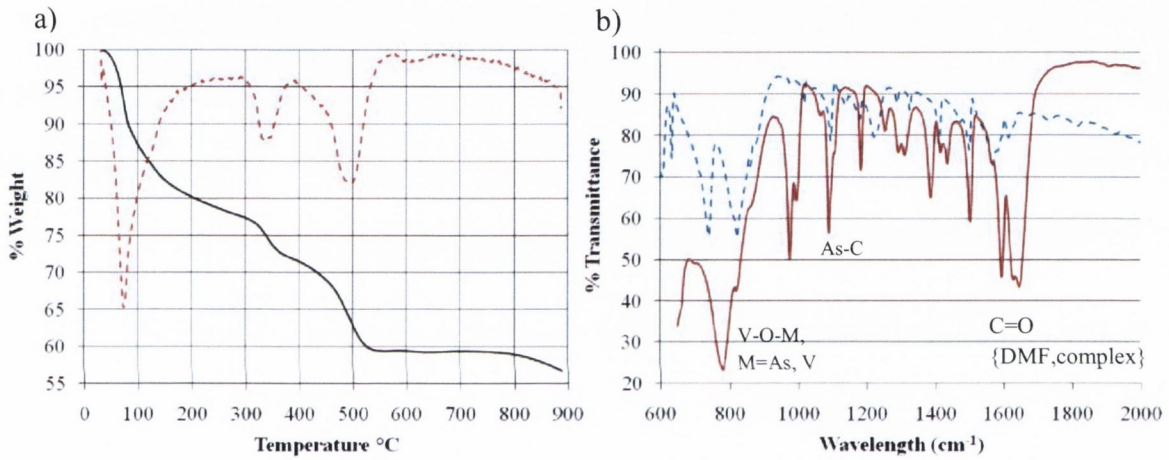

Figure 2.9 – The solid state characterisation of **2**. (a) Thermogravimetric analysis carried out in an air atmosphere. (b) An infrared spectrum of **2** (solid line) compared with that of the (4-carboxylphenyl)arsonic acid (dashed line) – full spectrum in appendix 2.

-Thermogravimetric analysis

A thermogravimetric analysis was carried out on **2** in a temperature range between 30°C to 900°C (Fig. 2.9a) in an air atmosphere. When the derivative of the TGA curve of **2** is calculated, three major weight loss events are observed centred at 75°C, 330°C and 500°C. The weight loss between 30°C and 200°C is associated with the loss of crystallisation water molecules and DMF molecules (22%). The thermogravimetric steps centred at 330°C and 500°C is expected to be associated with the ligand undergoing degradation in two

decomposition steps leading to the destruction of the cluster (6.25%, 12.43%). The formation of a stable inorganic phase is observed at 530°C.

- *Infrared spectroscopy*

An infrared spectrum of **2** was recorded (Fig. 2.9b) prior to the structure determination by single crystal X-ray diffraction. Notable stretches observed include signals at 1095 cm^{-1} (s, ν, As-C), 996 cm^{-1} (V^{IV}=O), 986 cm^{-1} (V^{V}=O), 831 cm^{-1} (s, ν, As-O) and 793 cm^{-1} (s, ν, V-O-V/V-O-As).[46, 47] The carbonyl stretch is present in the infrared spectrum of (4-carboxylphenyl)arsonic acid at 1684 cm^{-1} (vs, ν, C=O) and in the complex at 1652 cm^{-1}(vs, ν, C=O).[88, 89] However, there is an underlying but not distinct carbonyl stretch present due to the presence of DMF solvent molecules in **2**. A broad signal at 3470 cm^{-1} can be attributed to OH stretches of the solvent water molecules (full spectrum in appendix 2).

2.3.4 Solution characterisation of 2: UV-vis spectroscopy

- *UV-vis spectroscopy*

Compound **2** only partially dissolves in pure DMSO and its UV-vis spectrum was recorded in a deoxygenated DMSO/water mixture. The resulting spectrum, shown in Fig. 2.10 is very similar to that of **1.** The spectrum is characterised by a broad absorption in the near UV region, while much weaker broad absorbencies occur due to the d(V)-d(V) transitions at 714 nm (ε = 320.6 $L.mol^{-1}cm^{-1}$). A small shoulder at 604 nm (ε = 259.3 $L.mol^{-1}cm^{-1}$) can be attributed to intervalence charge transfers.[38, 42] The UV-vis spectrum suggests that the compound is stable under these experimental conditions. However in pure H_2O, **2** seemed to decompose: the absorptions due to the d(V)-d(V) transitions shift to 731 nm (ε = 634.7

$L.mol^{-1}cm^{-1}$) whilst the intervalence charge transfer absorptions undergo a blue shift to 575 nm (ε = 559.6 $L.mol^{-1}cm^{-1}$).

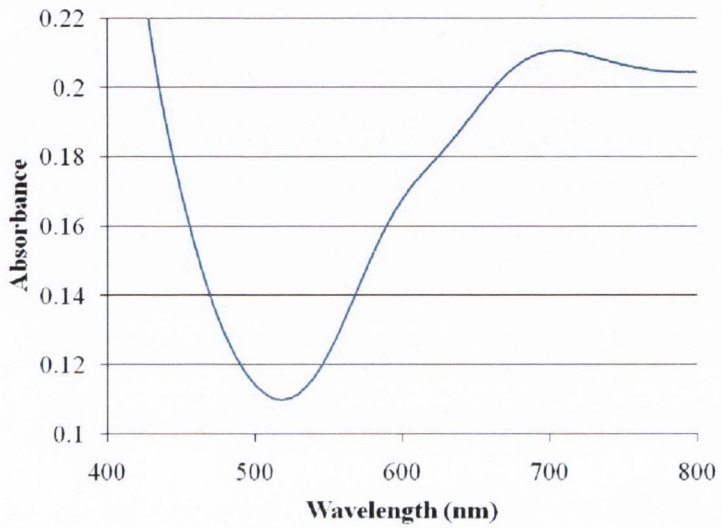

Figure 2.10 – UV-Vis spectrum of **2** in a deoxygenated DMSO/H_2O (9:1 w:w) mixture (1mM).

Table 2.4 – Crystal data and structure refinement for **2**.

Identification code	Compound **2**	
Empirical formula	$C_{46}\ H_{61}\ As_4\ N_6\ Na_9\ O_{62}\ V_5$	
Formula weight	2451.30 g mol^{-1}	
Temperature	150(2) K	
Wavelength	0.71073 Å	
Crystal system	Monoclinic	
Space group	$P2_1/n$	
Unit cell dimensions	a = 18.026(4) Å	α = 90°.
	b = 23.202(5) Å	β = 121.29(2)°.
	c = 26.312(9) Å	γ = 90°.
Volume	9404(4) $Å^3$	
Z	4	
Density (calculated)	1.731 Mg/m^3	
Absorption coefficient	2.026 mm^{-1}	
F(000)	4884	
Crystal size	0.2 x 0.2 x 0.1 mm^3	
Theta range for data collection	1.26 to 25.00°.	
Index ranges	-21<=h<=21, -27<=k<=27, -25<=l<=31	
Reflections collected	73662	
Independent reflections	16358 [R(int) = 0.0505]	
Completeness to theta = 25.00°	98.8 %	
Refinement method	Full-matrix least-squares on F^2	
Data / restraints / parameters	16358 / 0 / 1201	
Goodness-of-fit on F^2	1.189	
Final R indices [I>2sigma(I)]	R_1 = 0.0883, wR_2 = 0.2815	
R indices (all data)	R_1 = 0.1221, wR_2 = 0.3568	
Largest diff. peak and hole	3.126 and -4.386 e.$Å^{-3}$	

2.4 Synthesis of a mixed-valent vanadium(V^{IV}/V^{V}) pentanuclear complex incorporating (4-hydroxyphenyl)arsonic acid

2.4.1 The synthesis of $Na_5[V_5O_9(O_3AsC_6H_4\text{-}4\text{-}OH)_4]\cdot 17.5H_2O\cdot 5DMF$ (3)

Compound **3**, $Na_5[V_5O_9(O_3AsC_6H_4\text{-}4\text{-}OH)_4]\cdot 17.5H_2O\cdot 5DMF$, was synthesised in a similar synthetic manner to **1**. Sodium metavanadate was partially reduced in the presence of (4-hydroxyphenyl)arsonic acid in a water/DMF solution using hydrazine hydrate. A dark black green solution resulted upon reduction of the vandate at pH 7.2 and black green cube shaped crystals where observed after two weeks. These crystals became opaque due to the loss of solvents molecules when left outside the mother solution at room temperature for several days.

2.4.2 The structural characterisation of $Na_5[V_5O_9(O_3AsC_6H_4\text{-}4\text{-}OH)_4]\cdot 17.5H_2O\cdot 5DMF$ (3)

$Na_5[V_5O_9(O_3AsC_6H_4\text{-}4\text{-}OH)_4]\cdot 17.5H_2O\cdot 5DMF$ (**3**), crystallises in an orthorhombic space group, *P*nn2, as opposed to lower symmetry groups observed for **1** and **2**. Similarly to **1** and **2**, **3** contains the mixed-valent pentanuclear $\{V^{V}O(\mu_3\text{-}O)_4V^{IV}{}_4O_{12}\}$ core with four (4-hydroxyphenyl)arsonate ligands each bridging between two V atoms in an O,O'-*syn, syn* coordination mode. The asymmetric unit consists of three vanadium centres and the complete pentanuclear unit is generated by a C_2 symmetry operation (Fig. 2.11). Bond valence sum analysis was again used to calculate the oxidation states (Table 2.5). The central V(1) was found to be in oxidation state +V with bond lengths between V(1) ions and the μ_3-O^{2-} ligands O(1) and O(2), to be 1.866(5) and 1.885(5) Å and the terminal V(1)=O_{term} bond is 1.619(8) Å

long (Fig. 2.11b). The peripheral vanadium ions V(2) and V(3) are calculated to be in oxidation state +IV which is consistent with the clusters in **1** and **2**.

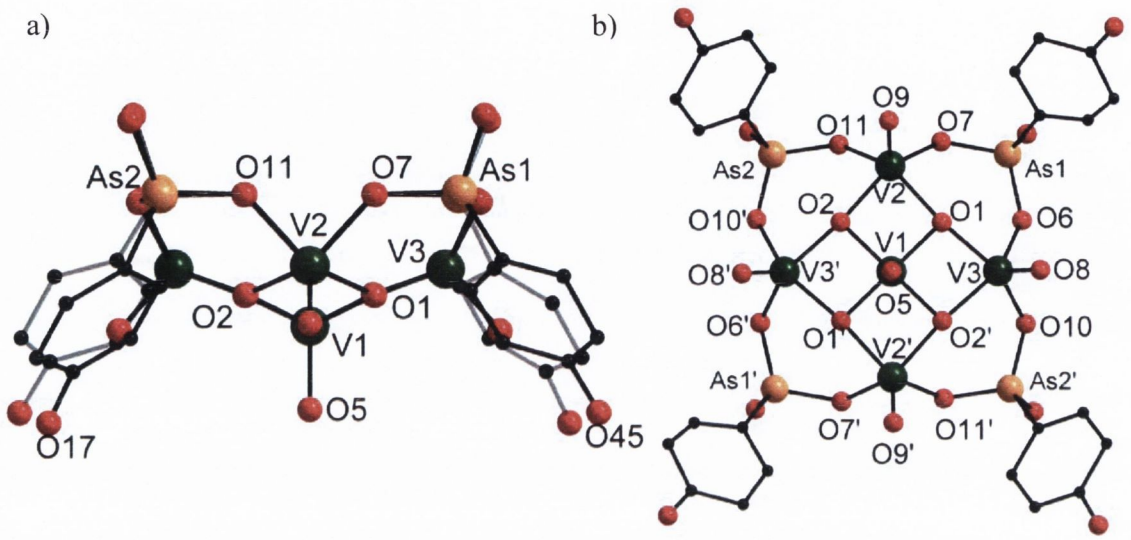

Figure 2.11 – (a) A ball and stick representation of the hybrid polyoxovanadate core as viewed along the crystallographic *b*-axis. (b) The plan view of the pentanuclear cluster as viewed along the crystallographic *c*-axis. Colour code: V green, As orange, O red, N blue, C black.

The range for these V-μ_3-O distances is 1.941(1) – 2.001(1) Å. The bond distances between these V centres and the organic ligand O donors vary between 1.967(6) – 2.009(6) Å whilst the terminal V=O bond distances range between 1.606(6) – 1.612(6) Å.

Table 2.5 – Bond sum valance analysis for **3**

V site	BVS	Assigned O.S.
V(1)	3.961	+4
V(2)	4.072	+4
V(3)	4.882	+5
μ_3-O (1) (2)	2.066, 2.064	-2
μ-O (6) (7) (10) (11)	1.830 – 1.928	-2
$O_{terminal}$ (8)(9)	1.575,1.731	-2

The hydroxy functions of the organic ligands remain protonated and the mixed-valent pentanuclear cluster has an overall charge of –5, which is compensated by five solvated sodium ions. Four of these solvated sodium ions coordinate to the rim of the pentanuclear structure in a fashion that was also observed in **2** (Fig. 2.12a, Fig. 2.12c).

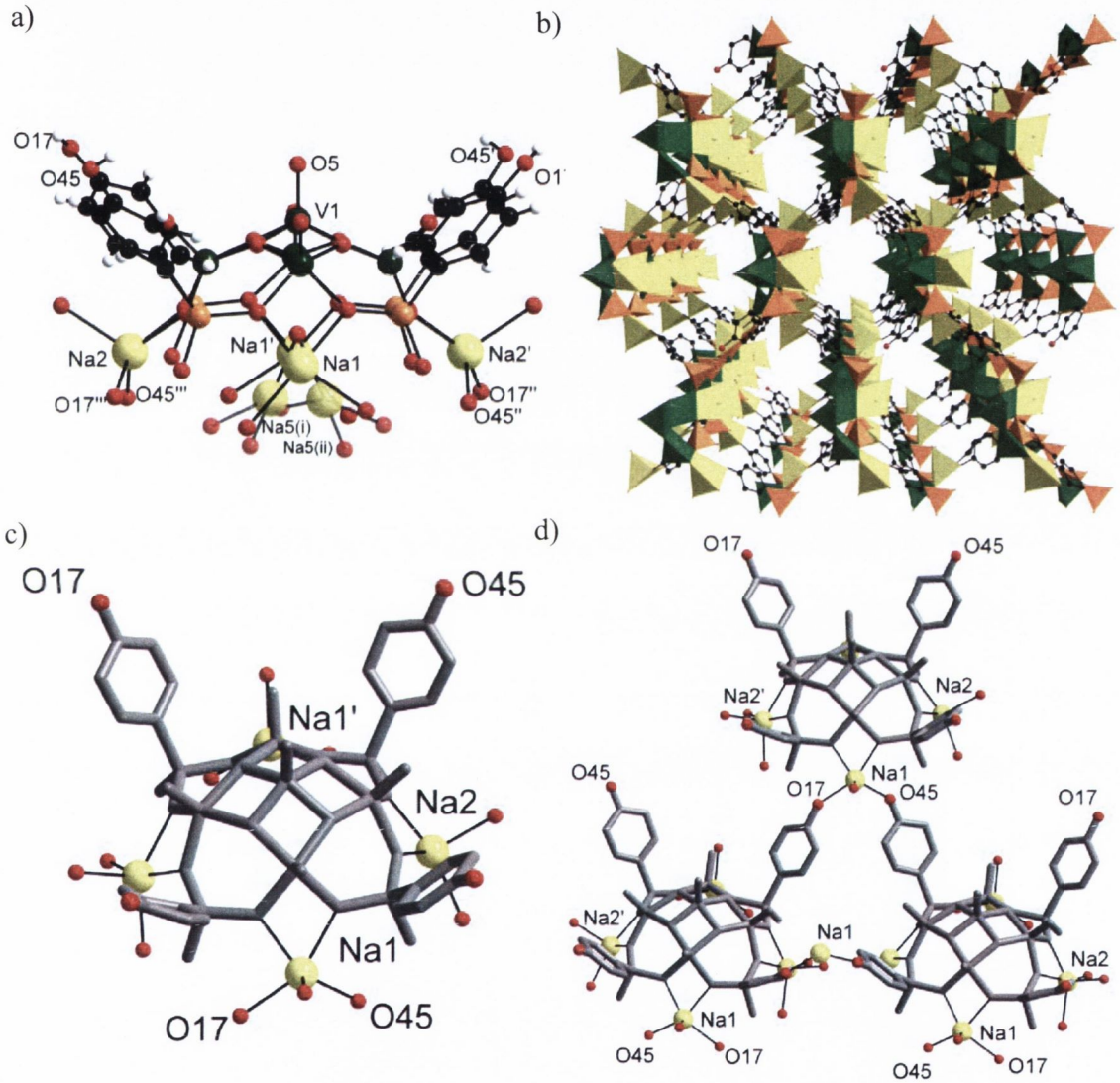

Figure 2.13 – (a) A ball and stick representation of the $Na_5[V_5O_9(O_3AsC_6H_4\text{-}4\text{-}OH)_4]$ in **3**. Na(5) is disordered over two positions and situated in the centre of the rim of the pentanuclear cluster; (b) A perspective view of the resulting channels in **3** viewed along the crystallographic *a*-axis. The solvent molecules in the channels have been omitted for clarity. (c) A grey wire frame representation of the pentanuclear anionic cluster of **3**. (d) The nature of the connectivity of the sodium counter-ions between neighbouring pentanuclear units is shown. Disordered water molecules have been omitted for clarity. (V, As and Na atoms are shown in polyhedral presentation in (b). Colour code: V green, As orange, Na yellow, O red, N blue, C black, H white).

The fifth isolated sodium ion Na(5) is disordered over two locations (Na5(i), Na5(ii)) located in the centre of the rim comprised of the other four bound sodium ions. The hydroxy groups of the organic ligands point in the direction of the V=O tips and bind to sodium counter-ions associated with a neighbouring cluster. The connectivity of the pentanuclear clusters is demonstrated in Fig. 2.12c & 2.12d. The sodium counter-ion Na(1) and its symmetry equivalents can be considered to have distorted octahedral coordination spheres. Two coordination sites of Na(1) are bound to the rim of the anionic vanadium cluster of **3** (Fig. 2.13c), whilst two *trans* coordination sites are bound by the hydroxy functional groups, O(17) O(45), of the adjacent neighbouring clusters (Fig. 2.12d). Two water molecules complete the coordination sphere of Na(1). This arrangement results in an open-framework structure in which solvent molecules are contained within channels that run in the direction of the crystallographic *a*-axis (Fig. 2.12b). Due to the large number of disordered solvent molecules contained in the channels of **3**, it was deemed appropriate to use the program SQUEEZE in order to model the structure.[90] It was noted from the CHN analysis (see 6.3.3) that **3** is most likely to contain three additional DMF molecules in its structure. Due to their disorder, we were not able to locate and refine these molecules.

2.4.3 Further solid state characterisation of 3: Thermogravimetric analysis and Infrared spectroscopy

- Thermogravimetric analysis

A TGA was carried out on the crystalline solid of **3** (Fig. 2.13a). The TGA analysis is comparable with that of **1** and **2**. The first broad weight loss is observed between 30°C to *ca.* 290°C. This weight loss corresponds to the loss of the crystallisation water molecules and DMF molecules (16.53%). A small weight loss centred at *ca.* 334°C is attributed to initial

decomposition of the organic ligands incorporated in the complex (5.31%) followed by a much larger weight loss (34.4%) at *ca.* 358 °C. An oxide formation is presumed to occur at 542 °C.

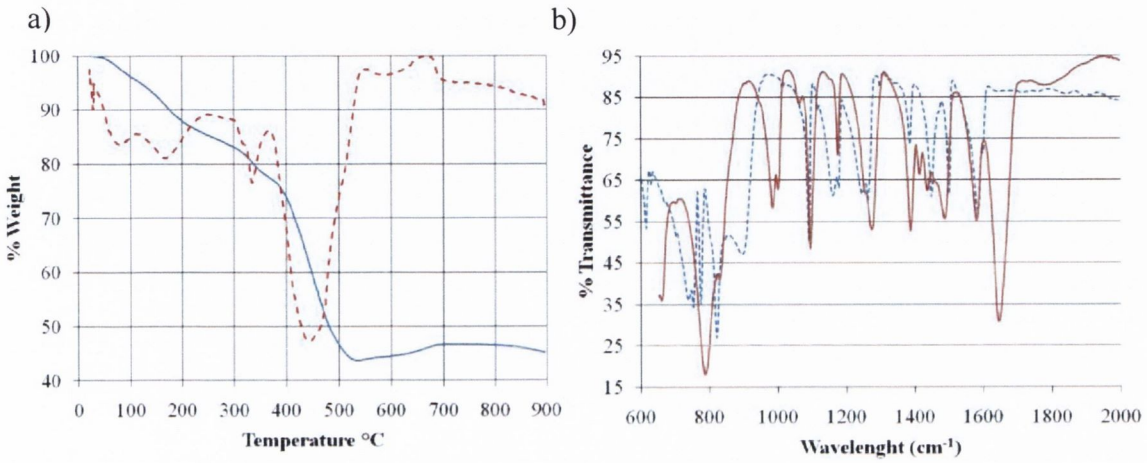

Figure 2.13 – Solid state characterisation of **3**. (a) TGA analysis of the crystalline powder of **3**. (b) The infrared spectrum of **3** (red) compared with the infrared spectrum of the starting arsonate ligand (blue dashed).

- *Infrared spectroscopy*

The infrared spectrum of **3** (Fig. 2.13b) is very similar to that of **1** and **2**. Notably, stretches include signals at 1096 cm^{-1} (s, ν, As-C), 1002 cm^{-1} (V^{IV}=O), 986 cm^{-1} (V^{V}=O), 831 cm^{-1} (s, ν, As-O) and 791 cm^{-1} (s, ν, V-O-V/V-O-As). Stretches that appear both in the ligand and in the complex are thought to originate from the aromatic C=C bonds which characteristically appear in the region of 1440-1625 cm^{-1} {m, ν, 1389 cm^{-1}; m, ν, 1430 cm^{-1}; m, ν, 1439 cm^{-1}; m, ν, 1491 cm^{-1}} for **3**.[88]

2.4.4 Solution characterisation of 3: Mass spectrometry and UV-vis spectroscopy

-Mass spectrometry

Compound **3** was dissolved in a DMSO and a mass spectrum was recorded (appendix 2 and Fig. 2.14a). The deprotonated (4-hydroxyphenyl)arsonate ligand is observed at m/z = 216.9350 ($AsO_3HC_6H_4OH^-$). A fragmentation of the ligand is also observed whereby a water molecule is lost to give a molecular formula of $[AsO_3C_6H_4]^-$ (m/z = 198.9380). An intense signal at m/z = 1266.3 is observed and modelled to correspond to the anionic complex of **3** with a molecular formula of $H_4[V_5As_4O_{25}C_{24}H_{24}]^-$ (appendix 2).

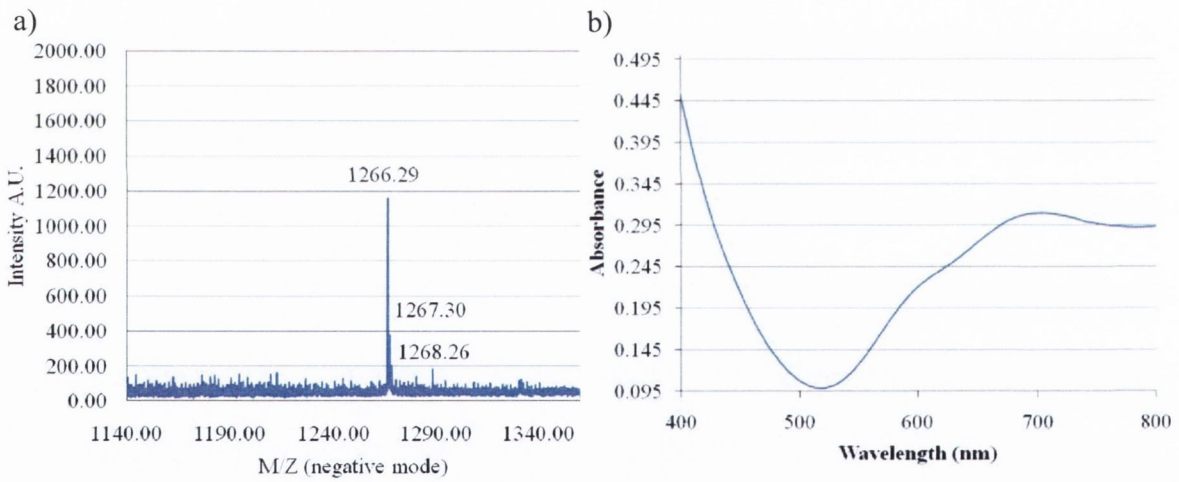

Figure 2.14 – The characterisation of **3** in solution. (a) Mass spectrum of **3** in DMSO. (b) UV-Vis spectroscopy of 1 mM solution of **3** in a deaerated DMSO solution.

-UV-vis spectroscopy

The UV-vis spectrum for **3** in DMSO is very similar to that of the UV-vis spectra of **1** and **2**. The solution of **3** displays the typically strong π(O) – d(V) charge transfer absorption in the near UV region. A weaker broad absorbence due to the d(V)-d(V) transitions is observed at 704 nm whilst a shoulder at 605 nm is the result of an intervalence charge transfer effect (Fig.

4.14b). The aqueous solution of **3** shows very low intensity absorbances in the visible region when compared to a DMSO solution of **3** with an equivalent molar concentration (see appendix 2). This is consistent with the decomposition of **3** in aqueous solutions which has similarly been observed for **2**.

Table 2.6 – Crystal data and structure refinement for **3**.

Identification code	Compound **3**	
Empirical formula	$C_{24}\ H_{16}\ As_4\ Na_5\ O_{33}\ V_5$	
Formula weight	1501.70 g mol^{-1}	
Temperature	150(2) K	
Wavelength	0.71070 Å	
Crystal system	Orthorhombic	
Space group	*P*nn2	
Unit cell dimensions	a = 14.512(7) Å	α = 90°.
	b = 22.664(12) Å	β = 90°.
	c = 13.699(8) Å	γ = 90°.
Volume	4506(4) $Å^3$	
Z	2	
Density (calculated)	1.107 Mg/m^3	
Absorption coefficient	2.034 mm^{-1}	
F(000)	1452	
Crystal size	0.35x 0.3 x 0.15 mm^3	
Theta range for data collection	2.23 to 25.00°.	
Index ranges	-17<=h<=12, -23<=k<=26, -16<=l<=16	
Reflections collected	19183	
Independent reflections	7712 [R(int) = 0.0541]	
Completeness to theta = 25.00°	99.9 %	
Refinement method	Full-matrix least-squares on F^2	
Data / restraints / parameters	7712 / 1 / 312	
Goodness-of-fit on F^2	1.027	
Final R indices [I>2sigma(I)]	R_1 = 0.0645, wR_2 = 0.1685	
R indices (all data)	R_1 = 0.0754, wR_2 = 0.1769	
Largest diff. peak and hole	0.609 and -0.547 e.$Å^{-3}$	

2.5 Synthesis of a mixed-valent vanadium(V^{IV}/V^{V}) pentanuclear complex incorporating (3-acetamido-4-hydroxyphenyl)arsonic acid

2.5.1 The synthesis of $Na_5[V_5O_9(O_3AsC_6H_4\text{-}3\text{-}NHCOCH_3\text{-}4\text{-}OH)_4]\cdot 19H_2O\cdot 3DMF$ (4)

$Na_5[V_5O_9(O_3AsC_6H_4\text{-}3\text{-}NHCOCH_3\text{-}4\text{-}OH)_4]\cdot 19H_2O\cdot 3DMF$ (**4**) was synthesised in the same synthetic manner as **3**. Sodium metavanadate was partially reduced with hydrazine hydrate in the presence of (3-acetamido-4-hydroxyphenyl)arsonic acid in a water/DMF solution. A dark black green solution resulted upon reduction at pH 7.2 and dark green cube shaped crystals where observed after a week. The crystals of **4** were more robust than those of **3.** The crystals did not become opaque when removed from the mother liquor due to the loss of solvents molecules, as was the case for crystals of **3**.

2.5.2 The structural characterisation of $Na_5[V_5O_9(O_3AsC_6H_4\text{-}3\text{-}NHCOCH_3\text{-}4\text{-}OH)_4]\cdot 19H_2O\cdot 3DMF$ (4)

Compound **4**, $Na_5[V_5O_9(O_3AsC_6H_4\text{-}3\text{-}NHCOCH_3\text{-}4\text{-}OH)_4]\cdot 19H_2O\cdot 3DMF$, crystallises in the orthorhombic space group, *I*mm2, a higher symmetry group than that of the crystal structure of **3**. Similarly to **3**, this hybrid cluster contains five vanadium ions, each with a square pyramidal coordination sphere. The central pyramid again shares common edges with its four surrounding $\{V^{IV}O_5\}$ polyhedra to give the typical convex mixed-valent $\{V^{V}O(\mu_3\text{-}O)_4V^{IV}{}_4O_{12}\}$ unit. In contrast to **3**, the two O donors from each $\{V^{IV}O_5\}$ peripheral square pyramid are provided by four (3-acetamido-4-hydroxyphenyl)arsonate ligands. Again, each

of these ligands bridges between two V atoms in an O,O'-*syn, syn* coordination mode (Fig 2.15).

Although the cluster core structure in **4** can be unambiguously resolved, the organic ligands were found to be highly disordered and a detailed location and refinement of the atoms was unattainable. It was noted that especially the flexible *meta* positioned amide side chains of the arsonic acid ligand were highly disordered.

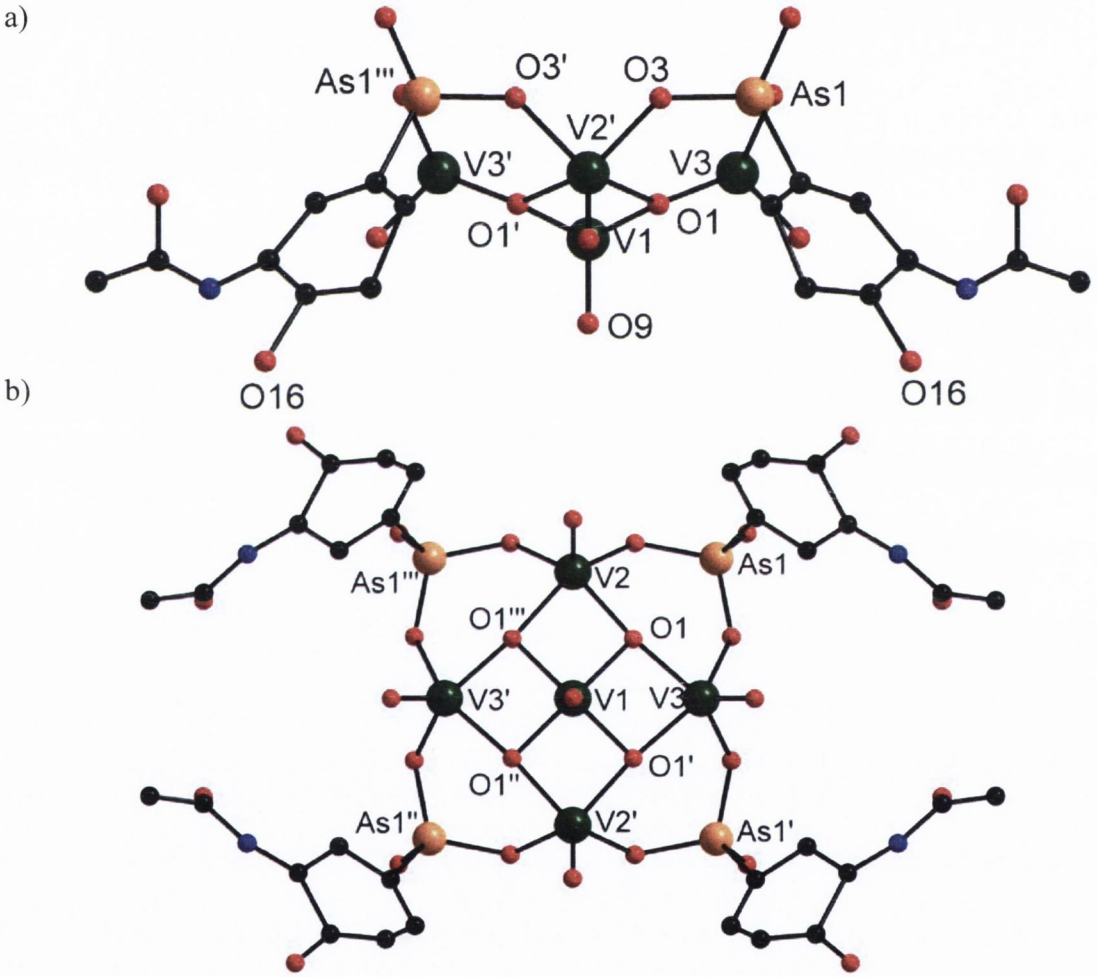

Figure 2.15 – (a) A ball and stick representation of the mixed-valent anionic core of **4** as viewed along the crystallographic *b*-axis. (b) The anionic core structure of **4** as viewed along the crystallographic *c*-axis. The amide functional groups are disordered over several positions as are the aromatic rings. Disordered atom positions have been deleted for clarity. Colour code: V green, As orange, O red, N blue, C black.

The phenomenon of disordered phenylarsonate ligands is well documented to hamper detailed structural analyses in comparable functionalised polyoxovanadate clusters.[46]

As previously discussed, bond valence sum analysis was used to calculate the oxidation states (see Table 2.7). The central V(1) was found to be in oxidation state +V with bond lengths between V(1) ions and the μ_3-O^{2-} ligands O(1), O(2), O(3), O(4) to vary between 1.867(1) – 1.883(1) Å and the terminal V(1)=O_{term} bond was found to be 1.633(1) Å long (Fig. 2.16a and 2.16b). The peripheral vanadium ions V(2), V(3), V(4) and V(5) are calculated to be in oxidation state +IV. These V-O distances range between 1.941(1) Å and 2.001(1) Å. The bond distances between these V centres and the organoarsonate ligand O donors vary between 1.958(1) – 1.990(1) Å whilst the terminal V=O bond distances vary between 1.608(1) – 1.615(1) Å.

Table 2.7 – Bond sum valance analysis for **4**

V & O site	Bond Valence Sum analysis	Assigned Oxidation State
V1	3.961	+4
V2	4.072	+4
V3	4.882	+5
μ_3-O (1) (2)	2.066,2.064	-2
μ-O (6) (7) (10) (11)	1.830 – 1.928	-2
$O_{terminal}$ (8)(9)	1.575,1.731	-2

The charge of the mixed-valent pentanuclear polyoxovanadate is compensated by five solvated sodium ions suggesting that the hydroxy functions of the organic ligands remain protonated. This observation is in agreement with the structure determination of **3** and applied synthetic conditions. Despite the disorder in the structure of **4**, four solvated sodium counter-ions were clearly located. These coordinate to the rim of the inorganic calyx structure (Fig. 2.16a) A fifth solvated sodium counter-ion appears to be disordered over two locations and

was located above the bowl-shaped cluster. A similar position was also occupied by a sodium counter-ion in **3**. The hydroxy groups O(16) and its symmetry equivalents extending from the exterior tips of the organoarsonate ligands of the complex coordinate to the rim-bound sodium counter-ions of neighbouring pentanuclear structures (Fig. 2.16b). This connectivity mode was also observed in **3**.

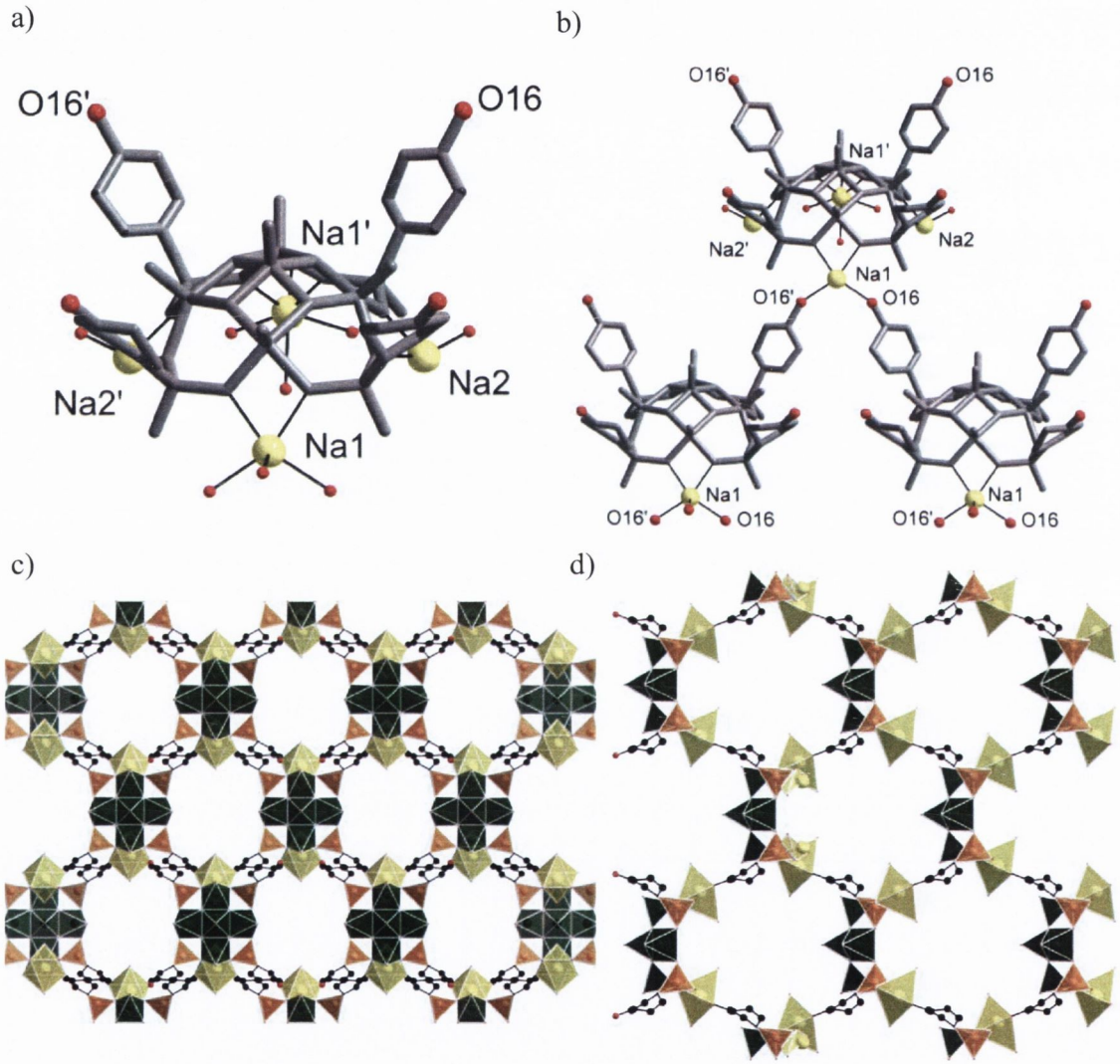

Figure 2.16 – (a) A wire frame representation of the anionic cluster core of **4** with the rim bound sodium counter-ions highlighted. (b) Highlighting the connectivity of the sodium counter-ion Na(1) which bridges between neighbouring clusters. (c) A polyhedral representation of the pentanuclear core with coordinating sodium counter-ions as viewed in the crystallographic *c*-axis. (d) A perspective view of the channels in crystal structure of **4** as viewed along the crystallographic *a*-axis. The disordered side chains, disordered aromatic ring atoms and disordered solvent molecules have been removed for clarity. Colour code: V green, As orange, Na yellow, O red, N blue, C black; Polyhedral representations: V green, Na yellow, As orange.

The arrangement results in an open framework structure in which solvent molecules reside in channels and these channels extend along the crystallographic *a*-axis (Fig. 2.16d). The *meta*-positioned amide groups of the arsonates seem to provide the walls of the solvent channels (Fig. 2.16c). Due to the large number of disordered solvent molecules contained in the channel of **4** it was deemed appropriate to use the program SQUEEZE in order to model the structure.[90] The molecular formula was assigned using the results of the CHN analysis.

2.5.3 Further solid state characterisation of 4: Thermogravimetric analysis, Infrared spectroscopy and BET surface area analysis

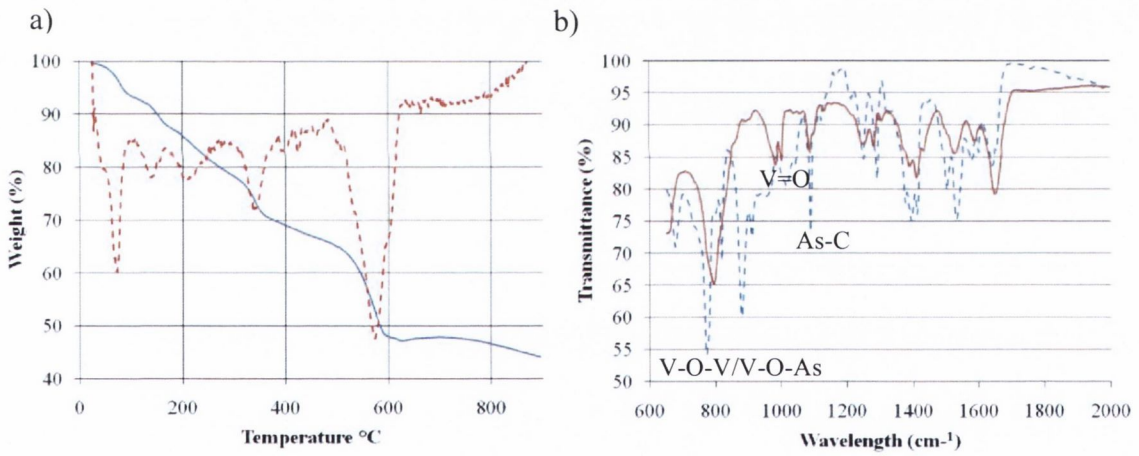

Figure 2.17 – Solid state characterisation of **4**. (a) TGA analysis of **4**; TGA analysis (blue line), derivation of the TGA curve (red dashed line). (b) Infrared spectrum of **4** (red solid line) and infrared spectrum of the organoarsonate ligand (blue dashed line).

-Thermogravimetric analysis

A TGA of **4** was performed in a temperature range between 30 °C and 900 °C in air (Fig. 2.17a). Three major events were observed in the temperature range between 30 °C and *ca.* 310 °C corresponding to loss of the crystallisation water molecules and DMF molecules

(22.7%). The fourth weight loss centred at 338 °C is presumed to correspond to the start of the decomposition of the complex and is associated with the loss of the hydroxy groups and the amide side chains from the aromatic organoarsonate ligands (12.2%). A subsequent weight loss observed between 476 °C and 635 °C results from the oxidative degradation of the remaining carbon atoms of the aromatic rings of the ligands (13.8%) as well as from the decomposition of the arsonate functionality.

-Infrared spectroscopy

Infrared spectroscopy was again utilised as a tool to determine the inclusion of the arsonate ligand as supported by the characteristic stretches of (3-acetamido-4-hydroxyphenyl)arsonic acid (Fig. 2.17b). Characteristic stretches arising from the aromatic moieties and the amide groups appear in the region 1400-1600 cm^{-1} (m, ν, 1400 cm^{-1}; m, ν, 1414 cm^{-1}; m, ν, 1536 cm^{-1}; m, ν, 1594 cm^{-1}).[88, 89] Additionally observed stretches include 1091 cm^{-1} (As-C), 1003 cm^{-1} (V^{IV}=O), 985 cm^{-1} (V^{V}=O) and 799 cm^{-1}.[46, 47] The latter signal is related to the V-O-As/V-O-V bonds within the anionic cluster core. A carbonyl stretch appears at 1654 cm^{-1} relates to the DMF solvent molecules (s, ν, C=O {DMF}) as well to carbonyl stretches due to the amide functionality on the ligand.

-BET

Compound **4** was heated under vacuum to 30°C for 24 hours. The Brunanuer-Emmett-Teller (BET) method was used to determine the surface area using nitrogen as the adsorbate at 77K. The slope was calculated to be 203.381 kg^{-1} with an intercept at 91.34 kg^{-1}. The correlation coefficient r was 0.981793 and the C constant was calculated to be 3.227. Using the BET

equation (appendix 2), the surface area analysis was calculated to be 11.816 m^2/g. When the sample was heated to higher temperatures under vacuum, no reliable BET surface area was could be determined indicating that the 3-D structure collapses.

2.5.4 Solution characterisation of 4: UV-vis spectroscopy

A 1mM solution of **4** in DMSO was prepared and the solution was characterised by UV-vis spectroscopy (see appendix 2). The UV-vis spectrum of **4** shows very similar absorptions to that of the DMSO solutions of **1** – **3**. The most notable absorptions in the visible region are a broad absorption at 703 nm (d-d transitions) and an accompanying shoulder at 603 nm due to the intervalence charge transfer within the mixed-valent pentanuclear complex. A UV-vis spectrum of **4** was also recorded in an aqueous solution but it indicated the decomposition of **4**.

Table 2.8 – crystal data and structure refinement for **4**.

Identification code	Compound **4**	
Empirical formula	$C_{27}\ H_9\ As_4\ N_{1.50}\ Na_5\ O_{38.50}\ V_5$	
Formula weight	1639.69 g mol^{-1}	
Temperature	118(2) K	
Wavelength	0.71075 Å	
Crystal system	Orthorhombic	
Space group	*I*mm2	
Unit cell dimensions	a = 15.314(6) Å	α = 90°.
	b = 20.284(8) Å	β = 90°.
	c = 15.268(6) Å	γ = 90°.
Volume	4743(3) $Å^3$	
Z	2	
Density (calculated)	1.169 Mg/m^3	
Absorption coefficient	1.943 mm^{-1}	
F(000)	1583	
Crystal size	0.2 x 0.2 x 0.2 mm^3	
Theta range for data collection	1.67 to 24.99°.	
Index ranges	-18<=h<=10, -16<=k<=24, -17<=l<=18	
Reflections collected	10307	
Independent reflections	4360 [R(int) = 0.0446]	
Completeness to theta = 24.99°	99.1 %	
Refinement method	Full-matrix least-squares on F^2	
Data / restraints / parameters	4360 / 1 / 252	
Goodness-of-fit on F^2	0.982	
Final R indices [I>2sigma(I)]	R_1 = 0.0730, wR_2 = 0.1919	
R indices (all data)	R_1 = 0.0855, wR_2 = 0.2033	
Largest diff. peak and hole	0.567 and -0.970 $e.Å^{-3}$	

2.6 Summary of mixed-valent vanadium(V^{IV}/V^{V}) pentanuclear complexes functionalised with organoarsonate ligands

In this chapter, we present four novel mixed-valent organoarsonate functionalised clusters. The compounds were structurally characterised using single crystal X-ray diffraction and found to contain the mixed-valent pentanuclear $\{V^{V}O(\mu_3\text{-}O)_4V^{IV}{}_4O_{12}\}$ unit. The introduction of different functional groups in the *para* position of the arsonate ligand (amine, carboxylate, hydroxy) does not hamper the self-assembly of this hybrid core structure (Fig. 2.18).

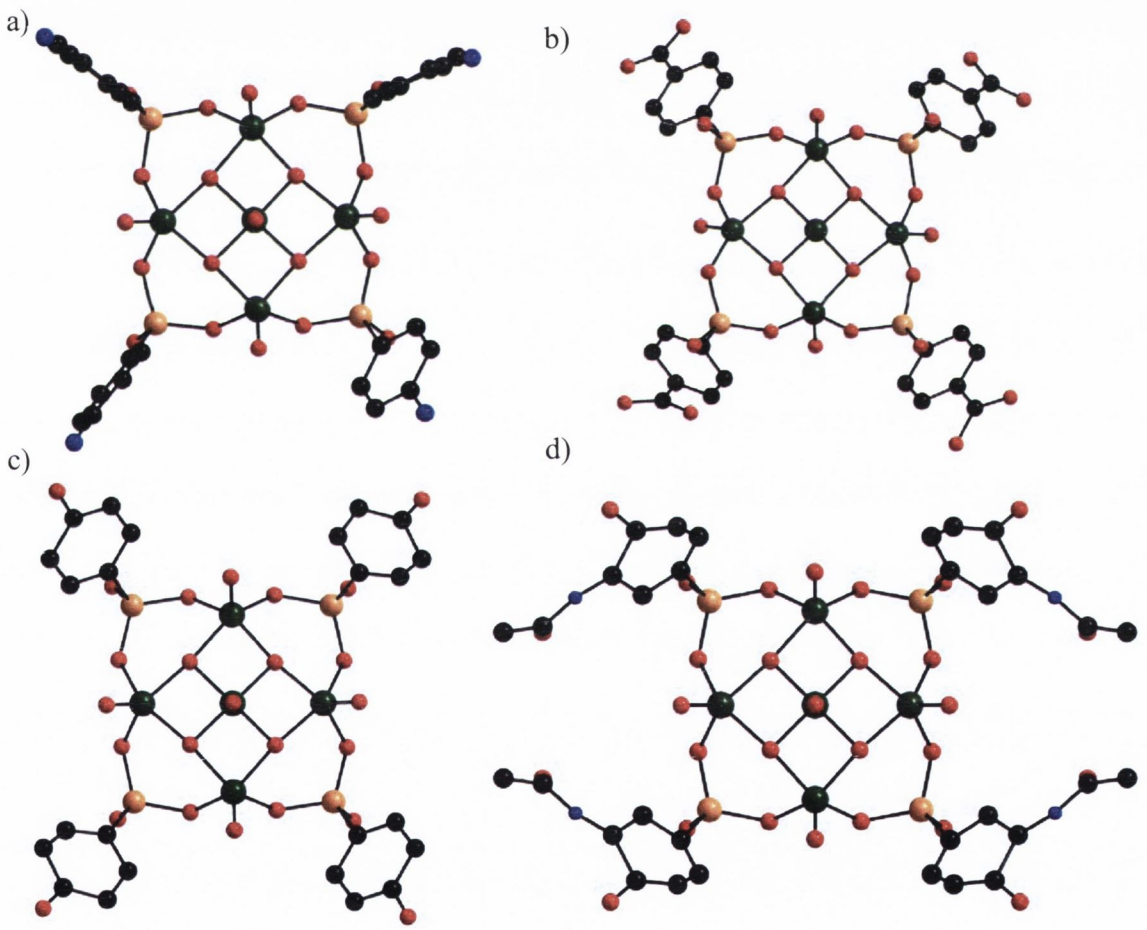

Figure 2.18 – (a – d) Summary of the anionic mixed-valent pentanuclear complexes stabilised by aromatic arsonate ligands. Disordered atom positions and hydrogen atoms have been removed for clarity. Colour code: V green, As orange, O red, N blue, C black.

UV-vis spectroscopy and mass spectrometry confirm that these compounds are stable in DMSO solutions. Mass spectra were recorded for **1** – **4** and modelled for the anionic clusters of **1** and **3**. Bond valence sum analysis characterises the oxidation states of the vanadium ions. Infrared spectroscopy and UV-vis spectroscopy are agreement with the mixed-valent nature of these compounds.[38, 42] Infrared spectroscopy was in addition used as a preliminary characterisation technique to confirm the incorporation of the organoarsonate ligands.

Our structural analyses demonstrate that the packing arrangements of the anionic clusters in **1** – **4** are strongly influenced by the different functionalising groups in *para* position to the arsonate functionality. The hybrid clusters containing peripheral hydroxy groups (**3** and **4**) were found to have open framework structures and accordingly, their surface areas were investigated. However, the BET surface area analyses strongly suggest that the 3-D arrangements of the anionic clusters in **3** and **4** collapse upon removal of the solvent molecules. The instability of these compounds to solvent removal can be attributed to weak intermolecular bonding between the anionic clusters in the packing structure of **3** and **4**. Future work will involve the synthesis of mixed-valent pentanuclear clusters whose functionalities will enable them to form stronger intermolecular bonds. A promising candidate for this work is the cluster in **2**. Its carboxylate functional group is ideal to coordinate to other transition metal ions producing stable 3-D frameworks.

Chapter Three

Assembly of pentanuclear secondary building units to produce hybrid cages

3.1 Introduction

The accessibility of the mixed-valent pentanuclear vanadium complex in **1** stabilised by (4-aminophenyl)arsonic acid in solution, instigated our motivation to exploit this structural motif for the preparation of hybrid cages. The aim of this chapter is to describe the isolation of novel nanodimensional hybrid polyoxovanadate cages functionalised by aryl arsonates. These hybrid polyoxovanadate caged structures are found to have different electronic environments within their respective cavities and can accommodate anionic guests or neutral solvent molecules depending on the respective compound. The synthesis of these novel hybrid polyoxovanadate cages can be procured by influencing the assembly process through slight perturbations in the reaction conditions, *e.g.* by changing the pH of the reaction conditions. In addition to pH changes, we decided to investigate the influence of increasing the vanadium(IV): ligand ratio and its consequences on the self-assembly process.

3.2 Synthesis of a vanadium(IV) dodecanuclear cluster incorporating (4-aminophenyl)arsonic acid

3.2.1 The synthesis of $Na_4[V_{12}O_{14}(OH)_4(H_2O)_4(O_3AsC_6H_4\text{-}4\text{-}NH_2)_{10}]\cdot 3DMF\cdot 16H_2O$ (5)

The novel complex $Na_4[V_{12}O_{14}(OH)_4(H_2O)_4(O_3AsC_6H_4\text{-}4\text{-}NH_2)_{10}]\cdot 3DMF\cdot 16H_2O$ (**5**) forms under almost identical reaction conditions to that of **1**. However in order to prepare **5**, the pH of the reaction solution was lowered to *ca.* pH 4.9. From this solution, blue cubic crystals of **5** formed after several hours. The structure of **5** was charcterised using single crystal X-ray diffraction.

*-UV-vis study of the transformation of the cluster **1** into that of **5***

Upon decreasing the pH of the reaction system that yielded **1**, the characteristic green colour transforms into a light blue appearance and the crystallisation of **5** begins within a few hours. The colour change and the transformation between the clusters in **1** and **5** can be monitored by UV-vis spectroscopy (Fig. 3.1) allowing us to optimise the formation conditions for **5**.

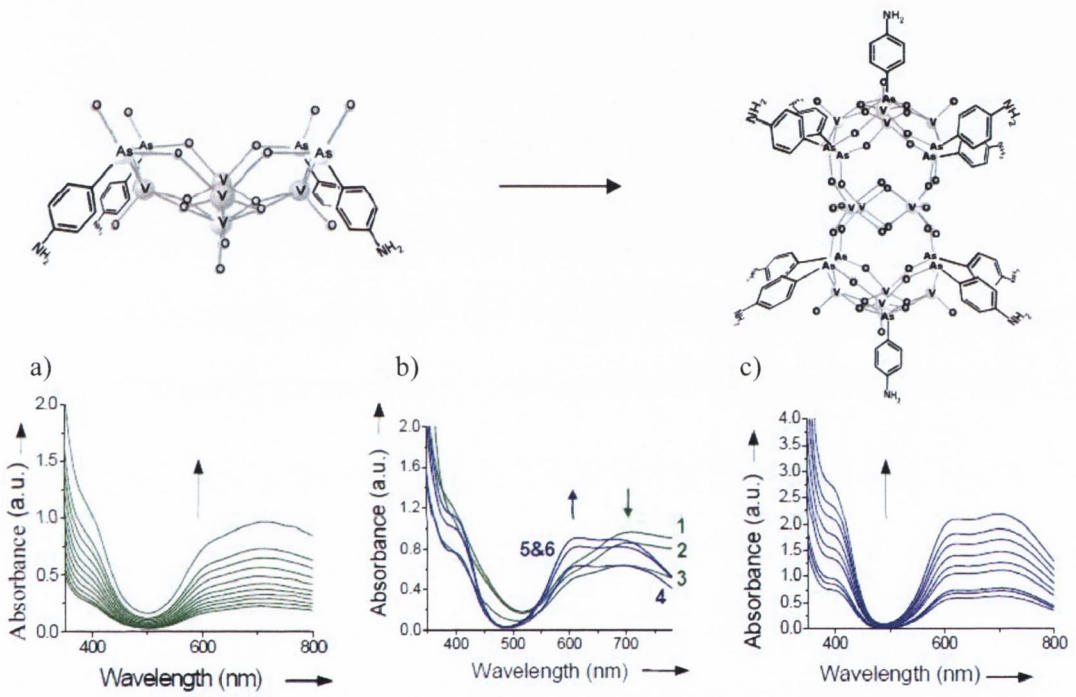

Figure 3.1 – The UV-vis spectra indicating the transformation of the anionic cluster of **1** into that of **5**. (a) and (c) concentration dependence of **1** and **5** in DMF/H_2O reaction mixtures, respectively (arrows indicate increasing concentration). (b) Transformation of the anionic cluster of **1** into that of **5** upon successively reducing the pH of five different reaction mixtures (spectrum 1 pH 7.3 to spectrum 6, pH = 4.86).

Reaction mixtures of **1** were stepwise acidified from pH 7.30 (green solution) to *ca.* pH 4.9 (turquoise/blue solution) and UV-Vis spectra were recorded at each different pH (Fig. 3.1b). The reaction mixtures containing the compounds are clearly disguisable in the visible region of the spectrum. DMF/H_2O reaction mixtures that produce **1** show absorption maxima at 721, 600 (sh) and 395 nm (Fig. 3.1a) whilst the solution that contains **5** which forms at pH 5

displays absorption maxima at 703, 624 and 404 nm (Fig. 3.1c). At this pH, these emerging bands reach a maximum and **5** separates, phase-pure from the solution.

3.2.2 The structural characterisation of $Na_4[V_{12}O_{14}(OH)_4(H_2O)_4(O_3AsC_6H_4\text{-}4\text{-}NH_2)_{10}]\cdot 3DMF\cdot 16H_2O$ (5)

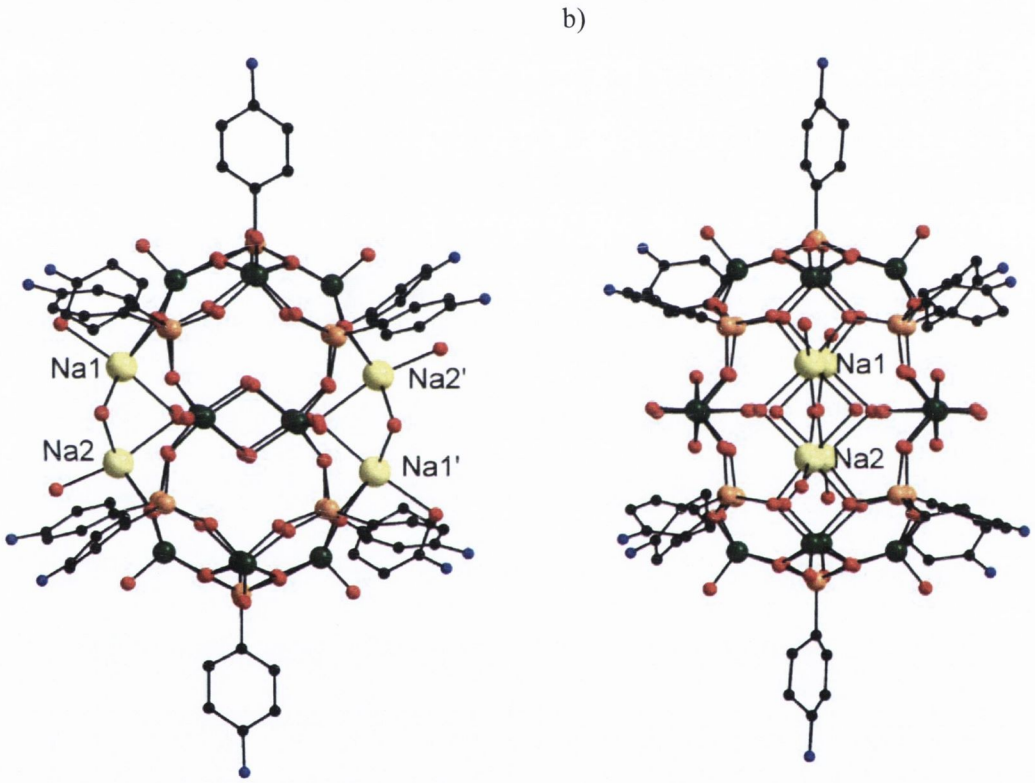

Figure 3.2 – (a - b) Ball and stick representations of the $Na_4(H_2O)_{10}[V_{12}O_{12}(OH)_4(H_2O)_4(O_3AsC_6H_4\text{-}4\text{-}NH_2)_{10}]$ cluster in **5** from two different perspectives; hydrogen atoms have been omitted for clarity. Colour code: V green, Na yellow, As orange, O red, N blue, C black.

$Na_4[V_{12}O_{14}(OH)_4(H_2O)_4(O_3AsC_6H_4\text{-}4\text{-}NH_2)_{10}]\cdot 3DMF\cdot 16H_2O$ (**5**) crystallises in the triclinc space group, *P*-1. The polyoxometalate cage in **5** contains 12 vanadium atoms, 10 (4-aminophenyl)arsonate ligands, 14 oxo ligands, 4 hydroxo ligands and four solvated sodium ions that are incorporated in the framework of the cage and compensate the negative charge

of the anionic hybrid polyoxovanadate cluster. The structure of the cluster contained within **5** can be seen in Fig. 3.2. The core structure is shown in Fig. 3.3.

The cluster can be visualised as the linkage of two 'calyx' clusters of **1** *via* eight arsonate functionalities and two $\{O_4V^{IV}(OH)_2V^{IV}O_4\}$ (Fig. 3.3b) units in which the V ions share a common edge of their distorted octahedral coordination polyhedra. Within one $\{O_4V^{IV}(OH)_2V^{IV}O_4\}$ unit the O-donors O(10), O(17), O(19), O(20) opposite to the common edge are provided by four (4-aminophenyl)arsonate ligands; two of these ligands link to the same 'calyx' rim.

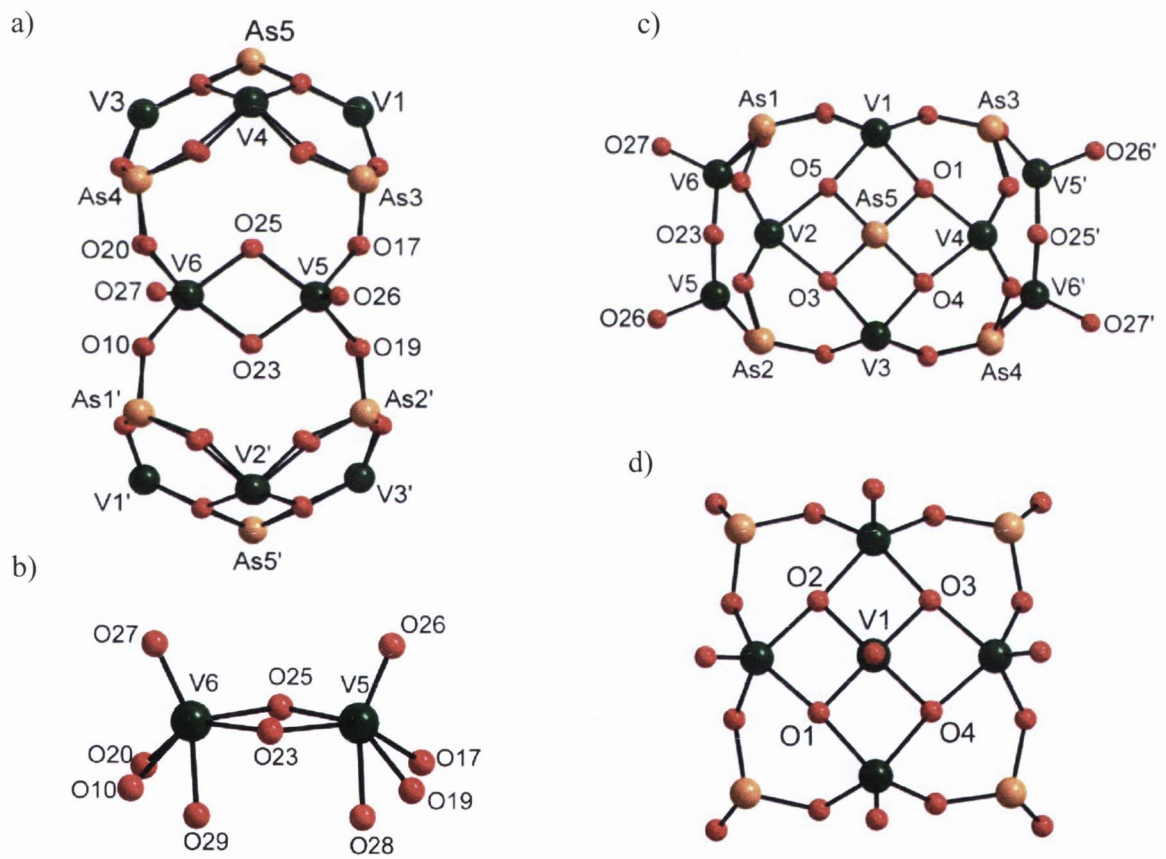

Figure 3.3 – Ball and stick representations of different perspective views of the V-O core structure in **5**. (a) The cluster core with a side on view onto the concave $\{AsO(\mu_2\text{-}O)_4V^{IV}{}_4O_{12}\}$ unit of **5** which is connected by four arsonate ligands to the two bridging dinuclear units. (b) The central dinuclear $\{O_4V^{IV}(OH)_2V^{IV}O_4\}$ bridging unit. (c) A plan view of the cluster core structure. (d) The vanadate centred mixed-valent pentanuclear cores present in **1** – **4**.

However, the $\{V^{V}O(\mu_3\text{-}O)_4V^{IV}{}_4O_{12}\}$ motif present in **1** is not exactly replicated in **5**; instead of the $\{V^{V}O_5\}$ unit, arsonate groups of the organic ligands extend the apex of the concave caps of the cage. The structural equivalence of the apical moieties, $\{As^{V}O_4\}$ and $\{V^{V}O_4\}$ can be explained by valence-bond considerations which predict similar As^{V}-O and V^{V}-O bond lengths.[46]

Table 3.1 – Bond sum valence analysis for **5**

V & O sites	Bond Valence Sum (BVS)	Assigned Oxidation State
V(1)	4.022	+4
V(2)	4.079	+4
V(3)	4.159	+4
V(4)	4.187	+4
V(5)	4.185	+4
V(6)	4.049	+4
μ_3-O (1) (3) (4) (5)	2.066-2.092	-2
μ-OH (23) (25)	1.191-1.206	-1
$O_{terminal}$	1.570-1.722	-2

Using bond valence sum analysis, the oxidation states of V(5) and V(6) were calculated to be +IV. The bond lengths between V(5), V(6) and the μ_2-hydroxo ligands O(23) and O(25) vary between 1.968(3) – 1.983(3) Å; bond distances between V(5), V(6) and the arsonate oxygen donors O(10), O(17), O(19), O(20) are in the range of 1.932(5) to 1.982(2) Å and the terminal V(5)=O_{term} and V(6)=O_{term} bond lengths are 1.603(2) and 1.610(3) Å long, respectively. The bond lengths between As(5) and μ_3-O^{2-} ligands O(1), O(3), O(4), O(5) vary between 1.801(3) – 1.815(2) Å (Fig. 3.3a). Bond valence sum analysis confirms that the peripheral vanadium ions of the concave capping unit, V(1), V(2), V(3) and V(4) adopt the oxidation state +IV, the bond distances between these vanadium centres and the μ_3-O^{2-} ligands range between 1.962(4) – 2.000(3) Å. The bond distances between these peripheral V centres and the peripheral arsonate ligand O donors vary between 1.920(5) – 1.959(5) Å whilst the terminal V=O bond distances for these ions are 1.596(4) and 1.621(3) Å long. The

calculated bond valence sum and the associated oxidation states of the vanadium and bridging oxygen atoms within the cluster anion of **5** are shown in Table 3.1.

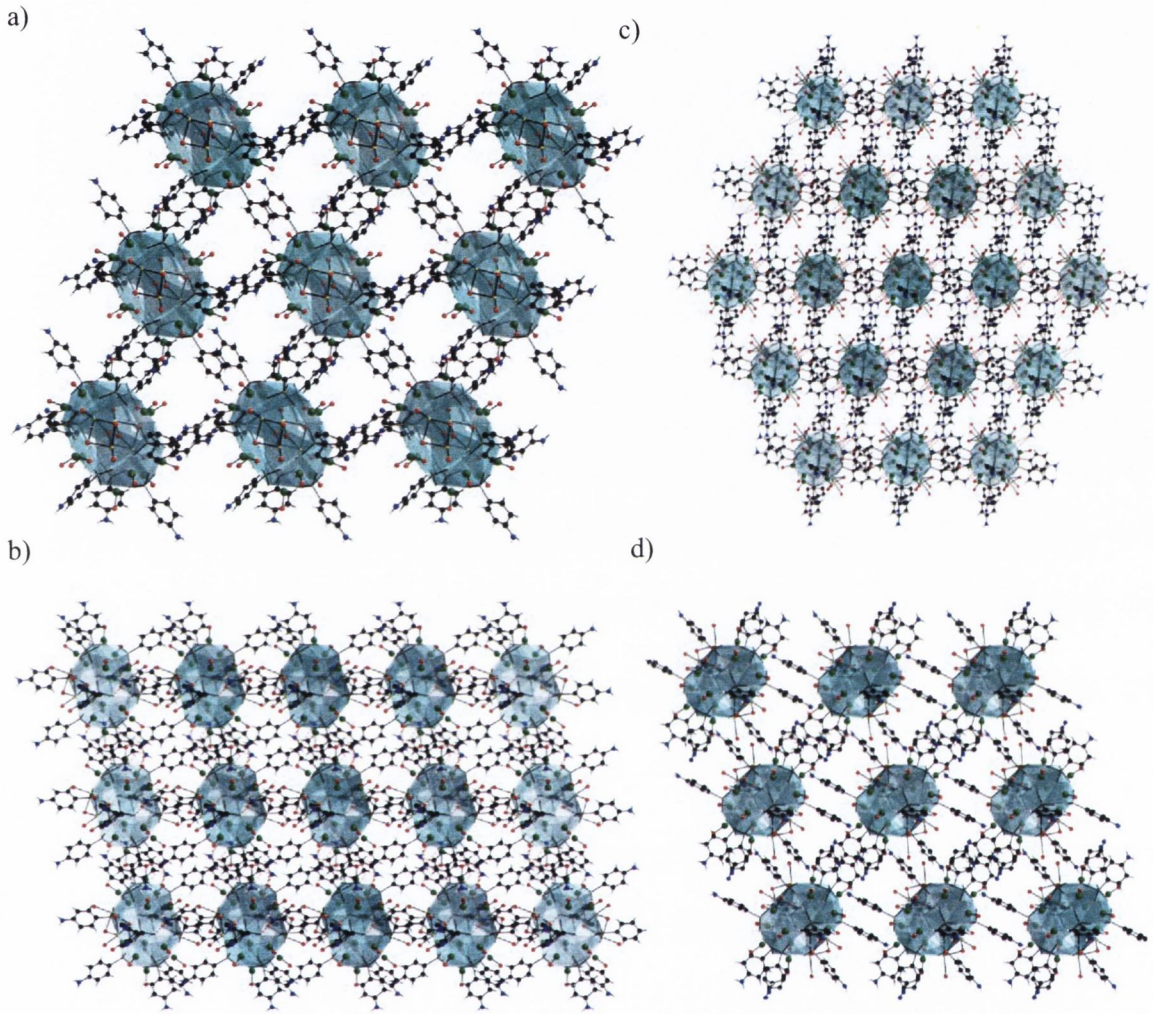

Figure 3.4 – Different perspective views of the $\{Na_4(H_2O)_{10}\}[V_{12}O_{12}(OH)_4(H_2O)_4(O_3AsC_6H_4\text{-}4\text{-}NH_2)_{10}]$ clusters in the crystal structure of **5**. (a) A view of the anionic cluster in the direction of the crystallographic *b*-axis; (b) in the [1,1,0] direction; (c) in the [1,1,1] direction and (d) in the direction of the crystallographic *c*-axis. Crystallisation solvent molecules have been omitted for clarity. Exterior cage dimensions shaded in light blue: approximately 11.8 Å x 8.6 Å x 8.2 Å. Colour code: V green, Na yellow, As orange, O red, N blue, C black, H white.

It is noted that a polyoxovanadate cluster with a similar core structure has been reported by Zubieta *et al.*[46] Differently to the structure reported by Zubieta *et al.*, the solid state structure of the cage in **5** is completed and closed by two $\{O_2(H_2O)Na(\mu_3\text{-}H_2O)_3Na\ (H_2O)O_2\}$ units to

give an overall neutral charge. Within this unit, distorted sodium octahedral coordination polyhedra share a common face and each of these dinuclear sodium units are linked *via* two arsonate O atoms to two vanadium atoms of the opposite concave cap of the cluster (Fig. 3.2b). The cavity of the cluster within the solid state structure of **5** might preferentially accommodate neutral guests considering that the four incorporated sodium counter-ions ions neutralise the negative charge on the anionic structure. The approximate dimensionality of the cavity in the anionic cluster of **5** is characterised by a rectangular arrangement of four peripheral As atoms in the capping motif with an As-As distance of 5.5 x 5.8 Å and a distance of 5.9 Å between the plane of these arsenic atoms in the two respective capping motifs within the cluster. Within the cavity of the anionic cluster of **5**, two symmetry related water molecules are located at the focal positions of the concave capping motifs. The interaction distances between the vanadium atoms V(1), V(2), V(3), V(4) and the residing water molecules vary from 3.146(7) Å to 3.476(4) Å.

The packing arrangement of the clusters cores in the crystal structure of **5** is shown in Fig. 3.4a – d. The clusters pack in such a way that a relatively open-framework structure results. The cavities between the clusters are occupied by constitutional water and DMF solvent molecules. The spacing between the clusters is a result of a rather complicated network of weak interactions between the H atoms of the amine functionalities and the terminal O atoms of the V=O bonds. The weak interaction distances between the donor and acceptor atoms range from 3.048(17) to 3.432(21) Å.

3.2.3 Further solid state characterisation of $Na_4[V_{12}O_{14}(OH)_4(H_2O)_4(O_3AsC_6H_4\text{-}4\text{-}NH_2)_{10}]\cdot 3DMF\cdot 16H_2O$ (5); Thermogravimetric analysis and Infrared spectroscopy

- Thermogravimetric analysis

The stability of **5** was investigated by thermogravimetric analysis in air between 30 °C and 900 °C (Fig. 3.5a). A broad step between 25 °C and 200 °C (13.6%) corresponds to the loss of constitution water molecules, coordinated water molecules and DMF solvent. The oxidative degradation of the organic ligands above 300 °C (23.6%) destroys the hybrid cluster. A thermogravimetric step at 565 °C is observed in air and is expected to be associated with oxide formation.

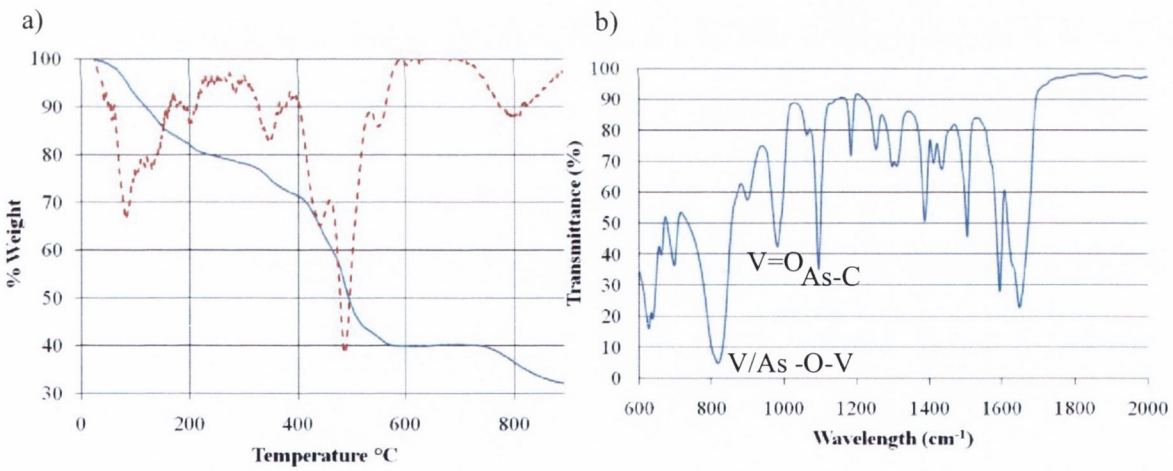

Figure 3.5 – (a) Thermogravimetric analysis of **5** in air (blue line) and the derivative of the measured TGA line (red dashed line). (b) An infrared spectrum of **5**.

- Infrared spectroscopy

An infrared spectrum of **5** was recorded and is shown in Fig. 3.5b. The infrared spectrum of **5** is very similar to that of **1**. The characteristic stretches of the (4-aminophenyl)arsonate ligand are present and include the As-C stretch at 1097 cm^{-1} and the As-O stretch at 898 cm^{-1}.[46, 47]

The stretches at *ca.* 822 cm^{-1} originate from {V-O-As} or {V-O-V} units in the cluster core. These infrared band stretches correspond to those previously reported for polyoxovanadates functionalised with organoarsonates.[46, 47] There is a carbonyl stretch at 1653 cm^{-1} due to the DMF molecules present in the structure of **5**. A broad band at *ca.* 3365 cm^{-1} can be attributed to the water of crystallisation (see appendix 3). There is a band stretch at 985 cm^{-1} due to the V=O bond. Similarly to **1**, the IR spectrum of **5** reveals bands that originate from the arsonate ligand and these bands were assigned by comparing the spectrum of (4-aminophenyl)arsonic acid with that of **5**. Stretches ranging between 1440-1625cm^{-1} are related to the aromatic functionalities of organic ligand.[88, 89]

3.2.4 Characterisation of $Na_4[V_{12}O_{14}(OH)_4(H_2O)_4(O_3AsC_6H_4\text{-}4\text{-}NH_2)_{10}]\cdot 3DMF\cdot 16H_2O$ (5) in solution; NMR, Mass spectrometry and UV-vis spectroscopy

- NMR

The cluster of **5** appears to be stable in DMSO. A ^1H NMR spectrum was recorded in deuterated DMSO and four broad peaks were observed. The broadening of the peaks can be attributed to the paramagnetic nature of the vanadium(IV) metal centres. The four peaks appear at 10.07 ppm (br, 20H, NH_2), 7.71 ppm (br, 4H), 7.05 ppm (br, 16H), 5.67 ppm (br, 20H) and integrate in a 5:1:4:5 ratio which is consistent with the crystallographically determined structure. The three most upfield peaks were assigned to the aromatic H atoms of the (4-aminophenyl)arsonate ligand while the most downfield peak was assigned to the amine H atoms of the organic ligand. The full spectrum can be found in the appendix 3.

-Mass spectrometry

Compound **5** was dissolved in DMSO and analysed by electrospray mass spectrometry. The mass spectrum of **5** was measured in the negative ionisation mode and consists of many defragmentation signals (see appendix 3).

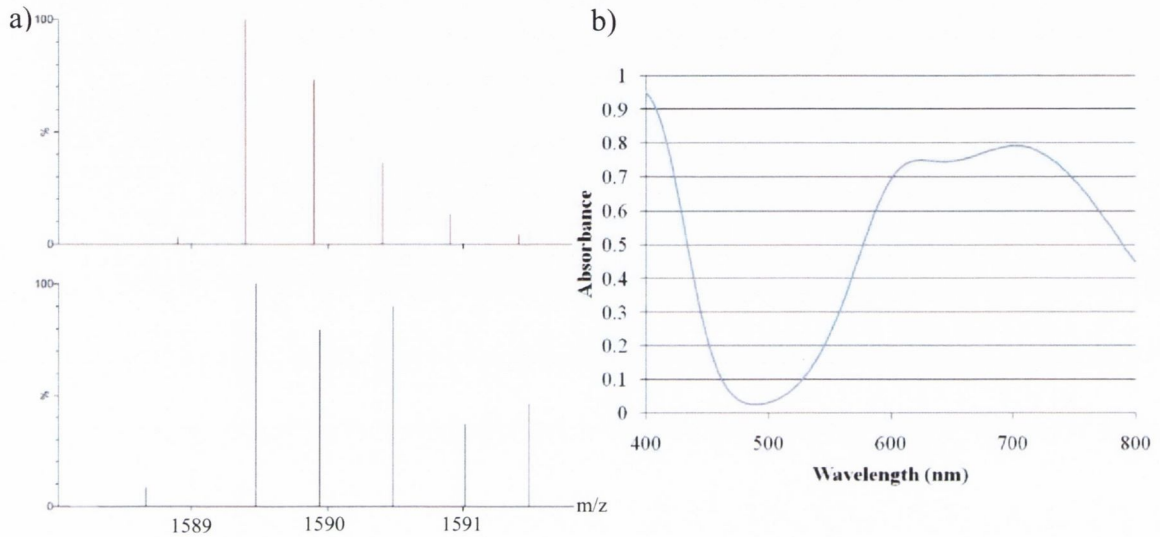

Figure 3.6 – The characterisation of **5** in solution. (a) Modelled isotopic envelope for $Na_4[(H_2O)_2\subset V_{12}O_{16}(OH)_2(O_3AsC_6H_4\text{-}4\text{-}NH_2)_{10}]^{2-}$ m/z = 1589.4 (top) and electrospray mass spectrometry in the negative mode of a DMSO solution of **5** (bottom). (b) UV-vis spectroscopy of 1mM solution of **6** in DMSO.

A signal arising from a -2 charged species is observed at m/z = 1571.82 and corresponds to the deprotonated anionic cluster of **5** with four coordinating sodium counter-ions, $Na_4[V_{12}O_{16}(OH)_2(O_3AsC_6H_4\text{-}4\text{-}NH_2)_{10}]^{2-}$. A second related signal arising from a -2 charged species is observed at m/z = 1560.83 and corresponds to the mono-deprotonated anionic cluster of **5** and three sodium counter-ions, $Na_3[V_{12}O_{15}(OH)_3(O_3AsC_6H_4\text{-}4\text{-}NH_2)_{10}]^{2-}$. The intense signal observed at m/z = 1589.4742 arising from a -2 charged species was modelled (Fig. 3.6a) and corresponded to the deprotonated anionic cluster of **5** with four sodium counter-ions and two water molecules, $Na_4[(H_2O)_2\subset V_{12}O_{16}(OH)_2(O_3AsC_6H_4\text{-}4\text{-}NH_2)_{10}]^{2-}$. There is also an intense signal at m/z = 1426.58 of a charged species present in the mass spectrum of **5**. Although this signal cannot be assigned, it is thought to be a stable

defragmentation ion as it appears in the mass spectra of the related compound **7** which will be discussed later within this chapter. An intense signal at m/z = 215.96 corresponds to the deprotonated (4-aminophenyl)arsonate ligand and is also observed in the mass spectrum of **1**.

-UV-vis spectroscopy

The UV-vis spectrum of **5** was measured in DMSO (Fig. 3.6b). A broad absorption between 400 nm and 480 nm is observed due to the π(O) – d(V) ligand to metal charge transfer between the (4-aminophenyl)arsonate ligand and the vanadium ions. In the visible region, two broad absorptions due to d-d transitions are observed at 710nm (ε = 789.2 $L.mol^{-1}cm^{-1}$) and 620nm (ε = 748.0 $L.mol^{-1}cm^{-1}$). The UV-vis spectrum of **5** in DMSO is in agreement with the UV-vis analysis of the reaction mixture when investigating the transformation of **1** into **5** (see 3.2.1).

Table 3.2 – Crystal data and structure refinement for **5**.

Identification code	Compound **5**	
Empirical formula	$C_{69}H_{52}As_{10}N_{13}Na_4O_{71}V_{12}$	
Formula weight	3651.68 g mol^{-1}	
Temperature	150(2) K	
Wavelength	0.71073 Å	
Crystal system	Triclinic	
Space group	*P* -1	
Unit cell dimensions	a = 16.554(3) Å	α = 115.32(3)°.
	b = 16.745(3) Å	β = 101.25(3)°.
	c = 16.777(3) Å	γ = 100.32(3)°.
Volume	3938.0(14) $Å^3$	
Z	1	
Density (calculated)	1.540 Mg/m^3	
Absorption coefficient	2.856 mm^{-1}	
F(000)	1775	
Crystal size	0.25 x 0.25 x 0.1 mm^3	
Theta range for data collection	1.41 to 25.57°.	
Index ranges	-20<=h<=20, -20<=k<=20, -20<=l<=20	
Reflections collected	30268	
Independent reflections	10690 [R(int) = 0.0504]	
Completeness to theta = 25.57°	99.9 %	
Refinement method	Full-matrix least-squares on F^2	
Data / restraints / parameters	10690 / 6 / 887	
Goodness-of-fit on F^2	1.229	
Final R indices [I>2sigma(I)]	R_1 = 0.0745, wR_2 = 0.2090	
R indices (all data)	R_1 = 0.1153, wR_2 = 0.2223	
Largest diff. peak and hole	1.052 and -1.063 e.$Å^{-3}$	

3.3 Synthesis of a mixed-valent vanadium tetradecanuclear cluster incorporating (4-aminophenyl)phosphonic acid

3.3.1 The synthesis of $Na_4H_2[V_{14}O_{22}(OH)_4(H_2O)_2(O_3PC_6H_4\text{-}4\text{-}NH_2)_8]\cdot 7DMF\cdot 12H_2O$ (6)

Upon the isolation of the organoarsonate functionalised hybrid cluster core in **5**, we set about to investigate if a structurally analogous organophosphonate cluster core could be synthesised. Following these investigations, the novel complex $Na_4H_2[V_{14}O_{22}(OH)_4(H_2O)_2(O_3PC_6H_4\text{-}4\text{-}NH_2)_8]\cdot 7DMF\cdot 12H_2O$ (**6**) was synthesised through the self assembly of (4-aminophenyl)phosphonic acid and sodium metavanadate using hydrazine hydrate in a water/DMF solution. The pH of the resultant reaction mixture was approximately neutral (pH 7.30). Green cubic crystal were observed in the solution after two weeks and the structure of **6** was determined by single crystal X-ray diffraction.

3.3.2 The structural characterisation of $Na_4H_2[V_{14}O_{22}(OH)_4(H_2O)_2(O_3PC_6H_4\text{-}4\text{-}NH_2)_8]\cdot 7DMF\cdot 12H_2O$ (6)

The mixed-valent tetradecanuclear compound $Na_4H_2[V_{14}O_{22}(OH)_4(H_2O)_2(O_3PC_6H_4\text{-}4\text{-}NH_2)_8]\cdot 7DMF\cdot 12H_2O$ (**6**) crystallises in the orthorhombic space group, *I*mmm. The asymmetric unit contains one (4-aminophenyl)phosphonate ligand and four vanadium ions. The complete cluster is generated through symmetry operations and is show in Fig. 3.7.

The functionalised core structure of **6** is very similar to that of **5**. However the substitution of arsonate ligands with phosphonate ligands results in a slight modification within the capping motif of the resulting cage structure. Two arsonate ligands situated in the apical positions of

the cage structure of **5** have formally been replaced by two $\{V^{V}O_5\}$ moieties in **6**. The resulting in a mixed-valent pentanuclear $\{V^{V}O(\mu_3\text{-}O)_4V^{IV}{}_4O_{12}\}$ that correlates to the core structures of **1** – **4**.

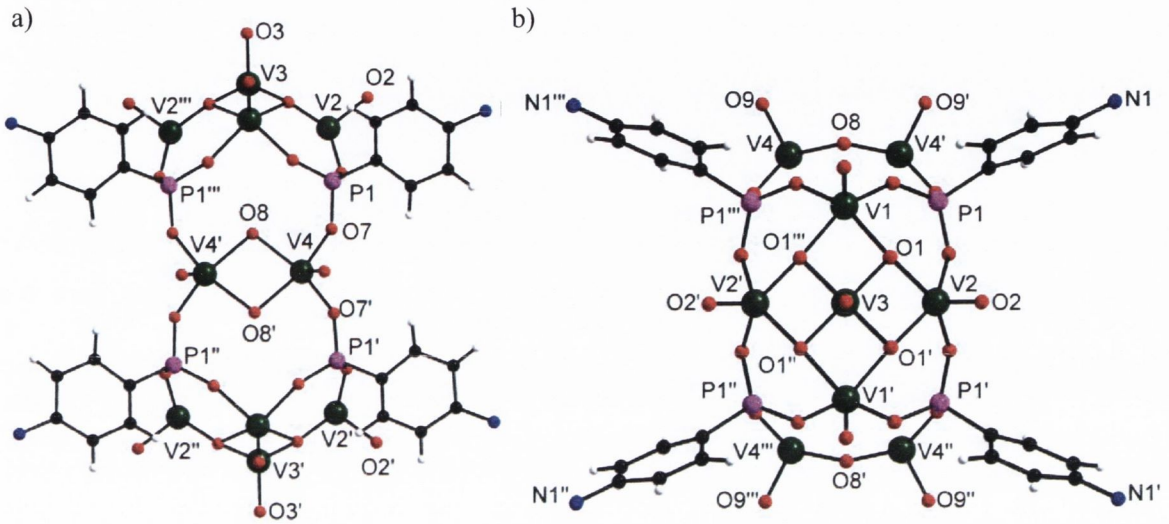

Figure 3.7 – (a) A ball and stick representation of the anionic cluster in **6** viewed along the crystallographic *a*-axis. (b) The anionic cluster in **6** when viewed in the crystallographic *c*-axis. Colour code: V green, P purple, O red, N blue, C black, H white.

Our investigations underline the structural equivalence of $\{AsO_4\}$ and $\{VO_4\}$ units in polyoxometalates (compare **1** – **4** with **5**). The mutual displacement of the $\{AsO_4\}$ and $\{VO_4\}$ units is the result of almost identical geometries and bond lengths. However in contrast, homologous organophosphonates display significantly shorter P-O distances thus limiting the displacement of $\{V^{V}\text{–}O\}$ units by $\{P\text{–}O\}$ units. Thus, the hypothetical phosphonate-containing capping motif could not be isolated throughout this study. Bond lengths comparisons based on bond valence sum calculations shown in Table 3.3 substantiate this observation.

The bond length between the central V(3) ion in the mixed-valent capping motif and the μ_3-O^{2-} ligand O(1) is 1.865(1) Å whilst the bond distance of the terminal $V(3)=O_{term}$ bond is 1.600(1) Å (Fig. 3.7). The bond distance between the peripheral vanadium ions V(1) and

V(2) and the μ_3-O^{2-} ligands is 1.967(2) Å and 1.968 Å respectively. The bond distances between these V centres and the (4-aminophenyl)phosphonate ligand O donors vary between 1.968(2) Å and 1.972(2) Å whilst the terminal V=O bond distances vary between 1.586(1) – 1.600(1) Å. The bond distance between V(4) in the bridging dinuclear unit and the μ_2-hydroxo ligand O(4) is 1.998(2) Å. The bond distance between the V(5) and the arsonate oxygen donor atom O(7) is 1.960(2) Å and the bond length of the terminal V=O_{term} term is 1.594(1) Å.

Using bond valence sum analysis, the peripheral vanadium V(1) and V(2) ions were calculated to be in oxidation state +IV. The central vanadium V(3) ion in the mixed-valent pentanuclear sub-unit is calculated to be in the oxidation state +V. The vanadium V(4) ion in the inorganic dinuclear bridging unit is calculated to be in oxidation state +IV. The calculated bond valence sum and the assigned oxidation states of the vanadium and bridging oxygen atoms are shown in Table 3.3.

Table 3.3 – Bond sum valence analysis for **6**

V & O sites	Bond Valence Sum (BVS)	Assigned Oxidation State
V(1)	4.163	+4
V(2)	4.104	+4
V(3)	5.115	+5
V(4)	3.883	+4
μ_3-O (1)	2.064	-2
μ-OH (8)	1.090	-1
$O_{terminal}$	1.671-1.731	-2
Reference Radius (Ro) used for BSV	Radius Ro (Å)	Difference (Å)
$V^V - O^{2-}$	1.803	
$As^V - O^{2-}$	1.767	0.036
$P^V - O^{2-}$	1.617	0.186

The approximate dimensionality of the cavity within **6** are similar to **5** and are characterised by a box arrangement of eight P atoms with an P-P distance of 5.2 x 5.6 Å in the capping

motif and a distance of 5.7 Å between the phosphorus atoms in the two respective capping motifs within the cluster.

As for **5**, the anionic cage in **6** is closed by two $\{O_2(H_2O)Na(\mu_3\text{-}H_2O)_3Na(H_2O)O_2\}$ units. Within this dinuclear sodium unit, the distorted octahedral coordination polyhedra share common faces. The two dinuclear sodium units are incorporated in the anionic cluster and are linked *via* two phosphonate oxygen donors to two vanadium atoms of the opposing mixed-valent pentanuclear concave caps of the cluster (Fig. 3.8a).

Figure (3.8a – d) shows the packing arrangement of clusters in the crystal structure of **6**. The anionic clusters in **6** pack so that a relatively open-framework structure ensues. The amine functionalities of the (4-aminophenyl)phosphonate ligands incorporated within the anionic clusters point at the terminal O atoms of the central V=O bonds of the mixed-valent pentanuclear concave caps of neighbouring anionic clusters (Fig. 3.8b). The nitrogen functionalities impose control in the self-assembly process resulting in a functionalised polyoxovanadate open-framework structure which contrasts similar functionalised polyoxovanadates.[38] The interaction distance between the nitrogen atoms in the amine group of the organophosphonate ligands and the oxygen atoms of the terminal oxygen ligands of the dinuclear vanadium units is 2.920(1) Å and is within the reported donor/acceptor distances reported for similar compounds displaying hydrogen bonding.[87] This open-framework structure contains channels between the clusters of *ca.* 1 nm diameter which are occupied by constitutional water molecules and disordered DMF molecules and these channels run parallel to the direction of the crystallographic *a*-axis.

The given formula for this compound was derived from CHN analysis. The partial dehydration and disorder of the solvent molecules in the crystal structure did not allow us to locate all the solvent molecules by single X-ray diffraction. It was deemed appropriate to use

the program SQUEEZE to model these disordered solvents within the crystal structure.[90]

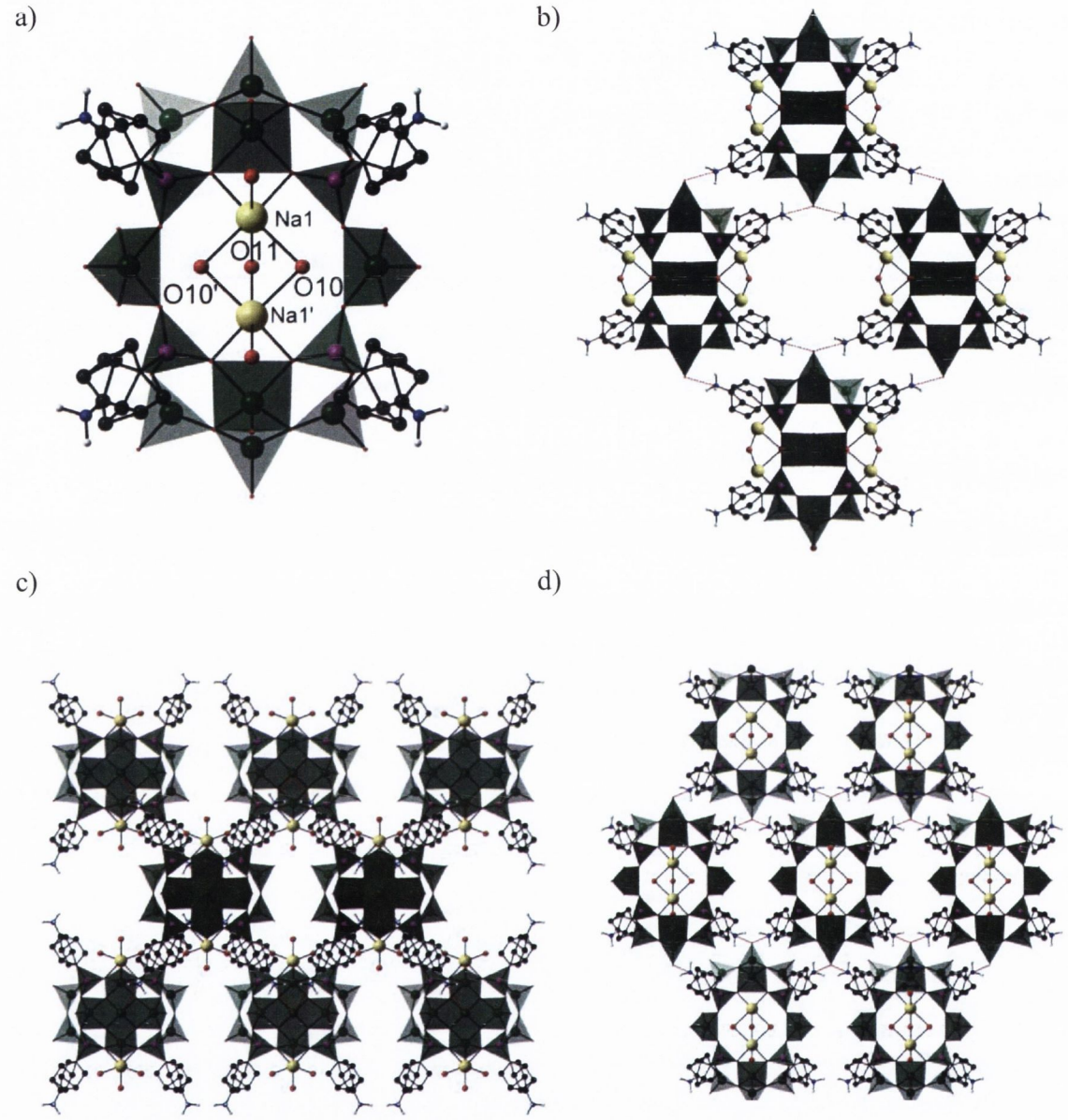

Figure 3.8 – A polyhedral representation of the anionic cluster core of **6**. (a) The incorporation of the dinuclear sodium counter-ions has been highlighted. Different perspective views of the crystal packing of the anionic cluster in **6** as viewed: (b) along the crystallographic *a*-axis; (c) along the crystallographic *c*-axis and (d) along the crystallographic *b*-axis. Selected hydrogen bonds have indicated with red dashed lines between the donor and acceptor atoms. Colour code: $\{VO_n\}$ polyhedra green, Na yellow, O red, N blue, C black, H white.

3.3.3 Further characterisation of the compound $H_2Na_4[V_{14}O_{22}(OH)_4(H_2O)_2(O_3PC_6H_4\text{-}4\text{-}NH_2)_8]\cdot 7DMF\cdot 12H_2O$ (6)

-Infrared spectroscopy

The infrared spectrum of **6** confirms the inclusion of the (4-aminophenyl)phosphonate ligand within the compound (Fig. 3.9a and appendix 3). Characterestic signals appear at 1652 cm^{-1} due to the carbonyl stretch of the DMF solvent molecules, at 1076 cm^{-1} for the P-C bond stretch of the phosphonate ligand, at 991 cm^{-1} due to the V^{IV}=O bond stretch and at 830 cm^{-1} as a result of the P-O bond stretch. The infrared stretch arising from the V^{IV}=O bond stetch is so broad that the V^{V}=O stretch could not be resolved. This assigment is in agreement with those of reported phosphonate structures.[38, 42, 88, 89]

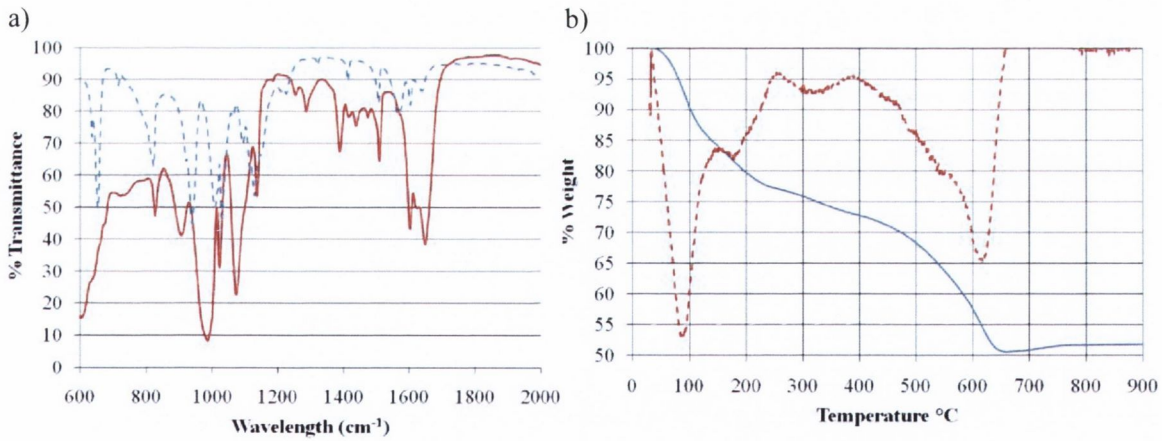

Figure 3.9 – Solid state characterisation of **6**: (a) Infrared spectrum of **6** (red) compared with that of (4-aminophenyl)phosphonic acid (blue dashed line). (b) A thermogravimetric analysis of **6** (blue line) carried out in air between 30 °C and 900 °C. The derivation of the thermogravimetric curve is also shown (red dashed line).

-Thermogravimetric analysis

The thermogravimetric analysis on the fresh crystals of **6** was performed in air in the temperature range between 30 °C and 900 °C (Fig. 3.9b). The first broad weight loss event between 30 °C and 250 °C corresponds to the loss of the crystallisation water molecules and the DMF molecules (33%). The second weight loss event centred at *ca.* 318 °C is presumed to correspond to the initial decomposition of the organic ligand and the destruction of **6** (4%). A third major broad weight loss event which is observed in a temperature range between *ca.* 390 °C and 660 °C is related to the complete oxidative degradation of the organic moieties in **6** (23%) and the formation of an inorganic oxide.

Table 3.4 – Crystal data and structure refinement for **6**.

Identification code	Compound **6**
Empirical formula	$C_{54}\ H_{32}\ N_{10}\ Na_2\ O_{68}\ P_8\ V_{14}$
Formula weight	2928.60 g mol^{-1}
Temperature	150(2) K
Wavelength	0.71073 Å
Crystal system	Orthorhombic
Space group	*I*mmm
Unit cell dimensions	a = 14.0233(11) Å $\alpha = 90°$.
	b = 19.8137(16) Å $\beta = 90°$.
	c = 26.169(2) Å $\gamma = 90°$.
Volume	7271.2(10) $Å^3$
Z	2
Density (calculated)	1.338 Mg/m^3
Absorption coefficient	1.028 mm^{-1}
F(000)	2881
Crystal size	0.15 x 0.15 x 0.1 mm^3
Theta range for data collection	1.65 to 25.05°.
Index ranges	-16<=h<=16, -23<=k<=23, -31<=l<=31
Reflections collected	38818
Independent reflections	3541 [R(int) = 0.1066]
Completeness to theta = 25.05°	99.7 %
Refinement method	Full-matrix least-squares on F^2
Data / restraints / parameters	3541 / 0 / 264
Goodness-of-fit on F^2	1.071
Final R indices [I>2sigma(I)]	$R_1 = 0.0670$, $wR_2 = 0.1893$
R indices (all data)	$R_1 = 0.0800$, $wR_2 = 0.1983$
Largest diff. peak and hole	1.259 and -0.828 e.$Å^{-3}$

3.4 Synthesis of vanadium(IV) tetradecanuclear cluster incorporating (4-aminophenyl)arsonic acid

3.4.1 The synthesis of $Na_4H_2[Cl_2{\subset}V_{14}O_{14}(OH)_8(O_3AsC_6H_4\text{-}4\text{-}NH_2)_{10}]\cdot 6DMF\cdot 15H_2O$ (7)

The novel complex $Na_4H_2[Cl_2{\subset}V_{14}O_{14}(OH)_8(O_3AsC_6H_4\text{-}4\text{-}NH_2)_{10}]\cdot 6DMF\cdot 15H_2O$ (**7**) forms through the self-assembly of (4-aminophenyl)arsonic acid and sodium vanadate in the presence of the reducing agent hydrazine monohydrate using similar synthethic conditions to those employed in the formation of **1** and **5**. However in this case, the metal ligand ratio was altered from a 1:2 ratio to a 3:2 ratio (metal in excess). The pH of the reaction solution was again lowered below pH 5 and from this solution, blue cubic crystals of **7** formed after four weeks. The structure of **7** was characterised through single crystal X-ray diffraction.

3.4.2 The structural characterisation of the tetradecanuclear vanadium cluster $Na_4H_2[Cl_2{\subset}V_{14}O_{14}(OH)_8(O_3AsC_6H_4\text{-}4\text{-}NH_2)_{10}]\cdot 6DMF\cdot 15H_2O$ (7)

Compound $Na_4H_2[Cl_2{\subset}V_{14}O_{14}(OH)_8(O_3AsC_6H_4\text{-}4\text{-}NH_2)_{10}]\cdot 6DMF\cdot 15H_2O$ (**7**) crystallises in the triclinic space group, *P*-1. The polyoxometalate core of **7** contains exclusively vanadium metal centers in the oxidation state +IV, similar to that of **5**. The structure of this anionic cluster is closely related to that of **5**, however, the core structure has now been extended and contains 14 vanadium atoms linked *via* 10 (4-aminophenyl)arsonate ligands (Fig. 3.10). There are four solvated sodium counter-ions incorporated in the cage structure. Again, the construction of this cage can be rationalised from the linkage of two 'calyx'-clusters of **1** *via* eight arsonate functionalities. However, the $\{V^{V}O(\mu_3\text{-}O)_4V^{IV}{}_4O_{12}\}$ motif present in **1** is not

exactly replicated in **7**. Comparably to **5** (Fig. 3.2a, 3.3c), the capping unit of **7** consists of a tetranuclear vanadium(IV) $\{NH_2C_6H_4AsO_3(\mu_3\text{-}O)V^{IV}{}_4O_{12}\}$ sub-unit with a centrally located organoarsonate ligand (Fig. 3.10).

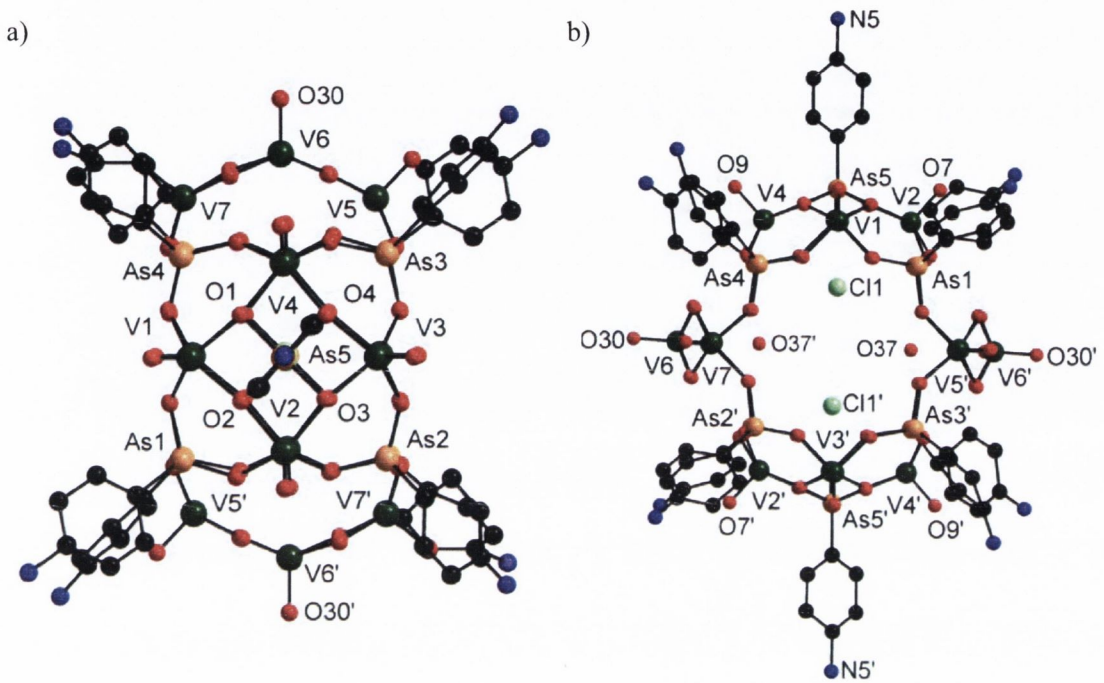

Figure 3.10 – (a) Anionic cluster in **7**, $[Cl_2{\subset}V_{14}O_{14}(OH)_8(O_3AsC_6H_4\text{-}4\text{-}NH_2)_{10}]^{4-}$ when viewed along the axial positioned (4-aminophenyl)arsonate ligand at the apex of the cluster; (b) The anionic cluster in **7** as viewed side on. H atoms have been omitted for clarity. Colour code: V green, Cl light green, Na yellow, As orange, O red, N blue, C black.

The structure of this sub-unit consists of the peripheral vanadium ions V(1), V(2), V(3) and V(4) linked through the $\mu_3\text{-}O^{2-}$ ligands O(1), O(2), O(3), O(4) and these have bond lengths that range between 1.968(3) – 2.009(3) Å. The $\mu_3\text{-}O^{2-}$ ligands originate from the arsonate ligand As(5) which is located at the apex of the concave caps of the cage. The distances between the $\mu_2\text{-}O^{2-}$ oxygen donors of the peripheral arsonate ligands and the vanadium ions of the capping unit range between 1.912(1) – 1.977(2) Å. The two dinuclear vanadium $\{O_4V^{IV}(OH)_2V^{IV}O_4\}$ bridging units that are present in **5** have now been extended to two trinuclear $\{O_5V^{IV}(OH)_2V^{IV}O(OH)_2V^{IV}O_5\}$ bridging units in **7**, thereby increasing the 'inorganic belt' within this type of cluster.

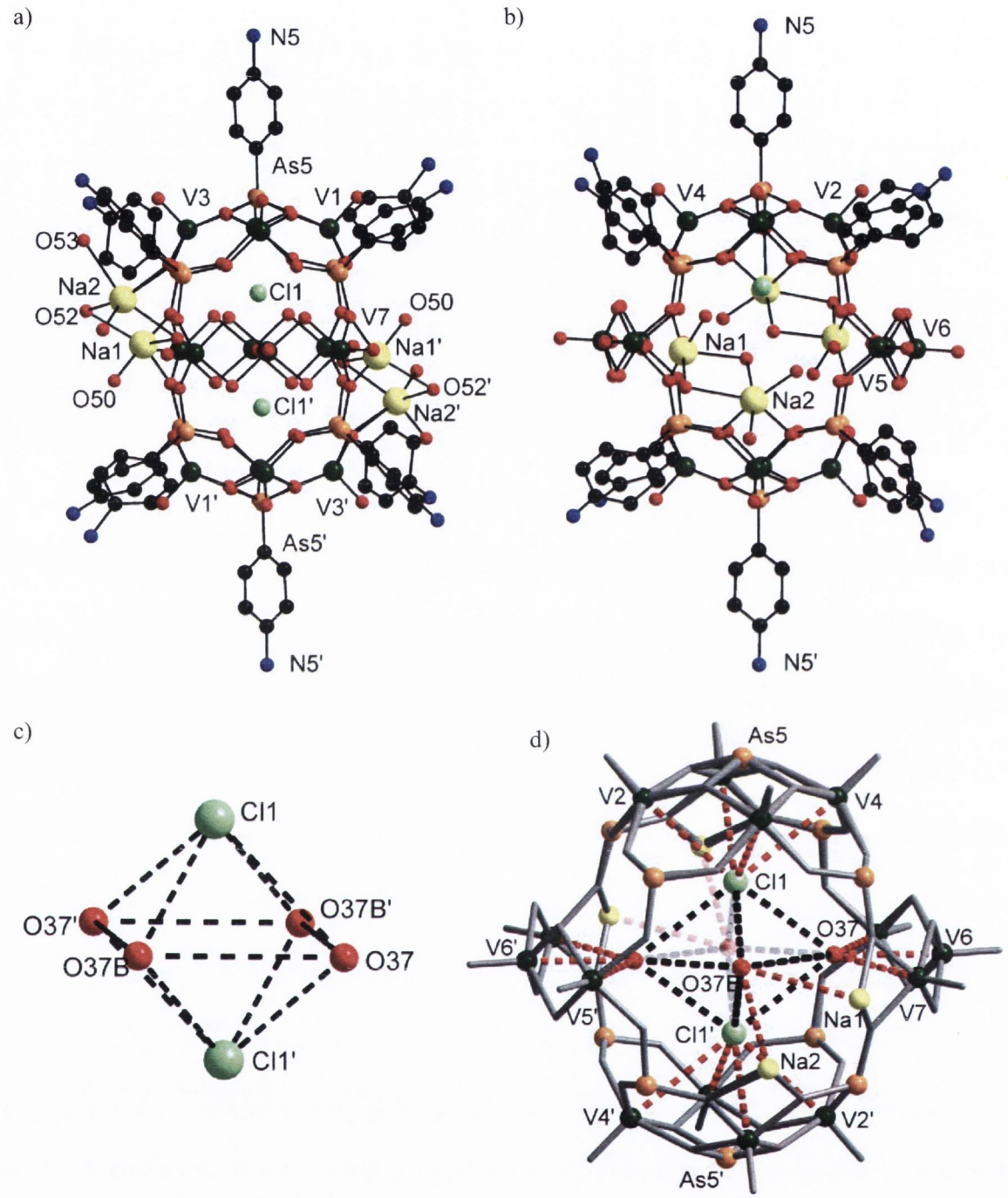

Figure 3.11 – A polyhedral representation of the cluster in **7**. (a) Side on view of the $\{Na_4(H_2O)_{10}\}[V_{12}O_{12}(OH)_4(H_2O)_4(O_3AsC_6H_4\text{-}4\text{-}NH_2)_{10}]$ (b) An adjacent side on perspective of the cluster in **8**. (c) Arrangement between the chloride ions and the water molecules within the cluster cavity, (O(37), 0.75 occupancy, O(37B) 0.25 occupancy) (d) The cluster core in **7** represented as a grey wire frame with the interactions between the guest molecules and the cluster core atoms highlighted using red dashed lines. Phenyl rings and H atoms have been deleted for clarity. Colour code: V green, Cl light green, Na yellow, As orange, O red, N blue, C black.

The bond distances between the vanadium ions in the trinuclear $\{O_5V^{IV}(OH)_2V^{IV}O(OH)_2V^{IV}O_5\}$ unit and the μ_2-hydroxo ligands are in the range 1.935(3) – 1.984(3) Å. The bond lengths between all the vanadium ions and their respective terminal oxo ligands are in the range of 1.524(2) – 1.585(2) Å. Bond valence sum analysis confirms that all the vanadium centres are in the oxidation state +IV. The results of this analysis are summarised in Table 3.5.

Table 3.5 – Bond sum valence analysis for **7**

V & O sites	Bond Valence Sum (BVS)	Assigned Oxidation State
V(1)	4.251	+4
V(2)	4.155	+4
V(3)	4.158	+4
V(4)	4.207	+4
V(5)	4.463	+4
V(6)	4.15	+4
V(7)	4.386	+4
μ_3-O (1) (2) (3) (4)	2.042-2.171	-2
μ-OH (23) (24) (25)(26)	1.161-1.237	-1
$O_{terminal}$	1.708-2.019	-2

The extension of the inorganic belt does not infer extra charge on the cluster as the terminal oxo ligands as well as the bridging hydroxo ligands neutralise the additional charge originating from the addition of the extra vanadium(IV) ions. The extension of the inorganic belt leads to a larger cage cavity in which two chloride ions and two water molecules are accommodated (Fig. 3.10b, Fig. 3.11). The cavity in the anionic cluster of **7** is slightly more symmetric when compared to the cavity in **5**. The cavity in the anionic cluster of **7** is characterised by an almost ideal cubic arrangement of eight As atoms with As-As-As distances of 5.8 x 5.8 x 5.9 Å along the cubic edges. Chloride ions are located at the focal points of the concave shaped capping units, $\{NH_2C_6H_4AsO_3(\mu_3\text{-}O)V^{IV}{}_4O_{12}\}$. The interaction distances between the central chloride ions and the vanadium ions of the capping sub-unit are in the range of 3.539(3) Å to 3.622(3) Å (Fig. 3.11d). The host-guest interaction of the

polyoxometalate cage with the halide atoms is a result of the weak interactions of the chloride anions with the Lewis acidic V^{IV} centers. [16, 38] However, there are also weak repulsive forces due to the presence of the oxygen O(1), O(2), O(3) and O(4) donors with negative partial charges that form part of the capping sub-unit. The interaction distance between these μ_3-O^{2-} oxygen donors and the chloride ions are in the range of 3.369(3) – 3.459(1) Å. Two water molecules (O(37), O(37')) are located at the centre of each arch shaped trinuclear bridging unit. Each of these water molecules is disordered over two positions (O(37) – 0.75% occupancy, O(37B) – 0.25% occupancy). The interaction distances between the water molecules and the vanadium centres in the inorganic belt is in the range from 2.997(2) Å to 3.352(3) Å. The distance between the chloride ions Cl(1) and Cl(1') and the water molecules (O(37), O(37')) is 3.481(3) Å and 3.495(3) Å, respectively (Fig. 3.11c). The incorporation of halide anions in other polyoxovanadate cages has previously been observed in the literature in both purely inorganic polyoxovanadates[16] as well as in hybrid polyoxovanadates[38] and has been discussed in Chapter 1, 1.2.2. The four sodium counter-ions do not seem to interact with the Cl^- ions; distances between the sodium ions and the central chloride anions are 5.071(2) and 5.325(7) Å long. The packing of the cluster anions in the crystal structure of **7** is seen in Fig. 3.12 and shows that these clusters pack in a similar manner to the clusters of **5** resulting in the formation a relatively open-framework structure. The framework contains cavities between the clusters that are occupied by constitutional water and DMF molecules. Within in the framework the clusters are linked *via* a rather complicated network of weak interactions between the H atoms of the amine functionalities and the terminal O atoms of the V=O bonds. Similar inter-cluster interactions were also seen in the crystal structure of **5**, however in the case of **7**, the interaction distances between the donor and the acceptor atoms are shorter and range between 2.800(3) and 2.944(2) Å. These donor/acceptor bond distances are similar to those reported for related compounds that display comparable hydrogen bonded

supramolecular structures.[87] The CHN analysis of **7** suggests that there are a total of six DMF molecules in the crystal structure. Some of these DMF molecules could not be fully resolved due to disorder of these solvent molecules.

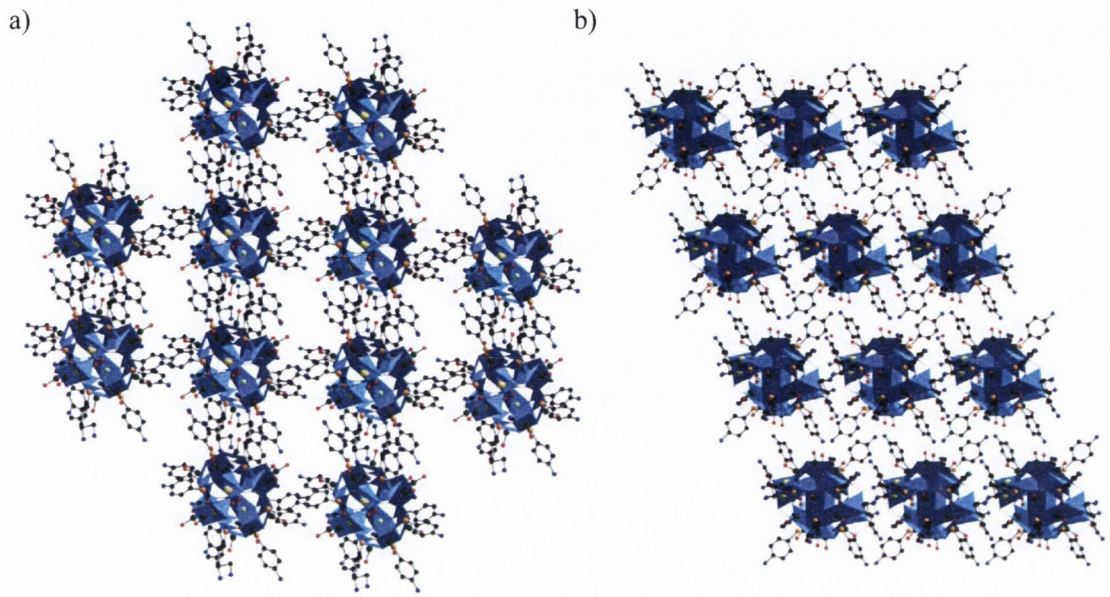

Figure 3.12 –The crystal packing diagram of **7** with a view in the direction of the crystallographic *a*-axis and (b) in the direction of the crystallographic *b*-axis; the anionic cluster core in **7** is represented by blue $\{VO_n\}$, $\{AsO_n\}$ and $\{NaO_n\}$ polyhedra. Colour code: O red, N blue, C black.

3.4.3 Further characterisation of $Na_4H_2[Cl_2{\subset}V_{14}O_{14}(OH)_8(O_3AsC_6H_4\text{-}4\text{-}NH_2)_{10}]\cdot 6DMF\cdot 15H_2O$ (7) : Mass spectrometry and Infrared spectroscopy

-Mass spectrometry

The characterisation of **7** proved to be problematic as it was found to undergo decomposition on exposure to air or common solvents. A similar sensitivity has also been observed for reduced hybrid polyoxovanadate compounds reported in literature.[46] A mass spectrum of the crystals dissolved in DMSO was obtained (Fig. 3.13a). However the compound seemed to

decompose after a short period. The decomposition is associated with a colour change from turqousie blue to black. However, despite the decomposition it was possible to identify signals in the mass spectrum that orginate from the cluster in **7**. Two signals originating from two -2 charged anionic species were observed and assigned to the cluster salts of **7**. The first signal corresponding to the formula $\{Na_2H_2[Cl_2{\subset}V_{14}O_{14}(OH)_8(O_3AsC_6H_4\text{-}4\text{-}NH_2)_{10}]\}^{2-}$ was observed at m/z = 1671.73. The second signal at m/z = 1682.25 can be assigned to the formula $\{Na_3H[Cl_2{\subset}V_{14}O_{14}(OH)_8(O_3AsC_6H_4\text{-}4\text{-}NH_2)_{10}]\}^{2-}$. Their isotopic distribution signals could not be modelled due to the weak intensity of the satellite signals. The highest intensity signal in the spectrum corresponds to the arsonate ligand which has a molecular mass of 216.9596 g mol^{-1} (M^-, 215.9688 m/z).

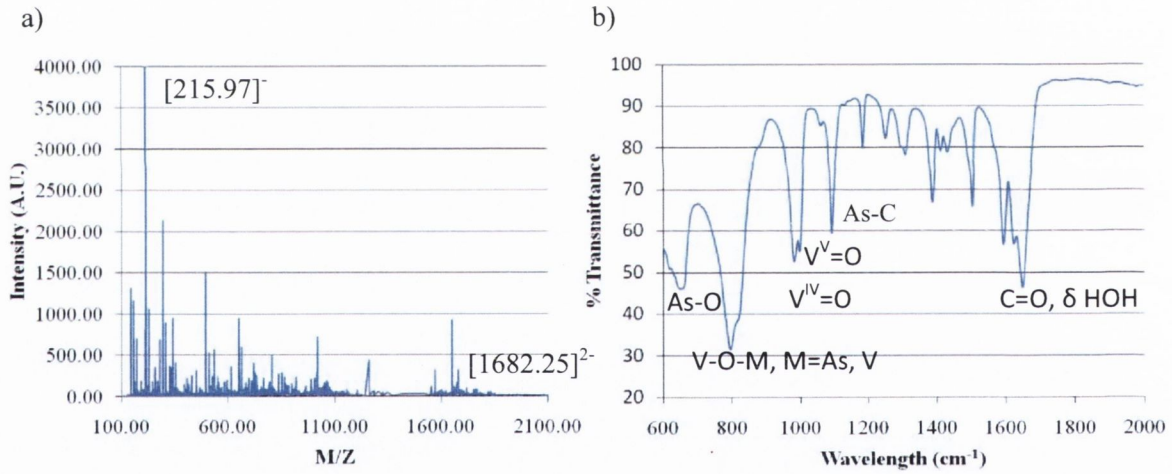

Figure 3.13 –Further characterisation of **7**: (a) Mass spectrum of **7** dissolved in DMSO (b) Infrared spectrum of **8**; a complete IR spectrum of **7** can be found in the appendix 3.

-Infrared spectroscopy

Infrared spectroscopy confirms the inclusion of the (4-aminophenyl)arsonate ligand within the complex (Fig. 3.13b). The IR spectrum of **7** is very similar to the infrared spectrum obtained for **5** as both clusters have a similar vanadium core structure containing exclusively V(IV) metal ions. However, there is a stretch at *ca.* 1000 cm^{-1} in the infrared spectrum of **7**

that relates to the V^{V}=O stretch. The explanation for the presence of such a stretch could be an indication that **7** undergoes a partial oxidation of the vanadium(IV) metal centres. Alternatively it may be possible that the bulk sample contains a small amount of V^{V} impurities which possibly originate from a related cluster that incoporates V^{V} centres in its structure.

Table 3.6 – Crystal data and structure refinement for **7**.

Identification code	Compound **7**	
Empirical formula	$C_{60}H_{34}As_{10}Cl_2N_{12}Na_4O_{66.50}V_{14}$	
Formula weight	3612.21 g mol^{-1}	
Temperature	150(2) K	
Wavelength	0.71073 Å	
Crystal system	Triclinic	
Space group	*P*-1	
Unit cell dimensions	a = 15.6447(12) Å	α = 78.330(2)°.
	b = 16.3423(13) Å	β = 67.724(2)°.
	c = 17.6625(14) Å	γ = 69.945(2)°.
Volume	3911.8(5) $Å^3$	
Z	1	
Density (calculated)	1.533 Mg/m^3	
Absorption coefficient	3.015 mm^{-1}	
F(000)	1740	
Crystal size	0.1 x 0.1 x 0.1 mm^3	
Theta range for data collection	1.47 to 25.00°.	
Index ranges	-18<=h<=18, -19<=k<=19, -21<=l<=21	
Reflections collected	30237	
Independent reflections	10606 [R(int) = 0.0667]	
Completeness to theta = 25.00°	99.8 %	
Refinement method	Full-matrix least-squares on F^2	
Data / restraints / parameters	10606 / 0 / 784	
Goodness-of-fit on F^2	0.936	
Final R indices [I>2sigma(I)]	R_1 = 0.0873, wR_2 = 0.2366	
R indices (all data)	R_1 = 0.1390, wR_2 = 0.2582	
Largest diff. peak and hole	1.071 and -0.964 e.Å-3	

3.5 Synthesis of a mixed-valent vandium hexadecanuclear cluster incorporating (4-aminophenyl)arsonic acid

3.5.1 The synthesis of $Na_2H_6[V_{16}O_{24}(OH)_8(O_3AsC_6H_4\text{-}4\text{-}NH_2)_8]\cdot 6DMF\cdot 13H_2O$ (8)

Whilst attempting to incoporate a transition metal into a polyoxovanadate cluster stablised by organoarsonate ligands, single crystals of the novel complex $Na_2H_6[V_{16}O_{24}(OH)_8(O_3AsC_6H_4\text{-}4\text{-}NH_2)_8]\cdot 6DMF\cdot 13H_2O$ (**8**) were obtained. Compound **8** is the result of the self-assembly of (4-aminophenyl)arsonic acid and sodium vanadate in the presence of hydrazine monohydrate and cobalt (II) chloride. The synthetic attempt yielded a green reaction mixture that contained a large amount of precipitate, which was removed by filtration. Green cube shaped crystals were observed in the resultant solution after six weeks. Compound **8** forms in low yields and its structure was investigated using single crystal X-ray diffraction.

3.5.2 The structural characterisation of $Na_2H_6[V_{16}O_{24}(OH)_8(O_3AsC_6H_4\text{-}4\text{-}NH_2)_8]\cdot 6DMF\cdot 13H_2O$ (8)

The novel compound $Na_2H_6[V_{16}O_{24}(OH)_8(O_3AsC_6H_4\text{-}4\text{-}NH_2)_8]\cdot 6DMF\cdot 13H_2O$ (**8**) crystallises in the monoclinic space group, *C*2/m. The asymmetric unit consists of six symmetry independent vanadium atoms and two arsonate ligands and the complete hexadecanulcear vanadium oxo cluster is generated by symmetry operations. The anionic cluster in **8** contains a similar core cluster to that observed in **7** with the formal difference that the two arsonate ligands in the apical position in **7** have been replaced by $\{V^VO_4\}$ units in **8**. The anionic cluster in **8** consists of 16 vanadium ions, eight (4-aminophenyl)arsonate ligands, 18 oxo ligands and 8 hydroxo ligands as seen in Fig. 3.14. The formation of the cluster can be

rationalised as the fusion of two mixed-valent pentanuclear units of **1** through two trinuclear di-hydroxo bridged $\{O_3V^{IV}(\mu\text{-}OH)_2VO(\mu\text{-}OH)_2V^{IV}O_3\}$ units. The mixed-valent pentanuclear capping units contain the typical concave mixed-valent $\{V^{V}O(\mu_3\text{-}O)_4V^{IV}{}_4O_{12}\}$ 'calix' unit as seen in Fig. 3.14a. Within the mixed-valent sub-unit, the bond distances between the central vanadium ion V(1) to the μ_3-O^{2-} ligand atoms O(2) and O(3) is 1.860(1) and 1.848(2) Å, respectively. The terminal V(1)=O_{term} bond is 1.563(1) Å long. The bond lengths between the symmetry independent peripheral vanadium metal centres V(2), V(3), V(4) and the μ_3-O^{2-} ligands O(2), O(3) are in the range between 1.943(1) – 1.957 (2) Å. These bond lengths compare very well with the bond lengths found in the core structure of **7**. The bond distances in the cluster in **8** between the vanadium centres and the μ_2-O^{2-} donors from the arsonate ligands range between 1.925(3) and 1.938(2) Å.

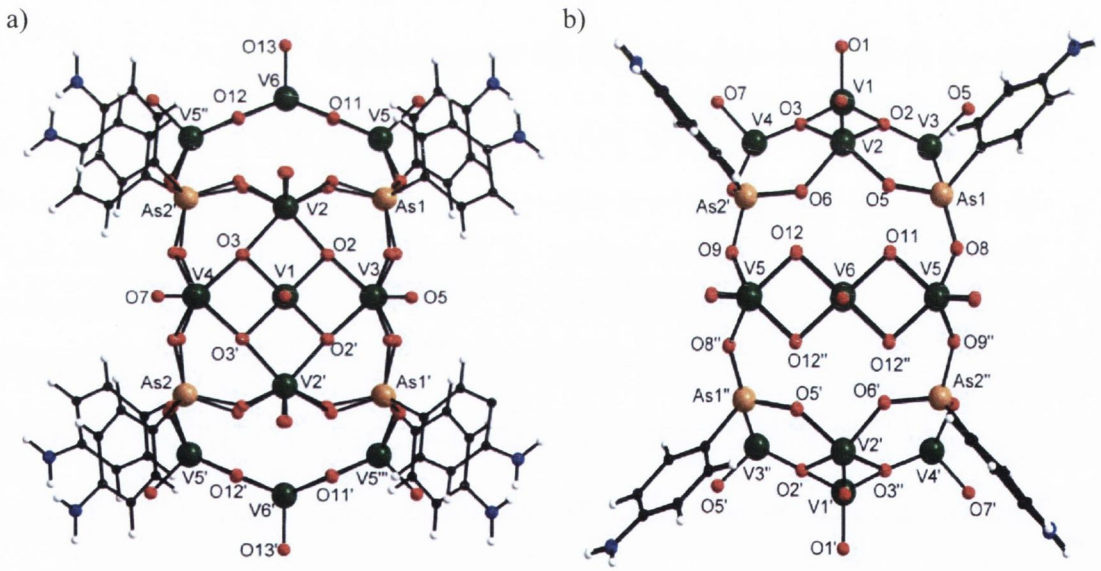

Figure 3.14 – A ball and stick representation of the anionic cluster core in **8**. (a) $\{V_{16}\}$ cluster in **8** when viewing onto the mixed-valent pentanuclear capping sub-unit. (b) A view of the $\{V_{16}\}$ cluster in **8** displaying the trinuclear $\{O_3V^{IV}(\mu\text{-}OH)_2VO(\mu\text{-}OH)_2V^{IV}O_3\}$ moieties that link the two pentanuclear sub-units (similar to **7**) viewed along the crystallographic *b*-axis. Disordered solvent molecules inside the cage structure and disordered phenyl ring atoms have been omitted for clarity. Colour code: V green, As orange, O red, N blue, C black.

The bond lengths of these peripheral vanadium centres to the terminal oxo ligands vary

between 1.561(3) and 1.592(3) Å. The two trinuclear units $\{O_3V^{IV}(OH)_2V^{IV}O(OH)_2V^{IV}O_3\}$ that inter-link the pentanuclear 'calix' units (Fig. 3.14b) are very similar to the trinuclear bridging units found in the cluster core in **7**. Again, the vanadium centres are linked *via* doubly-bridging hydroxo ligands with the peripheral oxygen donors being supplied by the arsonate ligands. The bond distances between the vanadium V(5) and V(6) centres and the hydroxo ligands O(11), O(12) within this inorganic belt are in the range of 1.980(3) to 2.013(3) Å. The bond distances from the vanadium centres V(5), V(6) to the terminal oxo ligands are 1.589(1) and 1.548 Å(1), long respectively.

Bond valence sum analysis was used to characterise the oxidation states of the vanadium centres. Comparable to **1**, the central vanadium ion, V(1), in the mixed-valent capping sub-unit was found to be in the oxidation state +V, with the four peripheral vanadium centres V(2), V(3) and V(4) found to be in the oxidation state +IV. The three vanadium centres V(5), V(6), V(5)' which form the trinuclear moieties that connect the mixed-valent pentanuclear motifs were found to be in the oxidation state +IV (Fig. 3.14b). The calculations for the bond valence sum analysis have been summarised in Table 3.7.

Table 3.7 – Bond sum valence analysis for **8**

V & O sites	Bond Valence Sum (BVS)	Assigned Oxidation State
V(1)	4.985	+5
V(2)	4.11	+4
V(3)	4.103	+4
V(4)	4.1	+4
V(5)	3.847	+4
V(6)	3.881	+4
μ_3-O (4), O(5)	2.095, 2.092	-2
μ-OH (11), (13)	1.146, 1.129	-1
$O_{terminal}$	1.653-1.913	-2

Figure 3.15 highlights different aspects of the anionic cluster in **8**. The anionic cluster with the sodium counter-ions incorporated in the cage structure is shown in Fig. 3.15a & b. The

cavity within the cluster has almost identical dimensions to those observed for **7**.

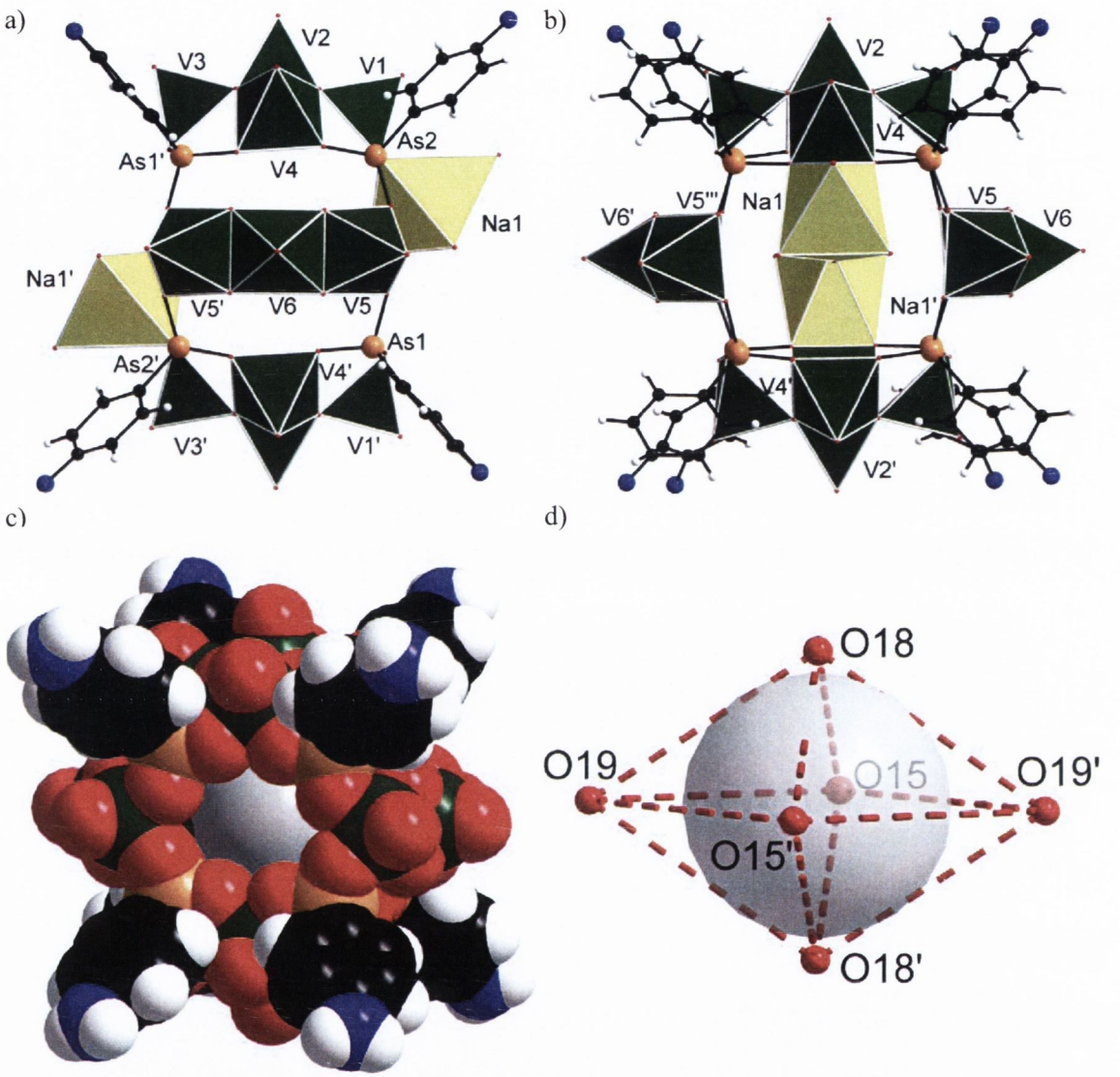

Figure 3.15 – Different aspects of the anionic cluster in **8**. (a) & (b) A polyhedral representation of the cluster core also showing the sodium counter-ions which are incorporated in the cage structure of **8**. (c) A space filling representation of the cage structure within **8**, potential cavity represented as a grey sphere (diameter *ca.* 2 nm). (d) The positions of the water molecules within the cavity of the cluster. Colour code: V green, As orange, Na yellow, O red, N blue, C black, H white.

The maximum theoretical cavity (without overlapping the covalent radii of the atoms of the framework of the cage) is represented as a grey space filling sphere with a radius of *ca.* 1 nm (see Fig. 3.15c). The cavity within the cluster is filled by water molecules (O(15), O(18), O(19)) and their symmetry equivalents. The electron density distribution in the cavity

suggests that the positions of O(15) and O(15') are only 50% occupancy so there are a total of five water molecules located within the cavity of the cluster. The inter-molecular distances between the water molecules range between 3.374(3) Å and 4.099(3) Å. These interaction distances are too long to be considered as hydrogen bonds for hydrogen bonded stabilised interactions.[87] The arrangement of water molecules must therefore be stabilised by weak interactions to the vanadium ions and the sodium counter-ions. The vanadium ions incorporated in the concave mixed-valent $\{V^{V}O(\mu_3\text{-}O)_4V^{IV}{}_4O_{12}\}$ stabilise O(18) and O(18') with interaction distances ranging between 3.383(4) Å to 3.519(3) Å.

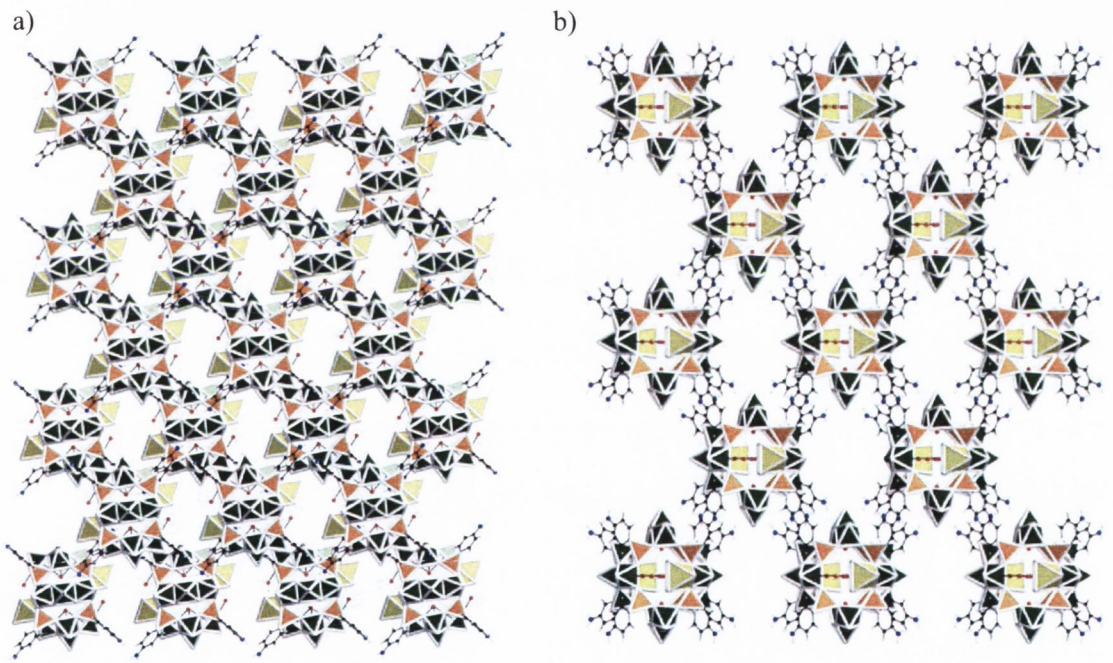

Figure 3.16 – A packing diagram of the crystal structure of **8** with a polyhedral representation of the cluster core when; (a) viewed along the crystallographic *b*-axis and (b) when viewed along the crystallographic *c*-axis. Solvent molecules have been omitted for clarity. Colour code: V green, As orange, Na yellow, C black, N blue.

The interaction distance between the water molecule O(19) and the central vanadium V(6) atom of the trinuclear bridging $\{O_3V^{IV}(\mu\text{-}OH)_2VO(\mu\text{-}OH)_2V^{IV}O_3\}$ unit is 2.882(1) Å, whilst the water molecule O(15) is coordinated to the sodium counter-ion with a bond distance of 2.609(7) Å. The positions and interactions distances of these water molecules in the cavity of

8 compare very well with those of the guest water molecules and chloride anions resolved in the cavity of **7**.

The packing arrangement of the clusters in **8** is reminiscent of that in **6** in that there are solvent filled channels which can be viewed in the crystallographic *c*-axis (Fig. 3.16). Inter-cluster interactions result in the generation of these channels with *ca.* 1.3nm diameter which are occupied by constitutional water molecules and disordered DMF molecules. The amine functionalities of the (4-aminophenyl)arsonate ligands in **8** point at the terminal O atoms of the vanadium centres in the bridging trinuclear units of a neighbouring cluster. The weak interactions between the donor and the acceptor atoms result in inter-atomic distances that range between 3.028(1) Å and 3.499(4) Å.

3.5.3 Further characterisation of the compound $Na_2H_6[(V_5O_9)_2(V_3O_3(OH)_4)_2(O_3AsC_6H_4\text{-}4\text{-}NH_2)_8]\cdot 6DMF\cdot 13H_2O$ (8)

The yield of the synthesis of **8** is low and substantial efforts to increase this yield proved unsuccessful. An infrared spectrum of **8** was recorded (Fig. 3.17). The spectrum confirmed the inclusion of the (4-aminophenyl)arsonate ligand in the complex. The spectrum of **8** displays the typical characteristic stretch for the As-C bond at 1095 cm^{-1}. Also observed are infrared stretches at 983 cm^{-1} and 1000 cm^{-1} corresponding to V^{V}=O and V^{IV}=O bonds respectively. The stretch due to the carbonyl functionality of the DMF was observed at 1652 cm^{-1}.

Only recently a related cluster was synthesised in high yield in our lab by Dr Lei Zhang in an attempt to incoporate a lanthanide ion into a polyoxovanadate cluster stablised by organoarsonates. Dr Zhang's synthesis similarly involves the self-assembly of (4-aminophenyl)arsonic acid and sodium vanadate in the presence of hydrazine monohydate.

This synthesis requires the addition of lathanide chloride to the reaction mixture instead of cobalt (II) chloride which was used in the synthesis of **8**. The addition of an additional chloride salt seems to be a requirement for the formation of **8**. Investigations into the mechanism of the cluster formation are on-going.

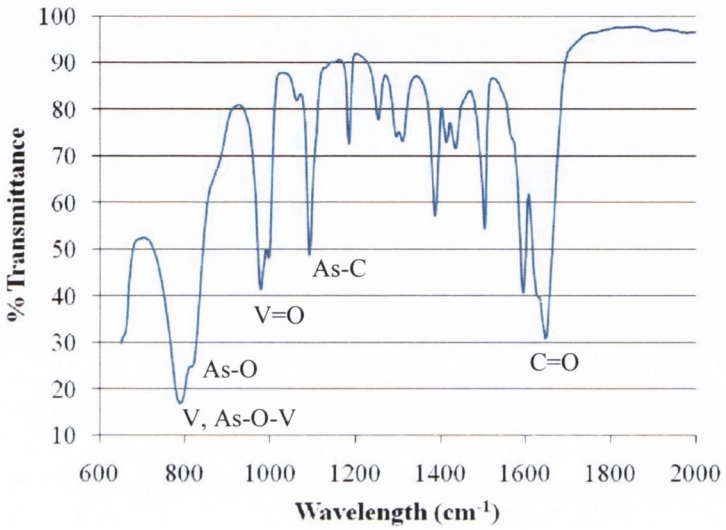

Figure 3.17 – Infrared spectrum of **8**, see appendix 3 for full spectrum.

Table 3.8 – Crystal data and structure refinement for **8**.

Identification code	compound **8**	
Empirical formula	$C_{63}\ H_{48}\ As_8\ N_{14}\ Na_2\ O_{74.5}\ V_{16}$	
Formula weight	3653.53 g mol^{-1}	
Temperature	150(2) K	
Wavelength	0.71075 Å	
Crystal system	Monoclinic	
Space group	*C*2/m	
Unit cell dimensions	a = 24.650(7) Å	α = 90°.
	b = 26.110(6) Å	β = 124.341(3)°.
	c = 15.089(4) Å	γ = 90°.
Volume	8019(4) $Å^3$	
Z	2	
Density (calculated)	1.513 Mg/m^3	
Absorption coefficient	2.610 mm^{-1}	
F(000)	3548	
Crystal size	0.2 x 0.15 x 0.15 mm^3	
Theta range for data collection	1.27 to 31.36°.	
Index ranges	-29<=h<=35, -37<=k<=37, -21<=l<=21	
Reflections collected	45258	
Independent reflections	12314 [R(int) = 0.0605]	
Completeness to theta = 31.36°	99 %	
Refinement method	Full-matrix least-squares on F^2	
Data / restraints / parameters	12314 / 0 / 429	
Goodness-of-fit on F^2	1.147	
Final R indices [I>2sigma(I)]	R_1 = 0.0978, wR_2 = 0.2646	
R indices (all data)	R_1 = 0.1362, wR_2 = 0.3124	
Largest diff. peak and hole	1.947 and -1.931 e.$Å^{-3}$	

3.6 Summary of large novel organoarsonate functionalised polyoxovanadate clusters

In chapter 1, we discussed the isolation of the novel mixed-valent pentanuclear vanadium cluster stabilised with (4-aminophenyl)arsonic acid (**1**). When we lowered the pH of the reaction mixture of **1**, we were able to isolate a hybrid dodecanuclear V(IV) cluster compound functionalised with 10 arsonate ligands (**5**). Upon reducing the pH of the reaction mixture, reduction of the vanadate ions from oxidation state +V to +IV is facilitated and the vanadate ions undergo a condensation reaction resulting in the generation of a larger cluster. Both these clusters, the penta- and dodecanuclear clusters from when the ligand is reacted in excess with vanadium ions (ligand:metal ratio 2:1).

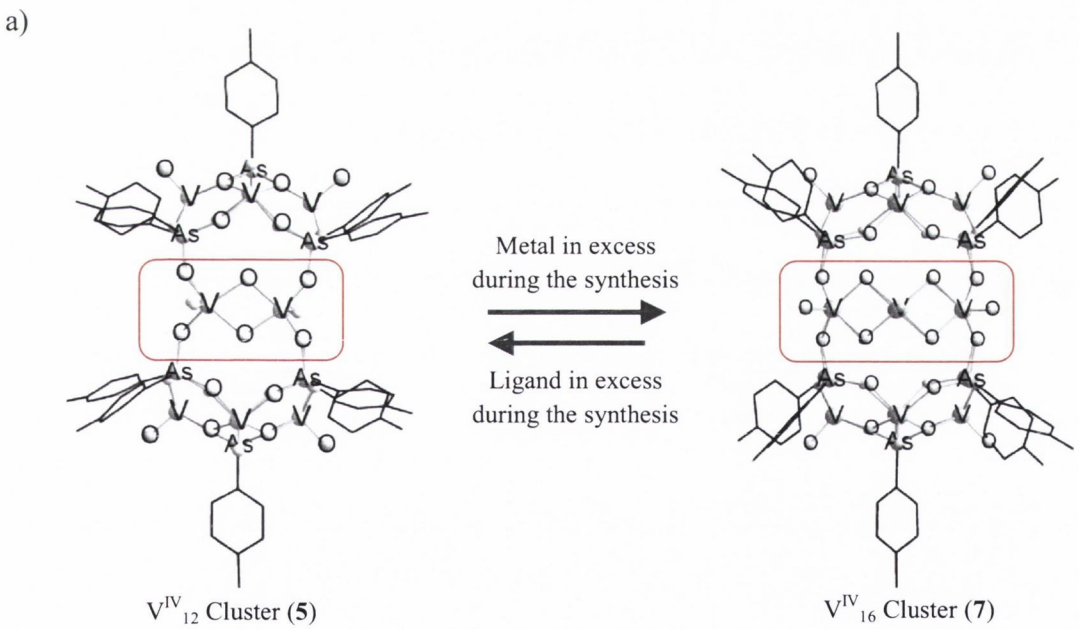

Figure 3.18 – Comparison of the anionic cluster core contained within **5** with that of anionic cluster within **7**. The inorganic belts in **5** (dinuclear vanadium bridging unit) and in **7** (trinuclear vanadium bridging unit) have been highlighted with a red box. The synthetic conditions of **5** differ from **7** due to a different metal/ligand ratio in the synthetic procedure.

When we replicated the same reaction conditions using an excess of metal ions, crystals of **7**

separated from the reaction mixture. Compound **7** has a related structure to that of the cluster of **5**. Both have a structure with exclusively V(IV) metal centres in their cluster core. However, the cluster in **7** has an expanded cavity with two extra vanadium ions in the trinuclear hydroxo bridged moieties that interlink the capping motifs (Fig. 3.18). From the relationship between **5** and **7**, we can conclude that an increased concentration of vanadyl ions in the reaction mixture leads to the enlargement of the inorganic belt within this type of cage compound. Future work would involve the synthesis of cluster core with even bigger inorganic bridging units such as tetranuclear hydroxo bridged units that could link the two capping motifs within the cluster.

Another important parameter in the self-assembly process of these large hybrid polyoxovanadate clusters is the ratio of reducing agent to vanadate species in solution. The reducing agent, hydrazine hydrate, controls the V^{IV}/V^{V} ratio of ions in solution and it appears that the ratio of these metal ions in solution is critical to the synthesis of different structural sub-units.

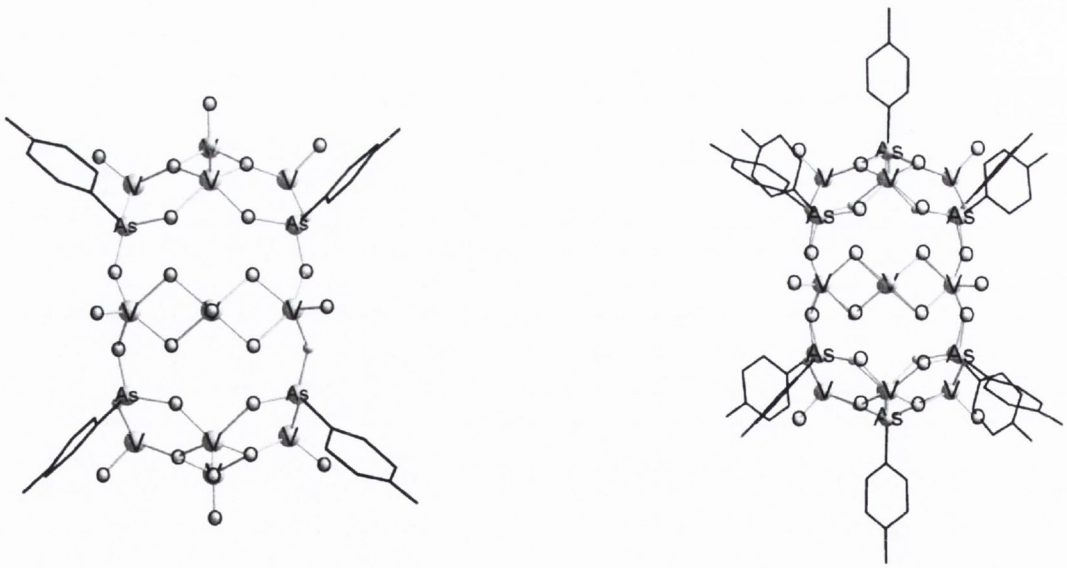

$V^{IV}_{14}V^{V}_{2}$ (Lig)$_8$ Cluster (**8**) V^{IV}_{14}(Lig)$_2$ (Lig)$_8$ Cluster (**7**)

Figure 3.19 – A structural comparison of the anionic cluster of **8** with that of **7**.

Compound **8** was inadvertently synthesised by attempts to incorporate a transition metal within the polyoxovanadate cluster. As mentioned previously the role of the transition metal in the assembly process is currently being investigated. The anionic cluster core of **8** is structurally comparable to the cluster within **7** (Fig. 3.19). Its core structure can be related to the cluster core of **7** where the arsonate group at the apex of the cluster have formally been replaced by a vanadium(V) ion.

It was noted that an octahedral arrangement of water molecules or a combination of water molecules and chloride ions were observed within the cluster cavities of the anionic clusters in **5** – **8**. Chloride ions are located at the focal points of the concave shaped $\{NH_2C_6H_4AsO_3(\mu_3\text{-}O)V^{IV}{}_4O_{12}\}$ capping units in **7** and **8**. The encapsulation of the halide atoms in the hybrid polyoxovanadate shell is a result of the weak interactions of the chloride anions with the Lewis acidic V^{IV} centers. Future work will involve understanding the assembly of related compounds in solution utilising the same starting materials with different anionic templates and reducing agents. The isolation of the predicted mixed-valent analogue of **5** will also be investigated. Host/guest interactions have been studied in related compounds[42] and we hope in future work to investigate the host/guest interaction of these novel structures.

Chapter Four

Mixed-valent decanuclear vanadium(V^{IV}/V^{V}) capsules stabilised by aryl diphosphonate ligands

4.1 Introduction

Having investigated the accessibility of mixed-valent pentanuclear structures stabilised by aryl arsonates (Chapter 2, **1** – **4**) over a wide range of reaction conditions and acquired the knowledge that organophosphonates can be incorporated into a mixed-valent cage (Chapter 3, **6**), we set about exploring the use of aromatic diphophonate ligands in the self-assembly of hybrid polyoxovanadate structures. This approach resulted in the formation of an unique hybrid organic-inorganic cage structure in $Na_8H_2[2H_2O\subset(V_5O_9)_2(O_3PC_6H_4\text{-}4\text{-}PO_3)_4]\cdot 34H_2O$ (**9**).

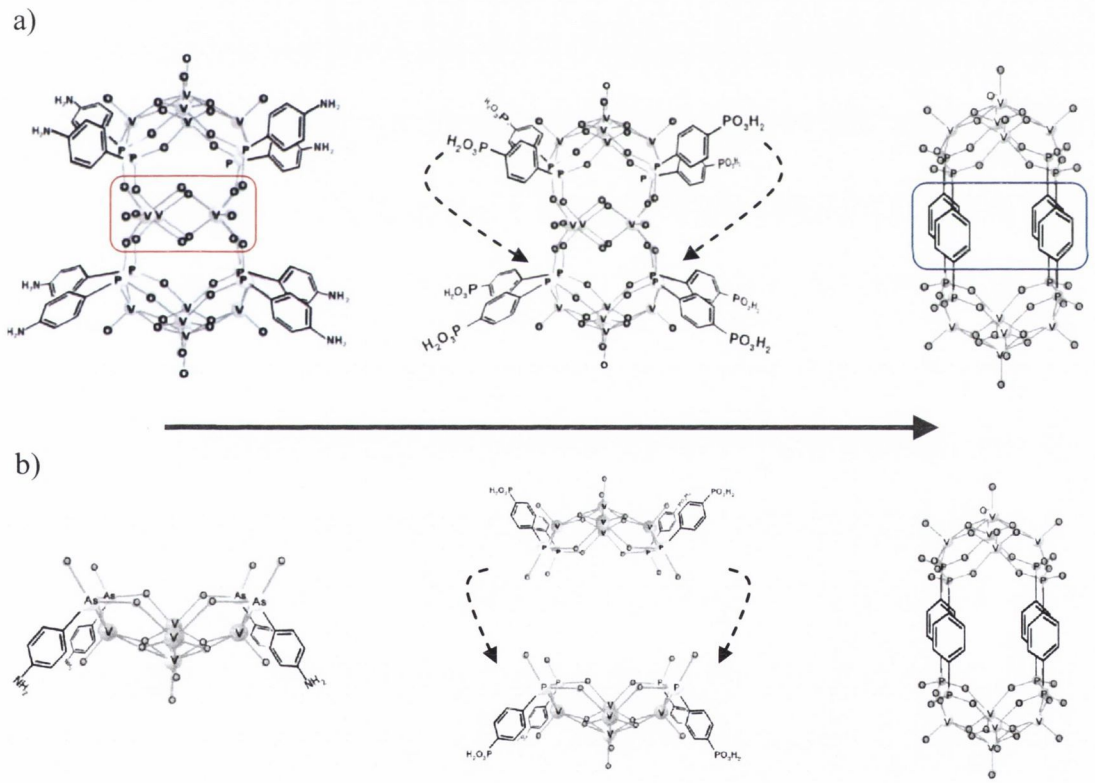

Figure 4.1 – Rationalisation of the formation of $[V_{10}O_{18}(O_3P\text{-}C_6H_4\text{-}PO_3)_4]^{10-}$ by comparison of its structure with those of $[V_5O_9(O_3AsC_6H_4\text{-}4\text{-}NH_2)_4]^{5-}$ (**1**) and $[V_{14}O_{22}(OH)_4(O_3PC_6H_4NH_2)_8]^{6-}$ (**7**). (a) The formal replacement of the bridging dinuclear unit in **9** (red box) with an aryl linker (blue box). (b) The formal replacement of arsonate ligands with phosphonate ligands for the intermolecular connectivity of two pentanuclear mixed-valent sub-units.

Considering the structure of **1** and the fact that the phosphonate functionalities are unlikely to substitute V^V ions, [46] the assembly of the molecular structure of **9** can be rationalised as the replacement of the arsonate ligands contained in $[V_5O_9(O_3AsC_6H_4\text{-}4\text{-}NH_2)_4]^{5-}$ (**1**) by diphosphonates. Rotational rearrangement of the tetrahedral phosphonate groups allows the linkage of two concave mixed-valent $\{V^VO(\mu_2\text{-}O)_4V^{IV}{}_4O_{12}\}$ sub-units resulting in the cage like structure seen within **9** (Fig. 4.1). Two variants of the hybrid cage within **9** are also discussed within this chapter: The synthesis of a related novel hybrid cage functionalised by an extended diphosphonate ligand, $Na_8H_2[(DMF)_2{\subset}(V_5O_9)_2(O_3PC_{12}H_8\text{-}4\text{-}PO_3)_4]\cdot 30H_2O$ (**11**) and the synthesis of a related hybrid cage that contains naphthyl diphosphonates, $Na_8H_2[(H_2O)_2{\subset}V_{10}O_{18}(O_3PC_{10}H_6\text{-}4\text{-}PO_3)_4]\cdot 44H_2O$ (**10**).

4.2 Aromatic phosphonate ligands

The ligands (1,4-benzene)bisphosphonic acid, (1,4-naphthalene)bisphosphonic acid and ([1,1'-biphenyl]-4,4'-diyl)bisphosphonic acid were synthesised by the modified Michaelis–Arbuzov reaction (Chapter 6, 6.2.1 – 6.2.5).[91] The reaction involves heating an aryl halide with an alkyl phosphite in the presence of the nickel(II) halide at 200 °C usually in the presence of 1,3-dissopropylbenzene as a solvent. The mechanism is considered to involve *in situ* reduction of nickel(II) halide to a nickel(0) phosphite complex which then undergoes oxidative insertion into the carbon–halogen bond of the aryl halide to form an aryl nickel(II) intermediate (Fig. 4.2). This intermediate then undergoes reductive elimination and gives an aryl(alkoxy)phosphonium salt, which rearranges to form the required phosphonate ester. This process also results in the generation of an alkyl halide which is continuously removed from the reaction mixture until the reaction is complete. Hydrolysis of the phosphonate ester under acidic conditions generates the desired phosphonic acids. The overall course of the reaction is

broadly similar to the more familiar Michaelis-Arbuzov phosphonylation of alkyl halides, in that the displaced halogen appears as a volatile alkyl halide (the alkyl group arises from the alkyl phosphite reagent). This synthetic approach was utilised to prepare a range of desired aryl phosphonic acids which include (1,4-benzene)bisphosphonic acid, (1,4-naphthalene)bisphosphonic acid, ([1,1'-biphenyl]-4,4'-diyl)bisphosphonic acid. (4-Aminophenyl)phosphonic acid and (1-naphthalene)phosphonic acid whose vanadium complexes are discussed in Chapters 3 and Chapter 5 were also prepared using this protocol using commercially available organic halides. The yields of these reactions and their respective ^{1}H and ^{31}P NMR spectra have been reported in the experimental.

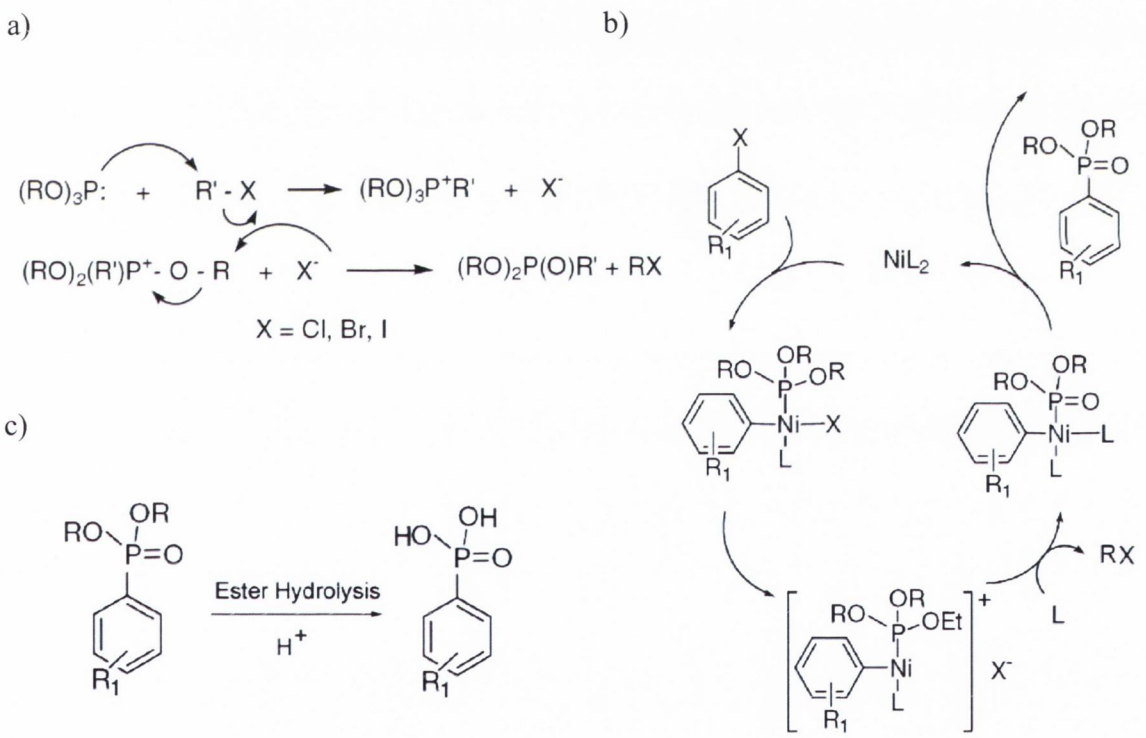

Figure 4.2 – Synthesis of phosphonic acids. (a) The Michaelis-Arbuzov reaction.[92] (b) The synthetic approach for the formation of aromatic phosphonic acids according to the modified Michaelis-Arbuzov reaction.[91, 93] (c) Ester hydrolysis under acidic conditions.[91]

4.3 Synthesis of a mixed-valent vanadium(V^{IV}/V^{V}) capsule incorporating (1,4-benzene)bisphosphonic acid

4.3.1 The synthesis of $Na_8H_2[(H_2O)_2{\subset}V_{10}O_{18}(O_3PC_6H_4\text{-}4\text{-}PO_3)_4]\cdot 34H_2O$ (9)

Compound **9**, $Na_8H_2[(H_2O)_2{\subset}V_{10}O_{18}(O_3PC_6H_4\text{-}4\text{-}PO_3)_4]\cdot 34H_2O$ is the product of the self-assembly of (1,4-benzene)bisphosphonic acid, sodium azide and sodium metavanadate in the presence of the reducing agent, hydrazine monohydrate, in a water/DMF solution. These reaction conditions are very similar to those used to generate the mixed-valent pentanuclear vanadium compounds **1** – **4**. Green cube shaped crystals of **9** which were suitable for X-ray diffraction measurements formed at pH 7.6 after several hours.

4.3.2 The structural characterisation of $Na_8H_2[(H_2O)_2{\subset}V_{10}O_{18}(O_3PC_6H_4\text{-}4\text{-}PO_3)_4]\cdot 34H_2O$ (9)

The crystal structure of **9** was refined in the *P*4/mnc space group. The anionic cluster of **9** consists of two typical concave mixed-valent $\{V^{V}O(\mu_3\text{-}O)_4V^{IV}{}_4O_{12}\}$ sub-units that are connected by four (1,4-benzene)bisphosphonate ligands (Fig. 4.3). Each ligand functionality bridges between two V atoms in O,O'- *syn, syn* coordination mode similar to coordination modes in **1** – **4**. However, the binding mode of the phosphonate functionalities is such that their terminal oxygen atoms and symmetry equivalents now point outwards in the same direction as the terminal oxygen atoms of the vanadium ions (Fig. 4.3b & 4.3c). This contrasts the binding modes of the arsonate functionalities in **1** in which the $\{RAsO_3\}$ tetrahedra are 180° rotated relative to the phosphonate group in **9**. The aromatic ring systems of the ligands are disordered over two positions.

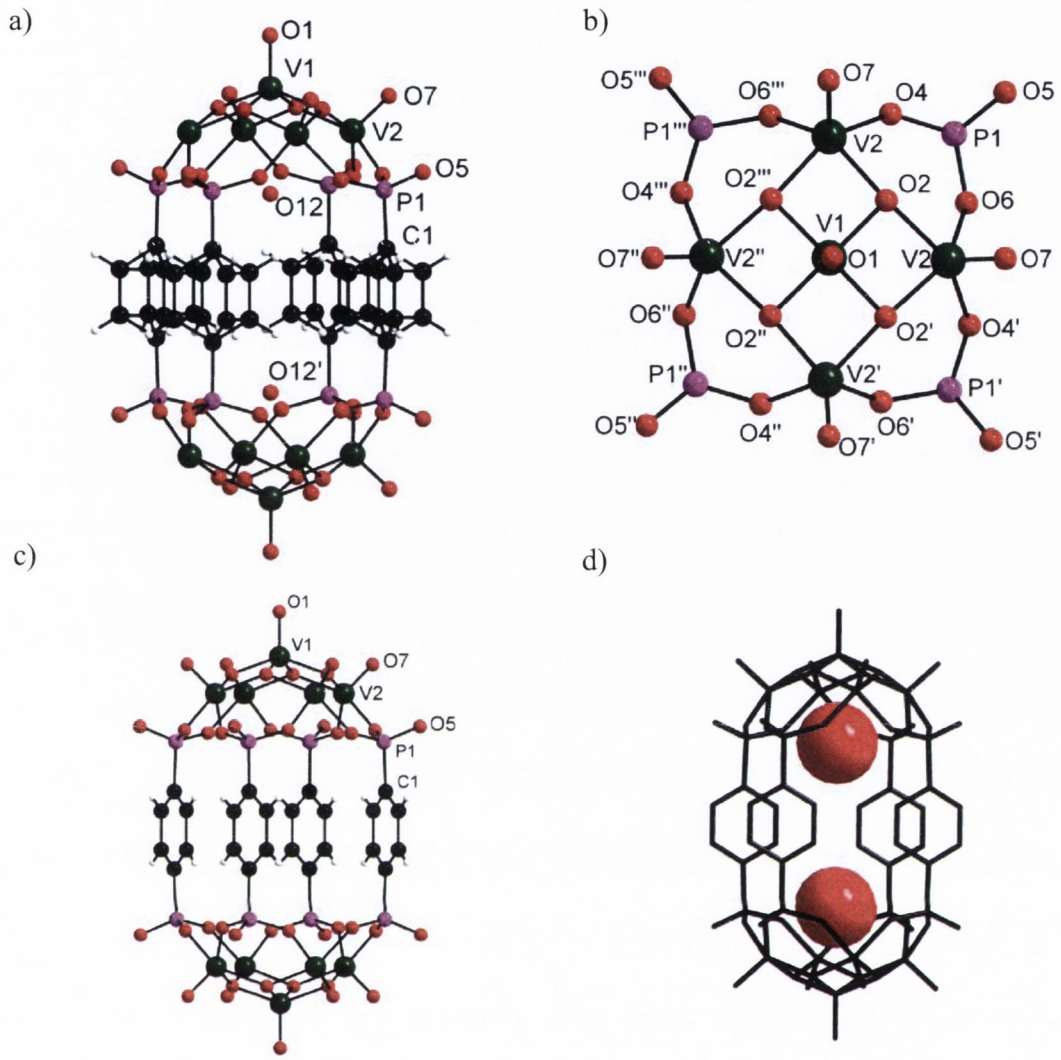

Figure 4.3 – (a) A ball and stick representation of the anionic cluster $[(V_5O_9)_2(O_3PC_6H_4\text{-}4\text{-}PO_3)_4]^{8-}$ contained in **9** as viewed in the direction of the crystallographic *b*-axis. (b) The core structure of the mixed-valent capping motif. (c) The residual solvent molecules as well as the disordered phenyl rings have been deleted for clarity. (d) The anionic cluster core in **9** is represented as a black wire frame with two space filling representations of the O atoms of the water molecules. Colour code: V green, P purple, O red, C black, H white.

Using bond valence sum analysis, the oxidation state of the central vanadium ion V(1) was calculated to be oxidation state +V (see Table 4.1). The bond length between V(1) and the μ_3-O^{2-} ligand O(2) is 1.880(1) Å and the terminal V(1)=O_{term} bond is 1.615(1) Å long (Fig. 4.3b). The peripheral vanadium ion V(2) is calculated to be in oxidation state +IV. The bond lengths between these vanadium metal centres V(2) and the μ_3-O^{2-} ligands O(2) range between 1.965(2) – 1.991(2) Å. The bond distances between these peripheral V centres and

the phosphonate O donors O(4) and O(6) vary between 1.943(3) – 1.964(3) Å whilst the terminal V=O bond distance is 1.602(2) Å.

Table 4.1 – Bond sum valence analysis for **9**

V & O sites	Bond Valence Sum (BVS)	Assigned Oxidation State
V(1)	4.91	+5
V(2)	4.086	+4
μ_3-O (2)	1.997	-2
μ-O (4) (6)	1.932, 1.882	-2
$O_{terminal}$ (1)(7)	1.662, 1.635	-2

Two symmetry related water molecules reside within the cavity of the cluster (Fig. 4.3d). A water molecule is located at the focal point of the concave mixed-valent capping motif at either end of the cluster. The distance between the water molecule O(12) and the central vanadium ion V(1) is 3.382(1) Å whilst the distance between the peripheral vanadium ion V(2) and the water molecule O(12) is 3.286(1) Å. The dimensions of the cage in **9** are characterised by an intramolecular V^V-V^V distance of 12.5 Å, a square arrangement of four P atoms with a P-P distance of 5.4 Å and a distance of 5.2 Å between the planes of parallel aligned aromatic rings.

The packing arrangements of the cages in the crystal structure of **9** are shown in Fig. 4.4. A distorted octahedrally coordinated sodium counter-ion is located in the cavity between adjacent clusters and is surrounded by six solvating water molecules (Fig. 4.4a). The oxygen atoms of the peripheral V=O bonds on each of the pentanuclear calix units are linked *via* solvated dimeric $\{O_2(H_2O)_2Na(\mu_2\text{-}H_2O)_2Na(H_2O)_2O_2\}$ units to an adjacent cluster cap resulting in a structural arrangement in which the caps act as pillars in a layered structure (Fig. 4.4b).

a)

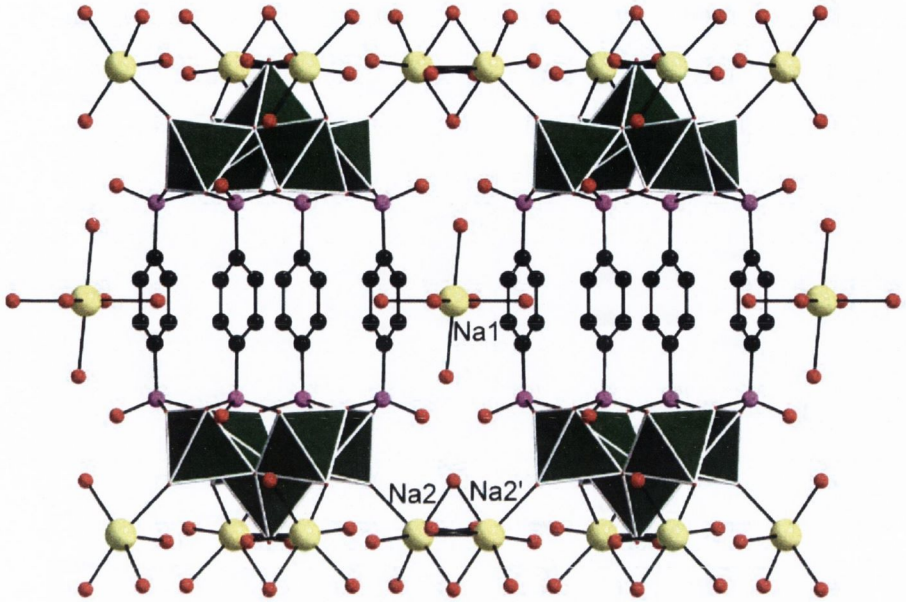

b)

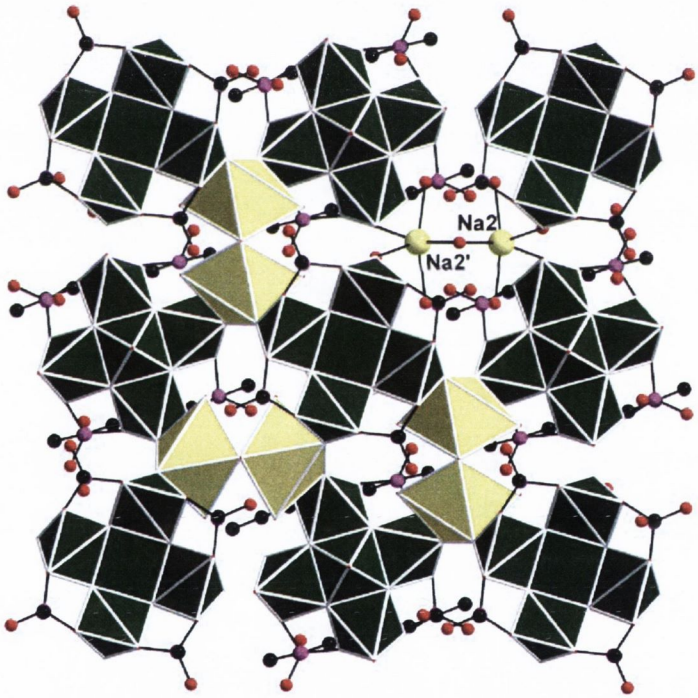

Figure 4.4 – (a) Packing arrangement of the clusters in **9** viewed in the direction of the crystallographic *b*-axis. (b) The packing arrangement of the mixed-valent pentanuclear vanadium units as viewed in the direction of the crystallographic *c*-axis. (Non-bonding crystallisation solvent molecules and the disordered phenyl rings have been omitted for clarity.) Polyhedral representation of $\{VO_5\}$ and $\{NaO_6\}$ units.

4.3.3 Further solid state characterisation of 9: Thermogravimetric analysis and Infrared spectroscopy

-Thermogravimetric analysis

Thermogravimetric analysis was carried out to investigate the thermal stability of **9** in air (Fig. 4.5). A thermogravimetric step between *ca.* 30 °C and 200 °C (24%) corresponds to the loss of all crystallisation solvent water molecules. Oxidation of the organic ligands starts at *ca.* 390 °C which leads to the destruction of the oxo-cluster and the formation of an inorganic oxide.[94]

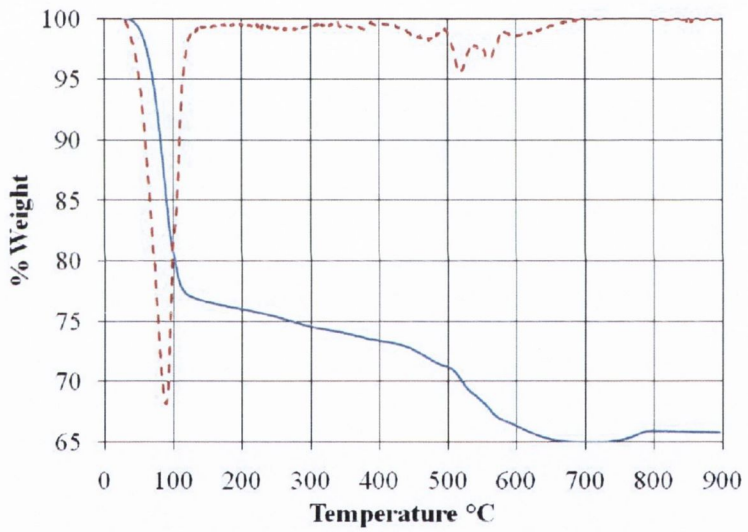

Figure 4.5 – (a) TGA of **9** in air (blue line). The derivative of the TGA curve is presented as a red dashed line.

-Infrared spectroscopy

An infrared spectrum of **9** was recorded and compared with that of the organic ligand. The infrared spectrum of the ligand, (1,4-benzene)bisphosphonic acid, displays a band at 1386 cm^{-1} which was attributed to the aromatic ring stretches whilst bands at 1098 cm^{-1}, 986 cm^{-1} and 982 cm^{-1} were attributed to the $\{PO_3\}$ functionality (Fig. 4.6). When this spectrum is compared to that of the infrared spectrum of **9**, some notable similarities are observed. A

stretch at 1390 cm^{-1} clearly underlines the incorporation of the aromatic ligand. Infrared bands originating from the $\{PO_3\}$ functionality are observed at 1152 cm^{-1}, 986 cm^{-1} and 894 cm^{-1}.[88, 89] Two strong bands at 1033 cm^{-1} and 1056 cm^{-1} are associated with ν(V=O) bond vibrations.[38, 42]

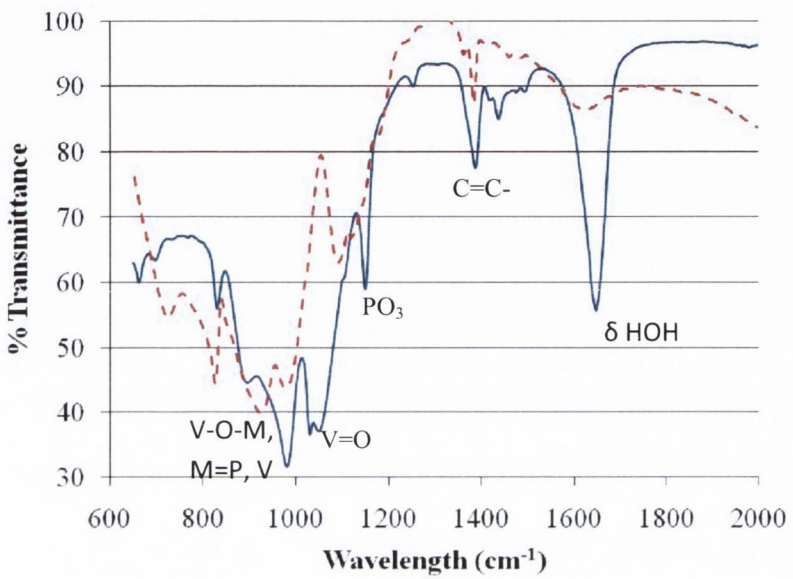

Figure 4.6 – (a) Infrared spectrum of **9** (blue) compared to the infrared spectrum of (1,4-benzene)bisphosphonic acid (red dash line), a complete IR spectrum of **9** can found in the appendix 4.

4.3.4 Solution characterisation of 9: Mass spectrometry and UV-vis spectroscopy

-Mass spectrometry

The mass spectrum of **9** in an aqueous solution was measured using electrospray mass spectrometry in the negative mode (Fig. 4.7). The most intense signal observed at m/z = 870.8967 corresponds to the -2 charged species of **9** with eight charge balancing protons, $H_8[V_{10}O_{18}(O_3PC_6H_4PO_3)_4]^{2-}$. A second related signal at m/z = 881.5903 corresponds to the -2

charged cluster of **9** with a sodium counter-ion and seven charge balancing protons, $NaH_7[V_{10}O_{18}(O_3PC_6H_4PO_3)_4]^{2-}$.

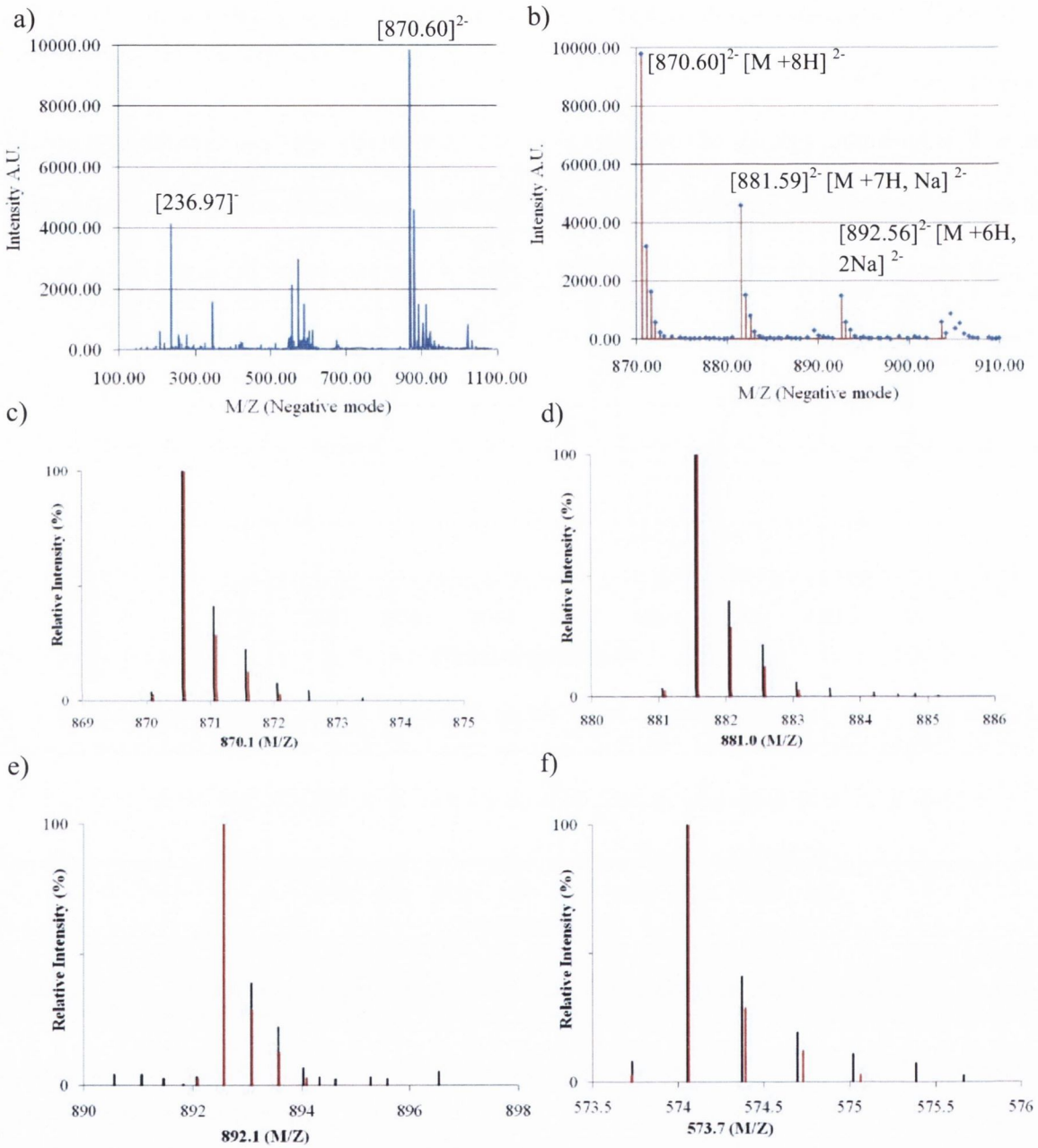

Figure 4.7 – (a) Mass spectrometry of **9** in an aqueous solution. (b) An anionic -2 charged species of **9** (M = $[V_{10}O_{18}(O_3PC_6H_4PO_3)_4]^{10-}$) with different numbers of sodium counter-ions. Comparison of the experimental isotopic envelopes (black spectra) with simulated patterns (red spectra) for: (c) $H_8[V_{10}O_{18}(O_3PC_6H_4PO_3)_4]^{2-}$ at m/z = 870.1, (d) $NaH_7[V_{10}O_{18}(O_3PC_6H_4PO_3)_4]^{2-}$ at m/z = 881.0, (e) $Na_2H_6[V_{10}O_{18}(O_3PC_6H_4PO_3)_4]^{2-}$ at m/z = 892.1 and (f) $H_7[V_{10}O_{18}(O_3PC_6H_4PO_3)_4]^{3-}$ $-H_2O$ at m/z = 573.7.

A third related signal at m/z = 892.5635 corresponds to the -2 charged cluster of **9** with two sodium counter-ions and six protons, $Na_2H_6[V_{10}O_{18}(O_3PC_6H_4\text{-}4\text{-}PO_3)_4]^{2-}$. An anionic -3 charged species is observed at m/z = 573.7 corresponding to the anionic cluster of **9** with seven proton counter-ions, $H_7[V_{10}O_{18}(O_3PC_6H_4\text{-}4\text{-}PO_3)_4]^{3}$ and a subsequent loss of a water molecule. All signals corresponding to these anionic species were modelled and their experimental and modelled isotopic distributions are shown in Fig. 4.7c – f and appendix 4. The deprotonated (1,4-benzene)bisphosphonic acid ligand is characterised by a signal at m/z = 236.97 in the mass spectrum of **9**.

- *UV-vis spectroscopy*

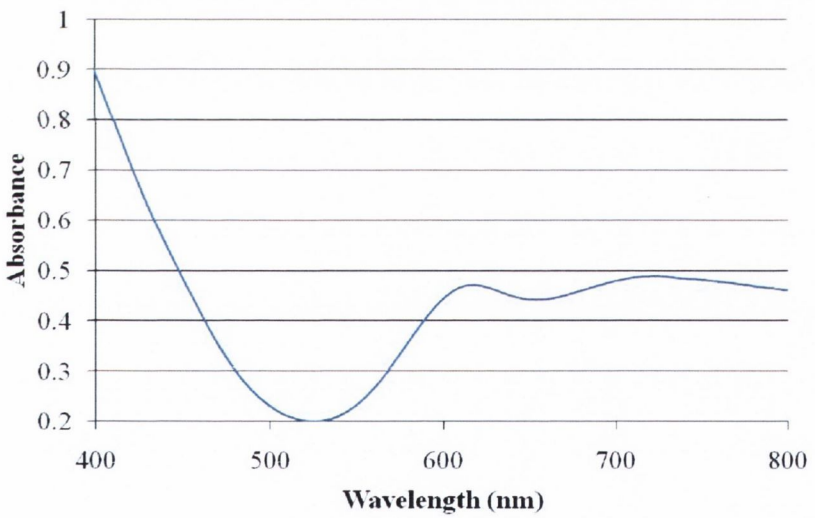

Figure 4.8 – The UV-vis spectrum of a 0.5mM aqueous solution of **9**.

Compound **9** was found to be soluble in water and the UV-vis spectrum was recorded of the aqueous solution (Fig. 4.8). An absorption is observed in the near UV region and is due to intensive charge transfer effects.[38] A much weaker broad absorbance originating the d-d transitions is observed at 724 nm (ε = 489 $L.mol^{-1}cm^{-1}$) with a small shoulder at 618 nm (ε = 471 $L.mol^{-1}cm^{-1}$) due to intervalence charge transfer.[38, 42]

Table 4.2 – Crystal data and structure refinement for **9**

Identification code	Compound **9**	
Empirical formula	$C_{24}\ H_{32}\ Na_8\ O_{78}\ P_8\ V_{10}$	
Formula weight	2509.58 g mol^{-1}	
Temperature	150(2) K	
Wavelength	0.71073 Å	
Crystal system	Tetragonal	
Space group	*P*4/mnc	
Unit cell dimensions	a = 12.128(1) Å	α = 90°.
	b = 12.128(2) Å	β = 90°.
	c = 30.574(6) Å	γ = 90°.
Volume	4496.8(12) $Å^3$	
Z	2	
Density (calculated)	1.853 Mg/m^3	
Absorption coefficient	1.292 mm^{-1}	
F(000)	2476	
Crystal size	0.2 x 0.2 x 0.1 mm^3	
Theta range for data collection	1.33 to 25.00°.	
Index ranges	-14<=h<=13, -10<=k<=14, -36<=l<=36	
Reflections collected	17802	
Independent reflections	2043 [R(int) = 0.1512]	
Completeness to theta = 25.00°	100.0 %	
Refinement method	Full-matrix least-squares on F^2	
Data / restraints / parameters	2043 / 3 / 186	
Goodness-of-fit on F^2	1.162	
Final R indices [I>2sigma(I)]	R_1 = 0.0856, wR_2 = 0.1921	
R indices (all data)	R_1 = 0.1157, wR_2 = 0.2053	
Largest diff. peak and hole	0.789 and -0.940 $e.Å^{-3}$	

4.4 Synthesis of a mixed-valent vanadium (V^{IV}/V^{V}) capsule incorporating (1,4-naphthalene)bisphosphonic acid

4.4.1 The synthesis of $Na_8H_2[(H_2O)_2{\subset}V_{10}O_{18}(O_3PC_{10}H_6\text{-}4\text{-}PO_3)_4]\cdot 44H_2O$ (10)

The synthesis of $Na_8H_2[(H_2O)_2{\subset}V_{10}O_{18}(O_3PC_{10}H_6\text{-}4\text{-}PO_3)_4]\cdot 44H_2O$ (**10**) was achieved by substituting (1,4-benzene)bisphosphonic acid with (1,4-naphthalene)bisphosphonic acid during the preparative procedure that led to the formation of **9**. The self-assembly process is initiated with the addition of the reducing agent, hydrazine hydrate, at neutral pH which instigates a colour change from bright yellow to a dark green solution and increases the pH of the reaction mixture. The pH was monitored and was re-adjusted to a neutral pH with hydrochloric acid. Small green cube-shaped crystals of **10** formed from the resultant reaction mixture after several days and were used for single crystal X-ray diffraction studies.

4.4.2 The structural characterisation of $Na_8H_2[(H_2O)_2{\subset}V_{10}O_{18}(O_3PC_{10}H_6\text{-}4\text{-}PO_3)_4]\cdot 44H_2O$ (10)

The anionic cluster contained within $Na_8H_2[(H_2O)_2{\subset}V_{10}O_{18}(O_3PC_{10}H_6\text{-}4\text{-}PO_3)_4]\cdot 44H_2O$ (**10**) can be described as containing two concave mixed-valent $\{V^{V}O(\mu_3\text{-}O)_4V^{IV}{}_4O_{12}\}$ sub-units linked *via* four (1,4 naphthalene)bisphosphonate ligands. The overall molecular cage structure is similar to that seen in **9** (Fig. 4.9). Bond valence sum analysis of **10** confirmed the oxidation states of the vanadium centres in the mixed-valent capping motif (Fig. 4.9c). The central vanadium ion V(1) is found to be in the oxidation state +V. The bond lengths between the central vanadium ion V(1) and the μ_3-bridging oxygen ligands (O(1), O(2), O(3), O(4))

are in the range between 1.899(2) – 1.912(1) Å. The peripheral vanadium metal centres (V(2), V(3), V(4), V(5)) are found to be in the oxidation state +IV. The bond distances between these vanadium metal centres and the μ_3-bridging oxygen ligands (O(1), O(2), O(3), O(4)) are in the range of 1.941(3) – 1.978(1) Å whilst the bond distances between these vanadium centres and the μ_2-bridging oxygen donors from the phosphonate ligands vary from 1.915(1) Å to 1.985(5) Å. The assignment of the oxidation states of the vanadium metal centres has been summarised in Table 4.3.

Table 4.3 – Bond sum valence analysis for **10**

V & O sites	Bond Valence Sum (BVS)	Assigned Oxidation State
V(1)	4.747	+5
V(2)	4.129	+4
V(3)	4.086	+4
V(4)	4.119	+4
V(5)	4.044	+4
μ_3-O (1) (2) (3) (4)	1.993-2.017	-2
μ-O (10) (11) (12) (13) (14) (15) (16) (17)	1.843-1.940	-2
$O_{terminal}$ (5) (6) (7) (8) (9)	1.566-1.703	-2

The dimensions of the cage in **10** are very similar to that observed for the cage structure of **9**. The intramolecular distances are characterised by V^V-V^V distances of *ca.* 12.6 Å, a square arrangement of four P atoms with a P-P distance of *ca.* 5.5 Å; a distance of *ca.* 7.9 Å between opposite parallel aligned aromatic rings. Similar to **9**, two disordered water molecules are found to reside within the hybrid capsule.

In contrast to **9,** the (1,4-naphthalene)bisphosphonate ligands in **10** are not disordered. This can be attributed to the increased size of the aromatic naphthalene moieties. The overall molecular entity in **10** appears to be not as symmetrical as that present in **9** and the compound crystallises in a lower symmetry space group, *P*-1. The symmetry and the increased size of

the 1,4 naphthalenebisphosphonate ligands also affect how the hybrid cages pack in the solid state.

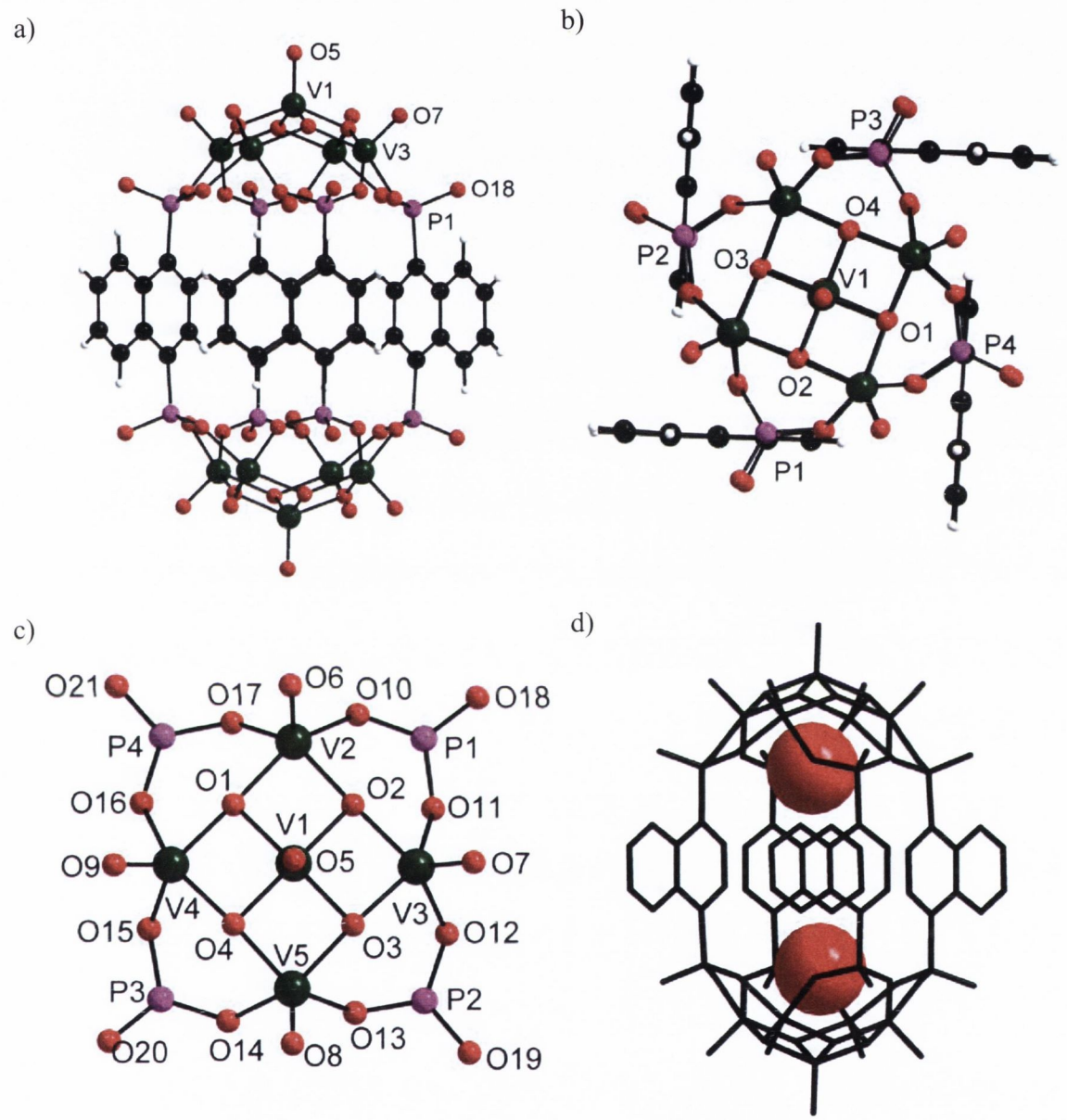

Figure 4.9 – Different perspective views of the anionic cluster $[(V_5O_9)_2(O_3PC_{10}H_6\text{-}4\text{-}PO_3)_4]^{8-}$ in **10**. (a) A ball and stick representation of the anionic cluster in **10** when viewed along the direction of the crystallographic *b*-axis; (b) a perspective view of the phosphonate ligand arrangement; (c) a perspective view of the core structure of the pentanuclear mixed-valent sub-unit. (d) The cluster core in **10** represented as a black wire frame with two space filling represented water molecules within the cage structure. Colour code: V green, P purple, O red, C black, H white.

The arrangement of the naphthalene rings is such that the aromatic rings point towards an adjacent neighbouring aromatic ring in an 'edge to face' arrangement (Fig 4.9b). The distances between the 'edge' C-atoms of the naphthalene moieties and the centre of the aromatic rings of adjacent phosphonate ligands range from 3.822(15) Å to 3.976(14) Å. Oxo ligands O(18), O(19), O(20), and O(21) from each of the phosphonate functionalities point outwards as observed for **9** (Fig 4.9c).

There are eight charge balancing solvated sodium counter-ions per anionic cluster in **10** which adopt a different packing arrangement than those observed in the crystal structure of **9**.

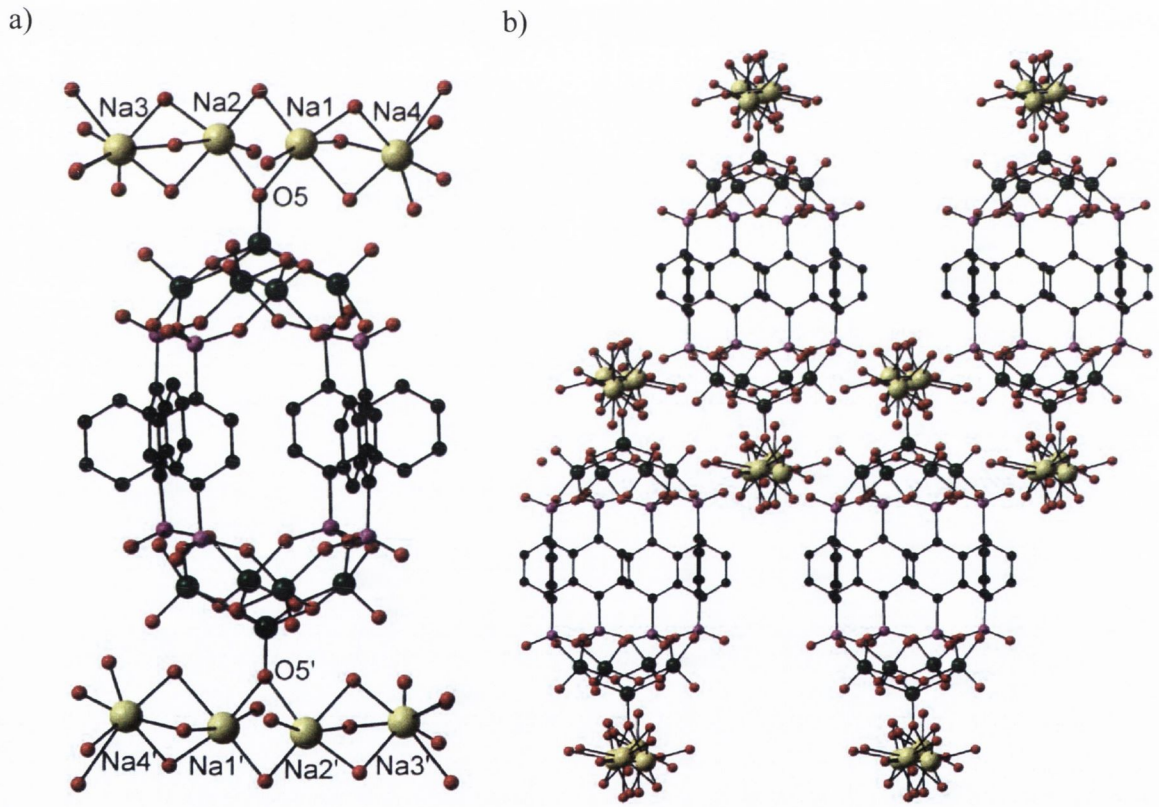

Figure 4.10 – (a) Connectivity of the solvated tetranuclear sodium unit (and symmetry equivalents) to the anionic cluster in **10**. (b) The packing arrangement of the sodium counter-ions in crystal structure of **10** when viewed along the crystallographic *b*-axis. Disordered solvents molecules and hydrogen atoms have been deleted for clarity. Colour code: V green, Na yellow, P purple, O red, C black.

Four solvated sodium counter-ions Na(1), Na(2), Na(3) and Na(4) are arranged to form tetranuclear chains in which the alkali ions are bridged through μ_2-bridging water ligands. These tetranuclear sodium units and their symmetry equivalents are connected to the anionic cluster *via* the apical terminal oxygen atoms O(5), O(5') of the capping motifs (Fig 4.10a). The sodium atoms Na(1) and Na(2) within these tetranuclear sodium chains are further centrally bridged by a μ_2-H_2O molecule leading to edge sharing distorted octahedra. The exterior sodium counter-ions Na(3) and Na(4) in the tetranuclear unit are bridged *via* three water molecules leading to octahedra that share a common face. The tetranuclear sodium motifs align parallel to the crystallographic *b*-axis (Fig 4.10b).

Further hydrogen bonds between the tertranuclear sodium sub-units and adjacent clusters link these entities into a complex network in which additional water and DMF solvent molecules are disordered within in the resulting cavities.

4.4.3 Further solid state characterisation of 10: Thermogravimetric analysis and Infrared spectroscopy

-Thermogravimetric analysis

A TGA was performed for **10** (Fig. 4.11a). An initial weight loss centred at *ca.* 68 °C (16.5%) corresponds to the loss of 26 water molecules with the remaining water molecules lost prior to the TGA measurement. A broad weight loss (16%) ranging between 340 °C and 790 °C corresponds to the loss of the organic moieties through an oxidative degradation process which leads to the decomposition of the capsular entity in **10**.[94]

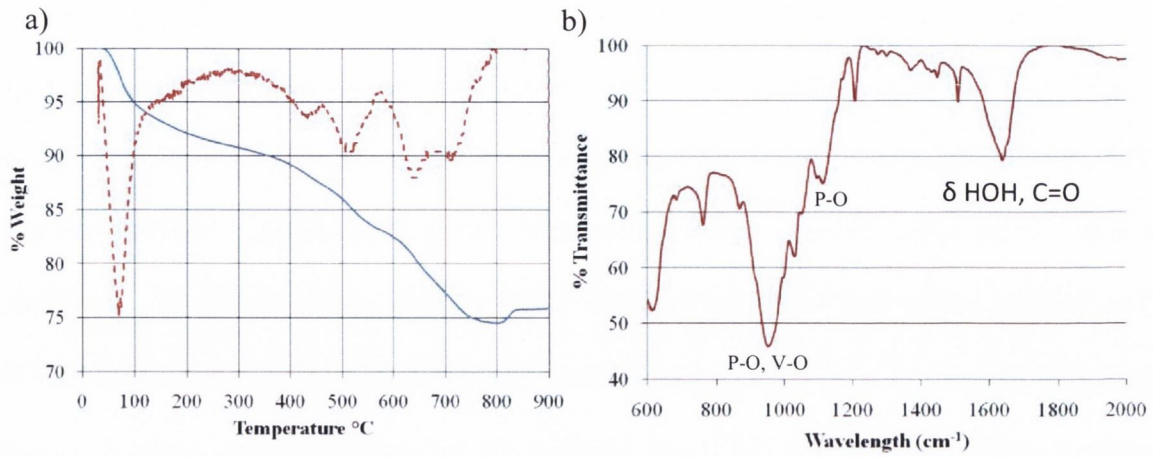

Figure 4.11 – The solid state characterisation of **10**: (a) Thermogravimetric analysis carried out in air (blue line). The derivative of the TGA cure is presented as a red dashed line. (b) Infrared spectrum of **10**, see appendix for full spectrum.

-Infrared spectroscopy

An infrared spectrum of **10** confirms the incorporation of the phosphonate ligand as the characteristic $\{PO_3\}$ bond vibrations are observed at 1108 cm^{-1} and 1119 cm^{-1} (Fig. 4.11b). A strong broad stretch is seen at 961 cm^{-1} which is related to the V-O-V/V-O-P bond vibrations.[38, 42] A shoulder is also observed at 1033 cm^{-1} and is related to the ν(V=O) bond vibration.

4.4.4 Solution characterisation of 10: UV-vis spectroscopy and mass spectrometry

-UV-vis spectroscopy

Compound **10** was dissolved in water and the UV-vis spectrum was recorded (Fig. 4.12a). The UV-vis spectrum displayed very similar absorption to that of the UV-vis spectrum of **9**. An absorption was observed in the near UV region and can be attributed to an intensive MLCT band. [38] A much weaker broad absorbance due to the d-d transitions occurs at 758.5 nm (ε = 537.6 $L.mol^{-1}cm^{-1}$). A shoulder at 618 nm (ε = 482.6 $L.mol^{-1}cm^{-1}$) originates from

intervalence charge transfer.[38, 42] The fluorescence behaviour of **10** was investigated; however, no significant fluorescence could be detected. This could be explained by the heavy atom effect and electron withdrawing abilities of the coordinated transition metals.[21]

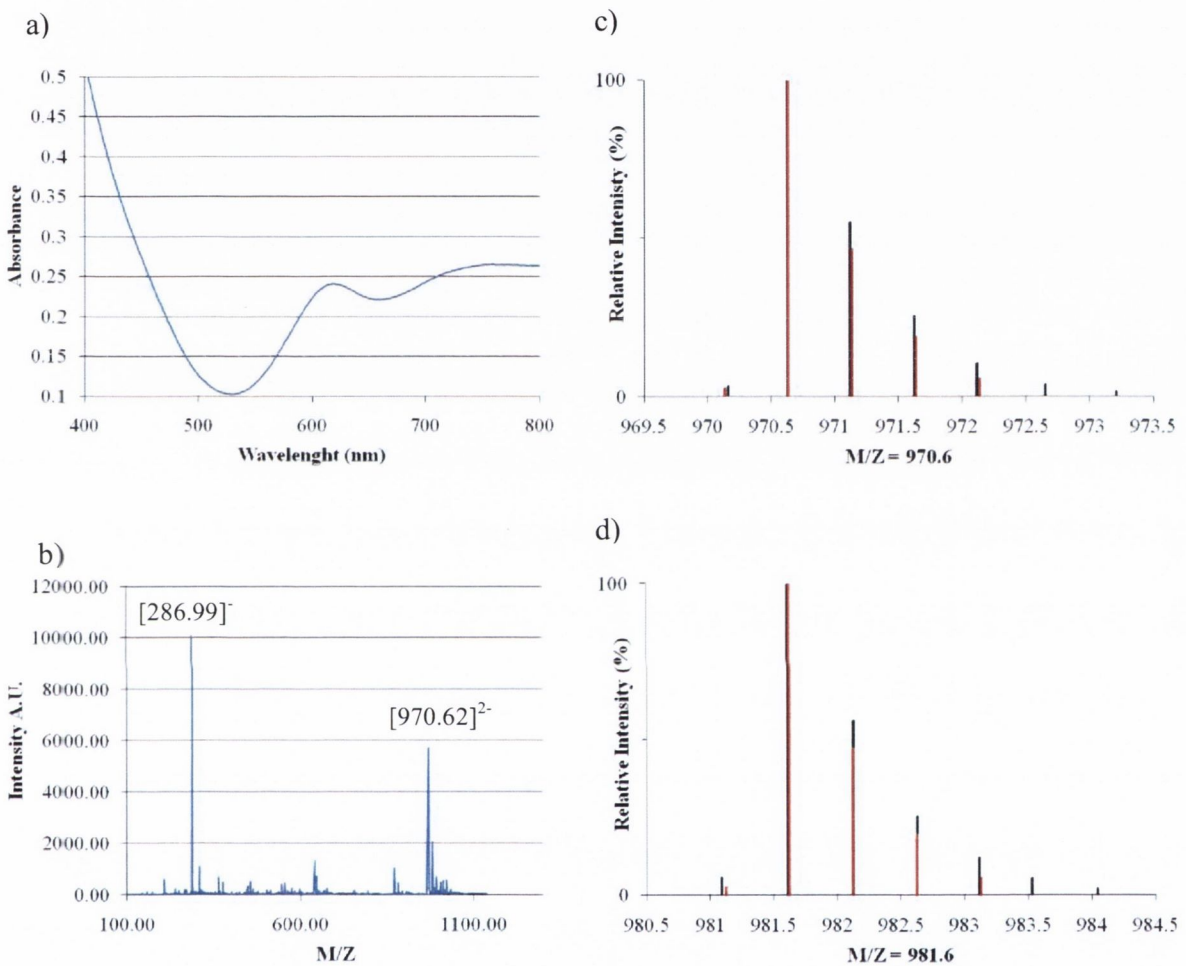

Figure 4.12 – (a) The UV-vis spectrum of a 0.5 mM aqueous solution of **10**. (b) The mass spectra of anionic molecular species of **10** in an aqueous solution: (c) $H_8[V_{10}O_{18}(O_3PC_{10}H_6PO_3)_4]^{2-}$ at m/z = 970.6, (d) $NaH_7[V_{10}O_{18}(O_3PC_6H_4PO_3)_4]^{2-}$ at m/z = 981.6.

-Mass spectrometry

An electrospray mass spectrum in the negative mode was recorded of an aqueous solution of **10** (Fig. 4.12b-d and appendix 4). Two signals were observed and modelled for the anionic cluster species contained within **10** (Fig. 4.12b). A signal at m/z = 970.62 corresponds to -2 charged species with the formula $H_8[(V_5O_9)_2(O_3PC_{10}H_6PO_3)_4]^{2-}$ while the signal at m/z =

981.61 corresponds to $NaH_7[(V_5O_9)_2(O_3PC_6H_4PO_3)_4]^{2-}$. The isotopic distribution patterns of these signals were successfully modelled (Fig. 4.12b-d). A signal is also observed at m/z = 992.60 corresponds to the formula $Na_2H_6[(V_5O_9)_2(O_3PC_6H_4PO_3)_4]^{2-}$. A signal at m/z = 286.99 originates from the deprotonated (1,4-naphthalene)bisphosphonic acid ligand.

Table 4.4 – Crystal data and structure refinement for **10**

Identification code	Compound **10**	
Empirical formula	$C_{40}\ H_{24}\ Na_8\ O_{88}\ P_8\ V_{10}$	
Formula weight	2853.67 g mol^{-1}	
Temperature	150(2) K	
Wavelength	0.71073 Å	
Crystal system	Triclinic	
Space group	*P*-1	
Unit cell dimensions	a = 14.9555(15) Å	α = 109.381(2)°.
	b = 15.1182(15) Å	β = 106.595(2)°.
	c = 17.0608(17) Å	γ = 107.314(2)°.
Volume	3141.7(5) $Å^3$	
Z	1	
Density (calculated)	1.508 Mg/m^3	
Absorption coefficient	0.940 mm^{-1}	
F(000)	1406	
Crystal size	0.3 x 0.2 x 0.2 mm^3	
Theta range for data collection	1.40 to 25.07°.	
Index ranges	-17<=h<=17, -18<=k<=17, -20<=l<=20	
Reflections collected	25572	
Independent reflections	9123 [R(int) = 0.0924]	
Completeness to theta = 25.07°	99.8 %	
Refinement method	Full-matrix least-squares on F^2	
Data / restraints / parameters	9123 / 0 / 701	
Goodness-of-fit on F^2	0.988	
Final R indices [I>2sigma(I)]	R_1 = 0.1049, wR_2 = 0.2876	
R indices (all data)	R_1 = 0.1448, wR_2 = 0.3048	
Largest diff. peak and hole	3.193 and -0.981 e.$Å^{-3}$	

4.5 Synthesis of a mixed-valent vanadium capsule(V^{IV}/V^{V}) incorporating ([1,1'-biphenyl]-4,4'-diyl)bisphosphonic acid

4.5.1 The synthesis of $Na_8H_2[(DMF)_2{\subset}V_{10}O_{18}(O_3PC_{12}H_8\text{-}4\text{-}PO_3)_4]\cdot 30H_2O$ (11)

The structure of the anionic cluster in **9** prompted us to use ([1,1'-biphenyl]-4,4'-diyl)bisphosphonic acid as a ligand in order to augment the cluster cage. This effort lead to the coordination compound $Na_8H_2[(DMF)_2{\subset}V_{10}O_{18}(O_3PC_{12}H_8\text{-}4\text{-}PO_3)_4]\cdot 30H_2O$ (**11**) which forms under the same synthetic conditions as **9**. Green tetragonally eleongated crystals of **11** formed after several hours and were used for single crystal X-ray diffraction studies.

4.5.2 The structural characterisation of $Na_8H_2[(DMF)_2{\subset}V_{10}O_{18}(O_3PC_{12}H_8\text{-}4\text{-}PO_3)_4]\cdot 30H_2O$ (11)

The structure of the anionic cluster in **11** is closely related to that observed in the structure of **9** and is found to crystallise in the same space group, *P*4/mnc. Similarly to **9** it consists of two typical concave mixed-valent $\{V^{V}O(\mu_3\text{-}O)_4V^{IV}{}_4O_{12}\}$ sub-units that are connected by four ([1,1'-biphenyl]-4,4'-diyl)bisphosphonate ligands which generate a cage-like structure. The ligands bind to the peripheral vanadium ions in an identical bridging mode that was observed in **9** (Fig. 4.13). In the case of **11**, we observe an elongation of the crystallographic *c*-axis due to the extra aromatic ring that has been introduced into the organic ligands. The aromatic ring systems of the ligands are disordered over two positions. Using bond valence sum analysis, the oxidation state of the central vanadium ion V(1) was calculated to be oxidation state +V. The bond length between V(1) and the $\mu_3\text{-}O^{2-}$ ligands O(2) is 1.885(11) Å and the bond

distance of the terminal V(1)=O_{term} bond is 1.630(10) Å long (Fig. 4.13a). The peripheral vanadium ion V(2) is calculated to be in oxidation state +IV. This vanadium ion binds to oxygen donor atoms with bond distances between 1.953(3) Å and 1.966(3) Å whilst the terminal V=O bond which has a bond distance is 1.606(2) Å.

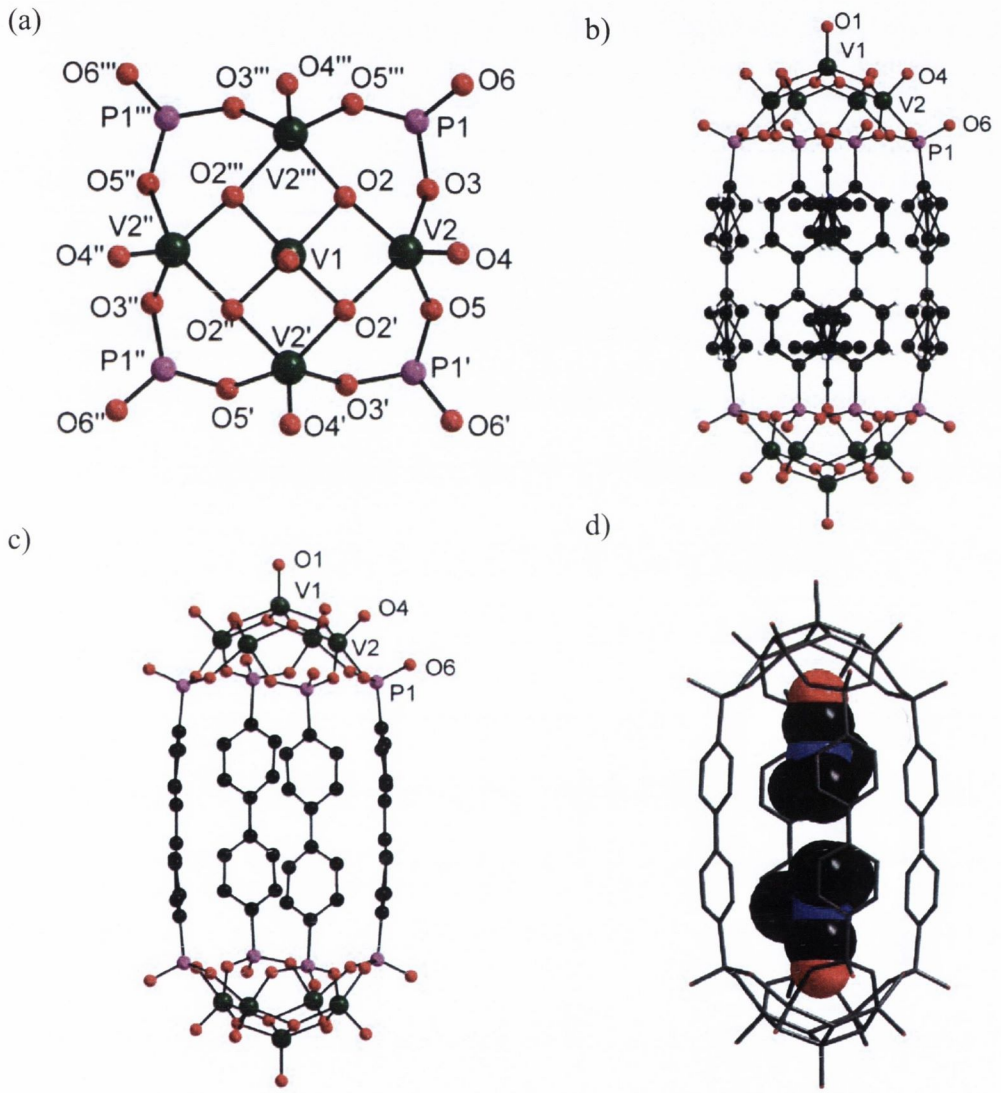

Figure 4.13 – (a) A ball and stick representation of the core structure of the mixed-valent sub-unit of the cage structure. (b) The anionic cluster within **11** as viewed in the direction of the crystallographic *b*-axis. (c) The anionic cluster within **11** with one set of the disordered phenyl rings deleted and with the encapsulated solvent molecules removed for clarity. (d) The anionic cluster core of **11** as a grey wire frame with two DMF molecules (space-filling representations) within the cage structure. Colour code: V green, P purple, O red, N blue, C black. H atoms omitted for clarity.

Table 4.5 – Bond sum valence analysis for **11**		
V & O sites	Bond Valence Sum (BVS)	Assigned Oxidation State
V(1)	5.125	+5
V(2)	4.166	+4
μ_3-O (2)	2.108	-2
μ-O (3) (5)	1.948, 1.977	-2
$O_{terminal}$ (1)(4)	1.644, 1.649	-2

The oxidation states of the vanadium ions have been summarised in Table 4.5. There are two DMF molecules encapsulated within the cage. The oxygen atoms of the DMF molecules are located directly below the central vanadium ions V(1) in the focal point of the concave mix-valent capping motif. The distances between the oxygen atoms of the DMF molecules and the vanadium metal centers in the mixed-valent capping motif vary from 3.040(1) Å to 3.064(1) Å. The position of the DMF methyl groups are disordered over four positions around the central N(1) atom (see Fig. 4.13b and Fig. 4.13d) and are directed towards the more hydrophobic centre of the capsule. The dimensions of the cage in **11** are characterised by an intramolecular V^V-V^V distance of 16.9 Å, a square arrangement of four P atoms with a P-P distance of 5.5 Å. The biphenyl moieties in **11** are slightly curved and the distances between the planes of parallel aligned aromatic rings deviate between 8.2 and 8.5 Å.

There are eight charge balancing sodium counter-ions per anionic cluster in **11**. Within the crystal structure, the solvated sodium counter-ions link the hybrid cages forming inorganic layers with interconnecting organophosphonate ligands. These inorganic layers are located in the *ab* plane of the crystal structure as shown in Fig. 4.14a. The peripheral V=O terminal oxygen atoms as well as the peripheral P=O terminal oxygen atoms of each cluster cap are linked through a complicated connectivity to the solvated sodium ions within the inorganic layers. Furthermore, distorted octahedrally coordinated sodium counter-ions are also located

within the cavities between adjacent clusters and are surrounded by six solvating water molecules (Fig. 4.14b). The overall crystal structure of **11** can be visualised as a layered structure in which the organic aromatic residues act as pillars (Fig. 4.14b).

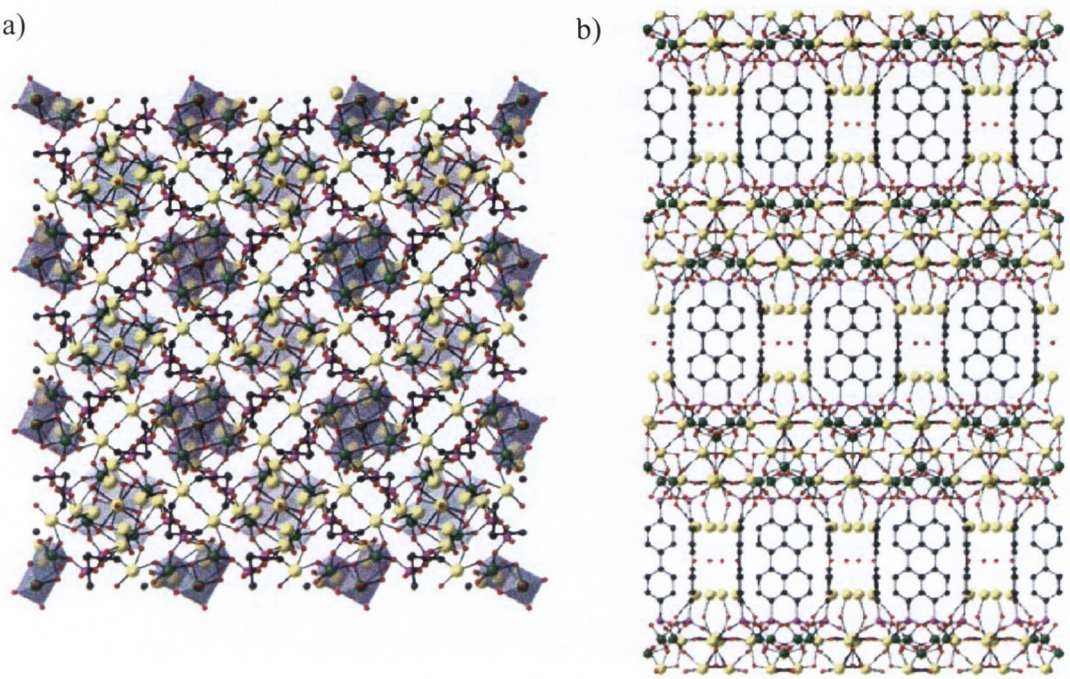

Figure 4.14 – (a) Packing arrangement of the clusters in the crystal structure of **11** when viewed in the direction of the crystallographic *c*-axis, ({VO_5} green). (b) A view of the packing arrangement of the hybrid cages in **11** as viewed in the crystallographic *b*-axis. The disordered solvent molecules and H atoms have been removed for clarity. The aromatic rings and sodium counter-ions are disordered. Colour code: V green, P purple, Na yellow, O red, C black.

4.5.3 Further solid state characterisation of 11: Thermogravimetric analysis and Infrared spectroscopy

-Thermogravimetric analysis

Thermogravimetric analysis was carried out to investigate the thermal stability of **12** in an air atmosphere in a temperature range between 30 °C and 900 °C (Fig. 4.15a). The overall decomposition behaviour of **11** is very similar to that of **9**. An initial step between 25 °C and 200 °C (9%) corresponds to the loss of the DMF and water molecules. Oxidation of the

organic ligands can be attributed to a broad thermogravimetric step at 425 °C and most likely results in the generation of an inorganic oxide.[94]

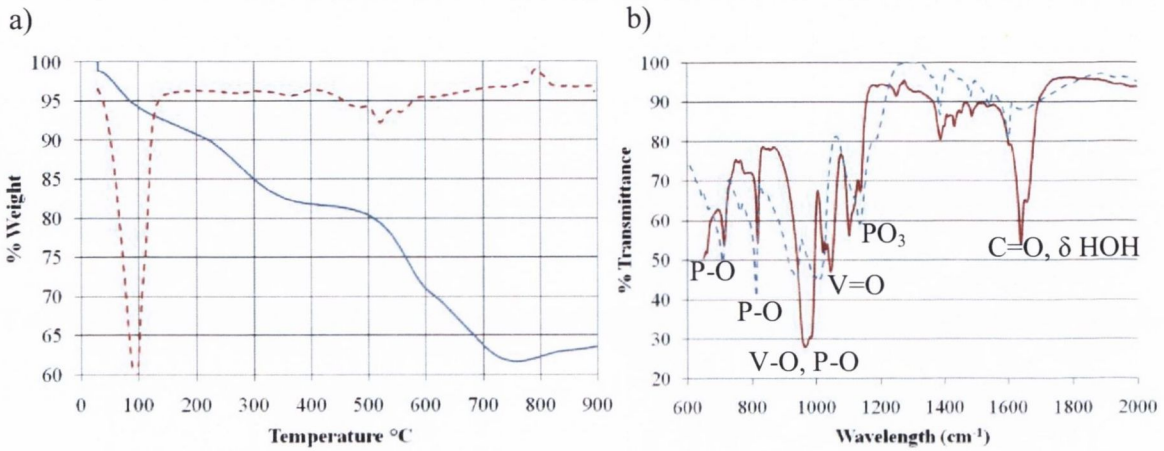

Figure 4.15 – (a) A TGA of **11** in air (blue line). The calculated derivative of the TGA curve has also been included (red dashed line). (b) The infrared spectrum of **11** (red) when compared to the infrared spectrum of ([1,1'-biphenyl]-4,4'-diyl)bisphosphonic acid (blue dashed line).

-Infrared spectroscopy

An infrared spectrum of **11** was measured and is shown in Fig. 4.15b and appendix 4. The infrared spectrum confirms the inclusion of the ([1,1'-biphenyl]-4,4'-diyl)bisphosphonate ligand in the complex through the observation of the characteristic $\{PO_3\}$ bands at 1105 cm^{-1}. A band appears at 1027 cm^{-1} corresponding to the ν(V=O) bond vibrations and several bands at 714 cm^{-1}, 804 cm^{-1} and 972 cm^{-1} were observed relating to the P-O and V-O vibration stretches of their respective bonds.

4.5.4 Solution characterisation of 11: Mass spectrometry and UV-vis spectroscopy

Similar to **9** and **10**, an electrospray mass spectrum in the negative mode was recorded of an aqueous solution of **11** (Fig. 4.16). A large number of anionic species with different numbers of counter-ions were observed for **11** in the mass spectrum. A summary of the recorded signals including weight signals that were observed but not modeled due to weak envelope intensities are displayed in Table 4.6

Table 4.6 – Molecular weight signals observed in the mass spectrum of **11** in solution

Molecular species	Charge	M/Z
$H_3[O_3PC_{12}H_8PO_3]^{1-}$	-1	313.0 (ligand)
$NaH_2[O_3PC_{12}H_8PO_3]^{1-}$	-1	335.0
$H_8[(V_5O_9)_2(O_3PC_{12}H_8PO_3)_4]^{2-}$	-2	1022.6 (modelled)
$NaH_7[(V_5O_9)_2(O_3PC_{12}H_8PO_3)_4]^{2-}$	-2	1023.1 (modelled)
$Na_2H_6[(V_5O_9)_2(O_3PC_{12}H_8PO_3)_4]^{2-}$	-2	1023.6 (modelled)
$Na_3H_5[(V_5O_9)_2(O_3PC_{12}H_8PO_3)_4]^{2-}$	-2	1024.1
$H_7[(V_5O_9)_2(O_3PC_{12}H_8PO_3)_4]^{3-}$ -H_2O	-3	675.4 (modelled)
$H_7[(V_5O_9)_2(O_3PC_{12}H_8PO_3)_4]^{3-}$	-3	681.4
$NaH_6[(V_5O_9)_2(O_3PC_{12}H_8PO_3)_4]^{3-}$	-3	688.7
$H_6[(V_5O_9)_2(O_3PC_{12}H_8PO_3)_4]^{4-}$ - H_2O	-4	501.8
$NaH_5[(V_5O_9)_2(O_3PC_{12}H_8PO_3)_4]^{4-}$ - H_2O	-4	507.3

The deprotonated ([1,1'-biphenyl]-4,4'-diyl)bisphosphonate ligand and its sodium salt were observed at m/z = 313.0, $H_3[O_3PC_{12}H_8PO_3]^{1-}$ and m/z = 335.0, $NaH_2[O_3PC_{12}H_8PO_3]^{1-}$ respectively. The anionic cluster species of **11** was observed in the mass spectrum as a -2 charged species at m/z = 1022.6, m/z = 1023.6, m/z = 1023.6 and m/z = 1024.1.

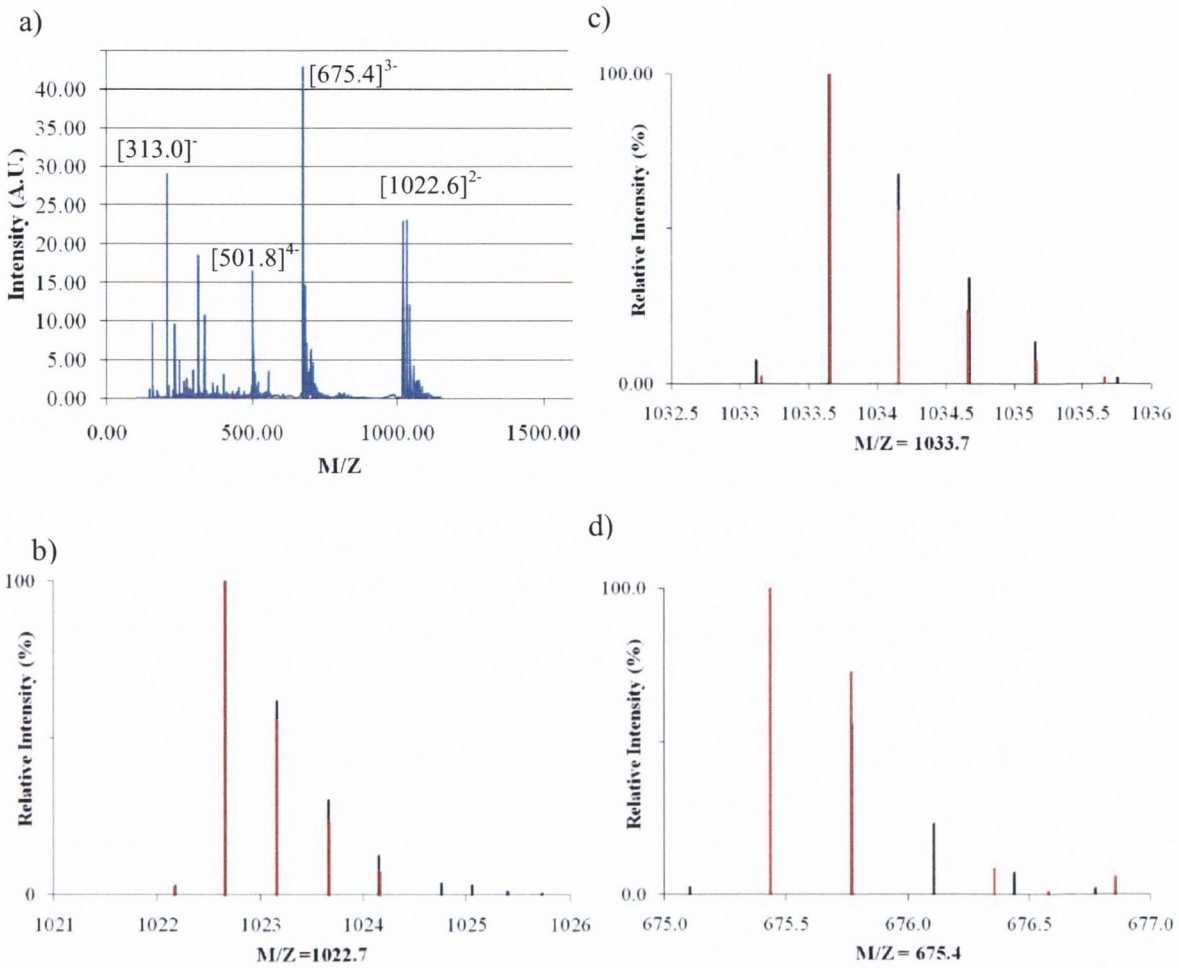

Figure 4.16 – (a) The mass spectrum of **11** dissolved in an aqueous solution. The experimental (black) and modelled (red) mass spectra: (b) $H_8[V_{10}O_{18}(O_3PC_{12}H_8PO_3)_4]^{2-}$ at m/z = 1022.7 and (c) $NaH_7[V_{10}O_{18}(O_3PC_{12}H_8PO_3)_4]^{2-}$ at m/z = 1033.7. (d) $H_7[V_{10}O_{18}(O_3PC_{12}H_8PO_3)_4]^{3-}$ - H_2O at m/z = 675.4

These signals correspond to the fully protonated anionic species, $H_8[V_{10}O_{18}(O_3PC_{12}H_8PO_3)_4]^{2-}$ and the sodium salts, $NaH_7[V_{10}O_{18}(O_3PC_{12}H_8PO_3)_4]^{2-}$, $Na_2H_6[V_{10}O_{18}(O_3PC_{12}H_8PO_3)_4]^{2-}$ and $Na_3H_5[V_{10}O_{18}(O_3PC_{12}H_8PO_3)_4]^{2-}$ respectively. Two -3 charged species are observed at m/z = 681.4 and m/z = 688.743 corresponding to the fully protonated anionic cluster, $H_7[V_{10}O_{18}(O_3PC_{12}H_8PO_3)_4]^{3-}$ and its respective sodium salt, $NaH_6[V_{10}O_{18}(O_3PC_{12}H_8PO_3)_4]^{3-}$. Two -4 charged species are observed at m/z = 501.8 and m/z = 507.3 corresponding to $H_6[V_{10}O_{18}(O_3PC_{12}H_8PO_3)_4]^{4-}$ and the respective sodium salt $NaH_5[V_{10}O_{18}(O_3PC_{12}H_8PO_3)_4]^{4-}$. In both cases the observed signals relate these species and a

sequential loss of one water molecule. The isotopic distribution patterns of the anionic species with the most intensive isotopic envelopes of the signals were modeled and are shown in Fig. 4.16b – d.

- *UV-vis spectroscopy*

A UV-vis spectrum of an aqueous solution of **11** was recorded (Fig. 4.17). Similarly to the solution of **9** and **10**, an intensive charge transfer absorption was observed in the near UV region.[38] A weaker broad absorbance due to the d-d transitions was observed at 723 nm (ε = 414.5 $L.mol^{-1}cm^{-1}$) with a small shoulder at 618 nm (ε = 439 $L.mol^{-1}cm^{-1}$) relating to an intervalence charge transfer.[38, 42]

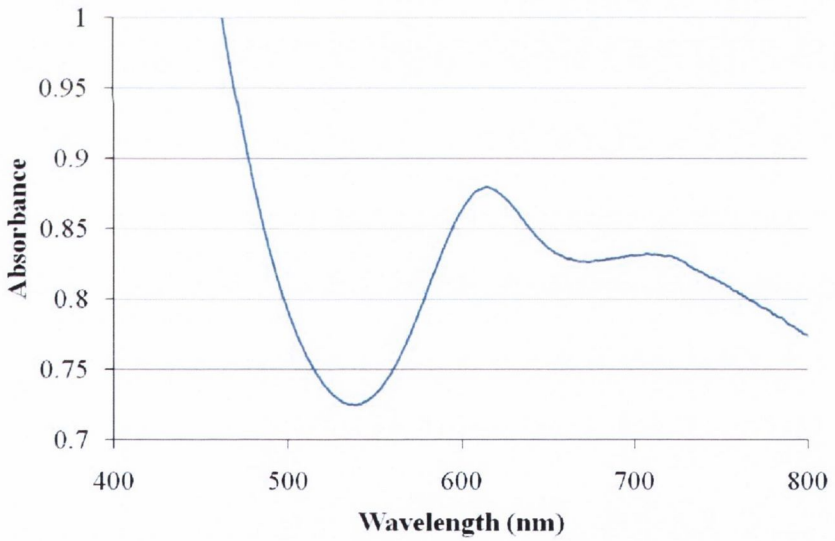

Figure 4.17 – (a) The UV-vis spectrum of a 1mM aqueous solution of **11**.

Table 4.7 – Crystal data and structure refinement for **11**

Identification code	Compound **11**	
Empirical formula	$C_{27}\ H_{46}\ N_1\ Na_4\ O_{36.5}\ P_4\ V_5$	
Formula weight	1439.19 g mol^{-1}	
Temperature	150(2) K	
Wavelength	0.71073 Å	
Crystal system	Tetragonal	
Space group	*P*4/mnc	
Unit cell dimensions	a = 12.2764(17) Å	α = 90°.
	b = 12.2764(17) Å	β = 90°.
	c = 38.948(8) Å	γ = 90°.
Volume	5869.9(16) $Å^3$	
Z	4	
Density (calculated)	1.630 Mg/m^3	
Absorption coefficient	0.998 mm^{-1}	
F(000)	2904	
Crystal size	0.1 x 0.1 x 0.2 mm^3	
Theta range for data collection	1.05 to 25.50°.	
Index ranges	-14<=h<=14, -14<=k<=14, -46<=l<=37	
Reflections collected	28789	
Independent reflections	2792 [R(int) = 0.0327]	
Completeness to theta = 24.99°	100.0 %	
Refinement method	Full-matrix least-squares on F^2	
Data / restraints / parameters	2792 / 13 / 292	
Goodness-of-fit on F^2	1.177	
Final R indices [I>2sigma(I)]	R_1 = 0.0570, wR_2 = 0.1801	
R indices (all data)	R_1 = 0.0641, wR_2 = 0.1873	
Largest diff. peak and hole	1.389 and -0.719 e.$Å^{-3}$	

4.6 An investigation of the bio-toxicity of 9 and 11 against three different cancer cells lines

The physiological activity of vanadium compounds has previously been discussed in chapter 1. In particular, Yamase and others have shown that polyoxometalates can display a wide variety of biological activity such as anti-tumour, anti-viral and anti-microbial activity.[78-80] Compounds **9** and **11** were shown to be stable in aqueous solution through their characterisation with mass spectrometry and their characteristic UV-vis spectra. In collaboration with Prof Clive William's group of the biochemistry department, Trinity College Dublin, we investigated in preliminary studies the toxicity effect of **9** and **11** on three different types of cancerous cells derived from the (a) chronic myelogenous leukaemia cancer cell line, K562 (b) lung carcinoma cancer cell line, A549 and (c) mutu-I: Burkitt's lymphoma cancer cell line. This study was also carried out to investigate the mechanistic effect, dose response and time response for each new hybrid compound.

The cell viabilities were tested in the presence of **9** and **11** at three standardised doses (100μm, 10μm, 1μm) (Fig. 4.18). A wide range of controls were carried out to ensure that additional factors implicating cell death were accounted for. The starting materials sodium orthovanadate, (1,4-benzene)bisphosphonic acid and ([1,1'-biphenyl]-4,4'-diyl)bisphosphonic acid were tested against the cancer cells and were found to have a negligible effect (see appendix 4). All the starting materials were dissolved in sterilised water for the dose administration to test cell viability. Compounds **9** and **11** were tested under similar conditions using sterilised water as a solvent.

The results are shown in Fig. 4.18 and demonstrate that the compounds are moderately toxic. The response of the cell viability for each cell line to the three different administered concentrations of **9** and **11** is very similar and the compounds do not show any significant

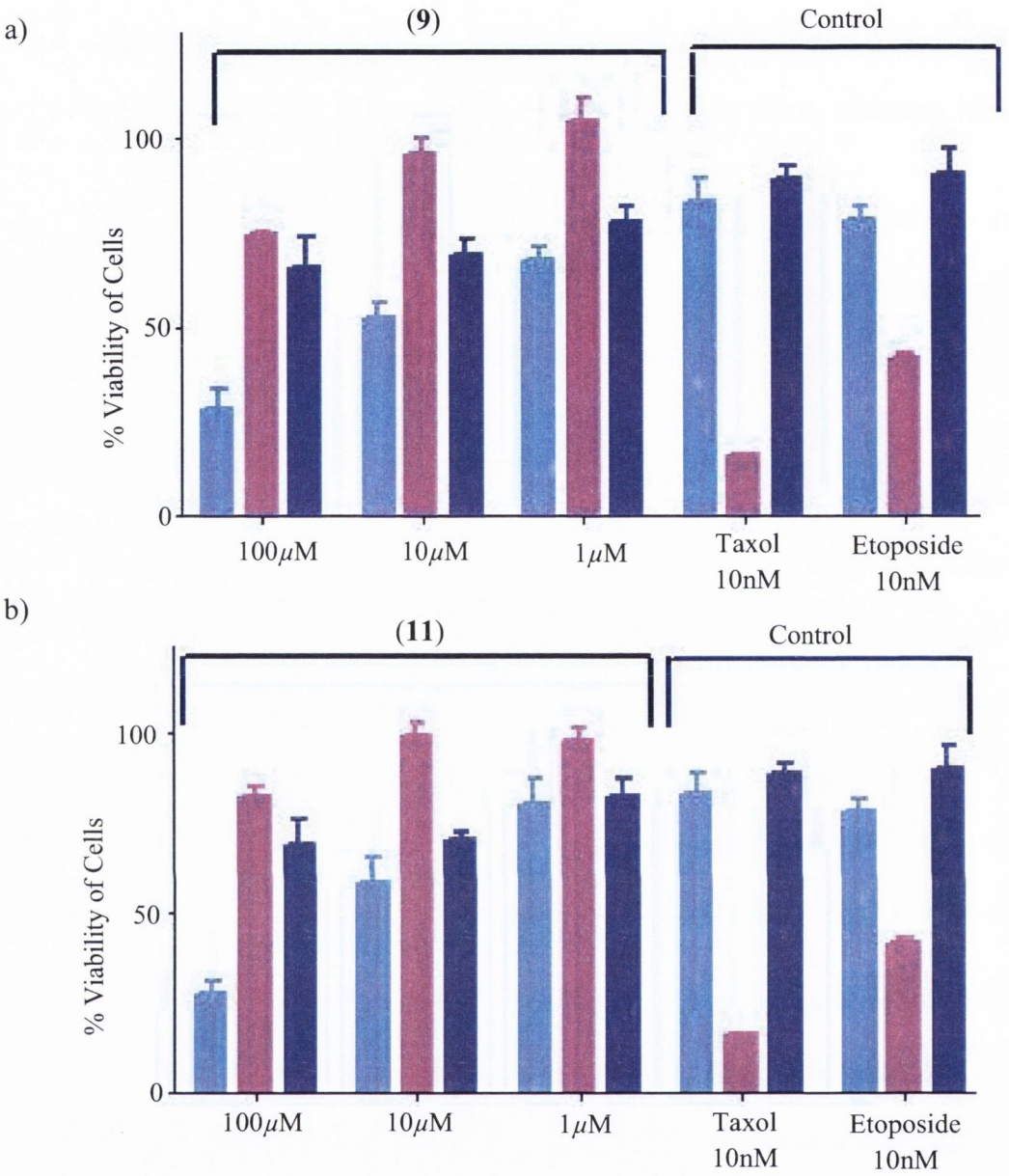

Figure 4.18 – (a) The viability of cells (%) versus the concentration of **9**. (b) The viability of cells (%) versus the concentration of **11**. The cell viability was also analysed against a control group as well as the solvent in which the compounds were dissolved in. Colour code: A549 light blue, Mutu-ls pink, K562 dark blue.

selectivity. The potency mechanism seems to be dependent on the polyoxovanadate cores and their compositions rather than on the actual size of the hybrid cages. The lung carcinoma cell viability shows approximately a linear relationship to the administered concentrations of **9** and **11**. The total percentage of the killed cells varies from 30 % - 70 % depending on the administered concentrations which range from 1 μM to 100 μM.

The Burkitt's lymphoma cancer cells show a more diminished response to **9** and **11**. The total percentage of killed Burkitt's lymphoma cells ranges between 25 % and 35 % for the concentrations of 1 μM and 100 μM, respectively. The leukaemia cancer cells show a very low dose response to **9** and **11** with the maximum dose concentration of 100 μM killing *ca.* 25 % of the leukaemia cells. Commercially available and licensed anticancer drugs Taxol and Etoposide, which operate at nanomolar concentrations were used as control drugs to verify our cell viability experiments.

Our results demonstrate that the investigated compounds have limited anticancer activity and cannot be regarded as promising candidates for anti-cancer treatment. However it might be interesting to establish the mechanism by which these polyoxometalates are inducing cell death. An understanding of the mechanism of action may help to overcome their limitations. In light of their low toxicity towards cancer cells, it would be of interest to determine their toxicity towards healthy cells. The capsular entities in this class of compound or in related host-guest systems could have the potential to be used in advanced drug delivery systems or sensors under physiological conditions.

4.7 Magnetic properties of 1, 5, 9 and 11

The compounds presented in this chapter possess structural motifs that are closely related to the structures of the compounds presented in chapter 2 and 3. We decided to investigate the magnetic properties of **9** and **11** and compare these with the representative compounds **1** and **5**. We were hoping that structure would allow us to elucidate magnetic interaction pathways within the core structures. The magnetic susceptibility measurements were recorded and

modeled by Dr. Rodolphe Clèrac using a Quantum Design SQUID magnetometer MPMS-XL housed at the Centre de Recherche Paul Pascal.

Compounds **1**, **9** and **11** can be considered from a magnetic point of view as squares of $S = ½$ V^{IV} spins with a central diamagnetic V^{V}. For **9** and **11**, these squares are assembled into pairs *via* bridging aromatic diphosphonate ligands resulting in the formation of molecular capsules. In the case of **6**, the same V_4 square motif (without the central V^{V}) is observed but it assembles through V^{IV} dinuclear motifs into a cage-like structure (3.2.2). In all cases, the interactions between the two motifs are likely to be weak and the main magnetic interactions should prevail within the tetranuclear and dinuclear moieties.

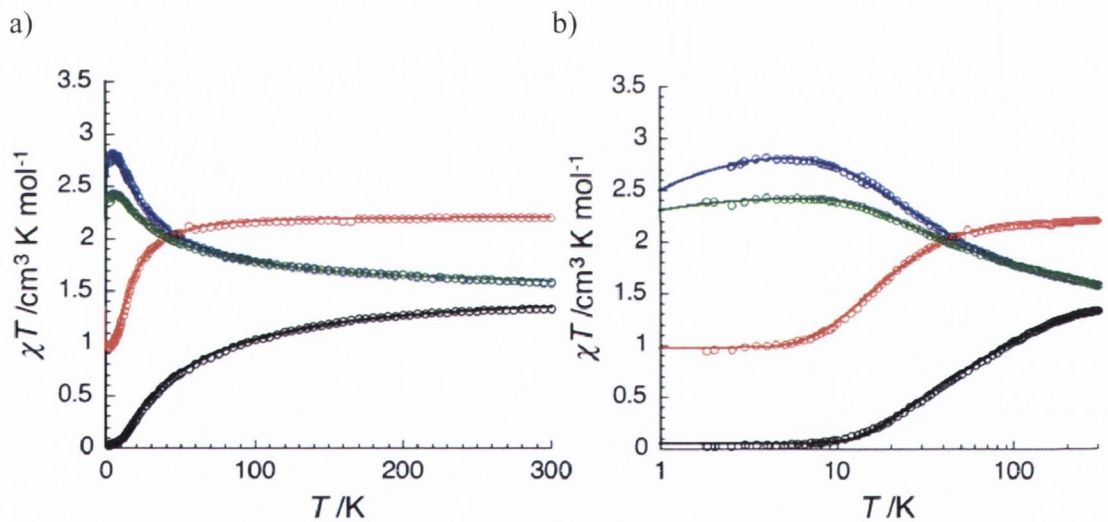

Figure 4.19 – (a) Temperature dependence of the χT product of **1** (black), **5** (red), **9** (blue), and **11** (green). (b) A magnified view of the χT product of (a) between 1 and 100 Kelvin.

At room temperature, the χT products have values of 1.33, 2.20, 1.58 and 1.57 cm^3 K mol^{-1} for **1**, **5**, **9** and **11**, respectively (Fig. 4.19). For **1**, **9** and **11**, the measured values are in good agreement with the expected value (1.50 cm^3Kmol^{-1}) for four V^{IV} metal ions ($S = 1/2$, $g = 2.0$: $C = 0.375$ cm^3 K mol^{-1}). In the case of **5**, the measured value is also in good agreement with the expected value (2.25 cm^3Kmol^{-1}) for six V^{IV} metal ions ($S = 1/2$, $g = 2.0$: $C = 0.375$ cm^3 K

mol^{-1}). Amongst the complexes that possess the mixed-valent pentanuclear $\{V^{IV}_4V^{V}\}$ core, **1** reveals a temperature dependence of the susceptibility that is significantly different from that of **9** and **11**.

4.7.1 Modelling the magnetic susceptibility of **1**

Decreasing the temperature, the χT product of **1** steadily decreases to vanish almost completely below 8 K with a residual value of 0.02 cm^3 K mol^{-1} at 1.8 K. This behavior suggests antiferromagnetic interactions between the V^{IV} ions resulting in a singlet ground state ($S_T = 0$). In an attempt to model the magnetic interactions between the V ions, two S = ½ tetranuclear Heisenberg models were proposed: Model 1 (Fig. 4.20a) proposes an equal magnetic interaction, *J*, between the four S = ½ metal ions. Model 2 (Fig. 4.20b) is similar to model 1 and proposes a magnetic interaction, *J*, between the four metal centres. However this model includes a second magnetic coupling constant, *J'*, allowing coupling between the four V^{IV} S = ½ through the central V^{V} diamagnetic centre.

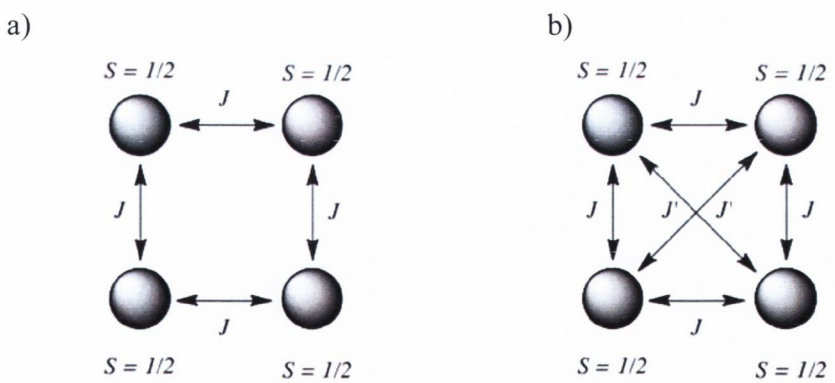

Figure 4.20 – (a) Model 1 only considers one coupling constant, *J*, between the V^{IV} centres. (b) Model 2 takes two coupling constants *J* and *J'* into account.

The application of the van Vleck equation[95] to the Kambe's vector coupling scheme[96] allows the determination of an analytical expression of the magnetic susceptibility from the following spin Hamiltonian:

$$H = -2J\{S_1 \bullet S_2 + S_2 \bullet S_3 + S_3 \bullet S_4 + S_1 \bullet S_4\} - 2J'\{S_1 \bullet S_3 + S_2 \bullet S_4\} \qquad \textbf{eq. 1}$$

where $\boldsymbol{S}_i$ are the spin operators (S = 1/2 for V^{IV}). The expression of the magnetic susceptibility for the models 1 and 2, in the low field limit is derived from literature.[97] As usual for the analysis of the magnetic properties, the model with the least parameters (J and g) was used to fit the experimental data.

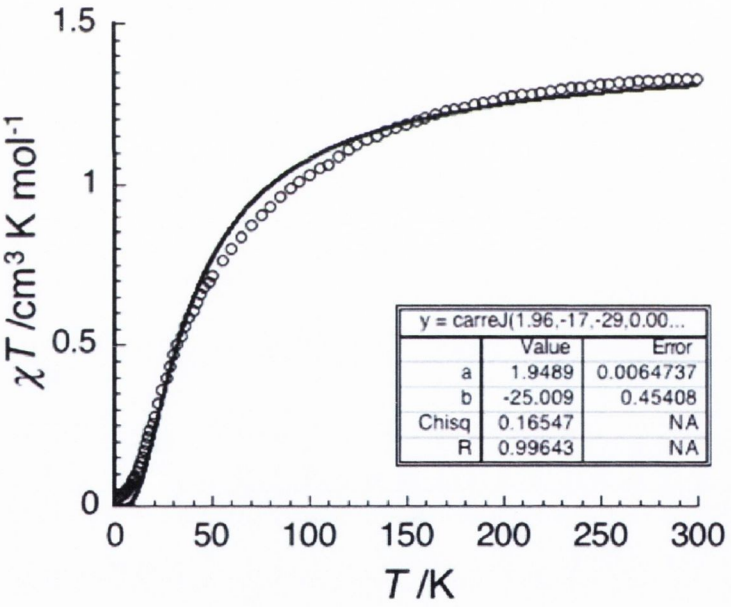

Figure 4.21 – Temperature-dependence of the χT product of **1**. Solid line: Fit using Model 2.

Unfortunately, model 1 (eq. 1 without J' term) failed to reproduce correctly the experimental data but gave a rough indication of the magnetic interaction between the V^{IV} ions, suggesting a coupling constant, J, of approximately -25 K. The initial trial experiment using model 1 underlines the relevance of the magnetic interaction, J', as proposed in model 2 (eq. 1).

Therefore model 2 was considered to be appropriate to fit the experimental data (Fig. 4.21). We found that the two proposed exchange pathways are of similar magnitude. The best fit between the modelled susceptibility and experimental data was obtained with $J/k_B = J'/k_B = -27.8(5)$ K and $g = 1.99(2)$.

4.7.2 Modelling the magnetic susceptibility of **9** and **11**

The analysis of the magnetic properties only considers the tetranuclear $\{V_4\}$ units in **9** and **11**. This approach allows a direct comparison with the magnetic properties of **1**. Decreasing the temperature, the χT products of **9** and **11** steadily increase to maxima at 5.0 and 6.1 K of 2.8 and 2.4 cm^3 K mol^{-1}, respectively (Fig. 4.18), demonstrating the presence of dominating ferromagnetic interactions within the $\{V^{IV}_4\ V^{V}\}$ cores and thus a possible $S_T = 2$ spin ground state per pentanuclear unit. It is worth mentioning that similar paramagnetic behaviour was observed by Karet *et al.* for related structural motifs.[41] At lower temperature, the χT products decrease slightly to 2.7 and 2.3 cm^3 K mol^{-1} at 1.8 K indicating the presence of weak inter-complex anti-ferromagnetic interactions.

Model 2 was used to fit the experimental data but in order to reproduce the decrease of the χT product below 6 K, inter-complex interactions have been included in the mean field approximation. In this approximation, the magnetic susceptibility is given by the following expression:

$$\chi = \frac{\chi_{V_4}}{1 - \frac{2zJ_{AF}}{Ng^2\mu_B^2}\chi_{V_4}} \qquad \textbf{eq. 2}$$

where J_{AF} is the inter-tetramer interaction, z the number of neighboring $\{V_4\}$ complexes and χ_{V4} is the expression of the magnetic susceptibility for the tetranuclear models 1 and 2 in the low field limit as derived from literature.[97] The best set of parameters obtained using this model are J/k_B = +32.4(2) K; J'/k_B = -12.4(1) K; zJ_{AF}/k_B = -0.04(1) K and g = 1.98(2) for **9** and J/k_B = +37(4) K; J'/k_B = -19(3) K; zJ_{AF}/k_B = -0.01(1) K and g = 1.98(2) for **11** (blue and green solid lines in Fig. 5.16). The sign of the magnetic interactions implies that the $\{V_4\}$ units possess S_T = 2 spin ground states even if the magnetic interactions, J', remain antiferromagnetic by nature. The S_T = 2 spin ground states of **9** and **11** are also supported by the good fits of the M *vs.* H data obtained using an S = 2 Brillouin function (Fig. 4.22; g = 1.99(1) for **9** and **11**). The presence of weak inter-complex antiferromagnetic interactions is confirmed by the negative values of the zJ_{AF} interactions that remain in an order of 40-10 mK.

a) b)

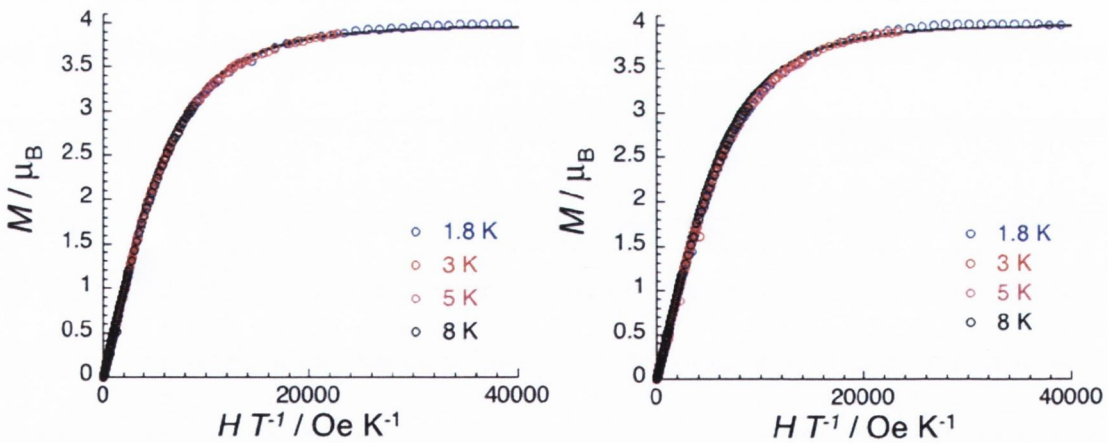

Figure 4.22 – Field-dependence of the magnetisation. Solid lines: calculated data using an S = 2 Brillouin function. (a) M *vs.* H data for **9**. (b) M *vs.* H data for **11**.

The most important difference between **9** / **11** and **1** is the sign of the coupling constant. While this magnetic interaction, is anti-ferromagnetic in **1** (J/k_B = -27.8(5) K), it becomes ferromagnetic in **9** and **11**, (J/k_B = +32.4(2) K and J/k_B = +37(4) K, respectively).

4.7.3 Modelling of the magnetic susceptibility of **5**

The analysis of the magnetic properties only considers half of the symmetric cluster core of **5** ($\{V_4\}$ + $\{V_2\}$ units). Decreasing the temperature, the χT product of **5** steadily decreases to reach a plateau below 6 K of *ca.* 1.0 cm^3 K mol^{-1} thus suggesting this complex has a triplet ground state (S_T = 1). This observation suggests a dominant anti-ferromagnetic interaction as observed in **1** but with a residual paramagnetic contribution. A hypothesis to explain this result predicts that the $\{V^{IV}_4\}$ core has the same behavior than that in **1** (stabilising a singlet ground state) and the connecting dinuclear units also present in **5** possess intra-molecular ferromagnetic interactions. In order to probe this assumption, the magnetic data were fitted to model 2 that treats the $\{V^{IV}_4\}$ core as in **1**. The $\{V^{IV}_2\}$ dinuclear unit was modelled using the following Hamiltonian:

$$H = -2J_d \{S_5 \bullet S_6\} \qquad \textbf{eq. 3}$$

The theoretical susceptibility is thus the sum of the susceptibilities for the tetranuclear and dinuclear unit that are given in the low field limit as defined in literature.[97, 98] The best set of parameters obtained using this model are J/k_B = -11.9(2) K; $J'/k_B \approx$ 0.0(5) K; J_d/k_B = +48(10) K and g = 1.98(2) (red solid line, Fig. 4.19). The sign of the magnetic interaction, J, implies that the $\{V^{IV}_4\}$ unit in **5** possesses an S_T = 0 spin ground state like in **1.** Our model also suggests that the J' interactions are close to zero (please note that in **5**, the central V^V is formally replaced by an As atom of an arsonate ligand). The result underlines the suitability of model 2 to analyse the magnetic properties of this series of compounds: Model 2 simplifies

itself to model 1 upon replacement of V^V ions by organoarsonate ligands. The analysis suggests that the organic arsonate ligands do not mediate anti-ferromagnetic interactions. The $S_T = 1$ spin ground state of the dinuclear unit in **5** is also supported by the good fits of the *M vs. H* data obtained using an $S = 1$ Brillouin function (Fig. 4.23; $g = 1.96(2)$).

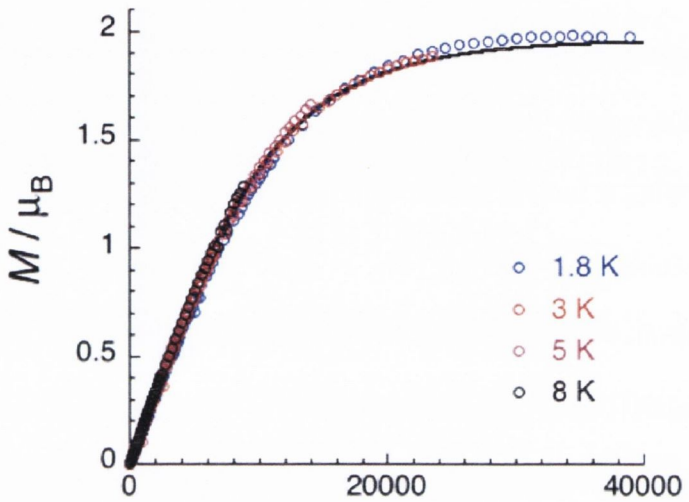

Figure 4.23 – (a) A plot of *M vs. H* data for **5**. Solid line: Fit using a S = 1 Brillouin function.

4.7.4 Summary of the magnetic properties of **1**, **5**, **9** and **11**

The magnetic data of **1**, **5**, **9** and **11** are in itself consistent and the used models were able to reproduce very well the experimental data. However different coupling constants *J* and *J'* were observed for the examined compounds. The differences are in agreement with literature reports [41] and might originate from slight geometrical differences within the arsonate and phosphonate stabilised compounds. The geometrical changes associated with a substitution of arsonate ligands by phosphonic ligands can significantly influence the magnetic properties. Substitution of V^V ions by arsonate ligands only results in subtle changes of the magnetic properties. The most important variable that determines the V•••V exchange interaction is the geometry of the oxo bridges and thus the orbital overlap.[73, 74] The V-O-V angle is an

appropriate parameter that characterises the bonding geometry and thus influences the magnetic interactions. As shown in Figure 4.24, the plot of the magnetic interaction, J, as a function of V-O-V angles within the square $\{V_4\}$ building units (in **1**, **5**, **9**, **11** and in the two compounds reported by Karet *et al.*[41]) substantiates this statement. The interpolated graph underlines the presence of an approximate linear relation between these two variables and the equation of the graph is given by $J/k_B = 600.1 - 4.21(\text{V-O-V}°)$. This very simple magneto-structural analysis underlines the consistency of the obtained magnetic data, and relates the magnitude and sign of J, to the bonding geometry with the tetranuclear subunit.

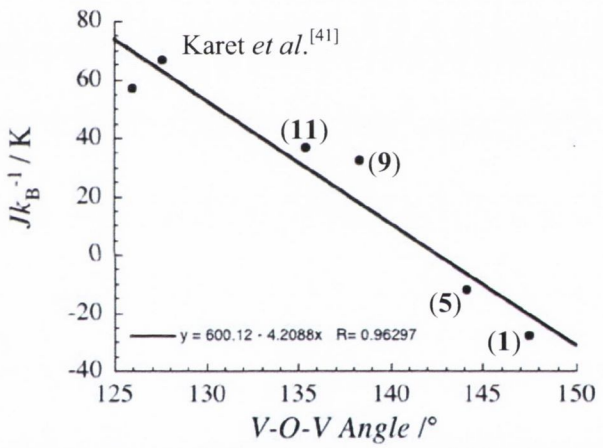

Figure 4.24 – (a) A plot of J/k_B *vs.* the V-O-V angles within the $\{V_4O_8\}$ structural motif of **1**, **5**, **9**, **11** and two compounds reported in the literature.

4.8 Summary of the mixed-valent decanuclear vanadium(V^{IV}/V^{V}) capsules stabilised by aryl diphosphonate ligands

Three novel hybrid polyoxovanadates capsules have been synthesised. These clusters have been structurally characterised using single crystal X-ray diffraction. The clusters have been characterised in solution utilising UV-vis spectroscopy and mass spectrometry. The clusters

of **9**, **10** and **11** encapsulate solvent molecules according to the respective sizes of their inner cavities.

For future work, the host-guest interactions of the solvent molecules within the hybrid cages of **9**, **10** and **11** will be investigated for molecular recognition purposes. Furthermore, the functionalisation of these hybrid clusters through the incorporation of bipyridine moieties in the bisphosphonate ligand will allow the incorporation of additional metal ions within these cage structures.

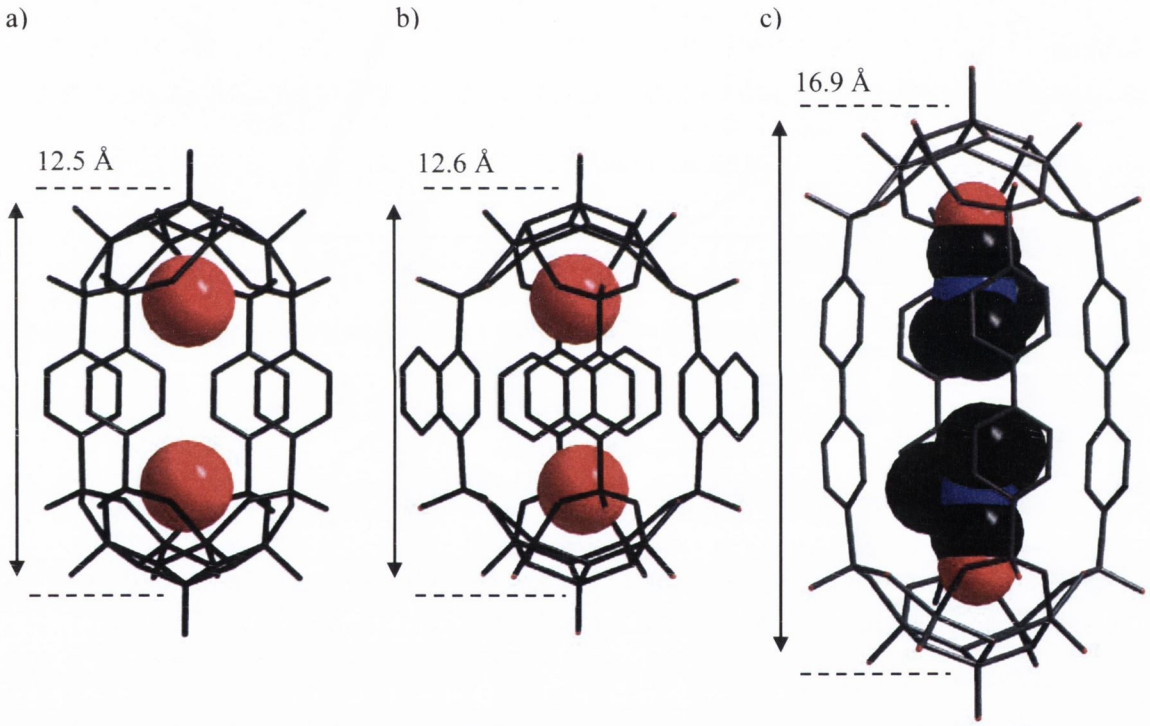

Fig 4.25 – Comparison of the external dimensions of the capsular entities in **9**, **10** and **11**. Wire frame representations of the anionic clusters encapsulating solvent molecules (space-filling representations). Colour code: O red, N blue, C black.

Two water molecules are observed to be encapsulated in the hybrid cages of **9** and **10** (Fig. 4.25). The pentanuclear mixed-valent vanadium capping motifs provide a polar environment allowing the encapsulation of hydrophilic molecules. Similar polar environments have been observed in **7**, **8** and **9** as well as in related compounds reported in the literature.[15, 16, 38, 42, 45,

[46] The inner cavity volume of the hybrid cage in **11** is increased due to the use of the elongated ([1,1'-biphenyl]-4,4'-diyl)bisphosphonate ligands. This increased cavity space within the cluster of **11** allows for the encapsulation of two DMF molecules. The oxygen atoms of the DMF molecules are located in the polar environments at the centre of the mixed-valent capping motifs whilst the methyl groups of the amide functionalities point toward the hydrophobic areas within the cage-structure. We further aim to explore the guest-host chemistry of these cages upon adjusting the cavity dimensions through the incorporation of different sized organophosphonate ligands.

The anti-cancer properties of **9** and **11** were investigated and both clusters were found to have very similar potency. These compounds were only moderately toxic and found to be mostly potent towards lung carcinoma cancer cells. The compounds showed a diminished potency against chronic myelogenous leukaemia cells and Burkitts's lymphoma cells.

The magnetic properties of **1**, **5**, **9** and **11** were also investigated. The magnetic susceptibilities for each compound were modelled and the coupling constants between the vanadium ions in each cluster were determined. Predominantly antiferromagnetic interactions are observed between the vanadium ions in **1** and **5**. Ferromagnetic exchange characterises the magnetic interactions between the vanadium ions in **9** and **11** at low temperatures. A simple magneto-structural analysis was obtained relating the magnitude and sign of J, to the bonding geometry of the vanadium ions within the capping motifs. In future we will extend this analysis to other compounds reported in this thesis.

Chapter Five

Assembly of condensed hybrid polyoxovanadates stabilised by organoarsonates or organophosphonates

5.1 Introduction

In this chapter, we describe the isolation of a series of novel condensed hybrid polyoxovanadate clusters stabilised by organoarsonates or organophosphonates ligands. These compounds were synthesised under acidic conditions which resulted in the stabilisation of a variety of differently coordinating, oligonuclear vanadium sub-units. Through the assembly of these vanadium subunits and the introduction of the tetrahedral moieties through the organoarsonates or organophosphonates ligands, we were able to isolate anionic hybrid clusters with unprecedented core structures. Condensed polyoxometalates have been described in literature and condensed structural motifs such as the Keggin structure, Wells-Dawson's structure and Evans-Anderson structure are well known and exploited in the polyoxometalate field. Historical aspects of these structures have been discussed in Chapter 1.

An investigation into the solvothermal synthesis of new hybrid polyoxometalates was also attempted. Although we successfully synthesised a hybrid polyoxovanadate cluster stabilised by organophosphonate ligands, we observed the *in situ* decomposition of the organoarsonates ligands under solvothermal conditions.

5.2 Synthesis of a condensed mixed-valent vanadium decanuclear complex incorporating (4-aminophenyl)arsonic acid

5.2.1 The synthesis of $NaH_4[V_{10}O_{18}(O_3AsC_6H_4\text{-}4\text{-}NH_2)_7(DMF)_2]\cdot 5H_2O\cdot 7DMF$ (12)

The novel mixed-valent decanuclear polyoxovanadate cluster, $NaH_4[V_{10}O_{18}(O_3AsC_6H_4\text{-}4\text{-}NH_2)_7(DMF)_2]\cdot 5H_2O\cdot 7DMF$ (**12**), was synthesised from sodium metavanadate and (4-

aminophenyl)arsonic acid under reducing conditions using hydrazine hydrate at lower pH values. The dark green mixture was stirred for 30 mins and was filtered hot. After several days, green needle shaped crystals were observed. After many attempts to obtain an appropriated size crystal for structural analyses, a large crystalline needle was isolated and examined using single crystal X-ray diffraction.

5.2.2 The structural characterisation of the mixed-valent decanuclear vanadium cluster $NaH_4[V_{10}O_{18}(O_3AsC_6H_4\text{-}4\text{-}NH_2)_7(DMF)_2]\cdot 5H_2O\cdot 7DMF$ (12)

$NaH_4[V_{10}O_{18}(O_3AsC_6H_4\text{-}4\text{-}NH_2)_7(DMF)_2]\cdot 5H_2O\cdot 7DMF$ (**12**) crystallises in the hexagonal space group, *P*6(3)/m. The asymmetric unit contains half of the anionic cluster core of **12** with the remainder generated by symmetry operations which include a reflection on a mirror plane running through the central atoms of the cluster. The hybrid polyoxovanadate cluster core in **12** consists of 10 vanadium atoms, seven (4-aminophenyl)arsonate ligands, 19 oxo ligands and two DMF molecules which are incorporated in the structure.

The cluster core in **12** is shown in Fig. 5.1 and Fig. 5.2. The structure of the anionic cluster core in **12** is different from those of the previously described hybrid polyoxovanadates. We can envisage the cluster as consisting of three different vanadium containing motifs: a $\{NH_2C_6H_4AsO_3(\mu_3\text{-}O)_4V_4O_{12}\}$ capping motif related to motifs observed in **6** and **8**, two corner sharing square pyramidal units $\{O_4V^{IV}(\mu_2\text{-}O)V^{IV}O_4\}$ and a central dimeric unit $\{O_4V^{V}(\mu_2\text{-}O)_2V^{V}O_3\}$ in which a distorted octahedron and a square pyramid share a common edge. These motifs are interconnected through six arsonate ligands. The coordination sphere

of the central vanadium ion V(3) has two *cis* coordinating terminal oxo ligands whilst all other vanadium ions reveal as observed in previous structures only one terminal oxo ligand.

a)

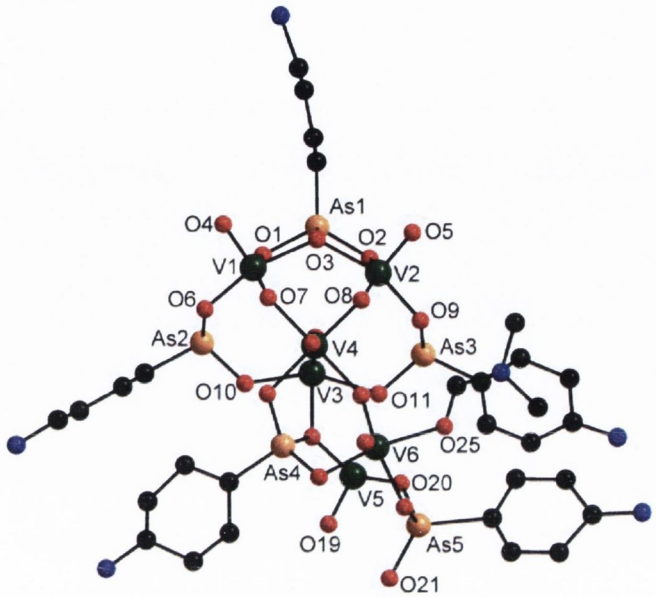

b)

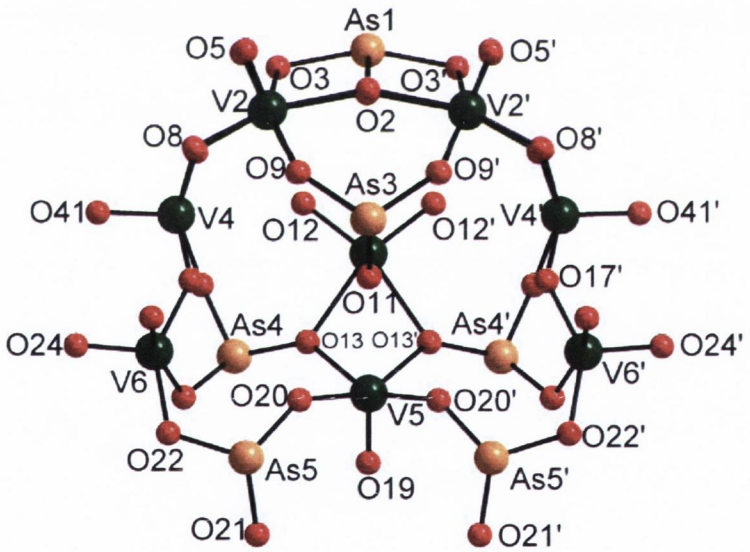

Figure 5.1 – Ball and stick representations of the anionic core, $[V_{10}O_{18}(O_3AsC_6H_4\text{-}4\text{-}NH_2)_7(DMF)_2]^{5-}$; (a) a view of the anionic cluster along the crystallographic *c*-axis and (b) a perspective view of the anionic core in which the aromatic ligands have been deleted. Colour code: V green, As orange, O red, N blue, C black.

The square-shaped $\{NH_2C_6H_4AsO_3(\mu_3\text{-}O)_4V_4O_{12}\}$ capping motif contains a central organoarsonate ligand coordinated to four corner sharing square pyramidal coordinated vanadium ions. While in **6** and **8**, this capping motif is stabilised by four peripheral arsonate

groups, in **12** two arsonate groups are replaced by symmetry related $\{O_4V^{IV}(\mu_2\text{-}O)V^{IV}O_4\}$ units which bind *via* O(7) and O(8) in a *syn, syn* bidentate bridging mode to opposite sides of the capping motif.

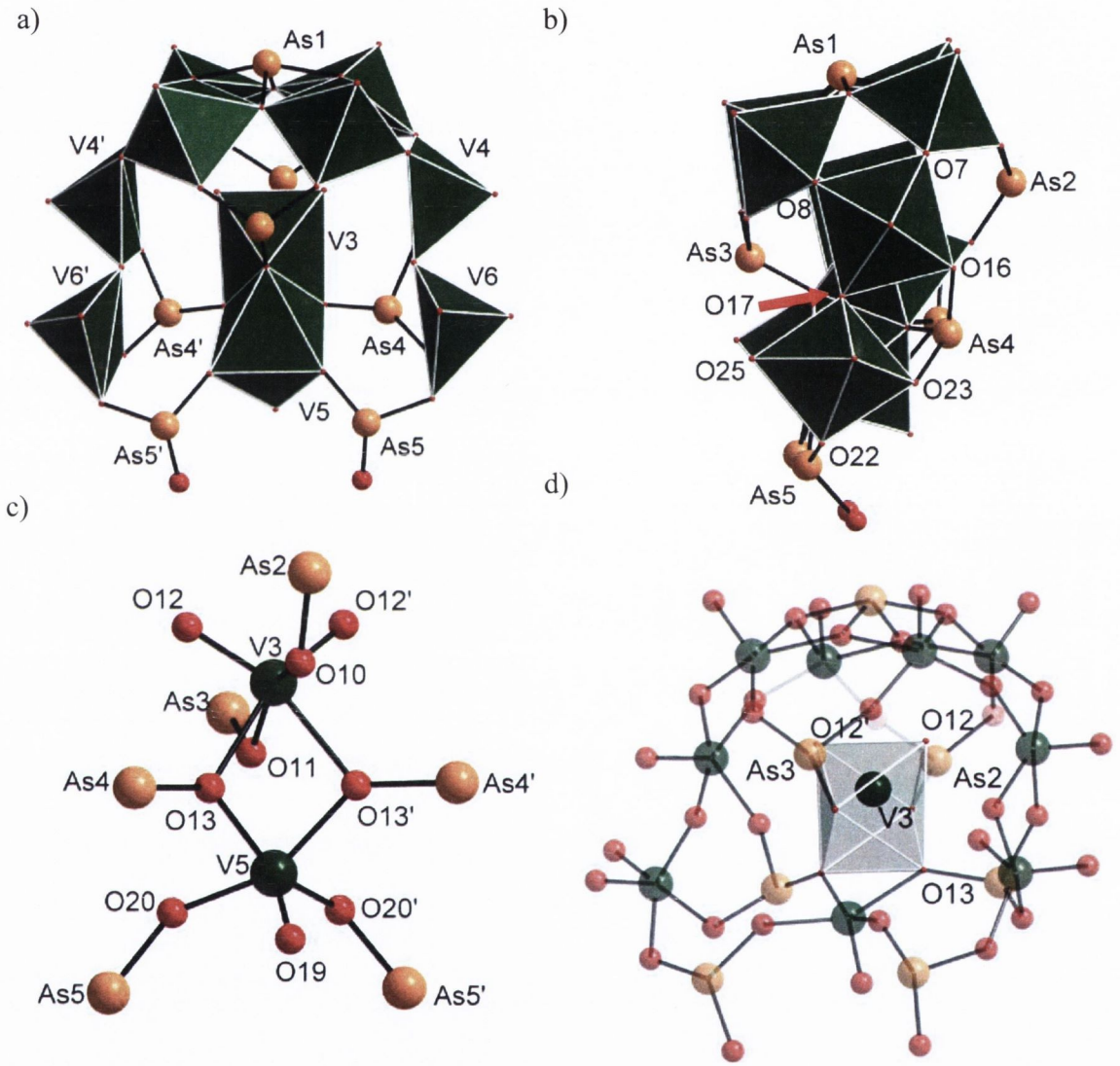

Figure 5.2 – (a) A polyhedral representation of cluster in **12**. (b) A polyhedral representation of the anionic core in **12** as viewed along the crystallographic *c*-axis. (c) A perspective view of the coordination environment of the central V(3) and V(5) vanadium ions. (d) A perspective view of the anionic core where the central V octahedral environment of V(3) has been highlighted. The phenyl rings of the organic ligands have been deleted for clarity. Colour code: V green, As orange, O red.

The $\{O_4V^{IV}(\mu_2\text{-}O)V^{IV}O_4\}$ dimer units located on either side of the capping motif can be visualised as square pyramidal coordinated vanadium ions V(4), V(6) which are linked

through an oxo ligand O(17) to each other. The bond distances between the metal centres V(6), V(4) and the μ_2-oxo donor O(17) are 1.693(9) and 1.954(12) Å, respectively. The vanadium ions in the dimer unit are further mutually bridged through O-donors O(16) and O(23) of an arsonate ligand. The oxygen donor O(22) of another arsonate ligand binds to the outer vanadium ion V(6) and resides in the *trans* position to the bridging oxo ligand O(17). The bond lengths between the metal centres and the oxygen donors from the arsonate ligands range from 1.907(10) to 1.967(11) Å. The square pyramidal coordination environment of V(6) is completed by the O-donor of a DMF molecule. The bond length between the vanadium centre and oxygen donor atom O(25) of the DMF molecule is 2.036(22) Å (Fig. 5.2a and Fig. 5.2b).

The remaining O-donors O(13) and O(20) of the two aforementioned arsonate ligands further link V(4) and V(6) with the central dimeric $\{O_4V^V(\mu_2\text{-}O)_2V^VO_3\}$ unit. Within this structural motif V(3) and V(5) are bridged through the symmetry related arsonate donors O(13) and O(13') providing a common edge of the between the polyhedra (Fig. 5.2c). The vanadium V(3) ion has a distorted octahedral coordinated environment whereby the μ-O donors O(13) and O(13') and two *cis* coordinating oxo ligands are located in the equatorial plane. The *trans* apical positions of the octahedron are provided by two O donors O(10) and O(11) from two arsonate ligands that link the central dinuclear motif with the $\{NH_2C_6H_4AsO_3(\mu_3\text{-}O)_4V_4O_{12}\}$ capping motif. The *cis* coordinating oxo ligands O(12) and O(12') that bind to V(3) point towards the interior of the concave capping unit. An example of an isolated vanadate cluster with two similar *cis* coordinating oxo ligands has previously been discussed in Chapter 1, 1.3.4.1. The bond lengths between the arsonate oxygen donors and V(3) and V(5) ions are in the range 1.960(14) – 2.170(8) Å whilst the bond distances between the metal centres and the terminal oxo ligands range between 1.524(15) – 1.660(8) Å. The remaining vanadium ions form V-O bonds to terminal oxo ligands which range between

1.567(11) Å to 1.615(10) Å. Some of the C – atoms of the aromatic organic rings are disordered.

Bond valence sum analysis was used to calculate the oxidation states of the vanadium metal centres. V(1) and V(2) in the capping motif $\{NH_2C_6H_4AsO_3(\mu_3\text{-}O)_4V_4O_{12}\}$ were found to be in the oxidation state +V. The vanadium atoms in the peripheral dimer units V(4) and V(6) are found to be in the oxidation state +IV (Fig. 5.2a). The central vanadium atoms V(3) and V(5) within the central dimer units are calculated in the oxidation state +V (Fig. 5.2d). The bond valence sum analysis of the vanadium ions has been summarised in Table 5.1.

Table 5.1 – Bond sum valence analysis for **12**

V & O sites	Bond Valence Sum (BVS)	Assigned Oxidation State
V(1)	5.197	+5
V(2)	4.980	+5
V(3)	5.018	+5
V(4)	4.253	+4
V(5)	4.876	+5
V(6)	4.272	+4
μ_3-O (1) (2) (3) (13)	2.068-2.163	-2
μ-O (6) (7) (8) (9) (10) (11) (16) (17) (20) (22) (23)	1.845-2.047	-2
O_{term} (4) (5) (12) (19) (24) (41)	1.472-2.126	-2

The clusters in **12** pack to form an open-framework structure. The packing structure of **12** is a result of the organisation of the anionic hybrid polyoxovanadate clusters involving mediating sodium counter-ions and hydrogen bonds (Fig. 5.3). The sodium counter-ions bind to the amine functionalities of the anionic clusters so that trimeric sub-units are observed (Fig. 5.3b). The interaction distances between the sodium counter-ions and the amine functionalities are in the range of 2.951(1) Å to 3.090 Å.

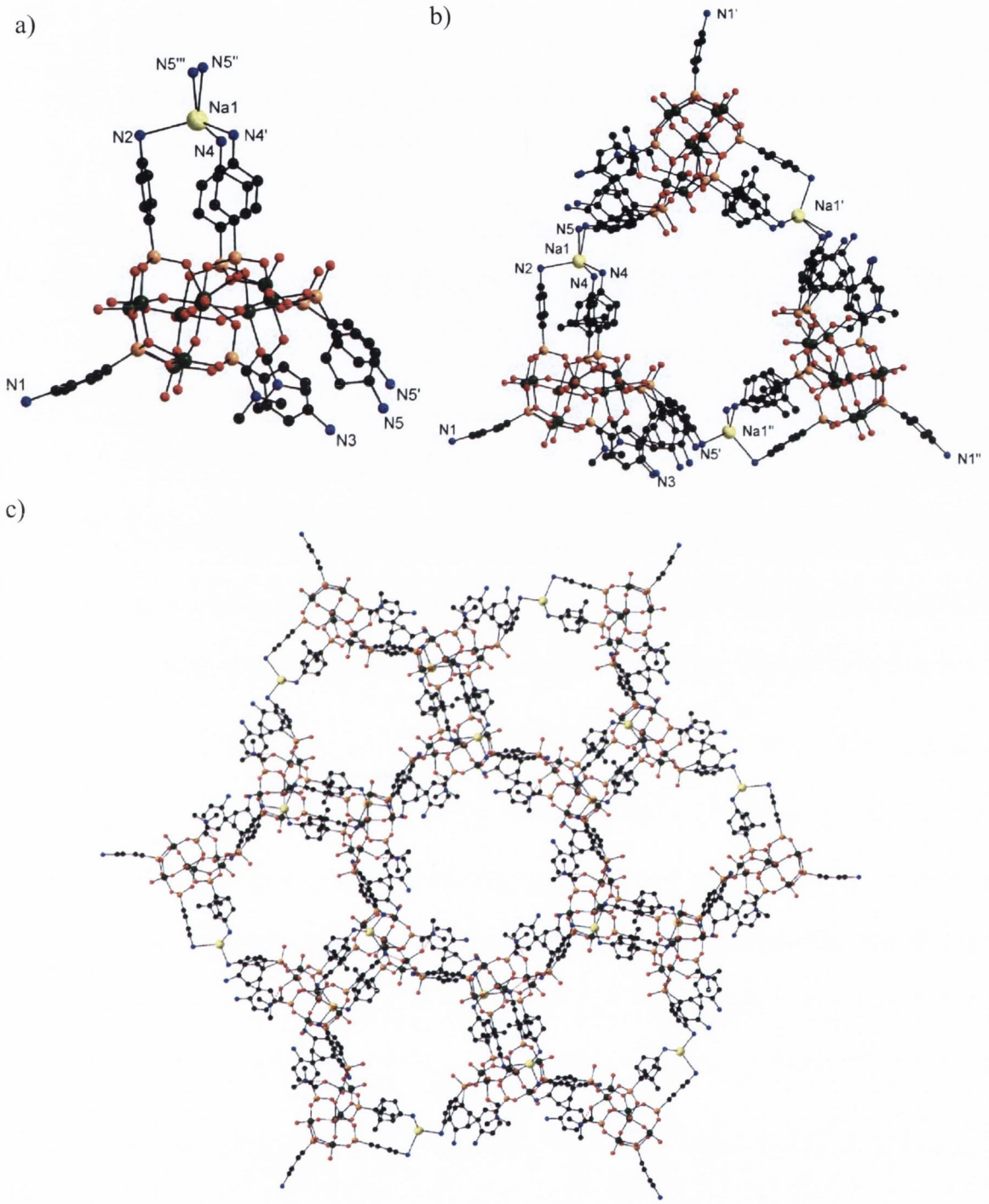

Figure 5.3 – (a) The binding environment of a sodium counter-ion Na(1) when coordinated through the amine groups of the anionic clusters within **12**. (b) A trimer of the anionic clusters within **12** linked through three sodium counter-ions. (c) The shown supramolecular structure is the result of the linking of the trimers units in (c) *via* hydrogen bonding (view in the direction of the crystallorgraphic *c*-axis). The hydrogen atoms, disordered phenyl rings and crystallisation solvent molecules have not been shown for clarity. Colour code: V green, As orange, Na yellow, O red, C black and N blue.

It is observed from the packing arrangement of the anionic clusters within the crystal structure of **12**, that solvent filled tubular cavities arise which run along the crystallographic *c*-axis (long crystal axis of the needle shaped crystals).

Two types of tubular cavities are observed; the smaller of these tubular cavities are constructed from trimers units of the anionic clusters within **12** while the larger tubular cavities are a result of a complex array of hydrogen bonding between the amine functionalities of the arsonate ligands and the terminal oxygen atoms of symmetrically adjacent neighbouring anionic clusters. The small tubular cavities have a maximum cross-sectional distance of *ca.* 1.2 nm and the terminal oxygen of the vanadium ions are seen to point inwards towards the cavity. The larger tubular cavities have a cross-sectional diameter of *ca.* 1.7 nm and it is observed that the methyl groups of the incorporated DMF molecule and the amine functionalities of the anionic clusters point inwards. The solvent molecules within these cavities are heavily disordered and it was deemed appropriate to model these disordered molecules using the SQUEEZE program.[90] According to CHN analysis, **12** contains five water molecules and seven DMF molecules per anionic cluster. It is likely that **12** contains additional solvent molecules in the large channels.

5.2.3 Further solid state characterisation of $NaH_4[V_{10}O_{18}(O_3AsC_6H_4\text{-}4\text{-}NH_2)_7(DMF)_2]\cdot 5H_2O\cdot 7DMF$ (12); Thermogravimetric analysis and Infrared spectroscopy

-Thermogravimetric analysis

The thermogravimetric analysis of **12** was performed in air between 30 °C and 900 °C (Fig. 5.4a). The derivative of the TGA revealed three significant weight losses centred at 77 °C,

300 °C and 618 °C. The first thermogravimetric step between 30°C and 200°C is associated with the loss of the solvents molecules (16.7%). The remaining solvent molecules were lost prior to the TGA measurement. The second thermogravimetric step centred at 300°C is expected to be associated with the oxidative degradation of the organic ligands within **12** and a further gravimetric step centred at *ca.* 620 °C is expected to result in the formation of an inorganic oxide.

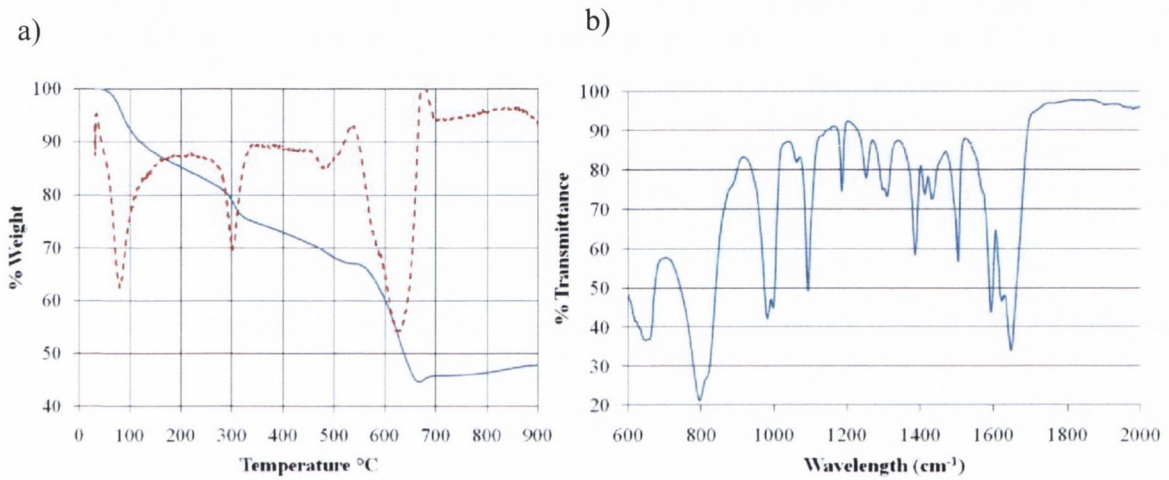

Figure 5.4 – (a) The recorded TGA of **12** in air between 30°C and 900°C. (b) An infrared spectrum of **12**.

-Infrared spectroscopy

The infrared spectrum of **12** confirms the inclusion of the arsonate functionality of the organic ligand (Fig. 5.4b). There is a band observed at 1096 cm^{-1} which is characteristic of the As-C bond stretch. A band at 898 cm^{-1} was assigned to the As-O bond stretch.[46, 47] A broad band of medium intensity observed at 997cm^{-1} is associated with the terminal V=O bond stretch and a strong broad band at 1650 cm^{-1} can attributed to the DMF molecules present within the crystal structure.[88, 89]

Table 5.2 – Crystal data and structure refinement for the squeezed data set of **12**.

Identification code	Compound **12**
Empirical formula	C_{48} As_7 N_9 Na O_{41} V_{10}
Formula weight	2415.40 g mol^{-1}
Temperature	150(2) K
Wavelength	0.71073 Å
Crystal system	Hexagonal
Space group	*P*6(3)/m
Unit cell dimensions	a = 36.752(2) Å α = 90°.
	b = 36.752(2) Å β = 90°.
	c = 16.2793(19) Å γ = 120°.
Volume	19043(3) Å3
Z	1
Density (calculated)	1.264 Mg/m^3
Absorption coefficient	2.575 mm^{-1}
F(000)	6906
Crystal size	0.05 x 0.05 x 0.3 mm^3
Theta range for data collection	1.67 to 20.00°.
Index ranges	-35<=h<=35, -35<=k<=35, -15<=l<=15
Reflections collected	124965
Independent reflections	6221 [R(int) = 0.2053]
Completeness to theta = 20.00°	99.9 %
Refinement method	Full-matrix least-squares on F_2
Data / restraints / parameters	6221 / 0 / 446
Goodness-of-fit on F2	0.946
Final R indices [I>2sigma(I)]	R_1 = 0.0565, wR_2 = 0.1336
R indices (all data)	R_1 = 0.1135, wR_2 = 0.1447
Largest diff. peak and hole	0.814 and -0.498 e.Å-3

5.3 Synthesis of a mixed-valent tridecanuclear vanadium complex incorporating (4-aminophenyl)arsonic acid

5.3.1 The synthesis of $Na_6[V_{13}O_{31}(O_3AsC_6H_4\text{-}4\text{-}NH_2)_3]\cdot 7H_2O\cdot 8DMF$ (13)

The synthesis of $Na_6[V_{13}O_{31}(O_3AsC_6H_4\text{-}4\text{-}NH_2)_3]\cdot 7H_2O\cdot 8DMF$ (**13**) was carried out under very similar synthetic conditions to those used for the formation of **7**. Concentrated hydrochloric acid was again used to adjust the pH but, in contrast, a smaller quantity of the reducing agent, hydrazine monohydrate was used in the preparation of **13**. The final pH of the reaction mixture was adjusted to pH 5.3. After approximately four weeks, small plate shaped turquoise crystals were observed and filtered off. These turquoise crystals were determined to have the same unit cell as **7**. When left in solution, crystals of **7** started to redissolve. After a total of *ca.* six weeks from the initial preparation of the reaction mixture, green plate shaped crystals were formed simultaneously with a white crystalline impurity. These green crystals were of suitable quality for structural analysis using single crystal X-ray diffraction and the structure of compound $Na_6[V_{13}O_{31}(O_3AsC_6H_4\text{-}4\text{-}NH_2)_3]\cdot 7H_2O\cdot 8DMF$ (**13**) was determined.

5.3.2 The structural characterisation of $Na_6[V_{13}O_{31}(O_3AsC_6H_4\text{-}4\text{-}NH_2)_3]\cdot 7H_2O\cdot 8DMF$ (13)

The compound $Na_6[V_{13}O_{31}(O_3AsC_6H_4\text{-}4\text{-}NH_2)_3]\cdot 7H_2O\cdot 8DMF$ (**13**) crystallises in the triclinic space group, *P*-1. The asymmetric unit contains two anionic $[V_{13}O_{31}(O_3AsC_6H_4\text{-}4\text{-}NH_2)_3]^{6-}$ clusters. The structures of the two clusters are almost identical and only one cluster will be discussed in detail. The cluster has approximate C_3 symmetry and can be described as a fragment of a sphere capped by three (4-aminophenyl)arsonate ligands (Fig. 5.5).

a)

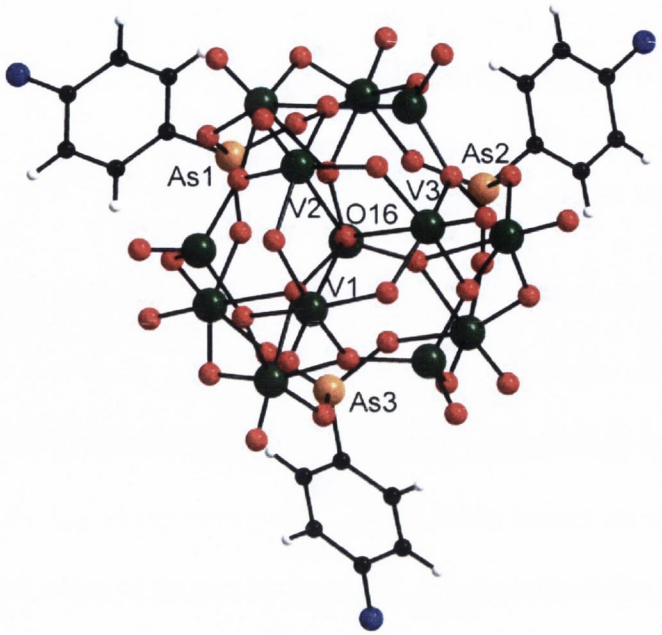

b)

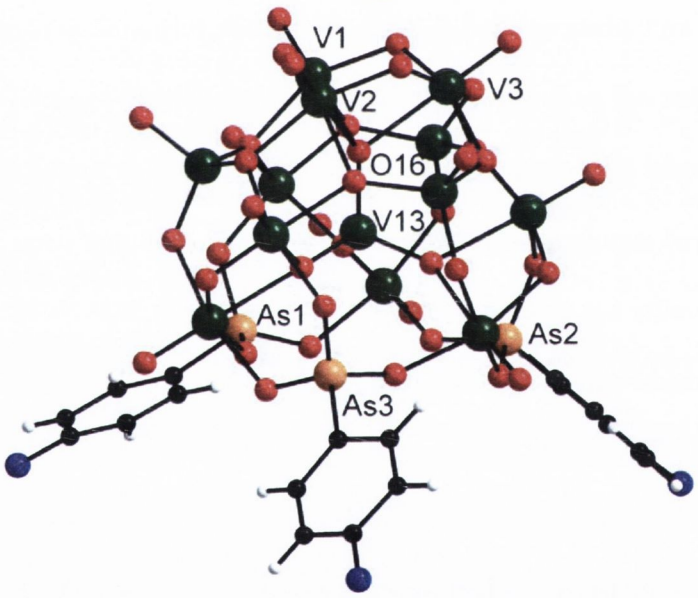

Figure 5.5 – Perspective views of the anionic cluster $[V_{13}O_{31}(O_3AsC_6H_4\text{-}4\text{-}NH_2)_3]^{6-}$ in **13**. Colour code: V green, As orange, O red, C black, N blue, H white.

The cluster is assembled from nine $\{VO_6\}$ octahedra, three $\{VO_4\}$ tetrahedra, three organoarsonate tetrahedra and one central VO_4 tetrahedra. The polyhedra connect through corner sharing and edge sharing interactions and the terminal oxo ligands of all the vanadium atoms point radially outwards. The bond lengths between the vanadium ions and the terminal oxo ligands are in the range of 1.596(1) Å - 1.636(2) Å.

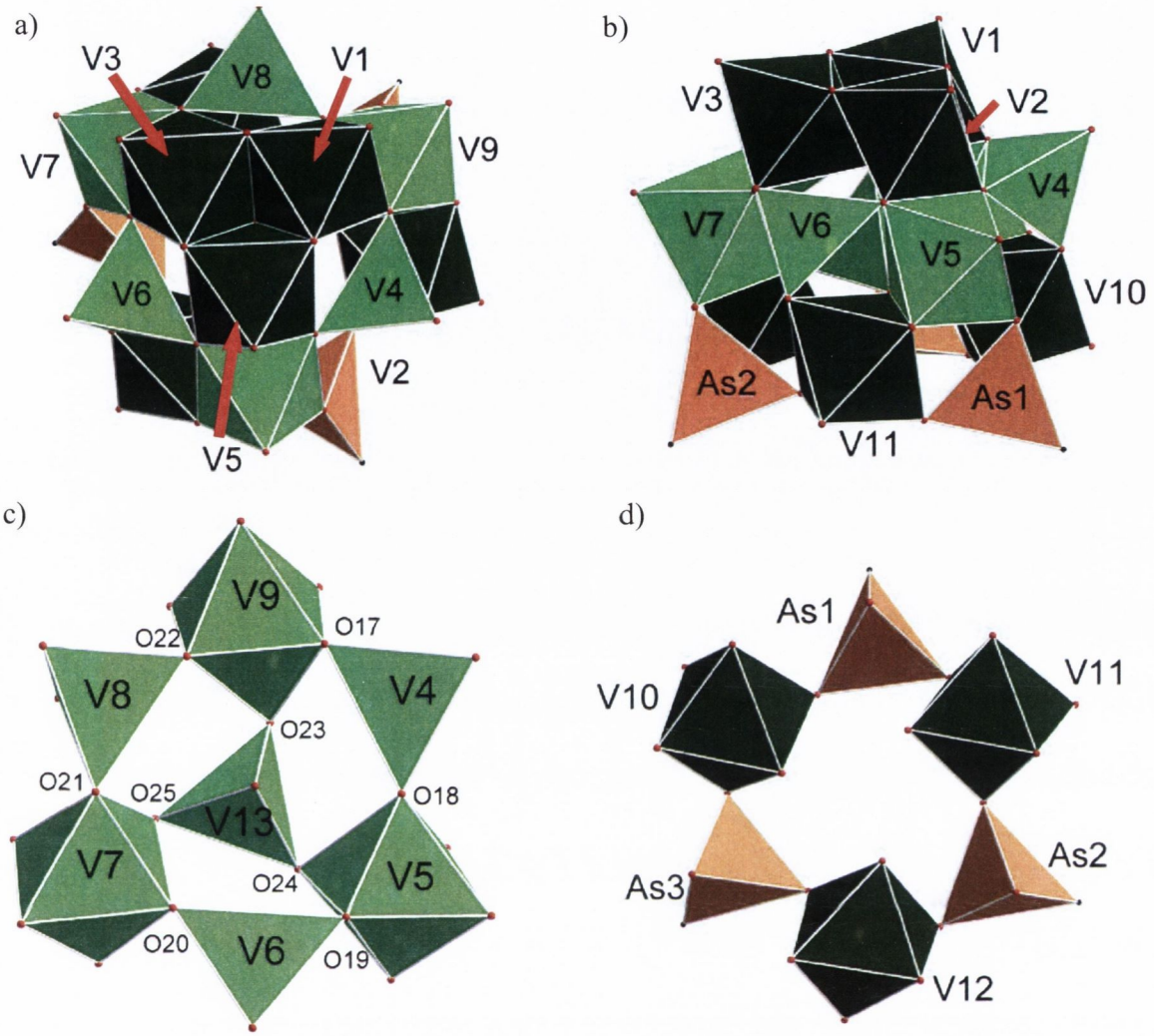

Figure 5.6 – Polyhedral representations of various building motifs within the cluster of **13**. (a) Plan view of the apex unit consisting of three edge sharing octahedra within the $[V_{13}O_{31}(O_3AsC_6H_4\text{-}4\text{-}NH_2)_3]^{6-}$ cluster. (b) A side on perspective of the cluster highlighting the hexanuclear $\{V_6O_{21}VO_4\}$ ring unit (lighter shade of green). (c) A plan view of the hexanuclear $\{V_6O_{21}VO_4\}$ unit incorporating a $\{VO_4\}$ motif in its centre. (d) Alternating pattern of the vanadium and arsonate polyhedra in the lower $\{V_3O_{12}(O_3AsC_6H_4\text{-}4\text{-}NH_2)_3\}$ rim unit of the cluster.

The structure is asymmetric and complicated, but can be visualised as consisting of three major structural motifs: a capping trinuclear unit $\{V_3O_{13}\}$, a hexanuclear ring unit $\{V_6O_{21}VO_4\}$ and a trinuclear motif $\{V_3O_{12}(O_3AsC_6H_4\text{-}4\text{-}NH_2)_3\}$ containing three organoarsonate ligands. The build-up of the cluster is shown in Fig. 5.6. The $\{V_3O_{13}\}$ capping motif consists of three distorted octahedrally coordinated vanadium ions V(1), V(2), V(3) which share common faces to adopt a triangular arrangement. This triangular motif has

been previously observed in other polyoxometalate clusters, *e.g.* in the Keggin structure. The bond distances between the vanadium ions and the bridging oxygen donors within this sub-unit are in the range from 1.819(1) Å to 2.060(1) Å whilst the bond distances between the vanadium ions and the central oxygen donor O(16) between 2.255(1) to 2.293(1) Å (Fig. 5.5a). The three vanadium polyhedra can be considered to form the apex of the cluster (Fig. 5.6a).

There are seven vanadium ions in the mid section of the anionic cluster. These vanadium ions can be visualised as a hexanuclear ring system in which three distorted octahedrally coordinated vanadium ions and three distorted tetrahedrally coordinated vanadium ions are connected in an alternate pattern. The tetrahedra and octahedra share common corners and the O-donors O(17), O(18), O(19), O(20), O(21) and O(22) bridge between the metal centres (Fig. 5.6). The bond distances between the octahedrally coordinated vanadium ions V(5), V(7), V(9) and the bridging oxo ligands are in the range between 1.938(2) Å to 2.090(2) Å. The bond lengths between the tetrahedrally coordinated metal centres and the oxo bridges are slightly shorter and range between 1.788(2) to 1.825(3) Å. In the centre of this hexanuclear ring, a tetrahedral $\{VO_4\}$ motif is connected through common corners to the distorted octahedrally coordinated vanadium ions. The bond distances between the central V(13) and its oxo ligands are 1.680(3) – 1.723(2) Å long. The bond lengths between the octahedrally coordinated vanadium ions V(5), V(7), and V(9) in the hexanuclear ring and O(23), O(24), O(25) of the central tetrahedron are 2.303(1) Å, 2.304(2) Å and 2.294(2) Å, respectively. The previously described trinuclear $\{V_3O_{13}\}$ capping motif is connected to the octahedra of the hexanuclear ring *via* common edges.

The lower $\{V_3O_{12}(O_3AsC_6H_4\text{-}4\text{-}NH_2)_3\}$ rim of the structure consists of three distorted octahedrally coordinated vanadium ions which are arranged in a triangular fashion and bridged through three arsonate functionalities from each organic ligand. The bond distances

between the octahedrally coordinated vanadium ions and the bridging oxygen donors from the arsonate ligands are 1.954(2) Å to 2.036(2) Å long. These three arsonate ligands bind in a tripodal fashion. The central vanadate ion situated in the hexanuclear $\{V_6O_{21}VO_4\}$ ring unit shares three oxygen donors with the three octahedra in the outer rim of the cluster. The lower rim $\{V_3O_{12}(O_3AsC_6H_4\text{-}4\text{-}NH_2)_3\}$ is further coordinated to the $\{V_6O_{21}VO_4\}$ hexanuclear ring through common corners.

Table 5.3 – Bond sum valence analysis for **13**

V & O sites	Bond Valence	Assigned	V & O sites	Bond Valence	Assigned
V(1)	4.99	+5	V(14)	4.732	+5
V(2)	4.779	+5	V(15)	4.799	+5
V(3)	4.891	+5	V(16)	4.902	+5
V(4)	4.937	+5	V(17)	4.98	+5
V(5)	5.025	+5	V(18)	5.018	+5
V(6)	4.857	+5	V(19)	5.048	+5
V(7)	5.017	+5	V(20)	4.952	+5
V(8)	5.044	+5	V(21)	4.968	+5
V(9)	5.048	+5	V(22)	4.98	+5
V(10)	4.21	+4	V(23)	4.146	+4
V(11)	4.3	+4	V(24)	4.28	+4
V(12)	4.276	+4	V(25)	4.279	+4
V(13)	5.377	+5	V(26)	5.243	+5

Bond valence sum analysis was used to calculate the oxidation states. The vanadium ions in the capping trinuclear $\{V_3O_{13}\}$ unit as well as the vanadium ions in the hexanuclear $\{V_6O_{21}VO_4\}$ ring motif were found to be oxidation state +V. The three vanadium ions in the lower $\{V_3O_{12}(O_3AsC_6H_4\text{-}4\text{-}NH_2)_3\}$ rim unit were found to be in oxidation state +IV. The oxidation states of the vanadium atoms of the cluster are summarised in Table 5.3. The second cluster in the asymmetric unit only reveals very minor geometrical differences and the oxidation states of the vanadium ions correspond to those of the discussed cluster.

The topology and connectivity of this condensed hybrid polyoxovanadate is related to that of the $\{VO_4\}$ centred $[V_{18}O_{46}(VO_4)]^{8-}$ cluster [17] and an $\{AsO_4\}$ functionalised

$[V_{12}As_3O_{39}(AsO_4)]^{6-}$ polyoxovanadate which contains an arsenate anion in the centre of the cluster core.[99]

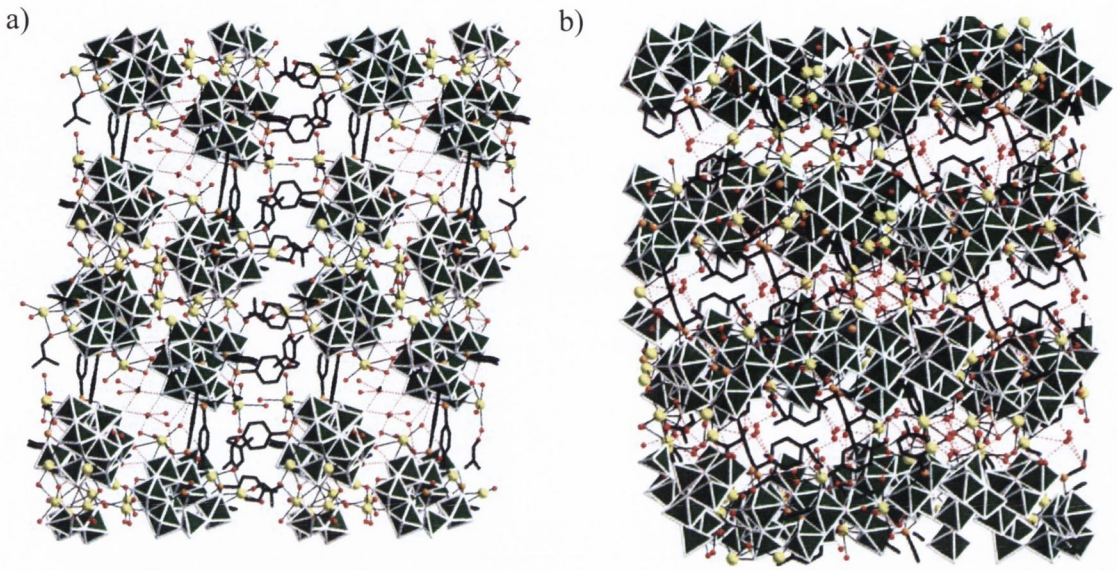

Figure 5.7 – (a) The polyhedral representation of the packing structure of the anionic cluster contained in **13** as viewed in the crystallographic *a*-axis and (b) as viewed in the [1,0,1] direction. Colour code: V green, As orange, Na yellow, N blue, O red, C black.

There are twelve charged balancing sodium counter-ions within the asymmetric unit. The sodium counter-ions bind to the terminal oxygen of the vanadium metal centres. These sodium counter-ions bridge between the anionic clusters to form a 3-D network structure (Fig. 5.7). The remaining void spaces within the crystal structure of **13** are filled with water and DMF crystallisation molecules which are bound through hydrogen bonds to the anionic clusters. These interactions result in the formation of a dense network structure.

5.3.3 Further solid state characterisation of $Na_6H[V_{13}O_{31}(O_3AsC_6H_4\text{-}4\text{-}NH_2)_3]\cdot 7H_2O\cdot 8DMF$ (13); Infrared spectroscopy and Thermogravimetric analysis

- Infrared spectroscopy

An infrared spectrum was recorded for **13** (Fig. 5.8a). The infrared spectrum confirmed the inclusion of the ligand through the presence of a band at 1092 cm^{-1} corresponding to the As-O stretch. There are bands present at 978 cm^{-1} and 999 cm^{-1} which correspond to the terminal V=O bond stretches. There is a strong band at 784 cm^{-1} due to the V-O-V/As-O-V structural motifs in **13**.[46, 47, 88, 89] There is also a strong band at 1652 cm^{-1} corresponding to the carbonyl stretch resulting from the DMF molecules in **13**.

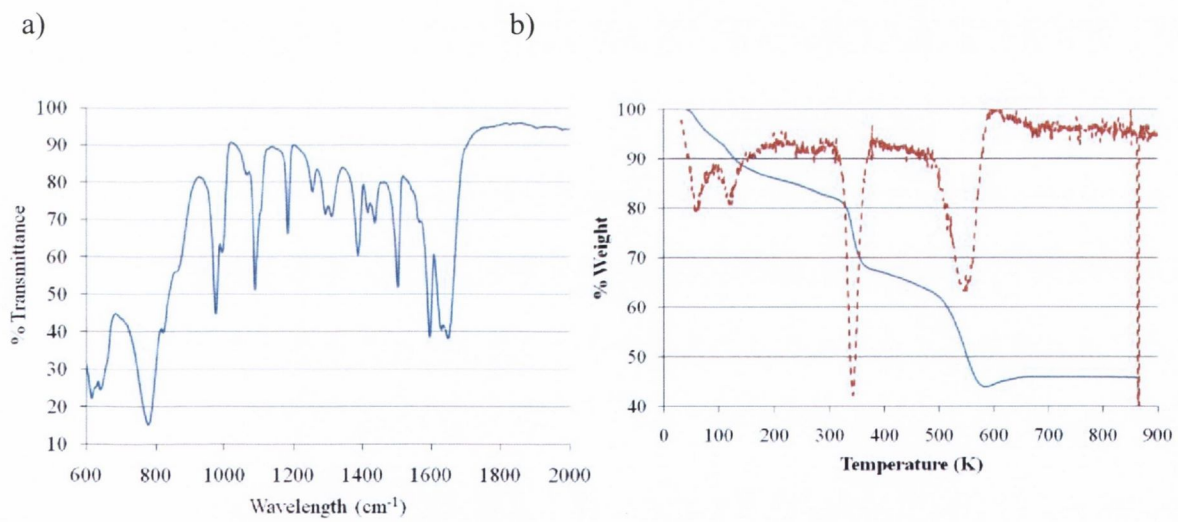

Figure 5.8 – (a) Infrared spectrum of **13**. (b) A TGA measurement of **13** between 30 °C and 900 °C in air atmosphere. Dotted line represents the derivative of the TGA curve.

- Thermogravimetric analysis

A thermogravimetric analysis of **13** was carried out in air in a temperature between 30°C and 900°C (Fig 5.8b). The derivative of the curve revealed three distinct processes of major weight losses. The first major weight loss which is characterised by two thermogravimetric

steps is observed between 30°C and 200°C and corresponds to the loss of the solvent molecules (14.4%). The remaining water and DMF molecules were lost prior to the TGA measurement. The second major weight loss centred at *ca.* 340°C corresponds to the degradation of the organic ligands (13.7%). A broader thermogravimetric step (19%) centred at *ca.* 540°C results in the formation of purely inorganic materials.

Table 5.4 – Crystal data and structure refinement for compound **13**.

Identification code	Compound **13**	
Empirical formula	$C_{28}\ H_{25}\ As_3\ N_{6.50}\ Na_6\ O_{60}\ V_{13}$	
Formula weight	2439.97 g mol^{-1}	
Temperature	150(2) K	
Wavelength	0.71073 Å	
Crystal system	Triclinic	
Space group	*P*-1	
Unit cell dimensions	a = 14.3442(11) Å	α = 96.021(2)°.
	b = 23.2835(18) Å	β = 102.948(2)°.
	c = 23.6319(18) Å	λ = 95.757(2)°.
Volume	7586.9(10) Å3	
Z	4	
Density (calculated)	2.136 Mg/m^3	
Absorption coefficient	2.972 mm^{-1}	
F(000)	4736	
Crystal size	0.2 x 0.15 x 0.15 mm^3	
Theta range for data collection	1.34 to 25.00°.	
Index ranges	-17<=h<=17, -27<=k<=27, -28<=l<=28	
Reflections collected	81782	
Independent reflections	26673 [R(int) = 0.0991]	
Completeness to theta = 25.00°	100.0 %	
Refinement method	Full-matrix least-squares on F^2	
Data / restraints / parameters	26673 / 0 / 2019	
Goodness-of-fit on F^2	1.032	
Final R indices [I>2sigma(I)]	R_1 = 0.0559, wR2 = 0.1607	
R indices (all data)	R_1 = 0.0750, wR2 = 0.1691	
Largest diff. peak and hole	2.187 and -1.251 e.$Å^{-3}$	

5.4 Synthesis of vanadium(IV) cubane incorporating (1-naphthalene)phosphonic acid

5.4.1 The synthesis of $H_2Na_2[(V^{IV}O)_4(OH)_4(O_3PC_{10}H_7)_4]\cdot 3DMF\cdot 12H_2O$ (14)

Compound **14**, $H_2Na_2[(V^{IV}O)_4(OH)_4(O_3PC_{10}H_7)_4]\cdot 3DMF\cdot 12H_2O$ is the product of the self-assembly process of the (1-naphthalene)phosphonic acid and sodium metavanadate under reducing conditions in a DMF/water solution. The assembly process was initiated with the addition of the reducing agent, hydrazine hydrate, at acidic pH value which instigates a colour change from bright yellow to a turquoise blue solution and an accompanying increase in pH. The pH of the solution was monitored and was re-adjusted to a neutral pH with hydrochloric acid after the addition of the reducing agent. Blue cube-shaped crystals of **14** formed from the reaction mixture after one day and were filtered. The resulting crystals were characterised by single crystal X-ray diffraction, CHN analysis, thermogravimetric analysis and infrared spectroscopy.

5.4.2 The structural characterisation of $H_2Na_2[(V^{IV}O)_4(OH)_4(O_3PC_{10}H_7)_4]\cdot 3DMF\cdot 12H_2O$ (14)

The compound $H_2Na_2[(V^{IV}O)_4(OH)_4(O_3PC_{10}H_7)_4]\cdot 3DMF\cdot 12H_2O$ (**14**) contains a tetranuclear vanadium complex in which the vanadium ions and μ_3-bridging oxygen donor atoms adopt a $[V_4(\mu_3\text{-}O)_4]^{8+}$ cubane structure. The crystal structure of **14** was solved in the monoclinic space group, $P2_1/c$ (Fig. 5.9). The topological arrangement of the vanadium ions in the tetranuclear complex can be visualised as four vanadium ions occupying four corners of a cube that are situated diagonally across from each other. The remaining four corners of the cube structure

are occupied by four μ_3-hydroxo ligands which each bind to three vanadium ions within the structure.

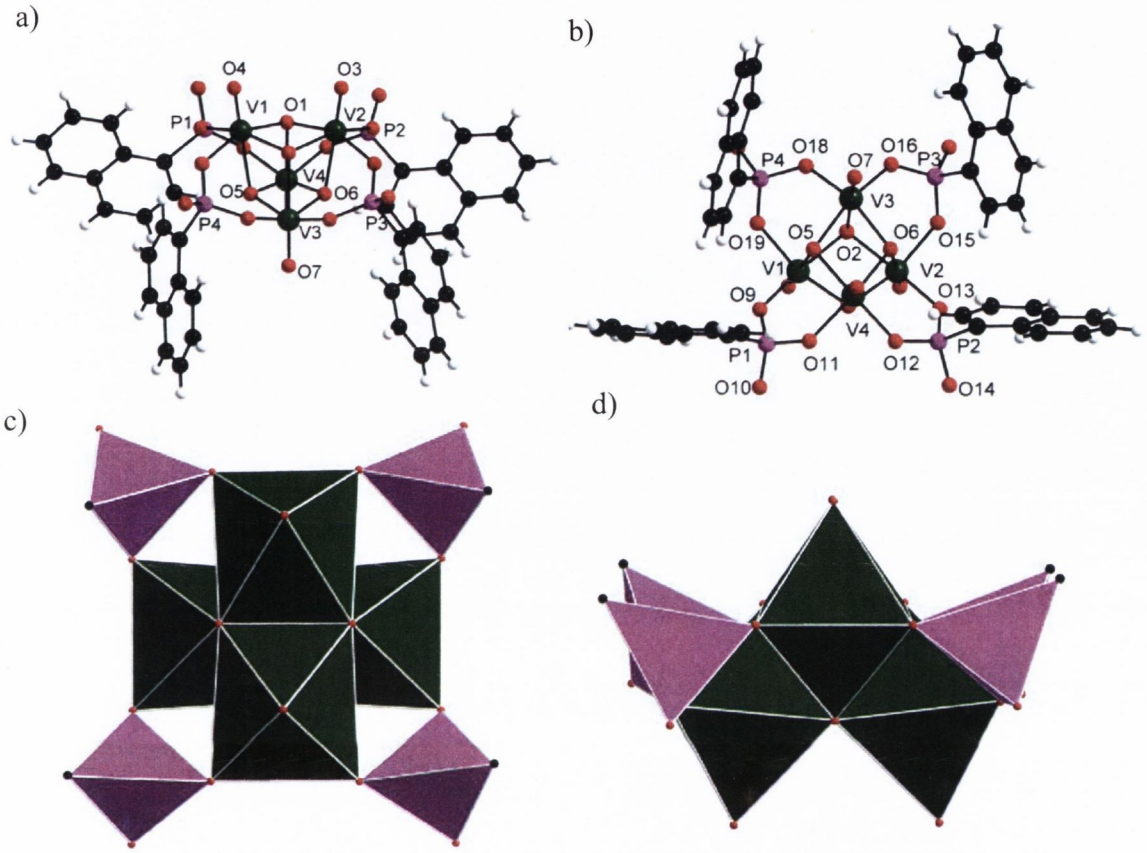

Figure 5.9 – (a) A perspective view of the ball and stick representation of the anionic $[(V^{IV}O)_4(OH)_4(O_3PC_{10}H_7)_4]^{4-}$ core in **14** and (b) as viewed along the crystallographic *b*-axis. (c) A plan view of the polyhedral representation of the cubane structure within **14** and (d) the polyhedral represented cubane structure as viewed side on. Colour code: V green, P purple, O red, C black, H white.

The tetranuclear structure is stabilised by four phosphonate ligands which each binding in O,O'-*syn, syn* bridging mode to two vanadium ions. The distorted octahedral coordination environment of each of the four vanadium ions is completed by terminal V=O bonds. These are situated in *trans* positions to the μ_3-O donor ligands. The cubane structure could also be visualised as a tetranuclear core of close-packed edge-sharing, distorted octahedra (Fig. 5.9c and Fig. 5.9d). The bond lengths between the vanadium ions (V(1) V(2), V(3), V(4)) and the μ_3-bridging hydroxo ligands O donors O(1), O(2), O(5) and O(6)) vary between 2.030(5) Å

and 2.337(1) Å. The terminal V=O bond lengths are comparable to those in previously described polyoxovanadate structures described within this thesis and range between 1.597(1) – 1.608(1) Å. The $[V_4(\mu_3\text{-}O)_4]^{8+}$ core structure deviates from the geometry of an ideal cube. The V-O-V and O-V-O angles range between 101.39(3)° – 104.55(5)° and 74.37(4) ° – 77.05(3)°, respectively, differing from the ideal angle of 90°. Bond valence sum analysis (see Appendix 1) confirms that all four V atoms in **14** adopt the oxidation state +IV. The results of the bond valence sum analysis has been summarised in Table 5.5.

Table 5.5 – Bond sum valence analysis for **14**

V & O sites	Bond Valence Sum (BVS)	Assigned Oxidation State
V(1)	3.891	+4
V(2)	3.827	+4
V(3)	3.835	+4
V(4)	3.846	+4
μ_3-O (1) (2) (5) (6)	1.161-1.215	-1
O_{term} (4) (5) (12) (19) (24) (41)	1.565-1.607	-2

Two protons and two sodium counter-ions balance the negative charge of the cubane structural motif in **14**. The sodium counter-ions bind to the anionic clusters resulting in a 1-D chains of alternating dinuclear sodium units and anionic cubane structural motifs that extend in the direction of the crystallographic *a*-axis (Fig. 5.10). The sodium counter-ions bind *via* μ_2-bridging oxygen donor atoms O(11), O(12), O(16), O(18) of phosphonate ligands to the cubane core (Fig. 5.9b and Fig. 5.10a). The distorted octahedral coordination spheres of the sodium counter-ions are completed by coordinating solvent molecules. These sodium octahedra are bridged *via* common faces and the donor atoms are provided by two μ_2-bridging water molecules and a μ_2-bridging DMF molecule. The crystal structure of **14** can be further observed to have a layered structure in which the hydrophilic polyoxovanadate clusters are separated by layers of the organic hydrophobic naphthalene moieties (Fig. 5.10b). The methyl functionalities of the DMF molecules are further found to point in the direction of

these hydrophobic regions. Figure 5.10b shows the packing structure in the direction of the crystallographic *a*-axis.

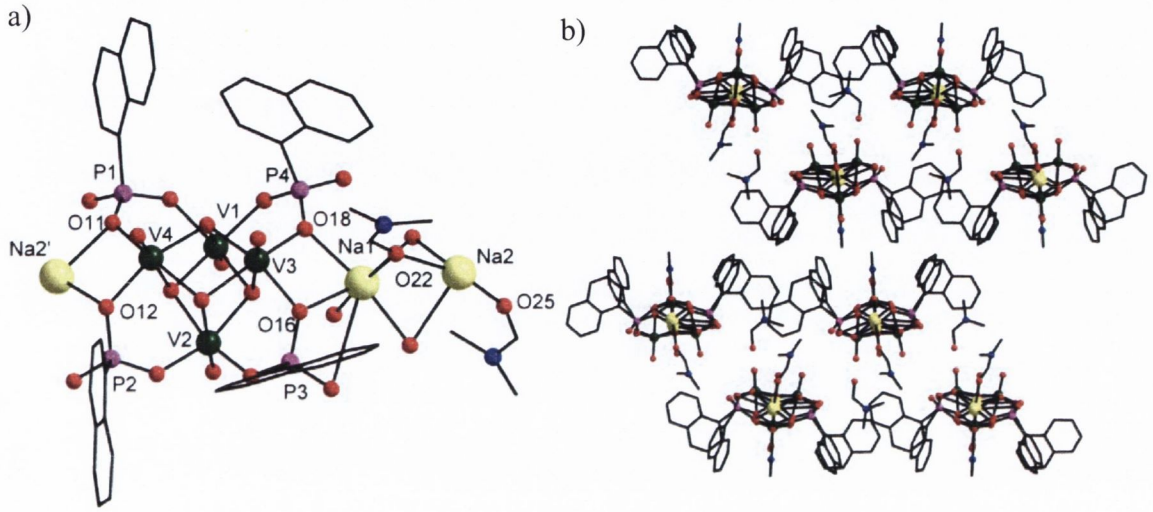

Figure 5.10 – (a) A perspective view of the 1-D polymer structure within **14**; the anionic $[(V^{IV}O)_4(OH)_4(O_3PC_{10}H_7)_4]^{4-}$ cluster is linked *via* solvated sodium counter-ions along the direction of the crystallographic *c*-axis. (b) The layered packing arrangement of these cubane clusters as viewed along the crystallographic *a*-axis. Colour code: V green, P purple, Na yellow, O red, N blue C black.

5.4.3 Further characterisation of $H_2Na_2[(V^{IV}O)_4(OH)_4(O_3PC_{10}H_7)_4]\cdot 3DMF \cdot 12H_2O$ (14); Thermogravimetric analysis and Infrared spectroscopy

-Thermogravimetric analysis

The thermal decomposition behaviour of **14** was investigated by thermogravimetric analysis in air in a temperature range between 30°C and 900°C and a series of small weight loss events were observed (Fig. 5.11a). A weight loss between 30 °C and 295 °C can be attributed to the solvent loss (10.5%). Consecutive steps above 300 °C are associated with the decomposition of the organic phosphonate ligands and the decomposition of the cluster.[94] A stable oxide phase is obtained above 720 °C.

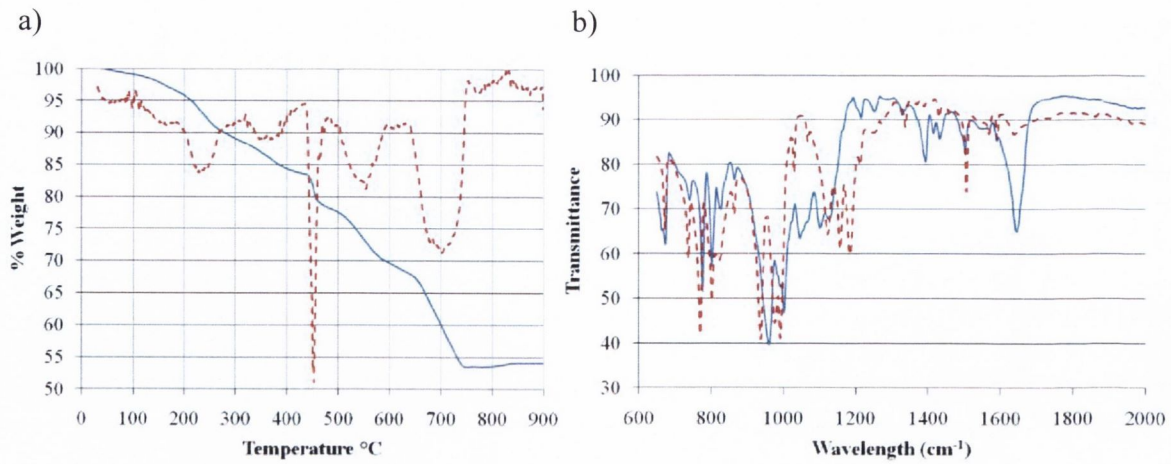

Figure 5.11 – A TGA of **14** between 30 °C and 900 °C in air. Red dash line represents the derivative of the TGA curve. (b) The comparison of an infrared spectrum of **14** (blue) with that of the spectrum of (1-naphthalene)phosphonic acid (red dash).

-Infrared spectroscopy

An infrared spectrum of **14** was recorded and was compared with the infrared spectrum of the (1-naphthalene)phosphonic acid ligand (Fig. 5.11b). Characteristic bands were observed at 1128 cm^{-1} and 1130 cm^{-1} confirming the incorporation of the phosphonate functionality.[38, 42] Additionally V-O-V/V-O-P bands were observed at 996 cm^{-1} and 964 cm^{-1}. P-O bond stretches appear at 766 cm^{-1} and 807 cm^{-1}. A carbonyl band at 1650 cm^{-1} originates from the DMF molecules.[88, 89]

Table 5.6 – Crystal data and structure refinement for compound **14**.

Identification code	Compound **14**	
Empirical formula	$C_{47.50}H_{44}N_{2.50}Na_2O_{31.50}P_4V_4$	
Formula weight	1527.47 g mol^{-1}	
Temperature	150(2) K	
Wavelength	0.71075 Å	
Crystal system	Monoclinic	
Space group	*P*21/c	
Unit cell dimensions	a = 12.335(8) Å	α = 90°.
	b = 34.77(2) Å	β = 107.067(9)°.
	c = 16.066(10) Å	γ = 90°.
Volume	6587(7) $Å^3$	
Z	4	
Density (calculated)	1.540 Mg/m^3	
Absorption coefficient	0.748 mm^{-1}	
F(000)	3090	
Crystal size	0.05 x 0.05 x 0.05 mm^3	
Theta range for data collection	2.54 to 22.50°.	
Index ranges	-12<=h<=13, -37<=k<=37, -17<=l<=17	
Reflections collected	41576	
Independent reflections	8540 [R(int) = 0.1050]	
Completeness to theta = 22.50°	99.1 %	
Refinement method	Full-matrix least-squares on F^2	
Data / restraints / parameters	8540 / 0 / 845	
Goodness-of-fit on F^2	1.262	
Final R indices [I>2sigma(I)]	R_1 = 0.1044, wR_2 = 0.2878	
R indices (all data)	R_1 = 0.1336, wR_2 = 0.3351	
Largest diff. peak and hole	0.996 and -0.815 e.$Å^{-3}$	

5.5 Investigation into the solvothermal synthesis of functionalised polyoxovanadates with organophosphonate and organoarsonates

We decided to investigate the assembly of phosphonate- or arsonate- stabilised polyoxovanadates under solvothermal conditions. It is widely known that compounds that are not unattainable under ambient conditions, can be synthesised at elevated temperatures and pressures.[100] Solvothermal reactions have made a significant contribution to the synthesis and structural determination of metal organic frameworks (MOFs).[51, 52, 101] The 3-D structures of these MOFs often make the resulting compounds very insoluble in common solvents and autoclave reactions have aided in the crystallisation of these compounds.

5.6 Solvothermal synthesis of a vanadium(IV) dodecanuclear cluster incorporating (1-naphthalene)phosphonic acid

5.6.1 The synthesis of $H_4[(VO)_{12}(OH)_{12}(O_3PC_{10}H_7)_8]\cdot 13H_2O\cdot 6DMF$ (15)

The phosphonate stabilised cubane structure in **14**, prompted us to investigate the reaction between vanadyl sulphate and (1-naphthalene)phosphonic acid under solvothermal conditions. We successfully synthesised a dodecanuclear polyoxovanadate cluster functionalised with eight naphthalene phosphonate ligands. Blue cubic crystals were obtained in high yields from a DMF/water solution in an autoclave at 160°C after three days. These single crystals were filtered from the mother liquor and the structure of $[H_4(VO)_{12}(OH)_{12}(O_3PC_{10}H_7)_8]\cdot 13H_2O\cdot 6DMF$ (**15**) was determined using single crystal X-ray diffraction.

5.6.2 The structural characterisation of $H_4[(VO)_{12}(OH)_{12}(O_3PC_{10}H_7)_8]\cdot 13H_2O\cdot 6DMF$ (15)

$H_4[(VO)_{12}(OH)_{12}(O_3PC_{10}H_7)_8]\cdot 13H_2O\cdot 6DMF$ (**15**) crystallises in the monoclinic space group, *C*2/m. The anionic cluster in **15** can be visualised as the linkage of six dinuclear $\{O_4V^{IV}(OH)_2V^{IV}O_4\}$ units *via* eight phosphonate tetrahedra (Fig. 5.12). Within these $\{O_4V^{IV}(OH)_2V^{IV}O_4\}$ units, distorted octahedrally coordinated V ions share a common edge.

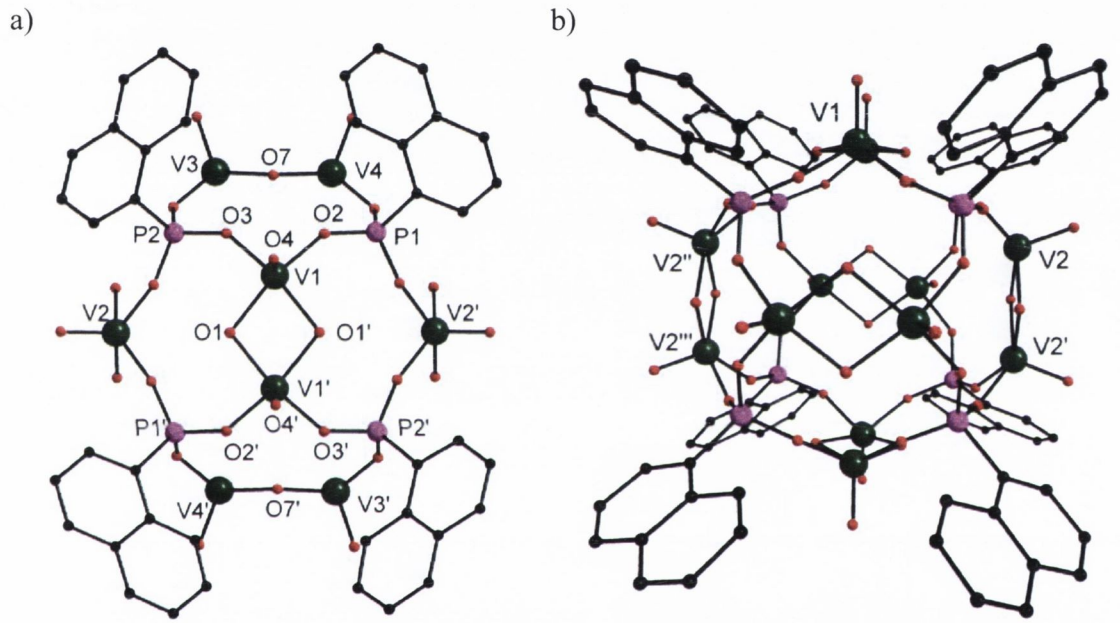

Figure 5.12 – (a) A ball and stick representation of the anionic $[(VO)_{12}(OH)_{12}(O_3PC_{10}H_7)_8]^{4-}$ core viewed along the crystallographic *b*-axis. (b) A perspective view of the anionic core in **15**. The hydrogen atoms have been removed for clarity. Colour code: V green, P purple, O red, C black.

Similar dinuclear bridging units have been observed within the hybrid cluster of **6**. The bond lengths between the vanadium ions and the μ_2-bridging hydroxo ligands vary between 1.961(38) Å and 1.980(9) Å. The bond distances of the terminal V=O oxygen bonds are in the range between 1.564(41) – 1.594(10) Å. Bond valence sum analysis confirms the oxidation states of all the vanadium metal centres as +IV (see table 5.7). Both the terminal V=O oxygen bonds and the naphthalene moieties protrude outwards from the cluster core.

Table 5.7 – Bond sum valence analysis for **15**		
V & O sites	Bond Valence Sum (BVS)	Assigned Oxidation State
V(1)	4.071	+4
V(2)	4.049	+4
V(3)	4.052	+4
V(4)	4.077	+4
μ_2-OH (1) (7) (11) (14)	1.143-1.212	-1
O_{term} (4) (6) (8) (12)	1.671-1.793	-2

The 12 vanadium and eight phosphorus atoms of each anion are located at the vertices of a pentagonal dodecahedron; each of its 12 faces is a distorted pentagon consisting of three vanadium atoms and two phosphorus atoms. The cluster cage encapsulates two disordered water molecules within its cavity.

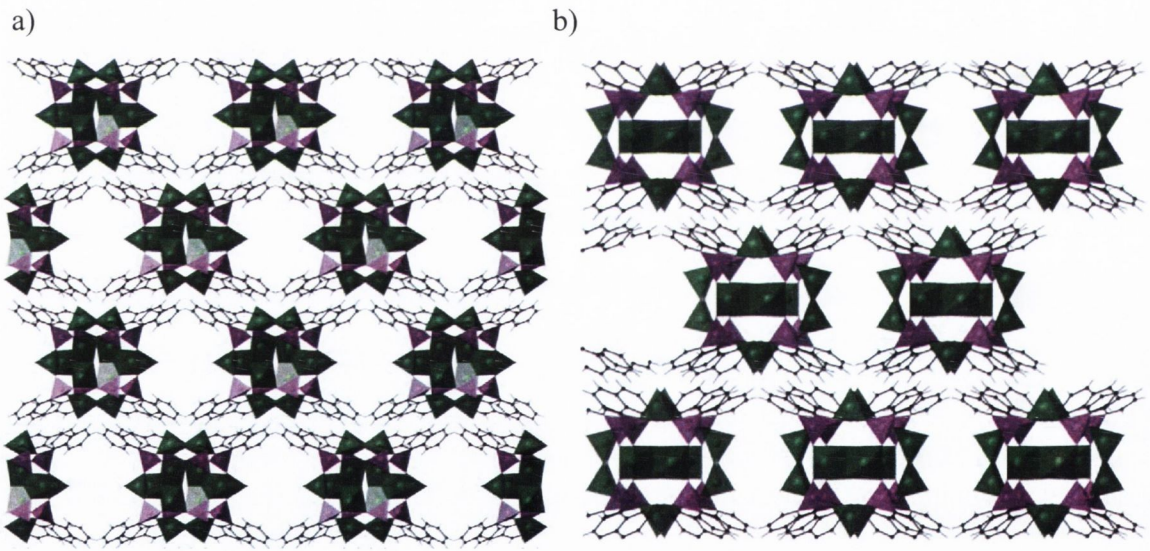

Figure 5.13 – (a) A polyhedral representation of the anionic $[(VO)_{12}(OH)_{12}(O_3PC_{10}H_7)_8]^{4-}$ core in the crystal structure of **15** as viewed along the crystallographic *c*-axis and (b) in the [1,0,1] direction. Crystallisation solvent molecules have been removed for clarity. Colour code: V green, P purple, O

It is noted that a similar polyoxovanadate cluster stabilised by (1-naphthalene)phosphonate ligands has been reported by Goshorn *et al.*[102] However in comparison to the compound reported by Goshorn *et al.*, the clusters in **15** adopt a different arrangement in the crystal

structure due to the structure directing effect of the naphthalene moieties. π-π Interaction prevail between the organic naphthalene moieties and the distances between relevant aromatic rings are in the range from 3.676(14) Å to 3.725(28) Å. The interactions involving these naphthalene moieties lead to the high symmetry packing of the clusters in the crystal structure. This packing arrangement results in the generation of a series of solvent filled channels throughout the crystal structure (Fig. 5.13). The largest channels which run in the direction of the crystallographic *c*-axes have dimensions of approximately 0.4 x 0.4 nm. It was deemed appropriate to use the SQUEEZE program in order to take account of the disordered solvent molecules.[90] The crystal structure of **15** was found to contain 13 water molecules and 6 DMF molecules as determined by microanalysis.

5.6.3 Further solid state characterisation of 15; Thermogravimetric analysis and Infrared spectroscopy

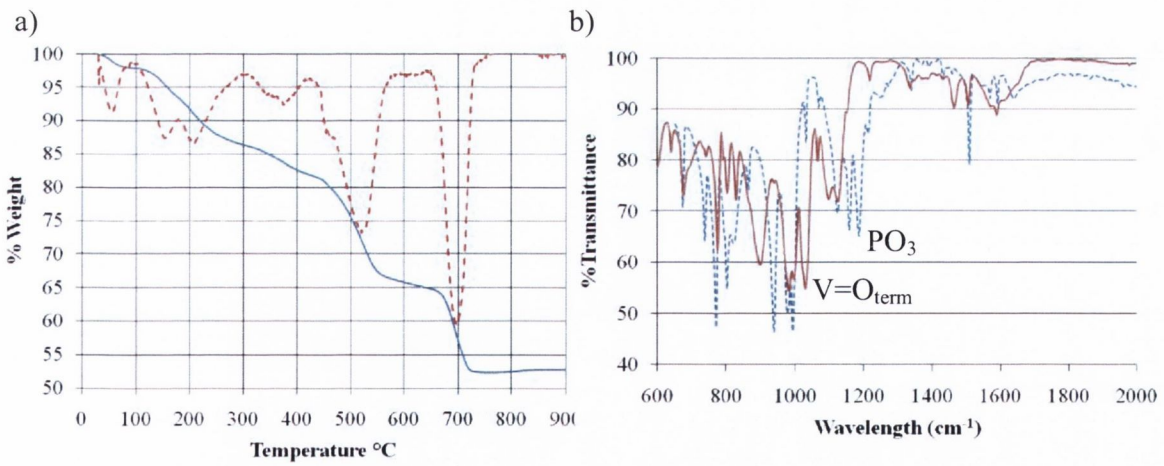

Figure 5.14 – (a) The TGA (blue) of **15** between 30°C and 900°C under an air atmosphere. The derivative of the %weight loss with respect to temperature has been highlighted with a red dashed line. (b) An infrared spectrum of **15** (red) overlaid on the infrared spectrum of (1-naphthalene)phosphonic acid (blue dashed line).

The thermogravimetric analysis of **15** was performed in a temperature range between 30 °C

and 900 °C in an air atmosphere (Fig. 5.14a). The loss of water molecules and DMF molecules is associated with two broad thermogravimetric steps (13.4%) between 30°C and *ca.* 270 °C. The remaining water molecules were lost prior to the TGA measurement. A thermogravimetric step between 300 °C and 400 °C to the oxidative degradation of the ligand and a further thermogravimetric step centred at *ca.* 520°C leads to the destruction of the cluster within **15**.

-Infrared spectroscopy

The infrared spectrum was recorded on a microcrystalline sample of **15** (Fig. 5.14b). The characteristic band at 1103 cm^{-1} arising for the phosphonate functionality confirms the inclusion the aromatic ligand. A band at 985 cm^{-1} originate from the V=O terminal bond. A broad band due to the carbonyl motif arising from the DMF molecules is present at 1593 cm^{-1}. Bands at 679 cm^{-1}, 777 cm^{-1}, 807 cm^{-1} and 832 cm^{-1} are present both in the infrared spectrum of the ligand and the complex. These bands are associated with the P-O bond stretches.[38, 42, 88, 89]

Table 5.8 – Crystal data and structure refinement for compound **15**.

Identification code	Compound **15**	
Empirical formula	$C_{80}\ H_{56}\ O_{55.50}\ P_8\ V_{12}$	
Formula weight	2764.29 g mol^{-1}	
Temperature	150(2) K	
Wavelength	0.71073 Å	
Crystal system	Monoclinic	
Space group	*C*2/m	
Unit cell dimensions	a = 21.379(4) Å	α = 90°.
	b = 24.962(5) Å	β = 123.62(3)°.
	c = 15.037(3) Å	γ = 90°.
Volume	6682(2) $Å^3$	
Z	2	
Density (calculated)	1.374 Mg/m^3	
Absorption coefficient	0.971 mm^{-1}	
F(000)	2752	
Crystal size	0.2 x 0.2 x 0.2 mm^3	
Theta range for data collection	1.63 to 28.30°.	
Index ranges	-28<=h<=22, -33<=k<=33, -12<=l<=20	
Reflections collected	22840	
Independent reflections	8068 [R(int) = 0.0202]	
Completeness to theta = 28.30°	94.9 %	
Refinement method	Full-matrix least-squares on F^2	
Data / restraints / parameters	8068 / 0 / 358	
Goodness-of-fit on F^2	1.044	
Final R indices [I>2sigma(I)]	R_1 = 0.0784, wR_2 = 0.2667	
R indices (all data)	R_1 = 0.0826, wR_2 = 0.2723	
Largest diff. peak and hole	3.060 and -2.276 e.$Å^{-3}$	

5.7 Investigation of the solvothermal synthesis of polyoxovanadate clusters incorporating arsonate ligands

Numerous attempts to synthesise polyoxovanadates clusters stabilised by organoarsonate ligands using hydrothermal and solvothermal methods were unsuccessful. In most cases we observed the cleavage of the As-C bond generating inorganic arsenates. For instance, black cubic crystals were obtained from the solvothermal reaction of vanadyl sulphate and (4-hydroxy)phenyl arsonic acid in a DMF/water solution at 200°C.

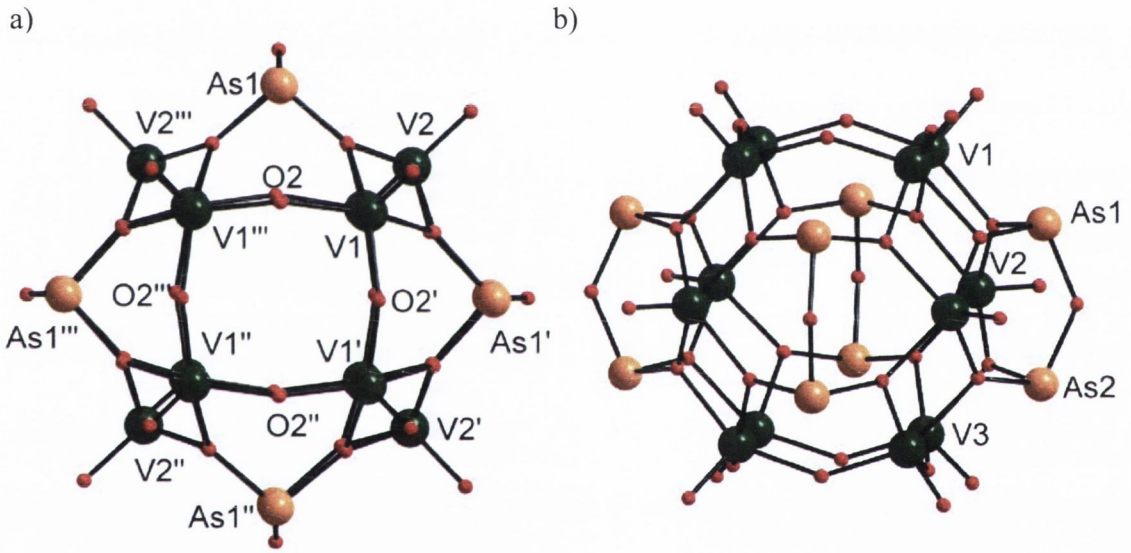

Figure 5.15 – Different perspective views of the product of the solvothermal synthesis of (4-hydroxy)phenylarsonic acid and vanadyl sulphate. The solvent molecule within the anionic $[V_{12}As_8O_{40}]^{4-}$ cluster has been removed for clarity. Colour code: V green, As orange, O red.

The reaction was carried out for three days. The single crystals were structurally characterised by single crystal X-ray diffraction. The crystals were found to contain the previously reported vanadoarsenate cluster, $[V_{12}As_8O_{40}(H_2O)]^{4-}$ as shown in Fig. 5.15.[113] The cell parameters were identical with those reported. The (4-hydroxy)phenyl arsonate ligands were found to decompose to arsenate (III) anions which are incorporated in the

vanadoarsenate cluster. The anionic $[V_{12}As_8O_{40}(H_2O)]^{4-}$ cluster consists of twelve distorted $\{VO_5\}$ square pyramids and four diarsenate units $\{As_2O_5\}$, whereby a hollow sphere is formed (Fig. 5.15).

The $[V_{12}As_8O_{40}(H_2O)]^{4-}$ cluster can be envisaged as the two tetranuclear $\{V_4O_8\}$ capping motifs linked *via* four $\{As_2O_5\}$ diarsenate units. The dinuclear arsenate units are mutually bridged by four vanadium ions that are located in mid section of the cluster. The diarsenate units bind to the tetranuclear capping motifs in a *syn*, *syn* coordination mode through oxygen donor atoms. These oxygen donor atoms further coordinate to square pyramidal coordinated vanadium ions which link the diarsenate units into a belt motif which forms the mid-section of the cluster. A disordered water molecule is encapsulated within the cluster. The twelve vanadium ions are in the oxidation state +IV.[103] This anionic cluster is structurally related to the vanadoarsenate clusters that have been discussed in Chapter 1, 1.3.3.

5.8 Summary of the assembly of condensed hybrid polyoxovanadates stabilised by organoarsonate or organophosphonate ligands

Manipulation of the reaction conditions allows us to obtain vanadium building units and connectivities different to those reported in previous chapters. Within this chapter, we report the synthesis and characterisation of condensed polyoxovanadate cores stabilised by (4-amino)phenylarsonate ligands at low pH, $NaH_4[V_{10}O_{18}(O_3AsC_6H_4\text{-}4\text{-}NH_2)_7(DMF)_2]\cdot 5H_2O\cdot 7DMF$ (**12**) and $Na_6[V_{13}O_{31}(O_3AsC_6H_4\text{-}4\text{-}NH_2)_3]\cdot 7H_2O\cdot 8DMF$ (**13**), a cubane structural $\{V_4O_4\}^{8+}$ motif in $H_2Na_2[(V^{IV}O)_4(OH)_4\ (O_3PC_{10}H_7)_4]\cdot 3DMF\cdot 12H_2O$ (**14**) stabilised using (1-naphthalene)phosphonate ligands and the solvothermal synthesis of a

functionalised polyoxovanadate, $H_4[(VO)_{12}(OH)_{12}(O_3PC_{10}H_7)_8]\cdot 13H_2O\cdot 6DMF$ (**15**). The synthetic strategy involved lowering the final pH of the reaction mixture which resulted in the formation of denser core structures which are characteristic for the compounds decribed in this chapter. The assembly of $V_{10}O_{18}(O_3AsC_6H_4\text{-}4\text{-}NH_2)_7(DMF)_2]^{5-}$ in **12** involving counter-ions results in a 3D network structure whose channels propagate in the direction of the crystallographic *c*-axis. The structural analysis reveals that the channels have cross-sectional diameters of 1.2 nm and 1.7 nm. The structural stability of the large solvent filled channels in **12** will be investigated in future work with a particular interest in the removal or exchange of the solvent molecules. Compound **13** represents another high nuclearity vanadate cluster that can be isolated from the original reaction mixture of **7** after a prolonged period of time. An important feature of this compound is that it represents an example of an organically functionalised vanadate that replicates the core structure of a previously reported inorganic cluster type. The functionalisation of this core structure resulted in a different packing arrangement in the crystal structure and gives rise to novel spectroscopic and electronic properties. Our synthetic efforts allowed us to stabilise an unprecedented V cubane core structure using (1-naphthalene)phosphonic acid. Redox-active transition metals that adopt cubane or related structures are of particular interest to scientists due their resemblance to active sites of enzymes and it has recently been suggested that such oxo-clusters might hold the key to catalyse the splitting of water.[104] In future experiments we will investigate the redox properties of this structural motif.

We have applied solvothermal synthesis for the functionalisation of vanadates to synthesise a dodecanuclear cluster compound as reported for **15**. However, this synthetic approach resulted in some cases in ligand decomposition and in one case; we were able to isolate the decomposition product which is a previously reported arsenate stabilised vanadate cluster. Despite many reaction attempts (several hundred), the method did not allow us to control the

reaction conditions and optimise the formation of desired compounds. Time constraints did not allow us to further investigate this synthetic approach.

- *Concluding remark*

Upon examining the formation conditions of all compounds, one can conclude that the $\{V_5O_9\}^{3+}$ mixed-valent sub-unit forms at higher pH vales (pH 6-8). Compounds that form under these pH conditions and incorporate this V^{IV}/V^{V} unit include the pentanuclear compounds **1** – **4**, the cage structures in **6** and **8** and the molecular capsules **9** – **11**. We noticed that pH-values above 8 only produce purely inorganic polyoxovanadates, *e.g.* the $[V_{18}O_{42}]^{12-}$ cluster. The cage structures in **5** and **7** that form below pH 6 contain the $\{NH_2C_6H_4AsO_3(\mu_3\text{-}O)_4V^{IV}{}_4O_{12}\}$ sub-unit replacing the $\{V_5O_9\}^{3+}$ mixed-valent sub-unit. This observation is in agreement with the UV-vis analysis of the reaction mixture of **1** and **5**. In all the above mentioned compounds, the coordination environments of the vanadium ions are best described as square pyramidal. It appears that lower pH values promote the condensation of vanadyl ions into denser core structures. Isolated compounds now also contain distorted octahedrally coordinated vanadium centres and observed connetivities resemble those in classical polyoxometalates (*e.g.* Keggin structure). It seems that template affects that results in cavitand and capsular entities only play a negligible role under these conditions.

The outlined results provide a synthetic protocol to a variety of functionalised structural motifs which now may be utilised as guest-host systems or functionalised building blocks of other metallosupramolecular systems (e.g. MOFs).

Chapter Six

Experimental

6.1 Materials and Methods

6.1.1 Reagents

All chemicals and solvents were of reagent grade and purchased from Aldrich Chem. Co. Ltd., Fluka Chemika-Biochemica (U.K.), ABCR GmbH & Co. KG (Germany) or local solvent suppliers, and were used as received. Water was deionised before use.

6.1.2 Magnetic Measurements

The magnetic susceptibility measurements were recorded and modeled by Dr. Rodolphe Clèrac using a Quantum Design SQUID magnetometer MPMS-XL housed at the Centre de Recherche Paul Pascal. This magnetometer works between 1.8 and 300 K for dc applied fields ranging from -7 to 7 T. Measurements were performed on polycrystalline samples of 12.24, 21.22, 10.70 and 15.08 mg, for **1**, **5**, **9** and **11** respectively. The magnetic data measurements were corrected for the sample holder and the diamagnetic contributions.

6.1.3 Nuclear magnetic resonance spectroscopy

^{1}H NMR, ^{13}C NMR and ^{31}P NMR spectra were recorded by either Dr. John O'Brien or Dr. Manuel Rüther on a Bruker DPX 400 spectrometer operating at 400.13 MHz; 100.14 MHz and 161.98 MHz respectively. Samples were carried out in deuterated solvents and are listed for each spectrum. Standard abbreviations for spectra: s, singlet; d, doublet; t, triplet; q, quaternary; m, multiplet; br broad, J, coupling constant.

6.1.4 Infrared spectroscopy

Infrared spectra were recorded on a PerkinElmer Spectrum One FT-IR spectrometer using either a universal ATR sampling accessory. Data were collected and processed using Spectrum v5.0.1 (2002 PerkinElmer Instrument LLC) software. The scan rate was 16 scans per minute with a resolution of 4 scans in the range 4000 – 650 cm^{-1}. The following abbreviations were used to describe the intensities: s, strong; m, medium; w, weak; br, broad.

6.1.5 Ultraviolet-visible spectroscopy

UV-vis spectra were recorded in the range 800 – 400 nm on a Cary Scan spectrophotometer at 20°C using quartz cells of 1 cm path length. Measurements were carried out on a 2 mL portion which was subsequently diluted. Measurements were also carried out on 2 mL portions that were abstracted at different time periods from the various reaction mixtures. The initial and final spectra were then characterised through super-imposing them on known solutions.

6.1.6 Mass spectrometry

Mass spectra were recorded and modelled by either Dr. Martin Feeney or Dr. J. Bernard Jean-Denis on a LCT Orthogonal Acceleration TOF Electrospray mass spectrometer operating in negative ionisation mode. Mass spectrometry was investigated on solution samples of the compounds which were dissolved either in DMSO or water and the solvent has been listed for each spectrum. Samples were loaded using a Waters 2690 HPLC interfaced to the mass spectrometer. The capillary voltage was held at 3.0 kV and the cone voltage at 30 V. The source temperature was 100 °C and desolvation temperature 300 °C. The desolvation gas flow was 500 L/hr. Masslynx 4.0 was used for isotope modelling.

6.1.7 X-ray diffraction analysis

Single crystal X-ray diffraction analyses for crystals described in this report were performed by Dr Tom Mc Cabe, Dr Wolfgang Schmitt or the candidate at Trinity College Dublin using a Bruker SMART APEX CCD diffractometer or a Rigaku Saturn-724 diffractometer. The candidate was involved in all aspects of structure determination at Trinity College Dublin.

The Bruker and the Rigaku diffractometers utilise a graphite-monochromated Mo-Kα radiation (λ = 0.71073 Å). The omega scan method was used to collect either a full sphere or hemisphere of data for each crystal with detector to crystal distance of either 5 or 6 cm at a temperature of 150 K. All data were collected, processed, and corrected for Lorentz and polarisation effects using SMART[105] and SAINT-PLUS[106] software. Absorption corrections for single crystals were applied using SADABS.[107] The structures were solved using either Patterson or direct methods and refined with the SHELXTL[108] program package.

All non-hydrogen atoms were refined anisotropically except for some atoms which were heavily disordered or reported as "non-positive definite" and thus refined isotropically. Hydrogen atoms (excluding water) were assigned to calculated positions using a riding model with appropriately fixed isotropic thermal parameters. Water molecules where applicable, were located from difference maps and in some cases their positions were refined with O-H distance restraints (DFIX, SAME, SADI) and isotropic thermal parameters (the same as that of the adjoining oxygen atom). Hydrogen atoms of some disordered molecules were not added.

In the case where there were a large number of solvent molecules disordered within a cavity, it was deemed appropriate to use the SQUEEZE/PLATON program.[90]

6.1.8 Solvothermal synthesis

Solvothermal synthesis was carried out using a Parr Instrument Company Series 4760/4765 general-purpose digestion bomb employing a 23 mL Teflon insert. Maximum loading of the insert was dependent on reagents but a typical volume of 8-10 mL was used. The heating cycles are specified for each reaction and were performed in a conventional oven.

6.1.9 Thermogravimetric Analysis (TGA)

Thermogravimetric analyses were carried out by Dr Manuel Rüther on a Perkin Elmer Pyris 1 TGA equipped with an ultra-micro balance with a sensitivity of 0.1 microgram. Sample weights were approximately 5 mg and the heating rate was 10 °C per minute within a temperature range of 30 °C to 900 °C in air.

6.2 Synthesis of the organic ligands

6.2.1 Synthesis of [4-(Diethoxy-phosphoryl)-phenyl]-phosphonic acid diethyl ester

This ligand was prepared by a slightly modified Arbusov reaction.[91,109] 4,4'-Dibromophenyl

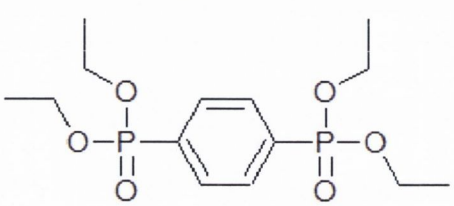

(4.72 g, 20.00 mmol) was dissolved in 50 nL diisopropylbenzene. The solution was heated to 185°C and $NiCl_2$ (0.50 g, 3.86 mmol) was added. Triethyl phosphite (10mL, 0.0583 mol) was added to this mixture over a 6 hrs period under a

gentle stream of N_2. The mixture was refluxed for 24 hrs and then $NiCl_2$ (0.25 g, 1.93 mmol) and triethyl phosphite (5 mL, 0.029 mol) were added. The resultant mixture was heated for a further 24 hrs, yielding a black solution which was distilled under vacuum to remove the solvent and unreacted triethylphosphite. The distillation yielded a black oil which was first washed with PET ether, and then subsequently with diethyl ether, until the consistency of the black material had changed from a liquid tar like state into a dry powder. Diethyl ether washings containing the ester were evaporated off yielding a white crystalline material which was finally washed sparingly with cold diethyl ether to obtain a pure white crystalline product. Yield: 4.69 g (67%).

^{1}H NMR ($CDCl_3$, 400 MHz): δ 7.91 (m, J_{PH} = 10.54 Hz, J_{HH} = 4 Hz, 4 H) 4.14 (m, J_{PH} = 9.0 Hz, J_{HH} = 3.01 Hz, 8 H), 1.34 (t, J_{HH} = 7.03 Hz, 12H).

^{31}P NMR ($CDCl_3$, 161 MHz): δ 18.07 (s, 2P).

6.2.2 Synthesis of (1,4-benzene)bisphosphonic acid

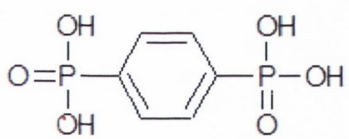

4-(Diethoxy-phosphoryl)-phenyl]-phosphonic acid diethyl ester (2.11 g, 6.00 mmol), concentrated hydrochloric acid (20 mL), and distilled water (20 mL) were refluxed for 14 hrs. The resultant solution was evaporated to dryness. Then the residue was dissolved in distilled water (30 mL), the solution was decolourised with charcoal, and the filtrate was evaporated under reduced pressure yielding a white solid.

Yield: 1.27 g (89.2%). FTIR (cm^{-1}) ν_{max} : 2613(br), 2251(br), 1622(m), 1487(w), 1460(w), 1362(m), 1119(sh), 1090(s), 977(s), 925(s), 826(s), 724(m).

^{1}H NMR (D_2O, 400 MHz): δ 7.64 (m, 4H).

^{31}P NMR (D_20, 161 MHz): δ 16.00 (s, 2P).

^{13}C NMR (D_2O, 101 MHz): δ 135.04 (s, q), 133.27 (s, q), 129.90 (s, CH).

6.2.3 Synthesis of [4'-(Diethoxy-phosphoryl)-biphenyl-4-yl]-phosphonic acid diethyl ester

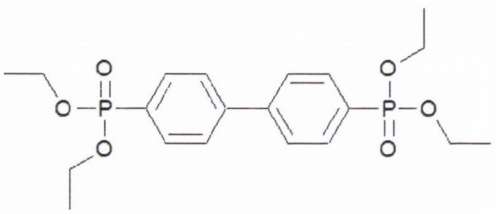

This ligand was prepared by a slightly modified Arbusov reaction.[91,109] 4,4'-Dibromobiphenyl (6.27 g, 20.00 mmol) was dissolved in diisopropylbenzene (50mL). The solution was heated to 185 °C and $NiCl_2$ (0.5 g, 3.89 mmol) was added. Triethyl phosphite (10 mL, 0.0583 mol) was added over a 6 hrs period under a gentle stream of N_2. The mixture was refluxed for 24 hrs. $NiCl_2$ (0.25 g, 1.93 mmol) and triethyl phosphite (5 mL, 0.029 mol) was then added. The resultant mixture was heated for a further 24 hrs yielding a black solution which was distilled under vacuum to remove the solvent and unreacted triethylphosphite. The resultant solid was extracted with petroleum ether and then recrystallised from methylene dichloride and petroleum ether yielding a white powder. Yield: 6.22 g (73%).

^{1}H NMR ($CDCl_3$, 400 MHz): δ 7.91 (m, 4H), 7.70 (m, 4H), 4.19 (m, 8H), 1.36 (t, J_{HH} = 7.04 Hz).

^{31}P NMR ($CDCl_3$, 161 MHz): 19.68 (s, 2P).

^{13}C NMR ($CDCl_3$, 101 MHz): 143.43 (s, q), 131.98 (s, CH), 128.51 (s, q), 126.80 (s, CH), 61.78 (s, CH_2), 15.93 (s, CH_3).

6.2.4 Synthesis of ([1,1'-biphenyl]-4,4'-diyl)bisphosphonic acid

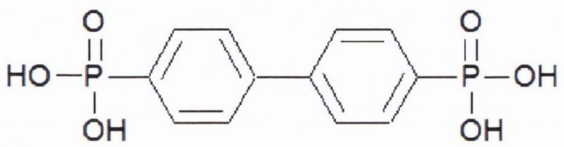

[4'-(Diethoxy-phosphoryl)-biphenyl-4-yl]-phosphonic acid diethyl ester (2.11 g 6.00 mmol), concentrated hydrochloric acid (20 mL), and distilled water (20 mL) were refluxed under stirring for 14 hrs. The resultant solution was evaporated to dryness. Then the residue was dissolved in distilled water (30 mL). The solution was decolourised with charcoal, and the filtrate was evaporated under reduced pressure to give a white solid.

Yield: 1.17 g (91.2%). FTIR (cm^{-1}) ν_{max} : 2572(br), 2166(br), 1837(m), 1690(m), 1625(m), 1486(w), 1410(w), 1384(m), 1362(w), 1120(sh), 1091(s), 982(s), 926(s), 827(s), 728(m).

^{1}H NMR (D_2O, 400 MHz): δ 7.64 (m, 4H).

^{31}P NMR (D_2O, 161 MHz): δ 16.00 (s, 2P).

^{13}C NMR (D_2O, 101 MHz): δ 135.61 (s, q) 133.45 (s, q) 129.95 (s, CH).

6.2.5 Synthesis of (1,4-naphthalene)bisphosphonic acid

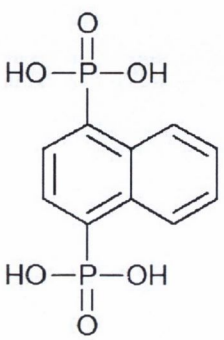

This ligand was prepared in an identical manner to the previous aryl-bisphosphonic acid ligands.[91,109] 4,4'-Dibromonaphthalene (5.72 g, 20.00 mmol) was dissolved in diisopropylbenzene (50mL). The solution was heated to 185 °C and $NiCl_2$ (0.5 g, 3.90 mmol) was added. Triethyl phosphite (10 mL, 0.06 mol) was added over a 6 hrs period under a

gentle stream of N_2. The mixture was refluxed for 24 hrs. $NiCl_2$ (0.25 g, 1.93 mmol) and triethyl phosphite (5 mL, 0.029 mol) was then added. The resultant mixture was heated for a further 24 hrs yielding a black solution which was distilled under vacuum to remove the solvent and unreacted triethylphosphite. The resultant solid was extracted with petroleum ether and then recrystallised from methylene dichloride and petroleum ether yielding a white powder. The (1,4-naphthalene)bisphosphonate ester product was refluxed in concentrated hydrochloric acid under stirring for 14 hrs. The resultant solution was evaporated to dryness. Then the residue was dissolved in distilled water (30 mL). The solution was decolourised with charcoal, and the filtrate was evaporated under reduced pressure to give a white solid. Yield: 2.42 g (42%).

FTIR (cm^{-1}) ν_{max} : 2760 (br), 2344 (br), 1497 (m), 1404 (m), 1267 (m), 1200 (m), 1189 (m), 1154 (m), 1107 (m), 997 (s), 949 (m), 925 (s), 827 (s), 770 (w), 747 (m), 712 (m).

^{1}H NMR (D_2O, 400 MHz): δ 8.67 (m, 2H), δ 8.05 (m, 2H), δ 7.66 (m, 2H).

^{31}P NMR (D_2O, 161 MHz): δ 12.29 (s, 2P).

6.2.6 Synthesis of (1-naphthalene)phosphonic acid

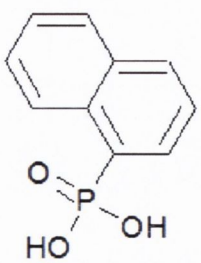

This ligand was prepared by a slightly modified Arbusov reaction.[91,109] 1-Bromo-naphthalene (4.14 g, 20.00 mmol) was dissolved in diisopropylbenzene (50 mL). The solution was heated to 185 °C and $NiCl_2$ (0.50 g, 3.86 mmol) was added. Triethyl phosphite (10 mL, 0.0583mol) was then added to the mixture over a 6 hrs period under a gentle stream of N_2. The mixture was refluxed for 24 hrs. $NiCl_2$ (0.25g, 1.93 mmol) and triethyl phosphite (5mL, 0.029mol) were added to the mixture which was heated at reflux for a further 24 hrs yielding

a black solution which was distilled under vacuum to remove the solvent and unreacted triethylphosphite. The resultant solid was extracted with petroleum ether and then recrystallised from methylene dichloride and petroleum ether. (1-Naphthalene)phosphonic acid diethyl ester, concentrated hydrochloric acid (60 mL), and distilled water (60 mL) were refluxed under stirring for 14 hrs. The resultant solution was evaporated to dryness. Then the residue was dissolved in distilled water (30 mL). The solution was decolourised with charcoal, and the filtrate was evaporated under reduced pressure to give a white solid. Yield: 3.53 g (85%).

FTIR (cm^{-1}) ν_{max} : 3578(w), 3287(w), 2258(br), 1637(w), 1591(m), 1570(w), 1508(s), 1458(w), 1431(w), 1389(w), 1369(w), 1338(m), 1215(m), 1184(s), 1151(s), 1108(m), 1069(w), 1029(m), 989(s), 942(s), 862(m), 826(m), 800(s), 771(s), 738(s), 673(s), 627(m).

^{1}H NMR (D_2O, 400 MHz): δ 8.44 (d, J_{HH} = 8.53 Hz, 1H), 7.70 (qt, 1H), 7.61 (d, 2H) 7.28 (m, 1H), 7.22 (d, 2H).

^{31}P NMR (D_2O, 161 MHz): 10.27 (s, 1P).

6.2.7 Synthesis of (4-aminophenyl)phosphonic acid

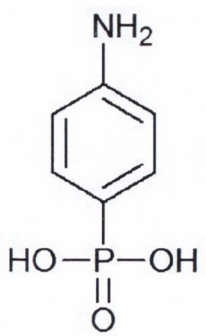

(4-aminophenyl)phosphonic acid was synthesised according to literature procedures.[110] 4-Bromoacetanilide (12.5 g, 52.5 mmol) and $NiCl_2$ (0.875 g, 7.5 mmol) were heated under N_2 at 190 °C and triethyl phosphite (11.25 ml, 65 mmol) was added dropwise. After the addition of the triethyl phosphite was complete, the reaction was allowed to cool to 150 °C and stirred for 1 h. The solution was allowed to cool to room temperature and stirred with petroleum ether overnight. The white solid which separated was recrystallised

from ethyl acetate to give (4-acetylaminophenyl)phosphonic acid diethyl ester, as white crystals. The (4-acetylaminophenyl)phosphonate ester was stirred at reflux (*ca.* 100 °C) in concentrated HCl overnight. Ethanol (50 ml) was added to aid dissolution. The solution was concentrated to 50 ml and placed in the fridge. The resulting white precipitate, 4-aminophenylphosphonic acid, **11** was collected and dried *in vacuo*. Yield (4.14 g, 45.6%).

FTIR (cm^{-1}) ν_{max} : 2863 (br), 2638 (br), 2147 (br), 1644 (w), 1605 (w), 1568 (m), 1507 (w), 1415 (w), 1323 (vw), 1151 (sh), 1131 (s), 1122 (sh), 1096 (m), 1029 (s), 1009 (s), 939 (s), 823 (s), 716 (vw), 654 (s), 644 (m).

^{1}H NMR (D_2O, 400 MHz): δ 7.32 (m, 2H), δ 6.56 (m, 2H).

^{31}P NMR (D_2O, 161 MHz): δ 14.50 (s, 1P).

6.2.8 Synthesis of (4-carboxyphenyl)arsonic acid

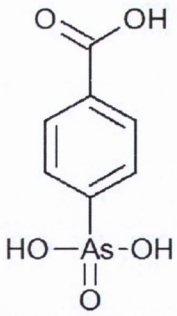

(4-Carboxyphenyl)arsonic acid was synthesized as reported in the literature.[49] 4-Aminobenzoic acid (16.00 g, 0.06 mol) was dissolved in 600 mL of H_2O and acidified with 30 mL of concentrated HCl at 0 °C. To the cold solution, a solution of 8.84 g (0.128 mol) of $NaNO_2$ in 80 mL of cold H_2O was added dropwise (solution 1). Solution 2, consisting of 17.32 g (0.088 mol) of As_2O_3, 21.0 g (0.524 mol) of NaOH, and 100 mL of H_2O, was prepared. Solution 1 was added to solution 2 dropwise with rapid stirring. Upon addition, N_2 was released and the solution turned orange. The solution was acidified to pH ~3 with concentrated HCl and filtered to remove any red precipitate. The yellow solution was then acidified to pH 1 with concentrated HCl, filtered again, and boiled to reduce the volume of

the solution to 75 mL. Upon cooling, an off-white precipitate was collected and washed with acetone. The product was recrystallized from ethanol/H_2O. Yield: 12.1 g (73%).

FTIR (cm^{-1}) ν_{max} : 2851 (br), 2684 (br),2574 (br), 2290 (br), 1684 (s), 1603 (w), 1569 (m), 1502 (w), 1424 (m), 1397 (m), 1323 (m), 1301 (s), 1284 (s), 1210 (br), 1190 (sh), 1130 (w), 1115 (w), 1091 (m), 1019 (w), 915 (sh), 865 (s), 800 (s), 760 (s), 701 (m), 688 (m).

^1H NMR (D_2O, 400 MHz): δ 8.17 (m, 2H), δ 7.82 (m, 2H).

6.3 Synthesis of the metal complexes

6.3.1 Synthesis of $Na_5[V_5O_9(O_3AsC_6H_4\text{-}4\text{-}NH_2)_4]\cdot 8H_2O$ (1)

A mixture of $NaVO_3$ (0.19 g, 1.53 mmol), NaN_3 (0.25 g, 3.85 mmol), (4-aminophenyl)arsonic acid (0.44 g, 2.027 mmol), H_2O (20 mL) and DMF (10 mL) was vigorously stirred at 70 °C until a clear solution formed (pH 7.00). $N_2H_4.H_2O$ (0.045 ml, 0.927 mmol) and 32% aqueous HCl (0.1 mL) were then added yielding a dark green solution (pH 7.30). The resulting dark green solution was stirred for 15 mins, then filtered hot, and allowed to cool to room temperature. The solution was filtered again after one day and plate shaped crystals were obtained from the solution after five days. Yield: 82%, based on $NaVO_3$. Green needle shaped crystals formed when sodium azide was not included in the synthetic procedure. These needle shaped crystals were characterised to contain the anionic cluster of **1** using mass spectrometry.

FTIR (cm^{-1}) ν_{max} : 3349(w), 3222(w), 2928(w), 2194(w), 1648(s), 1621(s), 1592(s), 1503(s), 1431(w), 1386(w), 1297(m), 1184(m), 1092(s), 980(s), 805(s), 731(w), 619(m).

CHN analysis on dried sample: expected for $As_4C_{24}H_{40}N_4Na_5O_{29}V_5$ (corresponding to the crystallographically determined formula and a loss of 3 DMF and 12.5 H_2O): C 18.99, H 2.66, N 3.69% found: C 18.29, H 2.83, N 4.54%.

^{1}H NMR (DMSO-d6, 400 MHz): δ 9.99 (br, 8H, NH_2), 7.19 (s, 8H), 5.49 (s, 8H).

MS(*m/z* - ES in DMSO): Found 1262.4789 (M^- - $5Na^+$ + $4H^+$: $C_{24}H_{28}N_4O_{21}V_5As_4$ Requires: 1262.5308).

UV-vis (in DMSO): λ[nm] = 395 (π(O) → d(V) - CT), 600 (d(V)), 701 (IVCT).

6.3.2 Synthesis of $Na_9[V_5O_9(O_3AsC_6H_4\text{-}4\text{-}COO)_4]\cdot 6DMF\cdot 15H_2O$ (2)

A mixture of $NaVO_3$ (0.19 g, 1.53 mmol), NaN_3 (0.25 g, 3.85 mmol), (4-carboxyphenyl)arsonic acid (0.492 g, 2.0 mmol), H_2O (20 mL) and DMF (10 mL) was vigorously stirred at 70 °C until a clear solution formed (pH 7.25). $N_2H_4.H_2O$ (0.045 mL, 0.927 mmol) and 32% aqueous HCl (0.1 mL) were added yielding a dark green solution (pH 7.50). This dark green solution was stirred for 25 mins, then filtered hot, and allowed to cool to room temperature. The solution was filtered again after one day and crystals from this solution were obtained after three days. Yield: 12%, based on $NaVO_3$.

FTIR (cm^{-1}) ν_{max} : 3476(br), 2939(w), 1652(vs), 1583(m), 1491(m), 1476(m), 1476(w), 1389(s), 1281(m), 1268(m), 1176(w), 1095(vs), 998(s), 996(sh), 833(s), 792(s), 662(sh), 635(sh), 617(s).

CHN analysis on dried sample: expected for $C_{46}H_{88}N_6O_{50}Na_9V_5As_4$ (corresponding to the crystallographically determined formula and a loss of 12 H_2O): C 24.16, H 3.88, N 3.68% found: C 24.20, H 4.26, N 3.91%.

UV-vis (in DMSO): λ[nm] = 604 (d(V)), 714 (IVCT)

6.3.3 Synthesis of $Na_5[V_5O_9(O_3AsC_6H_4\text{-}4\text{-}OH)_4]\cdot 7H_2O\cdot 5DMF$ (3)

A mixture of $NaVO_3$ (0.19 g, 1.53 mmol), NaN_3 (0.25 g, 3.85 mmol), (4-hydroxyphenyl)arsonic (0.436 g, 2 mmol), H_2O (20 mL) and DMF (10 mL) was vigorously stirred at 70 °C until a clear solution formed (pH 7.3). After the addition of $N_2H_4.H_2O$ (0.045 mL, 0.927 mmol) and 32% aqueous HCl, a dark green solution was observed (pH 7.40) which was stirred for 30 mins, then filtered hot, and allowed to cool to room temperature. The solution was filtered again after one day and crystals were obtained from the solution after 14 days. Compound **3** could also be reproduced with H_2SO_4 (conc.) as an acid, however white colorless crystals were always observed as a co-crystallising impurity. Yield: 19%, based on $NaVO_3$.

FTIR (cm^{-1}) ν_{max} : 3443(br), 2940(w), 1649(vs), 1584(s), 1491(s), 1473(m), 1389(s), 1278(s), 1176(w), 1096(s), 1002(sh), 987(s), 832(sh), 792(vs).

CHN analysis on dried sample: expected for $C_{39}H_{69}N_5O_{37}Na_5V_5As_4$ (corresponding to the crystallographically determined formula and a loss of $10.5H_2O$): C 25.06, H 3.72, N 3.75% found: C 25.04, H 3.45, N 4.20%.

MS(*m/z* – ES in DMSO): Found 1266.4916 (M^- - $5Na^+$ + $4H^+$: $C_{24}H_{24}O_{25}V_5As_4$ Requires: 1266.4669).

UV-vis (in DMSO): λ[nm] = 605 (d(V)), 704 (IVCT).

6.3.4 Synthesis of $Na_5[V_5O_9(O_3AsC_6H_4\text{-}3\text{-}NHCOCH_3\text{-}4\text{-}OH)_4]\cdot 19H_2O$

·3DMF (4)

A mixture of $NaVO_3$ (0.189 g, 1.525 mmol), NaN_3 (0.25 g, 3.850 mmol), (3-acetamido-4-hydroxyphenyl)arsonic acid (0.558 g, 2.027 mmol), H_2O (30 mL) and DMF (30 mL) was vigorously stirred at 65 °C until a clear solution formed (pH 6.65). The pH of the solution was adjusted to pH 6.02 with concentrated hydrochloric acid and upon addition of $N_2H_4.H_2O$ (0.045 mL, 0.927 mmol), a dark green solution was observed (pH 7.20). This solution was stirred for 20 mins, then filtered hot, and allowed to cool to room temperature. The solution was filtered and green cube shaped crystals were obtained from the solution after nine days. Yield: 15%, based on $NaVO_3$.

FTIR (cm^{-1}) ν_{max} : 3327(br), 1653(s), 1622(m), 1533(m), 1411(s), 1405(sh), 1286(m), 1259(m), 1090(m), 1002(m), 984(s), 797(vs).

CHN analysis on dried sample: expected for $C_{41}H_{95}N_7O_{51}Na_5V_5As_4$ (corresponds to the crystallographically determined formula): C 22.68, H 4.41, N 4.52% found: C 22.66, H 3.56, N 4.61%.

UV-vis (in DMSO): λ[nm] = 603 (d(V)), 703 (IVCT).

6.3.5 Synthesis of $Na_4[V_{12}O_{14}(OH)_4(H_2O)_4(O_3AsC_6H_4\text{-}4\text{-}NH_2)_{10}]$ ·3DMF·12H_2O (5)

A mixture of $NaVO_3$ (0.19 g, 1.53 mmol), NaN_3 (0.25 g, 3.85 mmol), (4-aminophenyl)arsonic acid (0.44 g, 2.027 mmol), H_2O (20 mL) and DMF (10 mL) was stirred at 70 °C until a clear solution formed (pH 7.0). After the addition of $N_2H_4·H_2O$ (0.045 mL), 32% aqueous HCl (0.50 mL) was added to adjust the final pH value to 4.9 (70 °C). Blue cubic crystals were obtained from this solution after five days. Yield 43%, based on $NaVO_3$.

FTIR (cm^{-1}) ν_{max} : 3365(br), 2932(w), 2035(m), 1650(s), 1594(m), 1505(m), 1438(w), 1413(w), 1388(m), 1312(w), 1254(w), 1183(w), 1095(s), 1062(w), 990(s), 898(w), 823(s), 695(m), 661(m).

CHN analysis for $C_{64.5}H_{95}As_{10}N_{11.5}Na_4O_{59.75}V_{12}$ (corresponds to the crystallographically determined formula and a loss of $4H_2O$), expected: C 22.52, H 2.78, N 4.68%; found: C 23.08, H 3.46, N 5.28%.

^1H NMR (DMSO-d6, 400 MHz): δ 10.07 (br, 20H, NH_2), 7.71 (br, 4H), 7.05 (br, 16H), 5.67 (br, 20H).

MS(*m/z* – ES in DMSO): Found 1589.4742 (M^{2-} - $2H^+$: $C_{60}H_{66}N_{10}O_{50}Na_4V_{12}As_{10}$ Requires: 1589.3983).

UV-vis (in DMSO): λ[nm] = 620 (d(V)), 710 (IVCT).

6.3.6 Synthesis of $Na_4H_2[V_{14}O_{22}(OH)_4(H_2O)_2(O_3PC_6H_4\text{-}4\text{-}NH_2)_8]\cdot 7DMF\cdot 12H_2O$ (6)

A mixture of $NaVO_3$ (0.19 g, 1.53 mmol), NaN_3 (0.25 g, 3.85 mmol), (4-aminophenyl)phosphonic acid (0.346 g, 2 mmol), H_2O (20 mL) and DMF (10 mL) was vigorously stirred at 70 °C until a clear solution formed (pH 7.25). After the addition of 0.045 mL of $N_2H_4.H_2O$ (0.045 mL, 0.927mmol) and aqueous HCl (32% 0.8 mL), a dark green solution was observed (pH 7.30). The resulting solution was stirred for 30 mins, then filtered hot, and allowed to cool to room temperature. The solution was filtered again after one day and crystals were obtained from this solution after seven days. Yield: 23%, based on $NaVO_3$.

FTIR (cm^{-1}) ν_{max} : 3378(br), 2047(m), 1652(s), 1635(sh), 1604(s), 1510(m), 1477(w), 1442(w), 1432(w0, 1392(m), 1292(w), 1259(w), 1139(m), 1076(s), 1025(s), 991(vs), 910(m), 830(m).

CHN analysis for $C_{69}H_{131}N_{15}O_{71}Na_4P_8V_{14}$ (corresponding to the crystallographically determined formula): C 24.67, H 3.93, N 6.25% found: C 24.35, H 3.71, N 6.72%.

6.3.7 Synthesis of $Na_4H_2[Cl_2{\subset}V_{14}O_{14}(OH)_8(O_3AsC_6H_4\text{-}4\text{-}NH_2)_{10}]\cdot 6DMF \cdot 15H_2O$ (7)

A mixture of $NaVO_3$ (0.19 g, 1.53 mmol), NaN_3 (0.25 g, 3.85 mmol), (4-aminophenyl)arsonic acid (0.166 g, 0.769 mmol), H_2O (20 mL), DMF (20 mL) was vigorously stirred at 65 °C until a clear solution formed. Aqueous HCl (32%) was added drop wise to adjust the reaction mixture to pH 5.0. $N_2H_4.{}_2H_2O$ (0.045 mL 0.927 mmol) was added, resulting in a colour change and the pH was again adjusted with Aqueous HCl 32% to pH 5.4. A dark green\turquoise solution was observed. The resulting reaction solution was stirred for 30 mins, then filtered hot, and allowed to cool to room temperature. The solution was filtered and turquoise block crystals were observed after 35 days. Yield: (5%), based on $NaVO_3$.

FTIR (cm^{-1}) ν_{max} : 3454(sh), 3357(br), 3249(sh), 1652(s), 1596(m), 1506(m), 1389(m), 1314(w), 1256(w), 1188(w), 1095(s), 1000(sh), 985(s), 821(sh), 800(s), 659(m).

CHN analysis for $C_{78}H_{142}N_{16}Na_4O_{73}Cl_2V_{14}As_{10}$ (corresponds to the crystallographically determined formula), expected: C 22.85, H 3.49, N 5.47%; found: C 22.91, H 3.31, N 6.11%.

UV-vis (in DMSO): λ[nm] = 403 ($\pi(O) \rightarrow d(V)$ - CT), 623 (d(V)), 731 (IVCT).

6.3.8 Synthesis of $Na_2H_6[V_{16}O_{24}(OH)_8(O_3AsC_6H_4\text{-}4\text{-}NH_2)_8]\cdot 6DMF\cdot 13H_2O$ (8)

A mixture of $NaVO_3$ (0.19 g, 1.53 mmol), (4-aminophenyl)arsonic acid (0.188 g, 0.870 mmol), H_2O (20 mL), DMF (10 mL) was vigorously stirred at 65 °C until a clear solution formed. $N_2H_4.2H_2O$ (0.045 mL, 0.927mmol) was added, resulting in a colour change and the pH was again adjusted with 0.1 mL of aqueous HCl (32%). A dark green solution was observed and $CoCl_2.6H_2O$ (0.182 g, 0.5 mmol) was then added to this resulting reaction solution. The resultant reaction mixture which became cloudy was stirred for 30 mins. The green reaction mixture was then filtered hot and allowed to cool to room temperature. A large amount of a pale pink precipitation was observed on the filter paper. The resultant green filtrate produced green cubed shaped crystals of **8** after 39 days. Yield: (2%), based on $NaVO_3$.

FTIR (cm^{-1}) ν_{max} : 3445(sh), 3353(br), 3233(sh), 1651(s), 1596(m), 1506(m), 1438(w), 1419(w0, 1389(m), 1315(w), 1312(w), 1256(w), 1187(w), 1094(m), 1000(m), 982(s), 824(sh), 797(s).

6.3.9 Synthesis of $Na_8H_2[(H_2O)_2\subset V_{10}O_{18}(O_3PC_6H_4\text{-}4\text{-}PO_3)_4]\cdot 30H_2O$ (9)

(1,4-Benzene)bisphosphonic acid (0.20 g, 0.86 mmol), Na_3VO_4 (0.28 g, 1.50 mmol), NaN_3 (0.25 g, 3.80 mmol), H_2O (15 mL), DMF 15 mL and triethylamine (0.25 mL, 1.79 mmol) were stirred at 70 °C for 15 mins. Aqueous HCl (32% 0.20 mL) was added and a yellow solution was observed (pH 6.50). $N_2H_4.H_2O$ (0.045 mL, 0.927 mmol) and further aqueous

HCl (32% 0.15 mL) solution were added resulting in a colour change to light green (pH 7.56). The solution was stirred for 1 hr, when dark green cube crystals were observed. The mother liquor was filtered off. Yield: (41%), based on Na_3VO_4.

FTIR (cm^{-1}) ν_{max} : 3187(br), 2616(br), 2164(w), 2039(m), 1756(w), 1641(s), 1604(sh), 1542(sh), 1488(w), 1434(w), 1384(m), 1306(w), 1249(w), 1135(sh), 1098(sh), 1050(s) 992(sh), 950(br), 818(m), 711(m).

CHN analysis expected for $C_{24}H_{82}Na_8O_{74}P_8V_{10}$ (corresponding to the crystallographically determined formula and a loss of $4H_2O$): C 11.55, H 3.31%; found: C 11.37, H 2.87%.

MS(*m/z* – ES in H_2O): Found 870.5706 (M^{2-} - $8Na^+$ + $6H^+$: $C_{24}H_{24}O_{42}P_8V_{10}$ Requires: 870.6025); 881.5607 (M^{2-} - $7Na^+$ + $5H^+$: $C_{24}H_{23}O_{42}NaP_8V_{10}$ Requires: 881.5607); 892.5694 (M^{2-} - $6Na^+$ + $4H^+$ -H_2O: $C_{24}H_{22}O_{42}Na_2P_8V_{10}$ Requires: 881.5845); $C_{24}H_{18}O_{50}Na_8P_8V_{10}$ Requires: 881.5607); 574.0540 (M^{3-} - $8Na^+$ +$5H^+$-H_2O: $C_{24}H_{21}O_{41}P_8V_{10}$ Requires: 574.0624).

UV-vis (in H_2O): λ[nm] = 619 (d(V)), 723 (IVCT).

6.3.10 Synthesis of $Na_8H_2[(H_2O)_2{\subset}V_{10}O_{18}(O_3PC_{10}H_6\text{-}4\text{-}PO_3)_4]\cdot 44H_2O$ (10)

(1,4-Naphthalene)bisphosphonic acid (0.247 g, 0.86 mmol), Na_3VO_4 (0.28 g, 1.50 mmol), NaN_3 (0.25 g, 3.80 mmol), H_2O (15 mL), DMF (15 mL) and triethylamine (0.25 mL, 1.79mmol) were heated at 70 °C for 15mins. Aqueous HCl (32% 0.18 mL) was added and a yellow solution was observed (pH 6.70). $N_2H_4.H_2O$ (0.045 mL, 0.927 mmol) and aqueous HCl (32% 0.13 mL) were added resulting in a colour change to light green (pH 7.50). The solution was stirred for 1 hr, when dark green cube shaped crystals were observed. The mother liquor was filtered off. Yield 30%, based on Na_3VO_4.

FTIR (cm^{-1}) ν_{max} : 3397(br), 3241(sh), 1645(s), 1510(m), 1453(w), 1384(w), 1209(w), 1119(sh), 1033(sh), 962(s), 889(sh), 765(m).

CHN analysis expected for $C_{40}H_{82}Na_8O_{70}P_8V_{10}$ (corresponding to the crystallographically determined formula and a loss of $18H_2O$): C 18.31, H 3.15%; found: C 18.03, H 2.87%.

MS(*m/z* – ES in DMSO): Found 970.6015 (M^{2-} - $8Na^+$ + $6H^+$: $C_{40}H_{32}O_{42}P_8V_{10}$ Requires: 970.6339); 981.5723 (M^{2-} - $7Na^+$ + $5H^+$: $C_{40}H_{31}O_{42}NaP_8V_{10}$ Requires: 981.6248); 992.5518 (M^{2-} - $6Na^+$ + $4H^+$: $C_{40}H_{30}O_{42}Na_2P_8V_{10}$ Requires: 992.6158);

UV-vis (in DMSO): λ[nm] = 618 (d(V)), 758 (IVCT).

6.3.11 Synthesis of $Na_8H_2[(DMF)_2{\subset}V_{10}O_{18}(O_3PC_{12}H_8\text{-}4\text{-}PO_3)_4]\cdot 30H_2O$ (11)

([1,1'-Biphenyl]-4,4'-diyl)bisphosphonic acid (0.27 g, 0.86 mmol), Na_3VO_4 (0.28 g, 1.50 mmol), NaN_3 (0.25 g, 3.80 mmol), H_2O (30 mL), DMF (10 mL) and triethylamine (0.25mL, 1.79mmol) were heated at 70°C for 15 mins. Aqueous HCl (32% 0.17mL) was added and a yellow solution was observed (pH 6.10). $N_2H_4.H_2O$ (0.045 mL, 0.927 mmol) was added to the solution, resulting in a colour change to light green (pH 7.28). The solution was left stirred for 1.5 hrs upon which dark green octahedron shaped crystals were observed. The mother liquor was filtered off. Yield: (36.3%), based on Na_3VO_4.

FTIR (cm^{-1}) ν_{max} : 3343(br), 2160(w), 2037(w), 1639(s), 1537(w), 1488(w), 1454(w), 1389(m), 1251(w), 1137(sh), 1102(s), 1045(s), 1030(s), 1022(s), 966(s), 857(w), 817(s), 760(w), 714(m).

CHN analysis for $C_{54}H_{98}N_2Na_8O_{73}P_8V_{10}$, (corresponding to the crystallographically determined formula): C 22.49, H 3.42, N 0.97%; found: C 21.82, H 2.79, N 1.51%.

MS(*m/z* – ES in H_2O): Found 1022.6624 (M^{2-} - $8Na^+$ + $6H^+$: $C_{48}H_{40}O_{42}Na_3P_8V_{10}$ Requires: 1022.6652); 1033.6523 (M^{2-} - $7Na^+$ + $5H^+$: $C_{48}H_{39}O_{42}Na_3P_8V_{10}$ Requires: 1033.6561); 675.4 (M^{3-} - $8Na^+$ + $5H^+$ - H_2O : $C_{48}H_{37}O_{41}P_8V_{10}$ Requires: 675.4375);

UV-vis (in H_2O): λ[nm] = 619 (d(V)), 724 (IVCT).

6.3.12 Synthesis of $NaH_4[V_{10}O_{18}(O_3AsC_6H_4\text{-}4\text{-}NH_2)_7(DMF)_2]\cdot 5H_2O\cdot 7DMF$ (12)

A mixture of $NaVO_3$ (0.19 g, 1.53 mmol), (4-aminophenyl)arsonic acid (0.221 g, 1.018 mmol), H_2O (20 ml), DMF (20 mL) was vigorously stirred at 65 °C until a clear solution formed. conc. HNO_3 was added dropwise to adjust the reaction mixture to pH 4.32 to form solution 1. $N_2H_4.2H_2O$ (0.045mL, 0.927mmol) was added to solution 1, resulting in a colour change and the pH was again adjusted with HNO_3 conc. to pH 3.63. A dark green\turquoise solution was observed. The resulting reaction solution was stirred for 30 mins, then filtered hot, and allowed to cool to room temperature. This reaction was filtered and green needle crystals appeared after 10 days. Yield (5.8%) based on $NaVO_3$.

FTIR (cm^{-1}) ν_{max} : 3354(br), 1651(s), 1628(sh), 1595(s), 1506(m), 1438 (w), 1416(w), 1388(m), 1314(w), 1256(w), 1188(w), 1094(m), 1000 (sh), 985(s), 801(s), 661(m).

CHN analysis expected for $C_{69}H_{119}N_{16}O_{53}As_7NaV_{10}$ (corresponding to the crystallographically determined formula with seven DMF molecules and five water molecules): C 26.93, H 3.9, 7.28%; found: C 27.04, H 3.64, 7.39%.

6.3.13 Synthesis of $Na_6H[V_{13}O_{31}(O_3AsC_6H_4\text{-}4\text{-}NH_2)_3]\cdot 7H_2O\cdot 8DMF$ (13)

A mixture of $NaVO_3$ (0.19 g, 1.53 mmol), NaN_3 (0.25 g, 3.85 mmol), (4-aminophenyl)arsonic acid (0.166 g, 0.765 mmol), H_2O (20 mL), DMF (20 mL) was vigorously stirred at 65 °C until a clear solution formed. Aqueous HCl 32% was added dropwise to adjust the reaction mixture to pH 5.0 to form solution 1. $N_2H_4.2H_2O$ (0.045 mL, 0.927 mmol) was added to 1 mL of deionised water to form solution 2. 0.4 mL of solution 2 was added to solution 1, resulting in a colour change and the pH was again adjusted with 32% aqueous HCl to pH 5.3. A dark green\turquoise solution was observed. The resulting reaction solution was stirred for 30 mins, then filtered hot, and allowed to cool to room temperature. The solution was again filtered and a small number of turquoise plate crystals were observed after 30 days. These turquoise crystals were characterised to be **7** using single crystal X-ray diffraction. Green plate shaped crystals of **13** appeared simultaneously with white crystalline impurity after a total of 43 days. Several attempts to optimise the formation conditions of **13** were unsuccessful and solid state characterisations were performed on single crystals of **13** which had been mechanically separated. Yield: (2.3%) based on $NaVO_3$.

FTIR (cm^{-1}) ν_{max} : 3341(br), 3227(br), 1652(s), 1639(sh), 1597(s), 1505(m), 1439(w), 1419(w), 1390(m), 1315(w), 1297(w), 1258(w), 1185(m), 1091(s), 998(sh), 978(s), 826(sh), 784(s).

CHN analysis expected for $C_{42}H_{89}N_{11}Na_6O_{55}As_4V_{12}$ (corresponding to the crystallographically determined formula with additional six DMF molecules and two water molecules): C 21.73%, H 3.38%, 5.81%; found: C 22.31, H 3.41%, 5.44%.

6.3.14 Synthesis of $Na_2H_2[(VO_2)_4(O_3PC_{10}H_7)_4] \cdot 3DMF \cdot 12H_2O$ (14)

A mixture of $NaVO_3$ (0.189 g, 1.525 mmol), (1-naphthalene)phosphonic acid (0.317 g, 1.525 mmol), H_2O (30 mL) and DMF (20 mL) was vigorously stirred at 65 °C until a yellow

solution formed (pH 5.7). Hydrazine monohydrate (0.045 mL, 0.927 mmol) was added and the pH was restored using concentrated hydrochloric acid (pH 5.9). A second addition of hydrazine monohydrate (0.045 mL, 0.927 mmol) resulted in a turquoise blue solution which was found to have a pH 5.9. The solution was left to stir on the hotplate for a 20 mins and the reaction mixture was filtered. A few turquoise cubed shaped crystals appeared within one day. Several attempts to optimise the yield of **14** were unsuccessful. Yield: 2.7% based on $NaVO_3$.

FTIR (cm^{-1}) ν_{max} : 3366(w), 1643(s), 1505(w), 1431(w), 1370(m), 1217(w), 1152(w), 1064(s), 1037(s), 956(s), 829(w), 803(s), 774(s), 695(s), 672(w).

CHN analysis expected for $C_{49}H_{73}Na_2O_{35}P_4V_4$ (corresponding to the crystallographically determined formula with three extra water molecules): C 35.94, H 4.49, 2.57%; found: C 35.72, H 4.24, 5.42%.

6.3.15 Synthesis of $H_4[(VO)_{12}(OH)_{12}(O_3PC_{10}H_7)_8]\cdot 13H_2O\cdot 6DMF$ (15)

A mixture of (1-naphthalene)phosphonic acid (0.11 g, 0.50 mmol), $VOSO_4.3H_2O$ (0.11 g, 0.40 mmol), H_2O (5 mL) and DMF (3 mL) was placed in a Teflon lined (23 mL) autoclave. The autoclave was then sealed and heated to 160 °C for three days. The final product mixture consists of blue cube crystals in a clear solution. The blue single crystals of **15** were collected in near quantitative yield by filtration.

Yield: 87mg (94.15%) based on $VOSO_4.3H_2O$. FTIR (cm^{-1}) ν_{max} : 3429(br), 3039(w), 2926(w), 2800(w), 2442(w), 1654(s), 1590(m), 1506(m), 1467(m), 1435(w), 1413(w), 1387(m), 1335(w), 1253(w), 1219(w), 1128(s), 1098(s), 1065(s), 1030(s), 996(s), 982(s), 898(s), 829(m), 804(m), 776(s), 741(w), 675(m).

CHN analysis expected for $C_{98}H_{140}N_6O_{67}P_8V_{12}$ (corresponding to the crystallographically determined formula with six additional unresolved DMF molecules and six unresolved water molecules): C 35.31, H 4.23, 2.52%; found: C 35.03, H 3.93, 2.57%.

Attached CD-ROM

The CD-ROM attached to this thesis contains electronic versions of various files for the structures given in this thesis. There are 2 folders that contain these files. (This information is also given in the ReadMe.txt file on the CD.)

The CIF folder contains all the crystallographic information files (*.cif). The naming of each file corresponds to the structure as given in the thesis (e.g. Compound 1 corresponds to 1 in the thesis). CIFs can be viewed in the Mercury program, which is a program available as a free download from the CCDC website (www.ccdc.cam.ac.uk).

The PDF folder contains a PDF type file of this entire thesis, should the reader require an electronic copy. PDF files can be viewed in the Adobe Acrobat Reader program, which is available as a free download from the Adobe website (www.adobe.com/products/acrobat/readermain.html).

References

[1] J. Berzelius, *Pogg. Ann. Phys.* **1826**, *6*, 380.

[2] C. Marignac, *Ann. Chem.* **1862**, *25*, 362.

[3] L. Pauling, *J. Am. Chem. Soc.* **1929**, *51*, 2868-2880.

[4] J. W. Illingworth, J. F. Keggin, *J. Chem. Soc.* **1935**, 575-580.

[5] L. C. W. Baker, J. S. Figgis, *J. Am. Chem. Soc.* **1970** *92*, 3794-3797.

[6] P. Kogerler, A. Müller, in *Polyoxometalated Molecular Science, Vol. 98* (Eds.: J. J. Borrás-Almenar, E. Coronado, A. Müller, M. T. Pope), Kluwer, Dordrecht, **2003**, pp. 297-326; M. T. Pope, A. Müller, *Angew. Chem. Int. Ed.* **1991**, *30*, 34-48; A. Müller, S. Roy, *Coord. Chem. Rev.* **2003**, *245*, 153-166.

[7] A. Müller, P. Kogerler, *Coord. Chem. Rev.* **1999**, *182*, 3-17; L. Cronin, P. Kogerler, A. Müller, *J. Solid State Chem.* **2000**, *152*, 57-67.

[8] A. Müller, S. Polarz, S. Das, E. Krickemeyer, H. Bögge, M. Schmidtmann, B. Hauptfleisch, *Angew. Chem. Int. Ed.* **1999**, *38*, 3241-3245; A. Müller, E. Krickemeyer, H. Bögge, M. Schmidtmann, P. Kogerler, C. Rosu, E. Beckmann, *Angew. Chem. Int. Ed.* **2001**, *40*, 4034-4037; A. Müller, E. Krickemeyer, H. Bögge, M. Schmidtmann, S. Roy, A. Berkle, *Angew. Chem. Int. Ed.* **2002**, *41*, 3604-3609; A. Müller, D. Rehder, E. Haupt, A. Merca, H. Bögge, M. Schmidtmann, G. Heinze-Bruckner, *Angew. Chem. Int. Ed.* **2004**, *43*, 4466-4470; A. Müller, L. Toma, H. Bögge, C. Schaffer, A. Stammler, *Angew. Chem. Int. Ed.* **2005**, *44*, 7757-7761; A. Müller, F. Sousa, A. Merca, H. Bögge, P. Miro, J. Fernandez, J. Poblet, C. Bo, *Angew. Chem. Int. Ed.* **2009**, *48*, 5934-5937.

[9] A. Müller, E. Beckmann, H. Bögge, M. Schmidtmann, A. Dress, *Angew. Chem. Int. Ed.* **2002**, *41*, 1162-1167.

[10] A. Müller, E. Krickemeyer, H. Bögge, M. Schmidtmann, C. Beugholt, P. Kogerler, C. Z. Lu, *Angew. Chem. Int. Ed.* **1998**, *37*, 1220-1223.

[11] A. Müller, S. Q. N. Shah, H. Bögge, M. Schmidtmann, *Nature* **1999**, *397*, 48-50.

[12] A. Müller, R. Rohlfing, J. Döring, M. Penk, *Angew. Chem. Int. Ed. Engl.* **1991**, *30*, 588-590.

[13] W. Klemperer, T. Marquart, O. Yaghi, *Angew. Chem. Int. Ed.* **1992**, *31*, 49-51.

[14] M. I. Khan, S. Ayesh, R. J. Doedens, M. H. Yu, C. J. O'Connor, *Chem. Commun.* **2005**, 4658-4660.

[15] A. Müller, E. Krickemeyer, M. Penk, R. Rohlfing, A. Armatage, H. Bögge, *Angew. Chem. Int. Ed.* **1991**, *30*, 1674-1676.

[16] A. Müller, R. Rohlfing, E. Krickemeyer, H. Bögge, *Angew. Chem. Int. Ed.* **1993**, *32*, 909-912.

[17] A. Müller, M. Penk, R. Rohlfing, E. Krickemeyer, J. Döring, *Angew. Chem. Int. Ed.* **1990**, *29*, 926-927.

[18] A. Müller, M. Penk, E. Krickemeyer, H. Bögge, Walberg, H. Juergen, *Angew. Chem. Int. Ed.* **1988**, *27*, 1719-1721.

[19] T. Kurata, A. Uehara, Y. Hayashi, Isobe, Kiyoshi, *Inorg. Chem.* **2005**, *44*, 2524-2530.

[20] W. Ouellette, M. H. Yu, C. J. O'Connor, J. Zubieta, *Inorg. Chem.* **2006**, *45*, 7628-7641.

[21] C. E. Housecroft, A. G. Sharpe, *Inorganic Chemistry*, Prentice Hall, Harlow, **2001**.

[22] D. E. Katsoulis, *Chem. Rev.* **1998**, *98*, 359-387.

[23] P. Gouzerh, A. Proust, *Chem. Rev.* **1998**, 77-111.

[24] A. Proust, R. Thouvenot, P. Gouzerh, *Chem. Commun.* **2008**, 1837-1852.

[25] S. T. Zheng, J. Zhang, B. Li, G. Y. Yang, *Dalton Trans.* **2008**, 5584-5587.

[26] A. Müller, J. Döring, *Z. Anorg. Allg. Chem.* **1991**, 251-274.

[27] G. Huan, M. Greaney, A. Jacobson, *J. Chem. Soc. Chem. Commun.* **1991**, 260-261.

[28] X. Cui, Y. Sun, G. Yang, *Inorg. Chem. Commun.* **2003**, 259-261; X. Cui, J. Xu, Y. Li, Y. Sun, L. Ye, G. Yang, *J. Mol. Struct.* **2003**, 395-398; Y. Gao, Y. Xu, Z. Han, C. Li, F. Cui, Y. Chi, C. Hu, *J. Solid State Chem.* **2010**, 1000-1006; Y. Qi, Y. Li, E. Wang, H. Jin, Z. Zhang, X. Wang, S. Chang, *Inorg. Chim. Acta* **2007**, 1841-1853; Y. Qi, Y. Li, E. Wang, H. Jin, Z. Zhang, X. Wang, S. Chang, *J. Solid State Chem.* **2007**, 382-389; A. Tripathi, T. Hughbanks, A. Clearfield, *J. Am. Chem. Soc.* **2003**, 10528-10529; T. Whitfield, X. Wang, A. Jacobson, *Inorg. Chem.* **2003**, 3728-3733; A. Wutkowski, C. Nither, P. Kogerler, W. Bensch, *Inorg. Chem.* **2008**, 1916-1918.

[29] D. Long, E. Burkholder, L. Cronin, *Chem. Soc. Rev.* **2007**, *36*, 105-121.

[30] I. Weinstock, E. Barbuzzi, M. Wemple, J. Cowan, R. Reiner, D. Sonnen, R. Heintz, J. Bond, C. Hill, *Nature* **2001**, *414*, 191-195.

[31] S. Mitchell, D. Gabb, C. Ritchie, N. Hazel, D. Long, L. Cronin, *Cryst. Eng. Comm.* **2009**, *11*, 36-39; S. Mitchell, S. Khanra, H. Miras, T. Boyd, D. Long, L. Cronin, *Chem. Commun.* **2009**, 2712-2714; C. Ritchie, F. Li, C. Pradeep, D. Long, L. Xu, L. Cronin, *Dalton Trans.* **2009**, 6483-6486; C. Ritchie, T. Boyd, D. Long, E. Ditzel, L. Cronin, *Dalton Trans.* **2009**, 1587-1592.

[32] C. Pradeep, D. Long, P. Kögerler, L. Cronin, *Chem. Commun.* **2007**, 4254-4256; L. Cronin, C. Beugholt, E. Krickemeyer, M. Schmidtmann, H. Bögge, P. Kögerler, T.

Luong, A. Müller, *Angew. Chem. Int. Ed.* **2002**, *41*, 2805-2808; T. Boyd, S. Mitchell, H. Miras, D. Long, L. Cronin, *Dalton Trans.* **2010**, 6460-6465; J. Thiel, C. Ritchie, C. Streb, D. Long, L. Cronin, *J. Am. Chem. Soc.* **2009**, *131*, 4180-4181; J. Yan, D. Long, L. Cronin, *Angew. Chem. Int. Ed.* **2010**, 4117-4120.

[33] G. Huan, J. W. Johnson, A. J. Jacobson, J. S. Merola, *Chem. Mater.* **1990**, *2*, 719-723; M. I. Khan, Y. S. Lee, C. J. Oconnor, R. C. Haushalter, J. Zubieta, *Inorg. Chem.* **1994**, *33*, 3855-3856; W. Ouellette, M. H. Yu, C. J. O'Connor, J. Zubieta, *Inorg. Chem.* **2006**, *45*, 3224-3239.

[34] C. Pradeep, D. Long, C. Streb, L. Cronin, *J. Am. Chem. Soc.* **2008**, *130*, 14946-14947.

[35] Q. Chen, J. Salta, J. Zubieta, *Inorg. Chem.* **1993**, 4485-4486.

[36] Y. D. Chang, J. Salta, J. Zubieta, *Angew. Chem. Int. Ed.* **1994**, *33*, 325-327.

[37] M. H. Chisholm, *Early transition metal clusters with [pi]-donor ligands*, VCH, New York ; Cambridge, **1995**.

[38] A. Müller, K. Hovemeier, R. Rohlfing, *Angew. Chem. Int. Ed.* **1992**, *31*, 1192-1195.

[39] S. Konar, A. Clearfield, *Inorg. Chem.* **2008**, *47*, 3492-3494.

[40] Q. Chen, J. Zubieta, *J. Chem. Soc. Chem. Commun.* **1994**, 1635-1636.

[41] D. D. Heinrich, K. Folting, W. E. Streib, J. C. Huffman, G. Christou, *J. Chem. Soc. Chem. Commun.* **1989**, 1411-1413; G. Karet, Z. Sun, D. Heinrich, J. McCusker, K. Folting, W. Streib, J. Huffman, D. Hendrickson, G. Christou, *Inorg. Chem.* **1996**, 6450-6460.

[42] A. Müller, K. Hovemeier, E. Krickemeyer, H. Bögge, *Angew. Chem. Int. Ed.* **1995**, *34*, 779-781.

[43] E. Burkholder, J. Zubieta, *Inorg. Chim. Acta* **2004**, *357*, 301-304; P. Hagrman, D. Hagrman, J. Zubieta, *Angew. Chem. Int. Ed.* **1999**, *38*, 2639-2684; V. Soghomonian, Q. Chen, R. C. Haushalter, J. Zubieta, *Angew. Chem. Int. Ed.* **1995**, *34*, 223-226.

[44] G. Bonavia, R. C. Haushalter, C. J. O'Connor, C. Sangregorio, J. Zubieta, *Chem. Commun.* **1998**, 2187-2188.

[45] J. Salta, Q. Chen, Y. D. Chang, J. Zubieta, *Angew. Chem. Int. Ed.* **1994**, *33*, 757-760.

[46] M. I. Khan, J. Zubieta, *Angew. Chem. Int. Ed.* **1994**, *33*, 760-762.

[47] M. I. Khan, Y. Chang, O. Chen, H. Hope, S. Parking, D. P. Goshorn, J. Zubieta, *Angew. Chem. Int. Ed.* **1992**, *31*, 1197-1200.

[48] J. Salta, Y. D. Chang, J. Zubieta, *J. Chem. Soc. Chem. Commun.* **1994**, 1039-1040.

[49] B. J. S. Johnson, R. C. Schroden, C. C. Zhu, A. Stein, *Inorg. Chem.* **2001**, *40*, 5972-5978.

[50] B. F. Hoskins, R. Robson, *J. Am. Chem. Soc.* **1989**, *111*, 5962-5964.

[51] O. M. Yaghi, M. O'Keeffe, N. W. Ockwig, H. K. Chae, M. Eddaoudi, J. Kim, *Nature* **2003**, *423*, 705-714.

[52] H. M. El-Kaderi, J. R. Hunt, J. L. Mendoza-Cortes, A. P. Cote, R. E. Taylor, M. O'Keeffe, O. M. Yaghi, *Science* **2007**, *316*, 268-272; J. L. C. Rowsell, E. C. Spencer, J. Eckert, J. A. K. Howard, O. M. Yaghi, *Science* **2005**, *309*, 1350-1354.

[53] Y. Gong, C. W. Hu, H. Liang, *Prog. Nat. Sci.* **2005**, *15*, 385-394.

[54] N. Mizuno, M. Misono, *Chem. Rev.* **1998**, *98*, 199-217.

[55] C. Hill, C. Prosser-McCartha, *Coord. Chem. Rev.* **1995**, 407-455.

[56] T. Hirao, *Chem. Rev.* **1997**, 2707-2724.

[57] T. Okuhara, *Chem. Rev.* **2002**, 3641-3665.

[58] J. Wang, L. Yan, G. Qian, X. Wang, *Tetrahedron Lett.* **2006**, 7171-7174.

[59] R. Noyori, M. Aoki, K. Sato, *Chem. Commun.* **2003**, 1977-1986; C. Hill, *Nature* **1999**, *401*, 436-437.

[60] L. Xu, E. Boring, C. Hill, *J. Cat.* **2000**, *195*, 394-405.

[61] K. Chary, C. Kumar, A. Murali, A. Tripathi, A. Clearfield, *J. Mol. Cat. A* **2004**, *216*, 139-146.

[62] A. Merca, E. T. K. Haupt, T. Mitra, H. Bögge, D. Rehder, A. Müller, *Chem. Eur. J.* **2007**, *13*, 7650-7658.

[63] A. Tsuda, E. Hirahara, Y. Kim, H. Tanaka, T. Kawai, T. Aida, *Angew. Chem. Int. Ed.* **2004**, 6327-6331; A. Müller, S. Roy, *J. Mater. Chem.* **2005**, 4673-4677.

[64] V. W. Day, W. G. Klemperer, O. M. Yaghi, *J. Am. Chem. Soc.* **1989**, *111*, 5959-5961.

[65] M. Rohmer, J. Devemy, R. Wiest, M. Benard, *J. Am. Chem. Soc.* **1996**, 13007-13014.

[66] P. Song, W. Guan, L. Yan, C. Liu, Z. Su, *Dalton Trans.* **2010**, 3706-3713.

[67] A. Müller, F. Peters, M. Pope, D. Gatteschi, *Chem. Rev.* **1998**, 239-271.

[68] B. Botar, P. Kogerler, A. Müller, R. Garcia-Serres, C. Hill, *Chem. Commun.* **2005**, 5621-5623; A. Todea, A. Merca, H. Bögge, T. Glaser, J. Pigga, M. Langston, T. Liu, R. Prozorov, M. Luban, C. Schroder, W. Casey, A. Müller, *Angew. Chem. Int. Ed.* **2010**, 514-519; A. Müller, A. Todea, H. Bögge, J. van Slageren, M. Dressel, A. Stammler, M. Rusu, *Chem. Commun.* **2006**, 3066-3068; A. Müller, A. Todea, J. van Slageren, M. Dressel, H. Bögge, M. Schmidtmann, M. Luban, L. Engelhardt, M. Rusu, *Angew. Chem. Int. Ed.* **2005**, *44*, 3857-3861.

[69] A. Müller, M. Luban, C. Schröder, R. Modler, P. Kögerler, M. Axenovich, J. Schnack, P. Canfield, S. Bud'ko, N. Harrison, *Chemphyschem* **2001**, 517-521.

[70] H. Zhang, Y. Li, Y. Lu, R. Clerac, Z. Zhang, Q. Wu, X. Feng, E. Wang, *Inorg. Chem.* **2009**, 10889-10891.

[71] A. Barra, D. Gatteschi, L. Pardi, A. Müller, J. Döring, *J. Am. Chem. Soc.* **1992**, 8509-8514.

[72] A. Müller, R. Sessoli, E. Krickemeyer, H. Bögge, J. Meyer, D. Gatteschi, L. Pardi, J. Westphal, K. Hovemeier, R. Rohlfing, J. Döring, F. Hellweg, C. Beugholt, M. Schmidtmann, *Inorg. Chem.* **1997**, *36*, 5239-5250.

[73] D. Gatteschi, L. Pardi, A. Barra, A. Müller, J. Döring, *Nature* **1991**, 463-465.

[74] W. Plass, *Angew. Chem. Int. Ed.* **1996**, 627-631.

[75] A. Rodriguez-Fortea, P. Alemany, S. Alvarez, E. Ruiz, *Eur. J. Inorg. Chem.* **2004**, 143-153.

[76] S. Khanra, L. Batchelor, M. Helliwell, F. Tuna, E. McInnes, R. Winpenny, *J. Mol. Struct.* **2008**, *890*, 157-162.

[77] S. Castro, Z. Sun, C. Grant, J. Bollinger, D. Hendrickson, G. Christou, *J. Am. Chem. Soc.* **1998**, 2365-2375.

[78] T. Yamase, *J. Mater. Chem.* **2005**, *15*, 4773-4782.

[79] B. Hasenknopf, *Front. Biosci.* **2005**, 275-287.

[80] A. Evangelou, *Crit. Rev. Oncol. Hemat.* **2002**, 249-265.

[81] D. Rehder, J. Pessoa, C. Geraldes, M. Castro, T. Kabanos, T. Kiss, B. Meier, G. Micera, L. Pettersson, M. Rangel, A. Salifoglou, I. Turel, D. Wang, *J. Biol. Inorg. Chem.* **2002**, 384-396.

[82] Z. Zhang, C. Huang, J. Li, S. Leonard, R. Lanciotti, L. Butterworth, X. Shi, *Arch. BioChem. Biophys.* **2001**, 311-320.

[83] C. Huang, Z. Zhang, M. Ding, J. Li, J. Ye, S. Leonard, H. Shen, L. Butterworth, Y. Lu, M. Costa, Y. Rojanasakul, V. Castranova, V. Vallyathan, X. Shin, *J. Biol. Chem.* **2000**, 32516-32522.

[84] K. Wozniak, J. Blasiak, *Arch. Toxicol.* **2004**, 7-15.

[85] N. C. Lloyd, H. W. M. Morgan, B. K. Nicholson, R. S. Ronimus, *J. Organomet. Chem.* **2008**, *693*, 2443-2450.

[86] G. O. Doak, L. D. Freedman, *Organometallic Compounds of Arsenic, Antimony and Bismuth*, Interscience, **1970**.

[87] S. C. Wallwork, *Acta. Cryst.* **1962**, *15*, 758-759.

[88] G. Socrates, *Infrared and Raman Characteristic Group Frequencies: Tables and Charts* 3rd ed., WileyBlackwell, Chichester, **2004**.

[89] K. Nakamoto, *Infrared and Raman spectra of Inorganic and coordination compounds. Part B, Applications in coordination, organometallic, and bioinorganic chemistry*, 5th ed., John Wiley, New York ; Chichester, **1997**.

[90] A. L. Spek, *J. Appl. Cryst.* **2003**, *36*, 7-13.

[91] Z. K. Wang, J. M. Heising, A. Clearfield, *J. Am. Chem. Soc.* **2003**, *125*, 10375-10383.

[92] A. K. Bhattachary, G. Thyarajon, *Chem. Rev.* **1981**, *81*, 415-430.

[93] Y. Qiang, S. Levchik, *Tetrahedron Lett.* **2006**, *47*, 277-281.

[94] V.V. Guiliants, J. B. Benziger, S. Sundaresan, *Chem. Mater.* **1995**, *7*, 1493-1498.

[95] J. H. Van Vleck, *The theory of electric and magnetic susceptibilities*, Oxford U.P, **1965**.

[96] K. Kambe, *J. Phys. Soc. Jpn.* **1950**, 48-51.

[97] J. Hall, W. Estes, E. Estes, R. Scaringe, W. Hatfield, *Inorg. Chem.* **1977**, 1572-1574.

[98] B. Bleaney, K. Bowers, *Proc. R. Soc. A.* **1952**, 451-465.

[99] A. Müller, M. Penk, J. Döring, *Inorg. Chem.* **1991**, *30*, 4935-4939.

[100] P. M. Foster, A. R. Burbank, C. Livage, G. Férey, A. K. Cheetham, *Chem. Commun.* **2004**, 368-369.

[101] T. Barton, L. Bull, W. Klemperer, D. Loy, B. McEnaney, M. Misono, P. Monson, G. Pez, G. Scherer, J. Vartuli, O. Yaghi, *Chem. Mat.* **1999**, *11*, 2633-2656; M. O'Keeffe, M. Eddaoudi, H. L. Li, T. Reineke, O. M. Yaghi, *J. Solid State Chem.* **2000**, *152*, 3-20.

[102] G. Huan, V. W. Day, A. J. Jacobson, D. P. Goshorn, *J. Am. Chem. Soc.* **1991**, *113*, 3188-3189.

[103] A. Müller, J. Döring, H. Bögge, *J. Chem. Soc. Chem. Commun.* **1991**, 273-274.

[104] H. I. Karunadasa, C. J. Chang, J. R. Long, *Nature* **2010**, *464*, 1329-1333.

[105] Bruker, SMART, Data collection program for the solution of crystal structures, Bruker AXS Inc., Madison, Wisconsin (USA), **2007**.

[106] Bruker, SAINT-Plus, Integration program for the solution of crystal structures, Bruker AXS Inc., Madison, Wisconsin (USA), **2007**.

[107] Bruker, SADAS, Absorption correction program for the solution of crystal structures, Bruker AXS Inc., Madison, Wisconsin (USA), **2001**.

[108] Sheldrick, G. M. *Acta Cryst.* **2008**, *A64*, 112-122.

[109] R. G. Harvey, E. R. Desombre, E. V. Jensen, *Tetrahedron,* **1966**, *22*, 1625-1640.

[110] R. J. Cooper, P. J. Camp, R. J. Gordon, D. K. Henderson, D. C. R. Henry, H. McNab, S. S. De Silva, D. Tackley, P. A. Tasker, P. Wightb, *Dalton Trans.*, **2006**, 2785-2793.

Appendix

Supplementary Information

Contents

v) A mass spectrum of **10** in water

vi) An infrared spectrum of **11** measured between 600 cm^{-1} and 4000 cm^{-1}

vii) An infrared spectrum of **11a** measured between 600 cm^{-1} and 4000 cm^{-1}

viii) An infrared spectrum comparing **11** with **11a**

ix) The full range of the mass spectra of **11** recorded in an aqueous solution

x) Control experiments testing the cell viability of the cancer cells lines against the starting materials of **9** and **11**

Appendix 1 – Bond Valence Sum Analysis

The bond sum valence analysis calculations were performed according to the bond valence equation derived by I. D. Brown.

Bond valences, S, are calculated from the bond lengths, R, using the function:

$$S = exp^{\left(\frac{(Ro-R)}{B}\right)}$$

where Ro is the predetermined bond valence value and B is the slope of the correlation curve (normally found to be 0.37 Å for all bonds).

Theory and Restrictions

The valence of a bond, *S*, is a quantity whose sum around each atom is equal to the oxidation state of the atom, *V*: *V*j =Σi*S*ij (1)

It correlates inversely with bond length, which allows the bond valence to be calculated if the bond length has been measured. Newly determined crystal structures can therefore be checked by comparing oxidation states (formal ionic charges) with bond valence sums.

The model is restricted to compounds which can, in a formal sense, be described as ionic, *i.e.* all atoms can be labelled as anions or cations in such a way that the compound contains no cation-cation or anion-anion bonds. It thus applies to most salts, minerals and ceramic compounds as well as to many of the environments of metal atoms in coordination complexes and metal ions in organic salts. The method cannot normally be used for metallic solids or organic molecules.

'Valence' program

A simple DOS program named 'Valence' developed by I. D. Brown was used within this thesis to calculate the total bond valence for each ion.

The 'Valence' software is deposited at the CCP14 website and is available either by downloading (free) or by contacting I.D. Brown at **idbrown@mcmaster.ca** or I.D. Brown Homepage at: http://www.physics.mcmaster.ca/people/faculty/Brown_ID.html

Appendix 2 – Additional experimental information for chapter 2

i) An infrared spectrum of **1** measured between 600 cm^{-1} and 4000 cm^{-1}

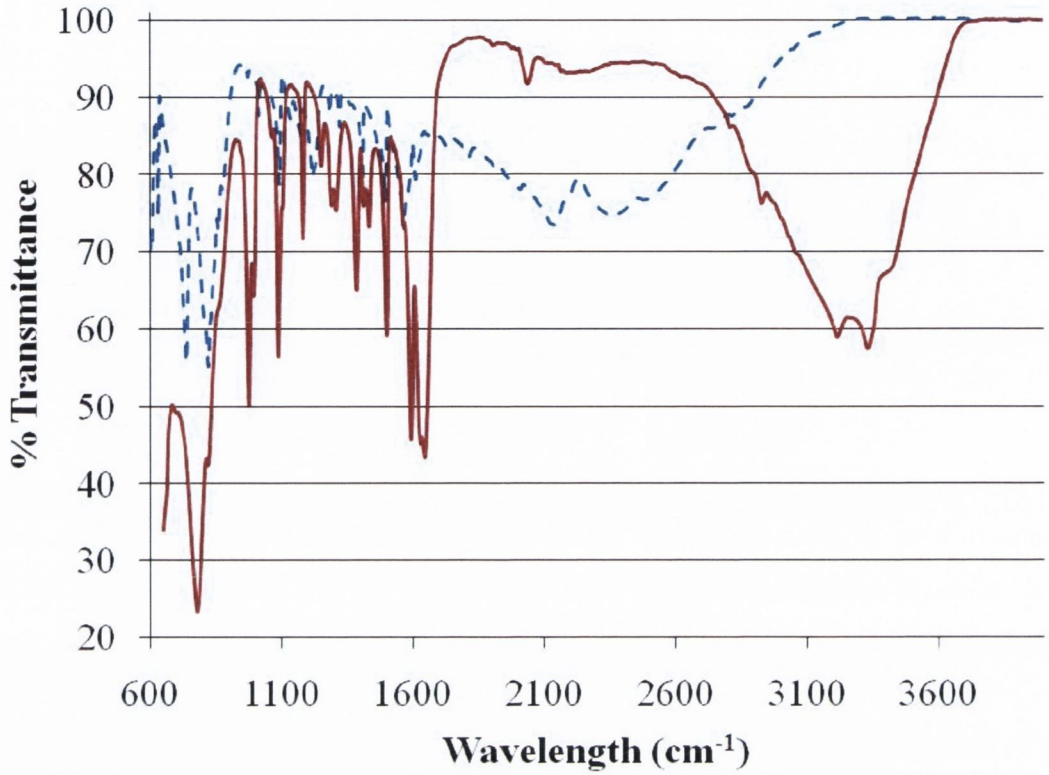

ii) The full range measured for the mass spectrum of **1** in DMSO

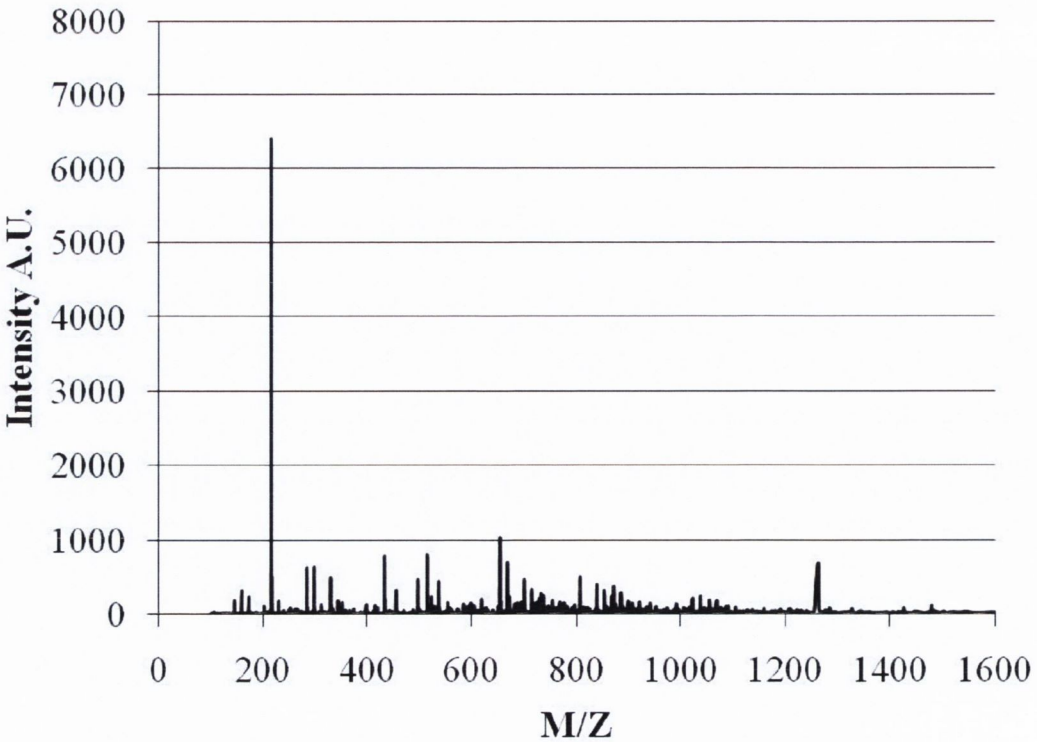

iii) Modelling of the mass spectra signal of the anionic signal of **1**

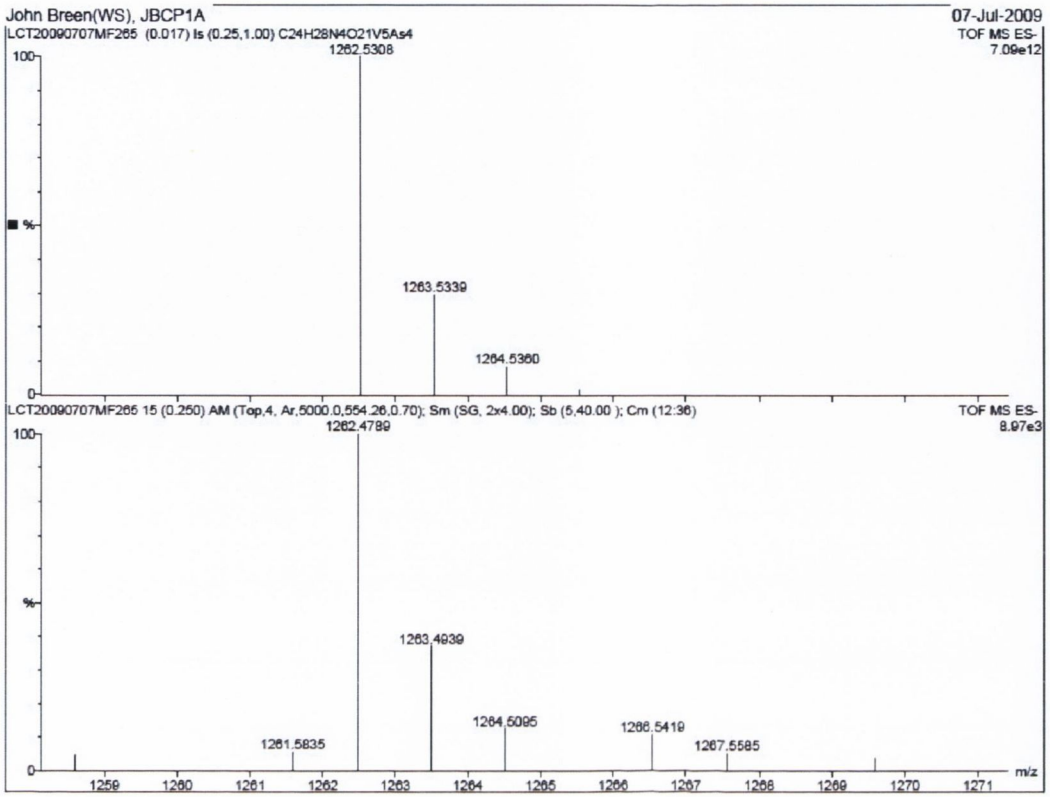

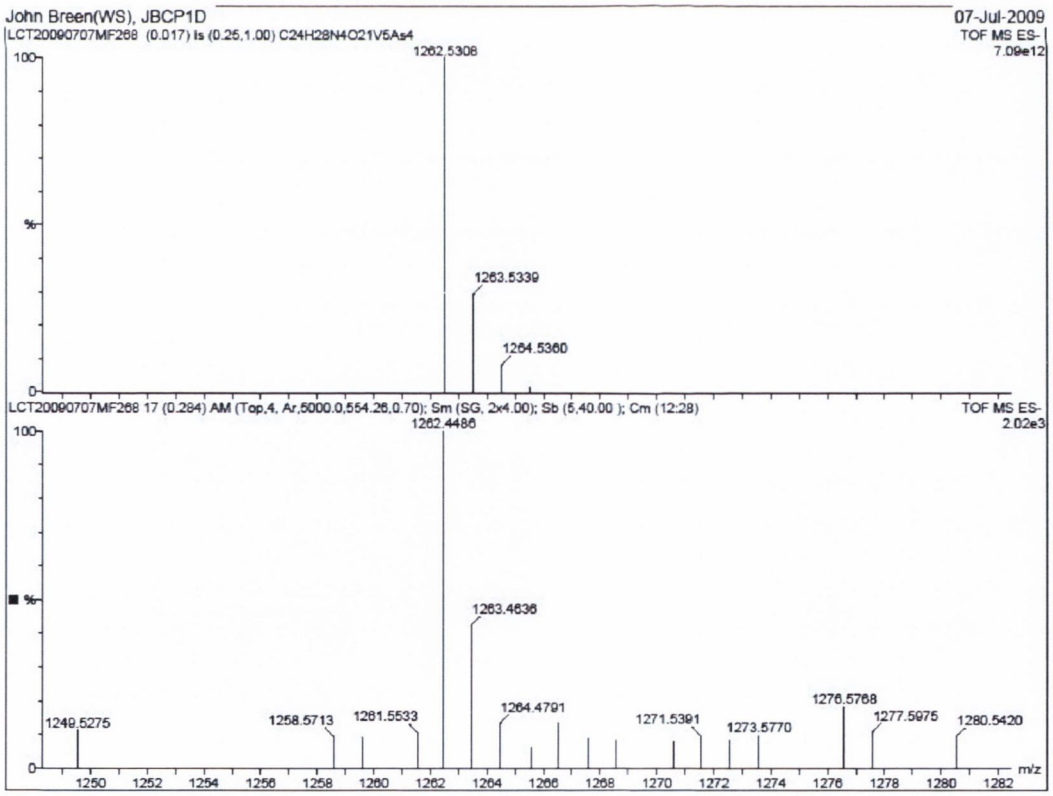

iv) NMR of **1** in deuterated DMSO

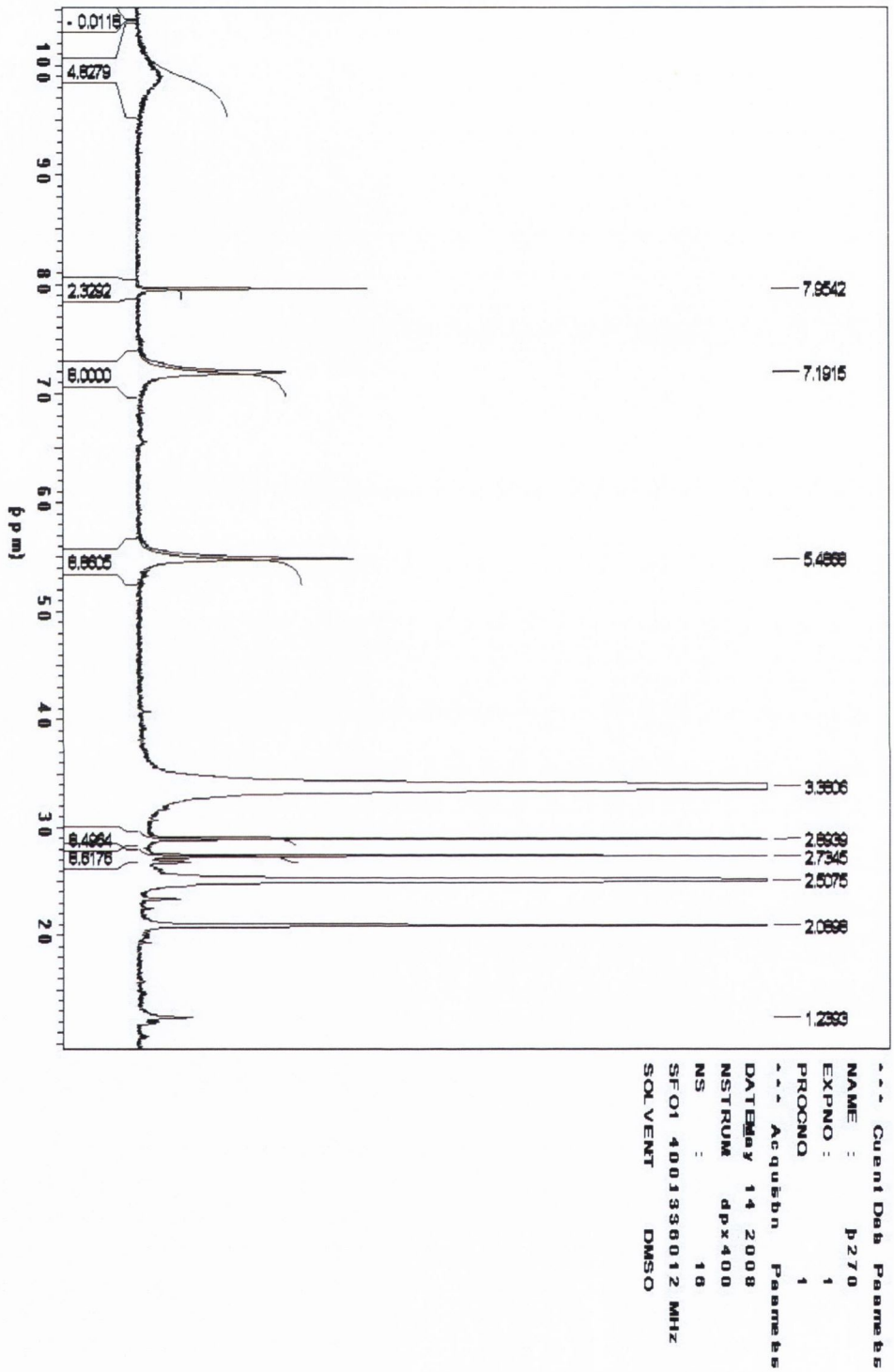

v) An infrared spetrum of **2** recorded between 600 cm^{-1} and 4000 cm^{-1}

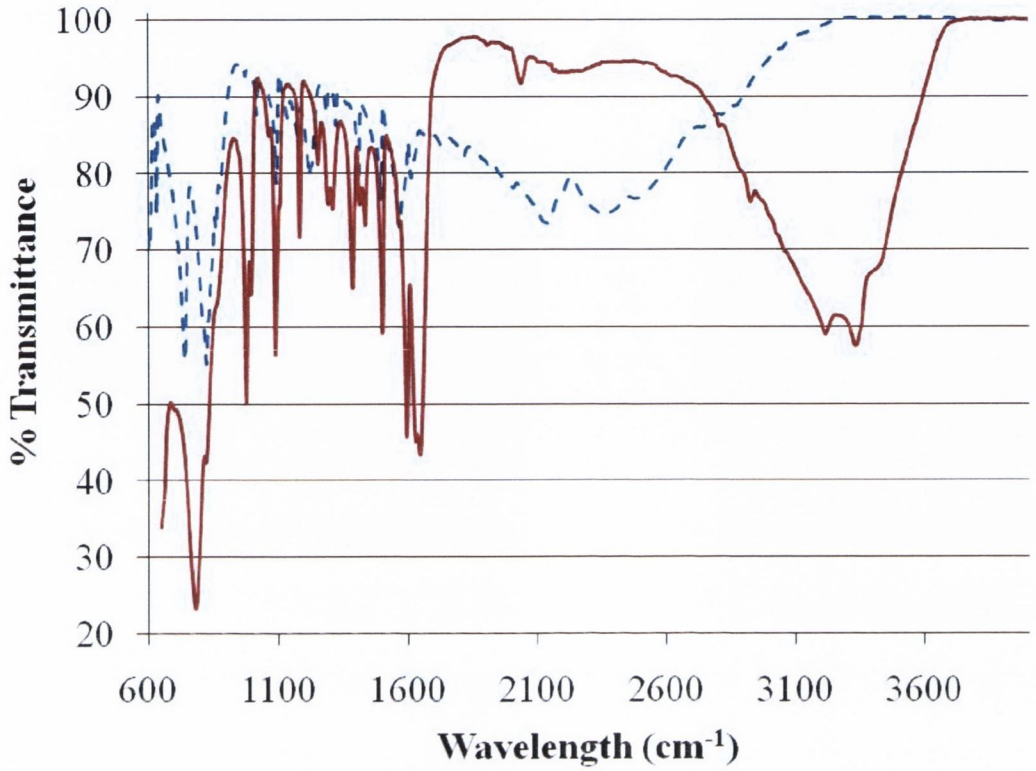

vi) UV-vis spectrum of **3** dissolved in water (1mM)

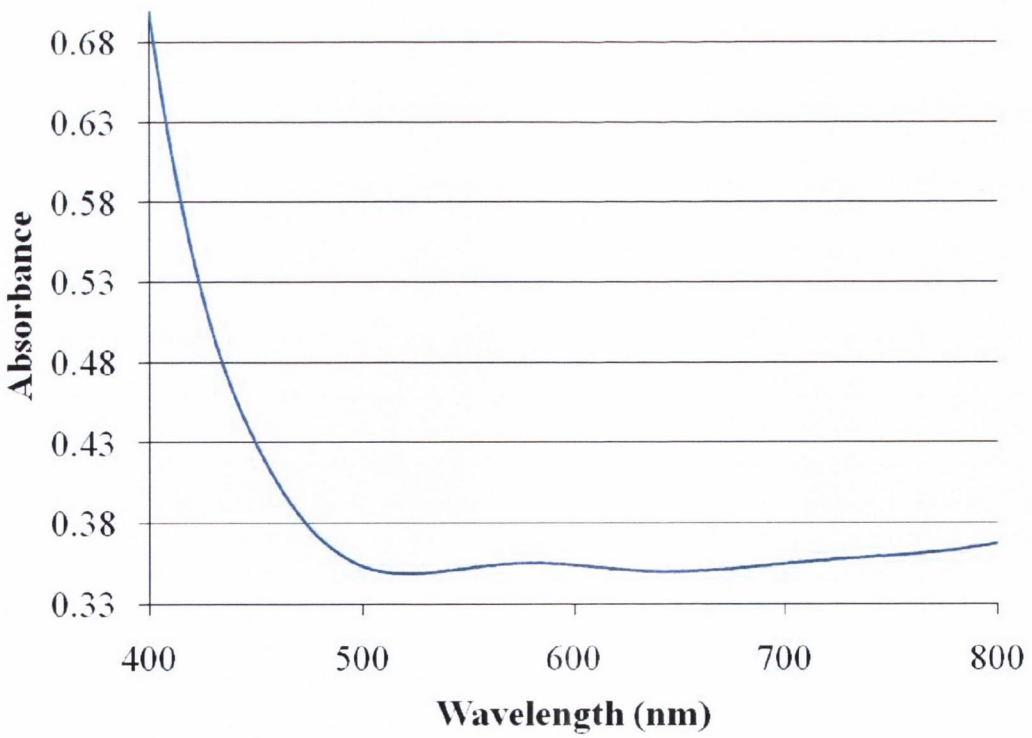

vii) Mass spectrum of **3** dissolved in DMSO

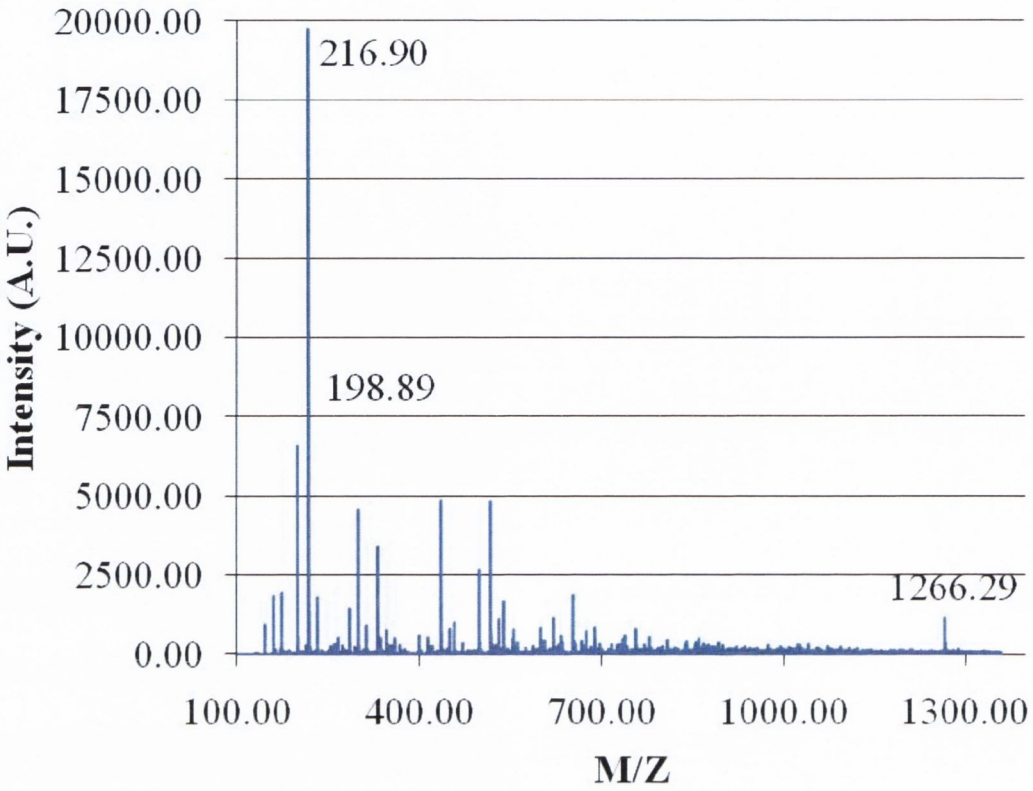

viii) Modelling of the mass spectra signal of the anionic cluster of **3** in DMSO

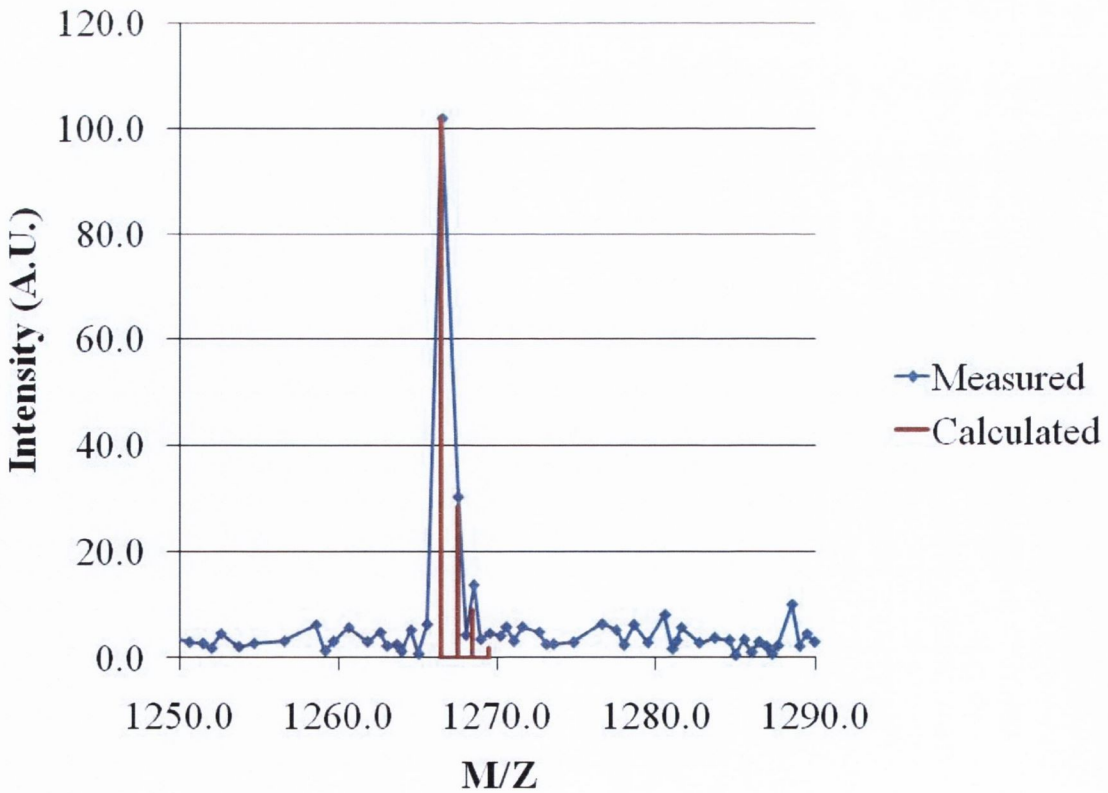

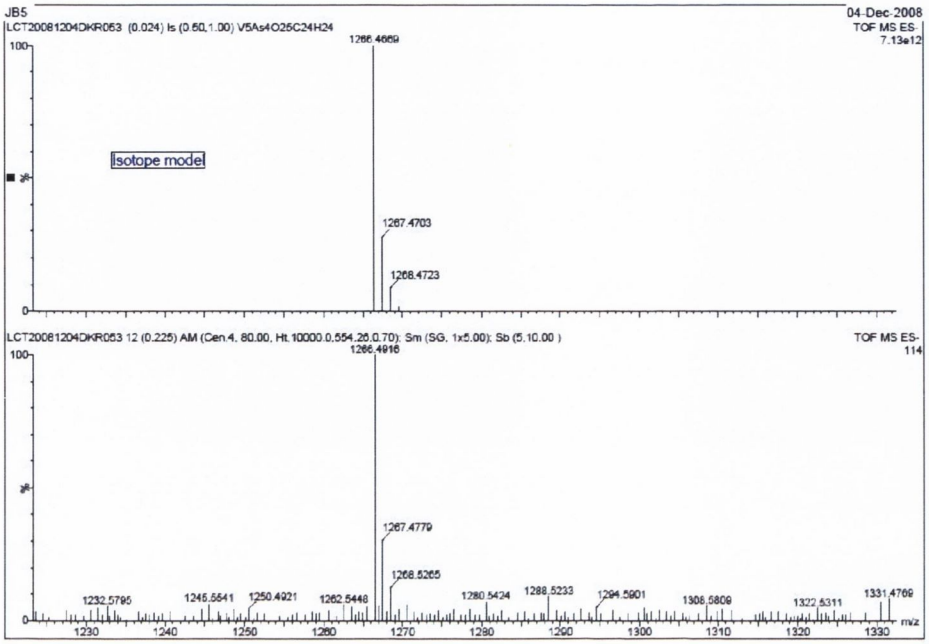
JB5
04-Dec-2008
LCT20081204DKR053 (0.024) Is (0.50,1.00) V5As4O25C24H24
TOF MS ES-
7.13e12
1266.4669
Isotope model
1267.4703
1268.4723
LCT20081204DKR053 12 (0.225) AM (Cen,4, 80.00, Ht,10000.0,554,26.0,70); Sm (SG, 1x5.00); Sb (5,10.00)
TOF MS ES-
1266.4916
1267.4779
1268.5265
1232.5795
1245.5541
1250.4921
1262.5448
1280.5424
1288.5233
1294.5901
1308.5809
1322.5311
1331.4769
m/z

ix) BET surface area analysis plot of **4**

-BET surface area analysis

The Brunauer-Emmett-Teller (BET) method is the most widely used procedure for the determination of the surface area of solid materials and involves the use of the BET equation.

$$\frac{1}{W\left(\left(\frac{Po}{P}\right)-1\right)} = \frac{1}{WmC} + \frac{C-1}{WmC}\left(\frac{P}{Po}\right) \qquad (\mathbf{a})$$

in which W is the weight of gas adsorbed at a relative pressure P/Po and Wm is the weight of adsorbate constituting a monolayer of surface coverage. The term C, the BET C constant is related to the energy of adsorption in the first adsorbed layer and consequently its value is an indication of the magnitude of the adsorbent/adsorbate interactions.

The BET equation requires a linear plot of 1/[W(Po/P)-1] vs P/Po which for most solids, using nitrogen as the adsorbate, is restricted to a limited region of the adsorption isotherm, usually in the P/Po range of 0.05 to 0.35. This linear region is shifted to lower relative pressures for microporous materials. The standard multipoint BET procedure requires a minimum of three points in the appropriate relative pressure range. The weight of a monolayer of adsorbate Wm can then be obtained from the slope 's' and intercept 'i' of the BET plot. For equation (**a**)

$$s = \frac{C-1}{WmC} \qquad (\mathbf{b})$$

$$i = \frac{1}{WmC} \qquad (\mathbf{c})$$

Thus, the weight of a monolayer Wm can be obtained by combing equations of (**b**) and (**c**).

$$Wm = \frac{1}{s+i} \qquad (\mathbf{d})$$

The second step in the application of the BET method is the calculation of the surface area. This requires a knowledge of the molecular cross-sectional area Acs of the adsorbate molecule. The total surface are St of the sampe can be expressed as:

$$St = \frac{Wm\ N\ Acs}{M} \qquad (\mathbf{e})$$

Where N is Avogadro's number ($6.023x10^{23}$ molecules/mol) and M is the molecular weight of the adsorbate. Nitrogen was the gas used for the surface area determinations since it exhibits intermediate C values for the C constant (50-250) on most solid surfaces. For the hexagonal close-packed nitrogen monolayer at 77K, the cross-sectional area Acs for nitrogen is 16.2 Å. The specific surface area S of the solid can be calculated from the total surface area St and the sample weight w, according to equation (**f**):

$$S = \frac{St}{W}$$

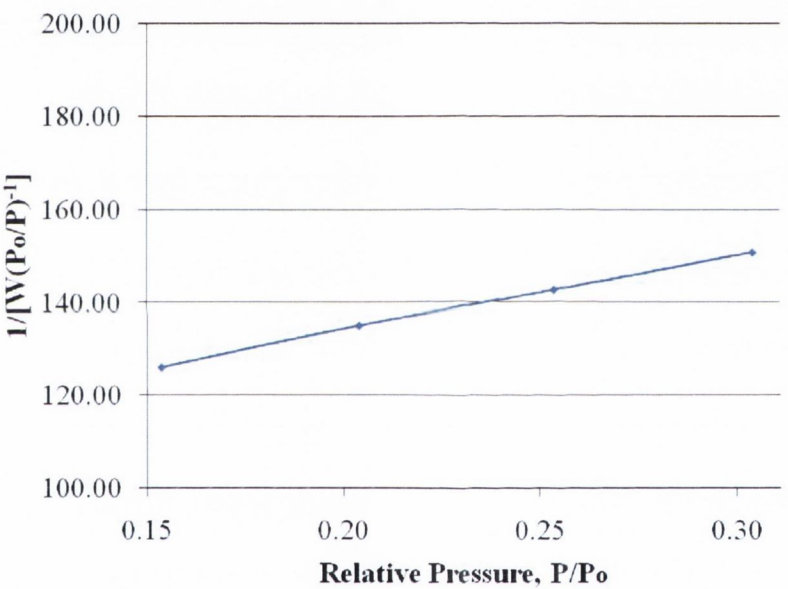

Figure – Surface area analysis of **4**; a linear plot of a multipoint BET used to calculate the surface area for **4** when using nitrogen as the adsorbate. The slope and intercept from the graph were used to calculate the surface area from the Brunanuer-Emmett-Teller method.

centre for microscopy and analysis

Quantachrome NovaWin2 - Data Acquisition and Reduction for NOVA Instruments ©1994-2006, Quantachrome Instruments version 2.2

Quantachrome INSTRUMENTS Optimizing particle performance

Analysis			**Report**		
Operator:	nleddy	**Date:** 2009/11/03	**Operator:**	nleddy	**Date:** 11/6/2009
Sample ID:	26010	**Filename:**	C:\Documents and Settings\Administrator\My Documents\BET\03110		
Sample Desc:	14	**Comment:**	Run 1		
Sample weight:	0.0757 g	**Sample Volume:**	0.02393 cc		
Outgas Time:	24.0 hrs	**OutgasTemp:**	50.0 C		
Analysis gas:	Nitrogen	**Bath Temp:**	77.3 K		
Press. Tolerance:	0.100/0.100 (ads/des)	**Equil time:**	60/60 sec (ads/des)	**Equil timeout:**	240/240 sec (ads/des)
Analysis Time:	180.9 min	**End of run:**	2009/11/03 17:12:12	**Instrument:**	Nova Station B
Cell ID:	32				

Data Reduction Parameters

Adsorbate	Nitrogen	Temperature	77.350K		
	Molec. Wt.: 28.013 g	Cross Section:	16.200 Å²	Liquid Density:	0.808 g/cc

MBET summary

Slope =	203.381
Intercept =	9.134e+01
Correlation coefficient, r =	0.981793
C constant=	3.227
Surface Area =	11.816 m²/g

Multi-Point BET Plot

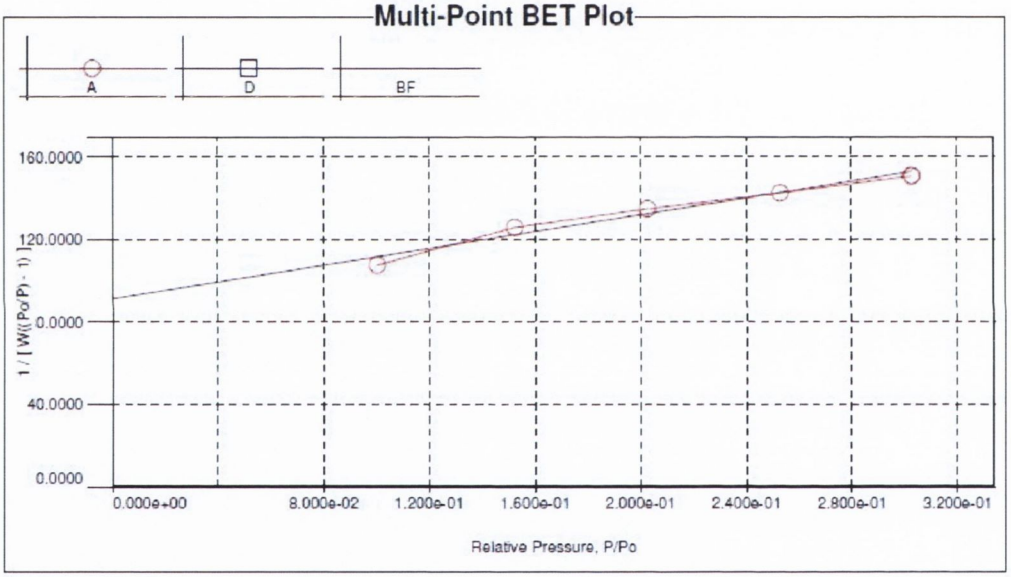

Multi-Point BET

Relative Pressure [P/Po]	Volume@STP [cc/g]	1 / [W((Po/P) - 1)]	Relative Pressure [P/Po]	Volume@STP [cc/g]	1 / [W((Po/P) - 1)]
1.00773e-01	0.8309	1.0791e+02	2.52917e-01	1.8985	1.4267e+02
1.52682e-01	1.1437	1.2606e+02	3.03117e-01	2.3066	1.5088e+02
2.02896e-01	1.5076	1.3509e+02			

centre for microscopy and analysis

Quantachrome NovaWin2 - Data Acquisition and Reduction for NOVA Instruments
©1994-2006, Quantachrome Instruments
version 2.2

Quantachrome INSTRUMENTS
Optimizing particle performance

Analysis
Operator: nleddy **Date:** 2009/11/03
Sample ID: 26010 **Filename:**

Report
Operator: nleddy **Date:** 11/6/2009
C:\Documents and Settings\Administrator\My Documents\BET\031109B32.qps

Single Point Surface Area

Relative Pressure [P/Po]	Volume@STP [cc/g]	1 / [W((P/Po) - 1)]	Slope	Surf. Area [m^2/g]
1.00773e-01	0.8309	1.0791e+02	1070.8290	3.2522
1.52682e-01	1.1437	1.2606e+02	825.6361	4.2180
2.02896e-01	1.5076	1.3509e+02	665.8016	5.2306
2.52917e-01	1.8985	1.4267e+02	564.1128	6.1734
3.03117e-01	2.3066	1.5088e+02	497.7576	6.9964

x) UV-vis spectrum of **4** in DMSO (1mM)

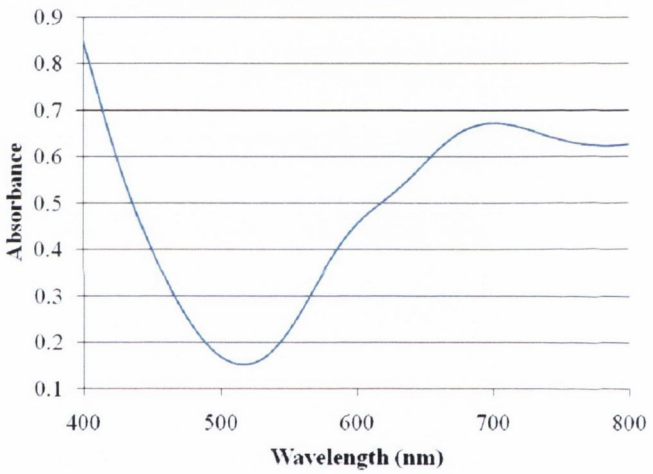

xi) UV-vis spectrum of **4** in water (1mM)

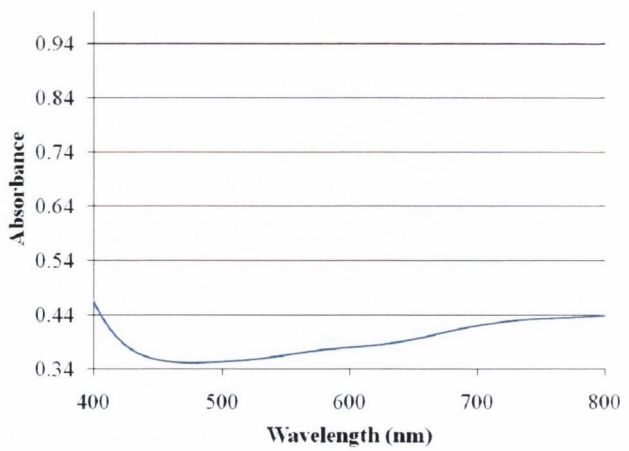

Appendix 3 – Additional experimental information for chapter 3

i) An infrared spectrum of **5** measured between 600 cm^{-1} and 4000 cm^{-1}

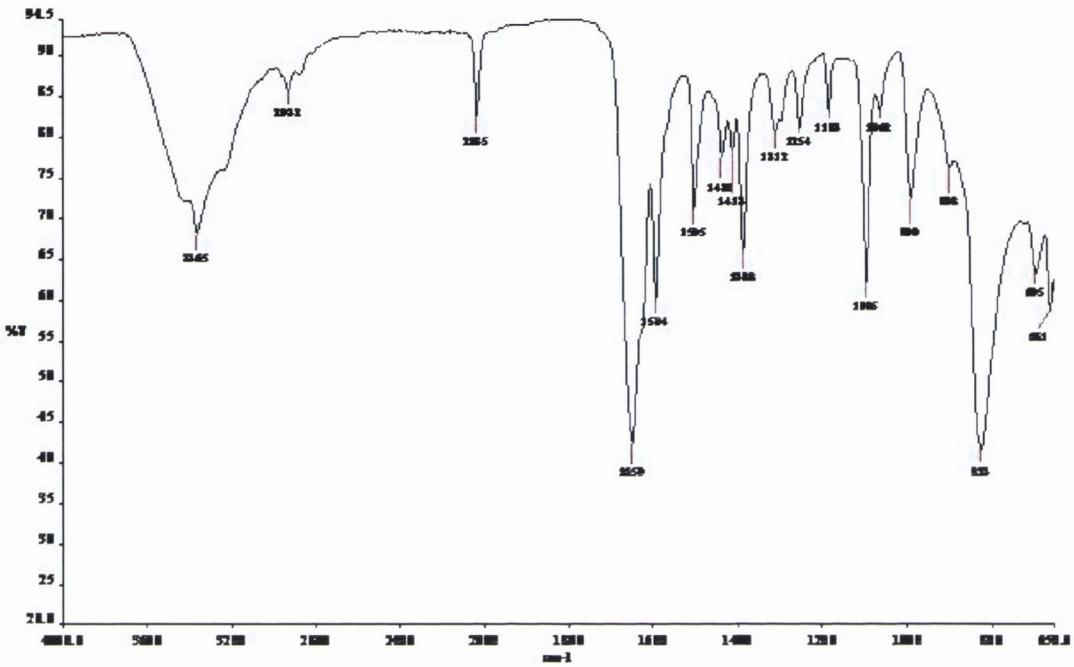

ii) NMR of **5** in deuterated DMSO

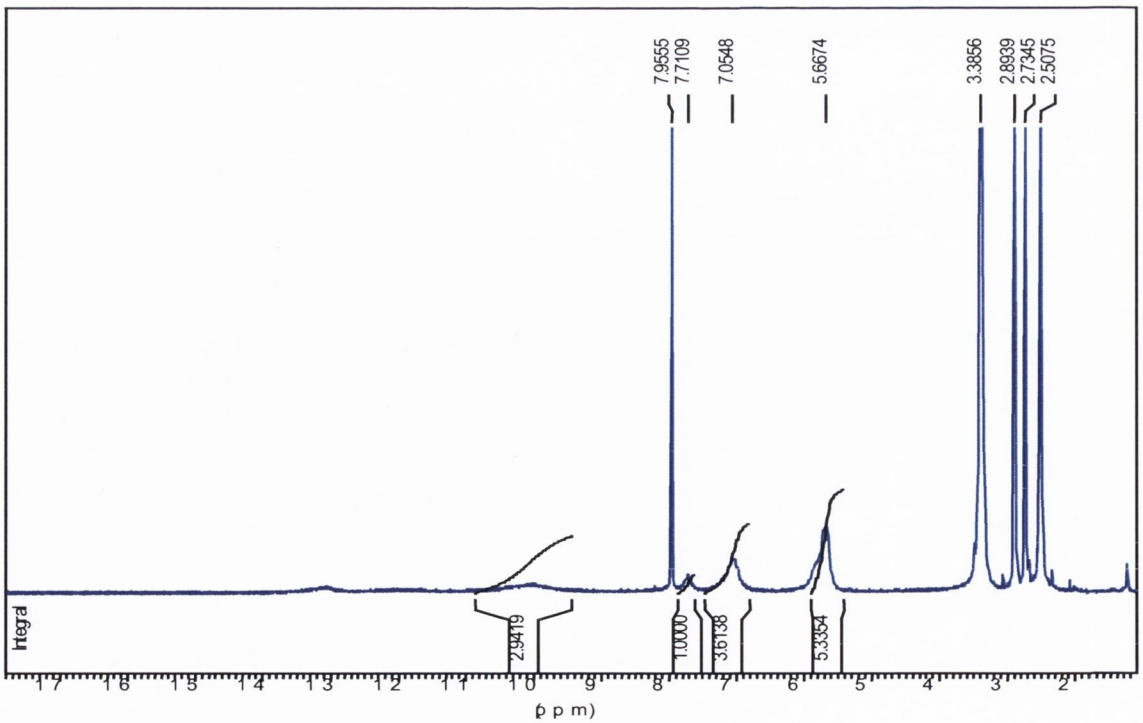

iii) The full range of the mass spectra of **5** in DMSO

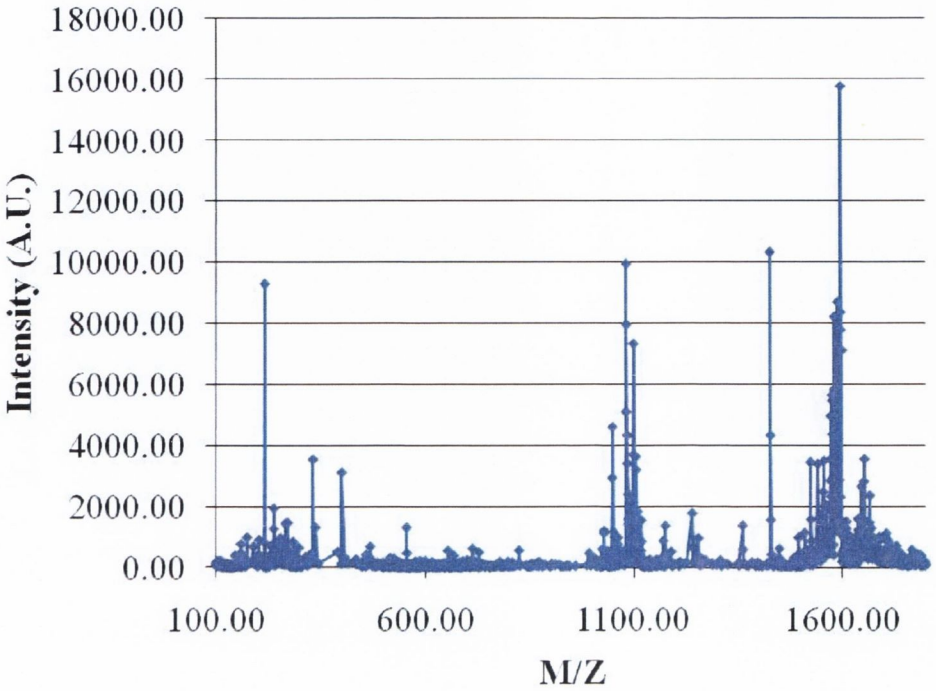

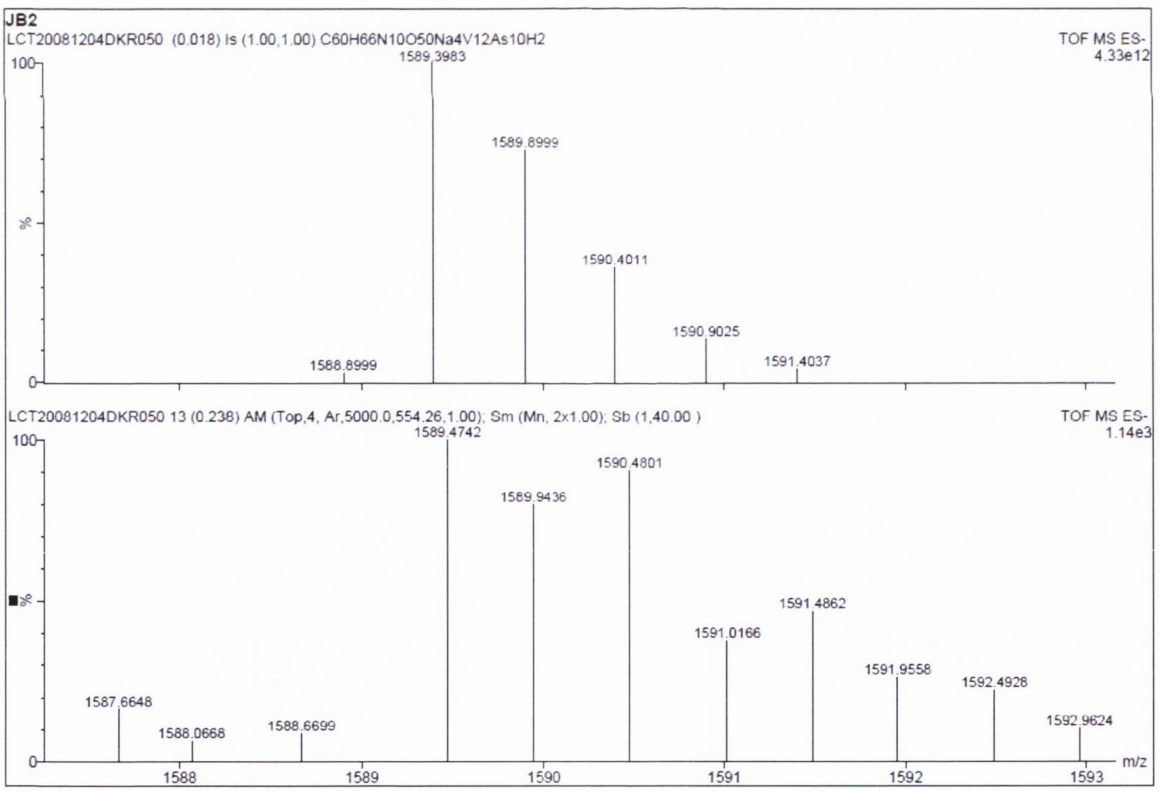

iv) An infrared spectrum of **6** measured between 600 cm^{-1} and 4000 cm^{-1}: **7** (red) and ligand (blue).

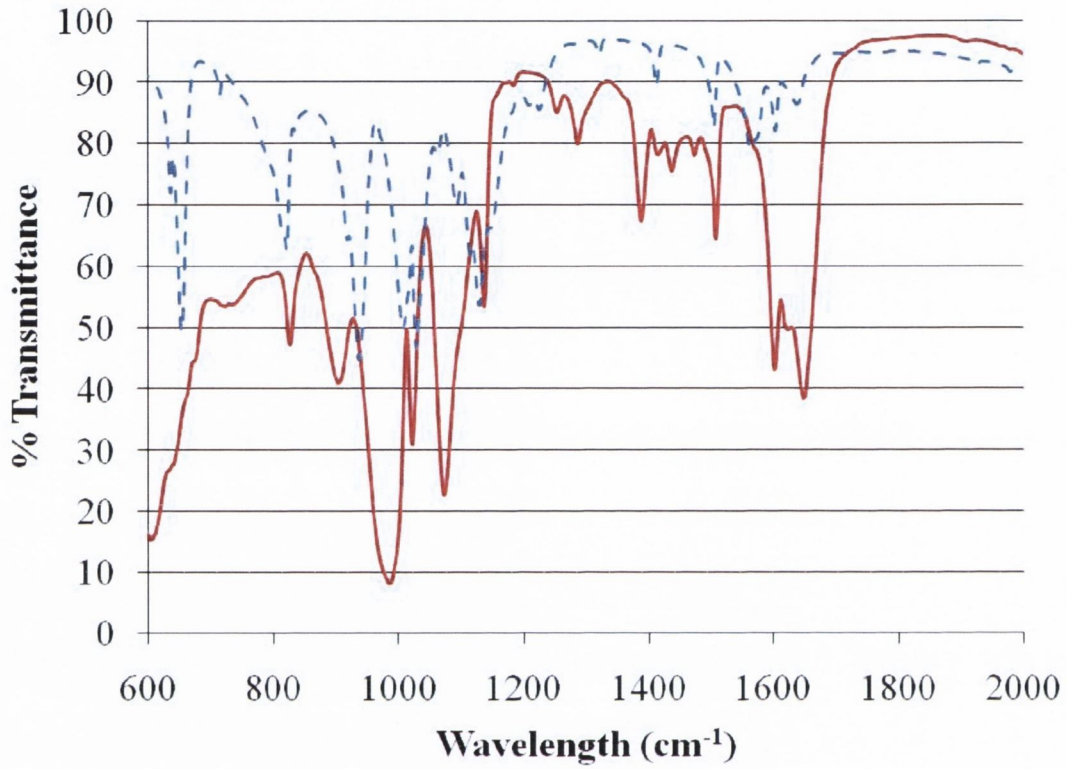

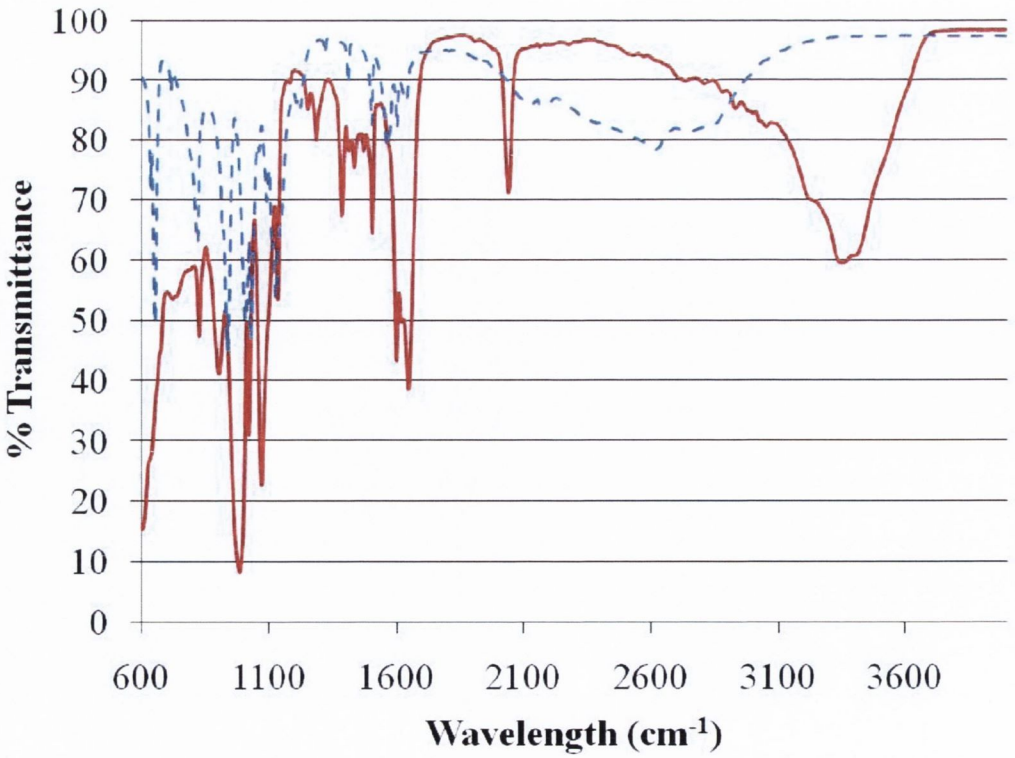

v) An infrared spectrum of **7** measured between 600 cm^{-1} and 4000 cm^{-1}

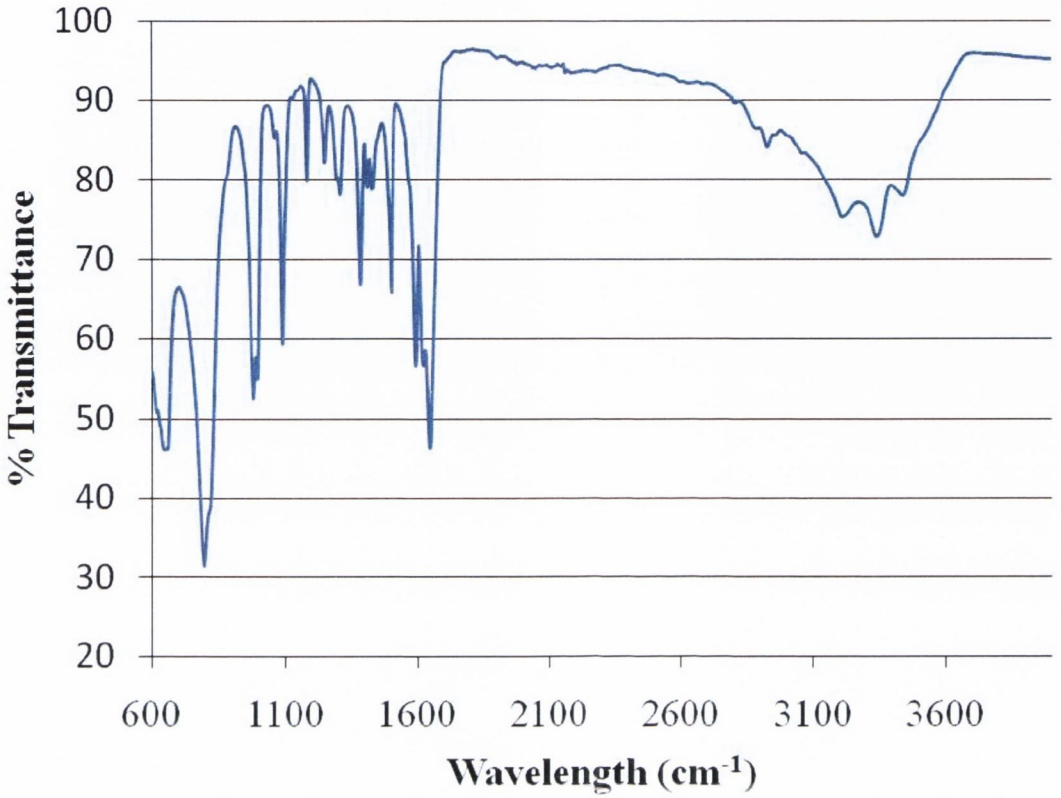

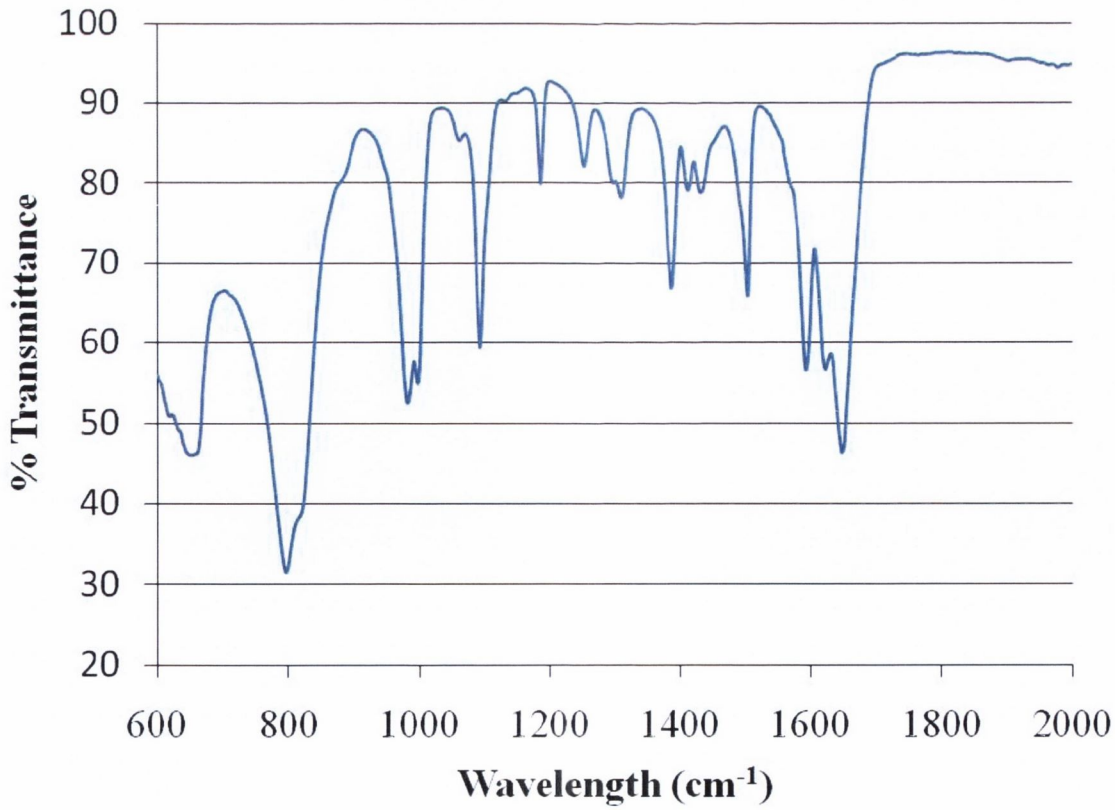

vi) An infrared spectrum of **8** measured between 600 cm^{-1} and 4000 cm^{-1}

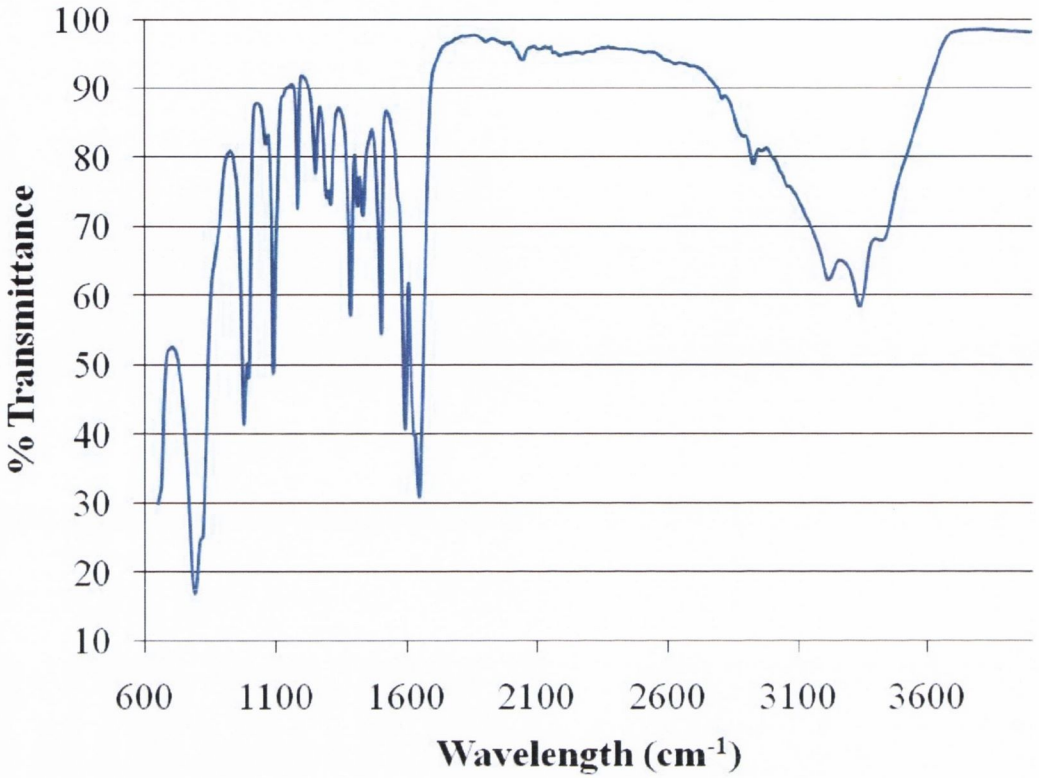

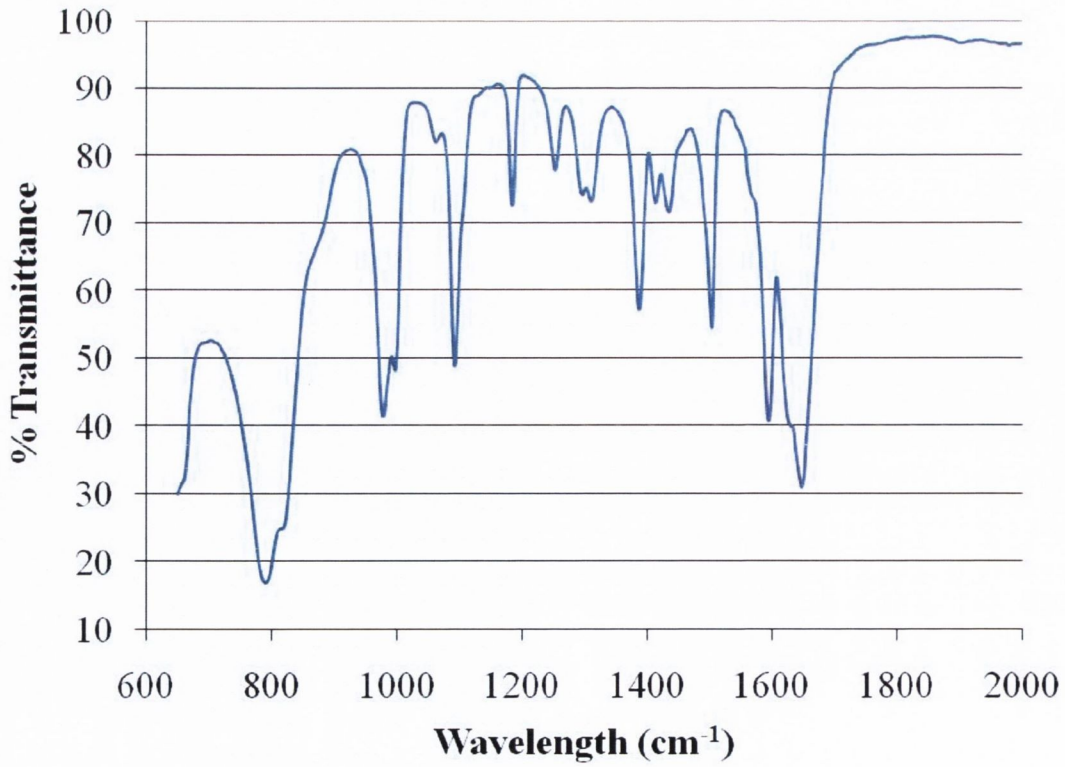

Appendix 4 – Additional experimental information for chapter 4

i) An infrared spectrum of (1,4-phenyl)bisphosphonic acid

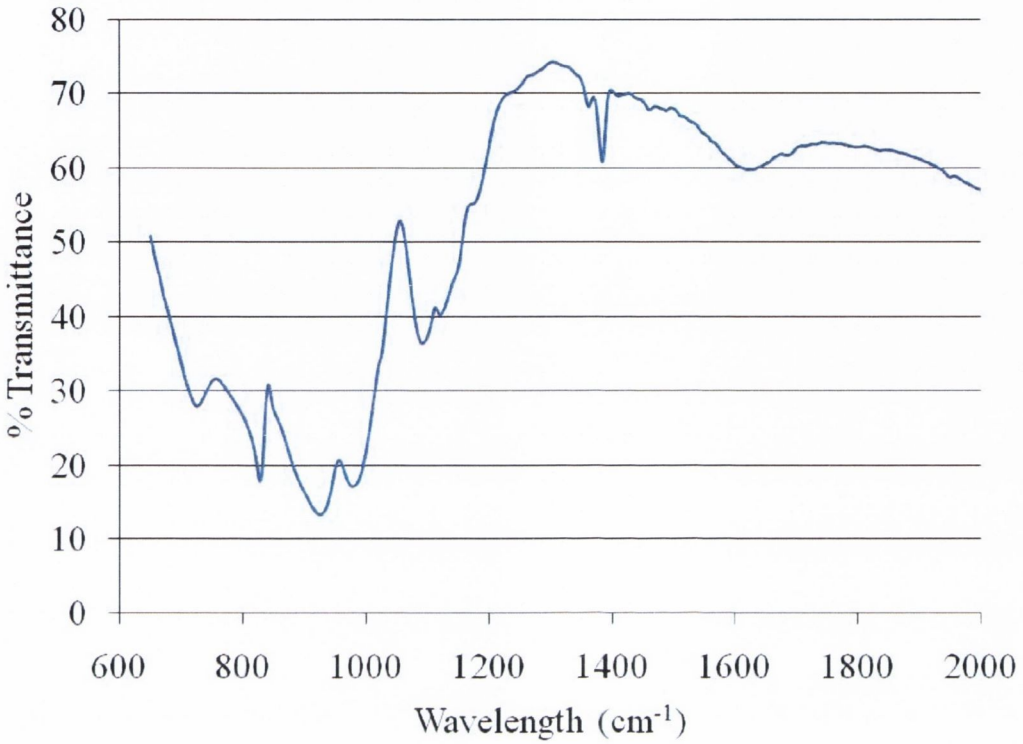

ii) An infrared spectrum of **9** measured between 600 cm^{-1} and 4000 cm^{-1}

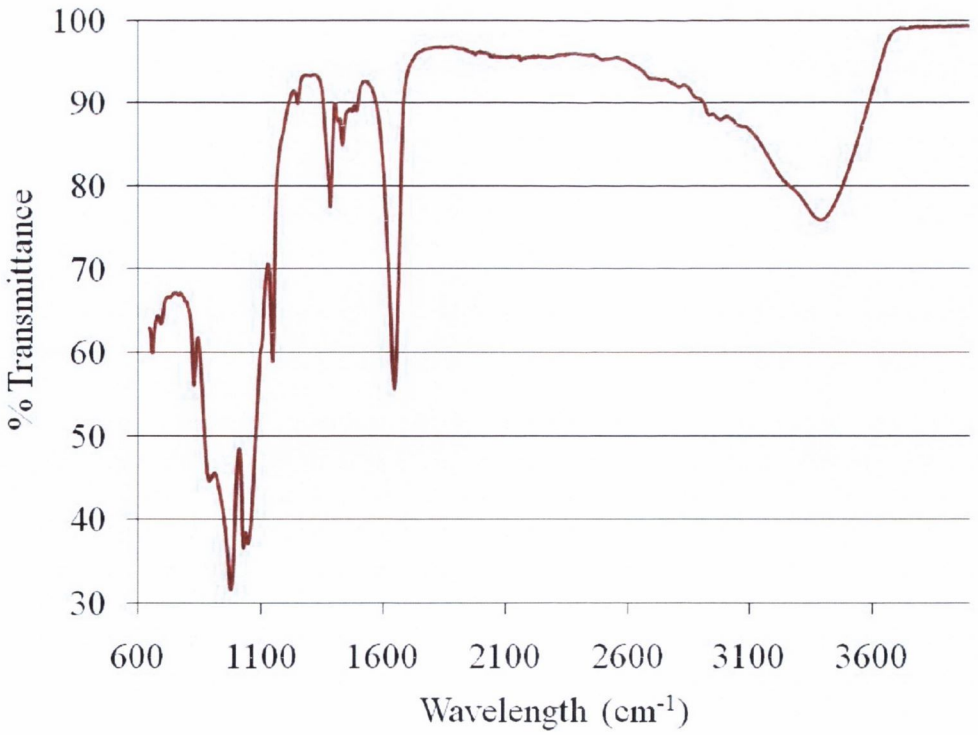

iii) A mass spectrum of **9** recorded in an aqueous solution (JB8 original code name)

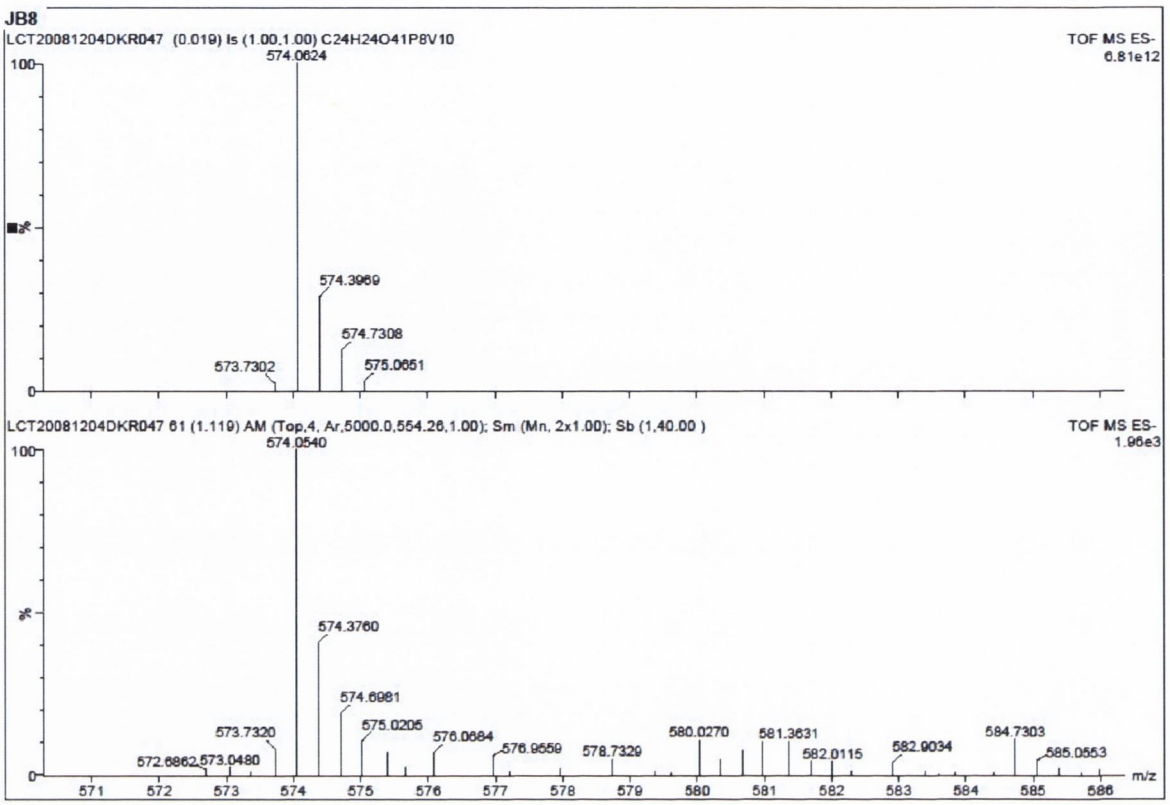

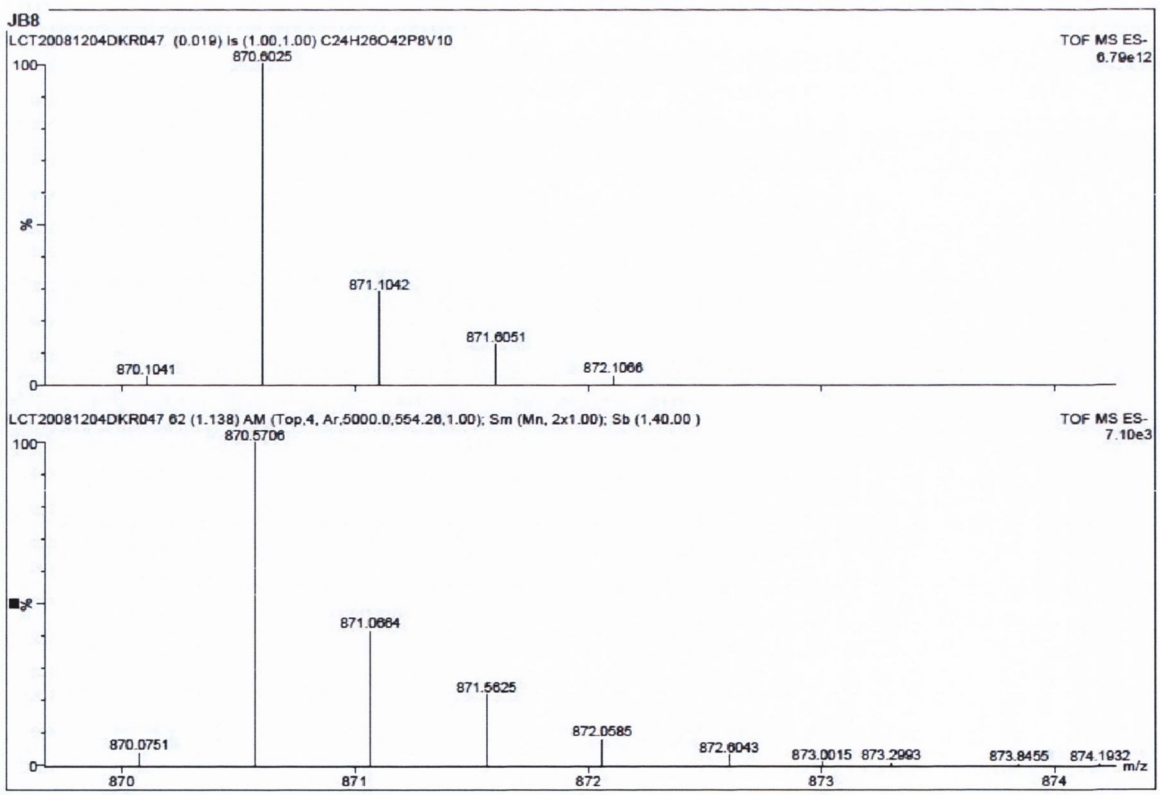

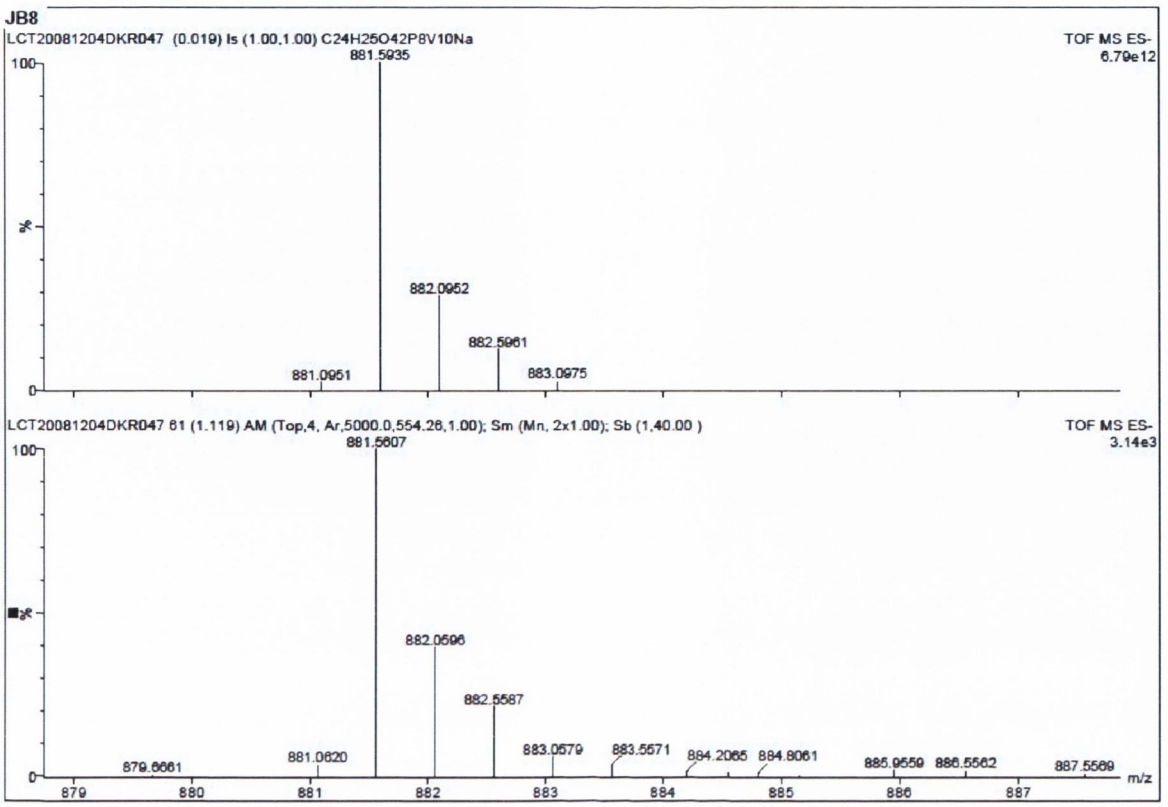
JB8
LCT20081204DKR047 (0.019) Is (1.00,1.00) C24H25O42P8V10Na
TOF MS ES-
6.79e12
881.5935
882.0952
882.5961
881.0951
883.0975
LCT20081204DKR047 61 (1.119) AM (Top,4, Ar,5000.0,554.26,1.00); Sm (Mn, 2x1.00); Sb (1,40.00)
TOF MS ES-
3.14e3
881.5607
882.0596
882.5587
879.6661
881.0620
883.0579
883.5571
884.2065
884.8061
885.9559
886.5562
887.5569
m/z

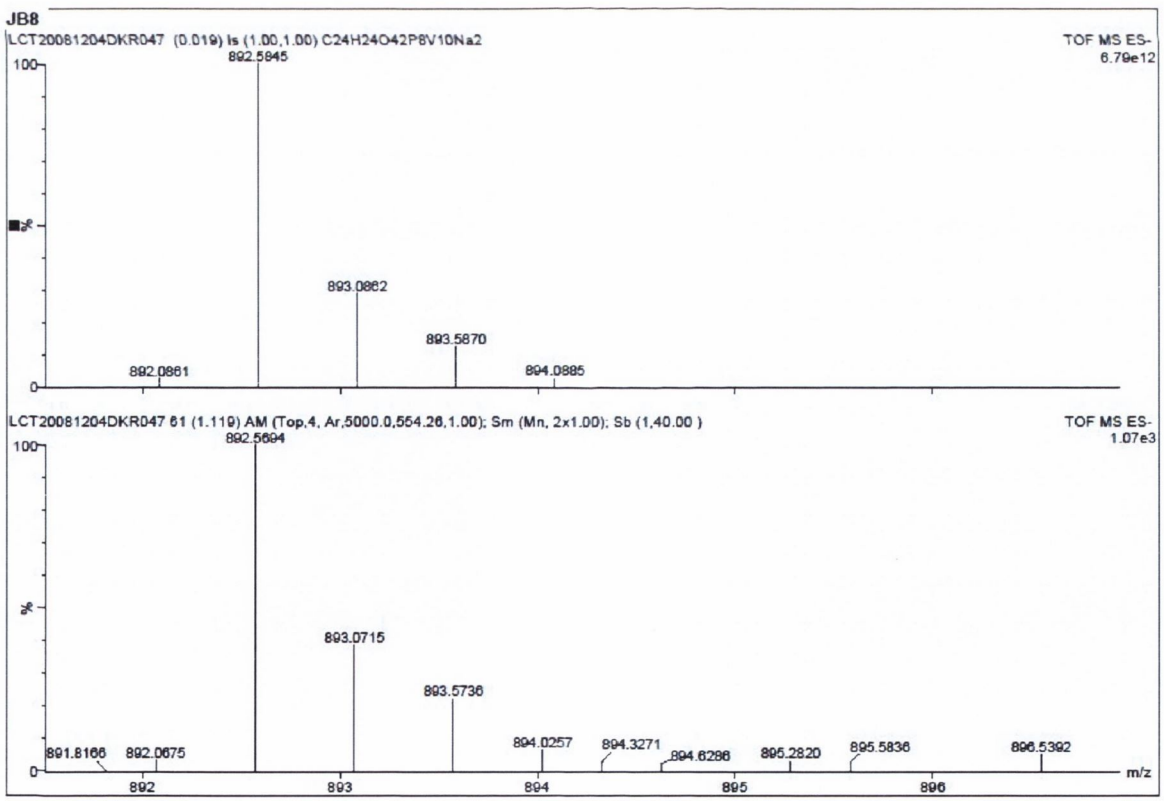
JB8
LCT20081204DKR047 (0.019) Is (1.00,1.00) C24H24O42P8V10Na2
TOF MS ES-
6.79e12
892.5845
893.0862
893.5870
892.0861
894.0885
LCT20081204DKR047 61 (1.119) AM (Top,4, Ar,5000.0,554.26,1.00); Sm (Mn, 2x1.00); Sb (1,40.00)
TOF MS ES-
1.07e3
892.5694
893.0715
893.5736
891.8166
892.0675
894.0257
894.3271
894.6296
895.2820
895.5836
896.5392
m/z

iv) An infrared spectrum of **10** recorded between 600 cm^{-1} and 4000 cm^{-1}

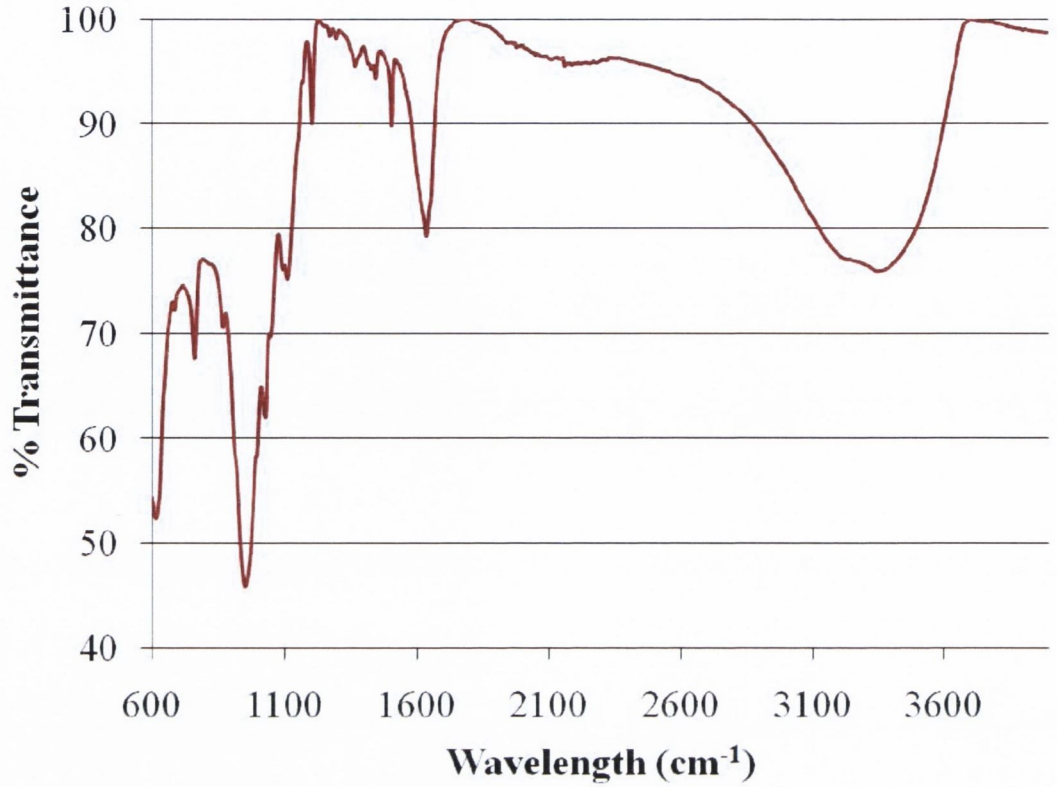

v) A mass spectrum of **10** in water

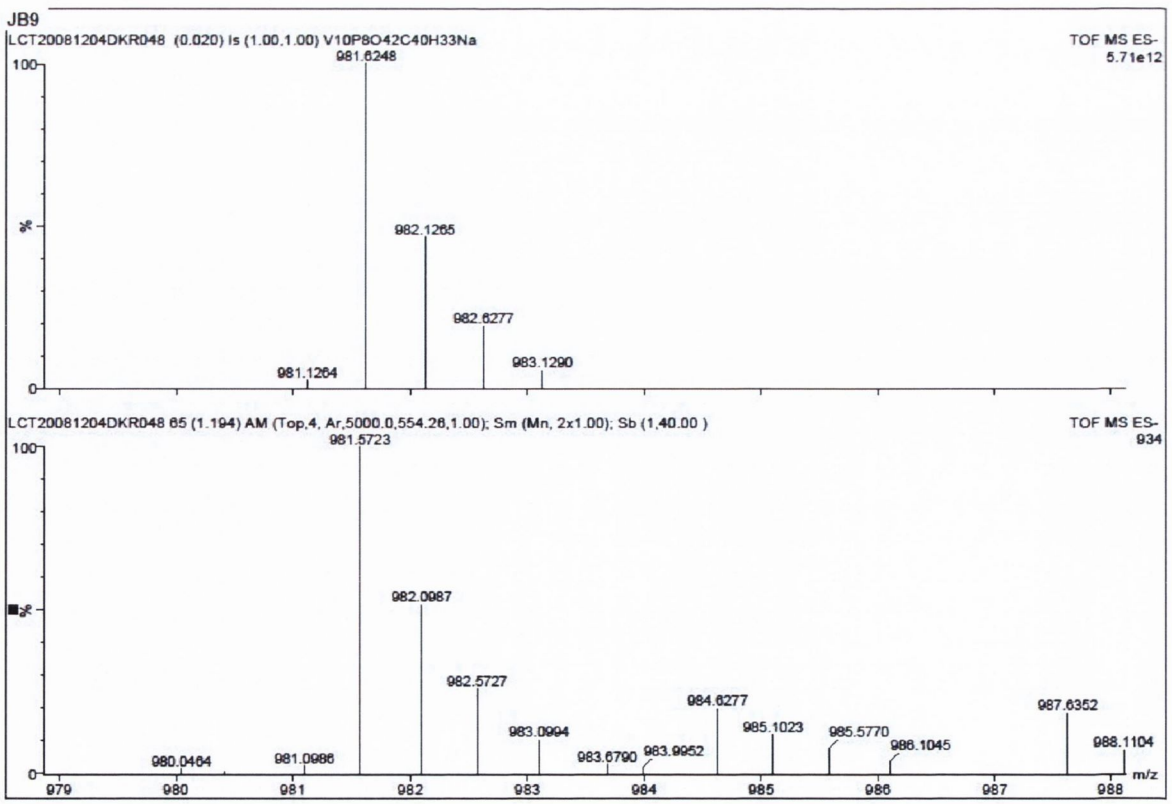

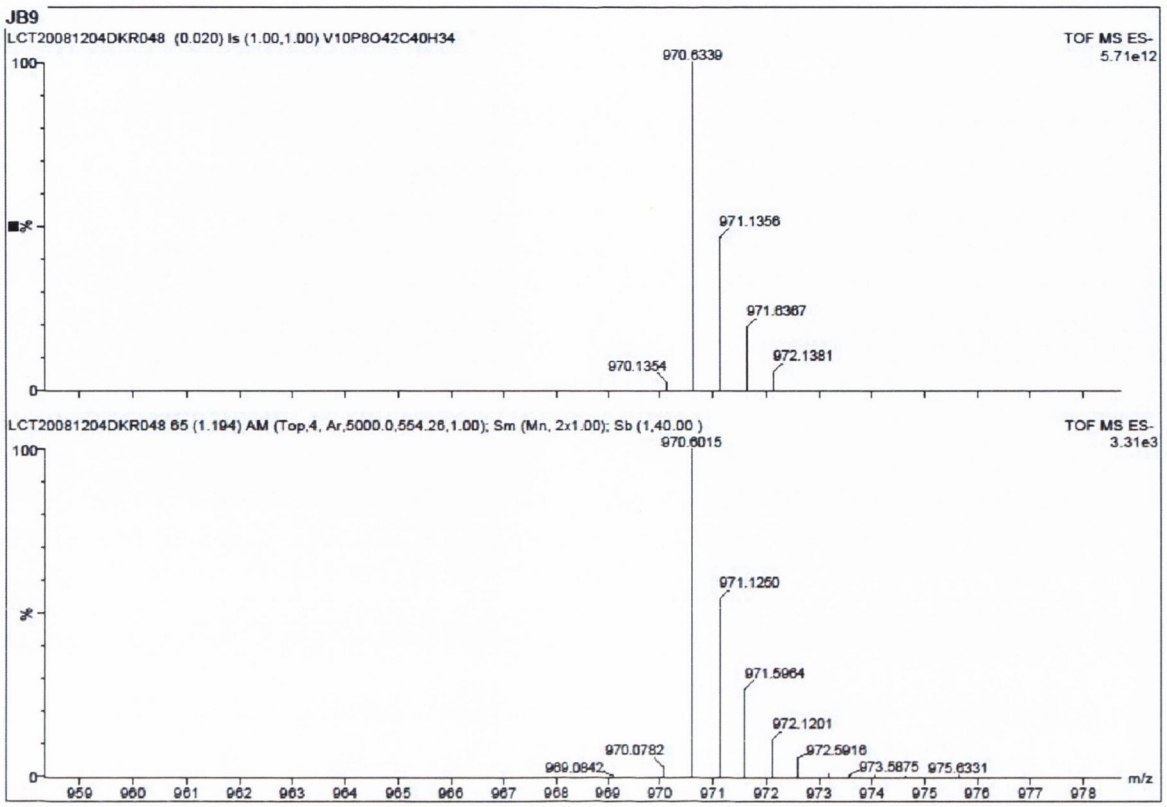
JB9
LCT20081204DKR048 (0.020) Is (1.00,1.00) V10P8O42C40H34
TOF MS ES-
5.71e12
100
%
0
970.6339
971.1356
971.6367
972.1381
970.1354
LCT20081204DKR048 65 (1.194) AM (Top,4, Ar,5000.0,554.26,1.00); Sm (Mn, 2x1.00); Sb (1,40.00)
TOF MS ES-
3.31e3
970.6015
971.1250
971.5864
972.1201
970.0782
972.5916
969.0842
973.5875
975.6331
m/z
959 960 961 962 963 964 965 966 967 968 969 970 971 972 973 974 975 976 977 978

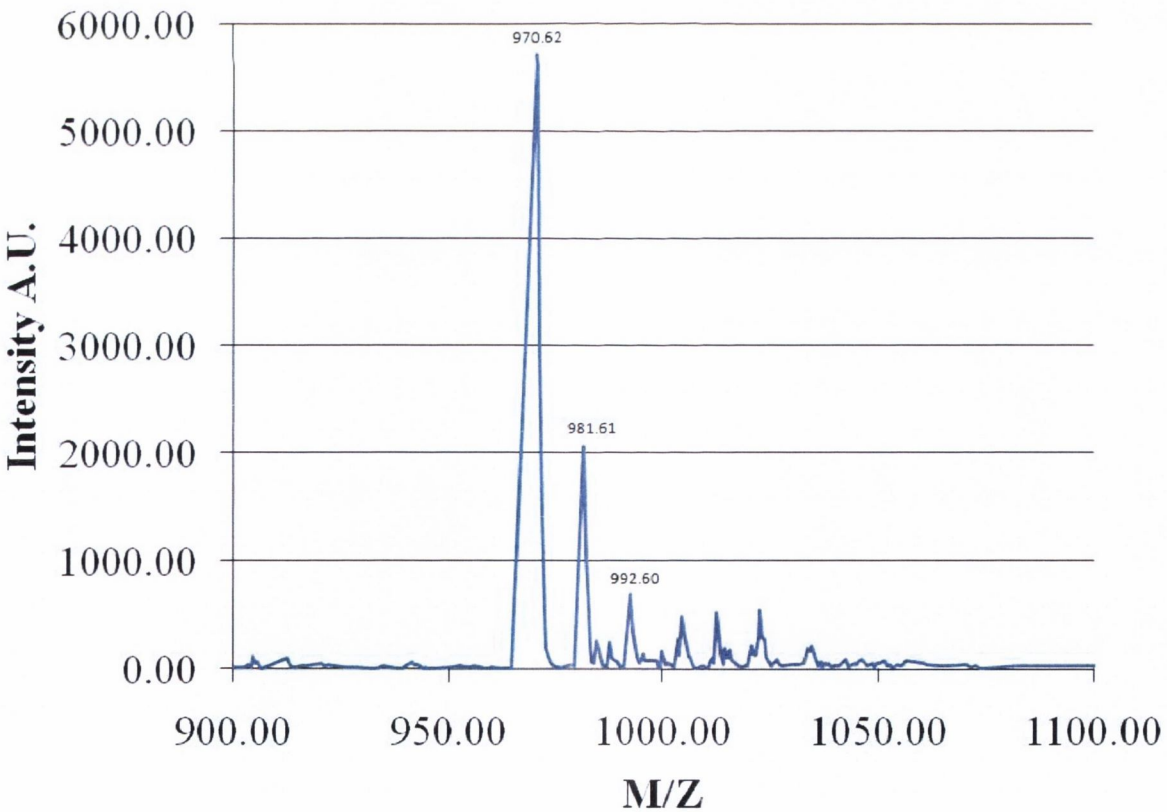
6000.00
5000.00
4000.00
3000.00
2000.00
1000.00
0.00
Intensity A.U.
970.62
981.61
992.60
900.00
950.00
1000.00
1050.00
1100.00
M/Z

vi) An infrared spectrum of **11** measured between 600 cm^{-1} and 4000 cm^{-1}

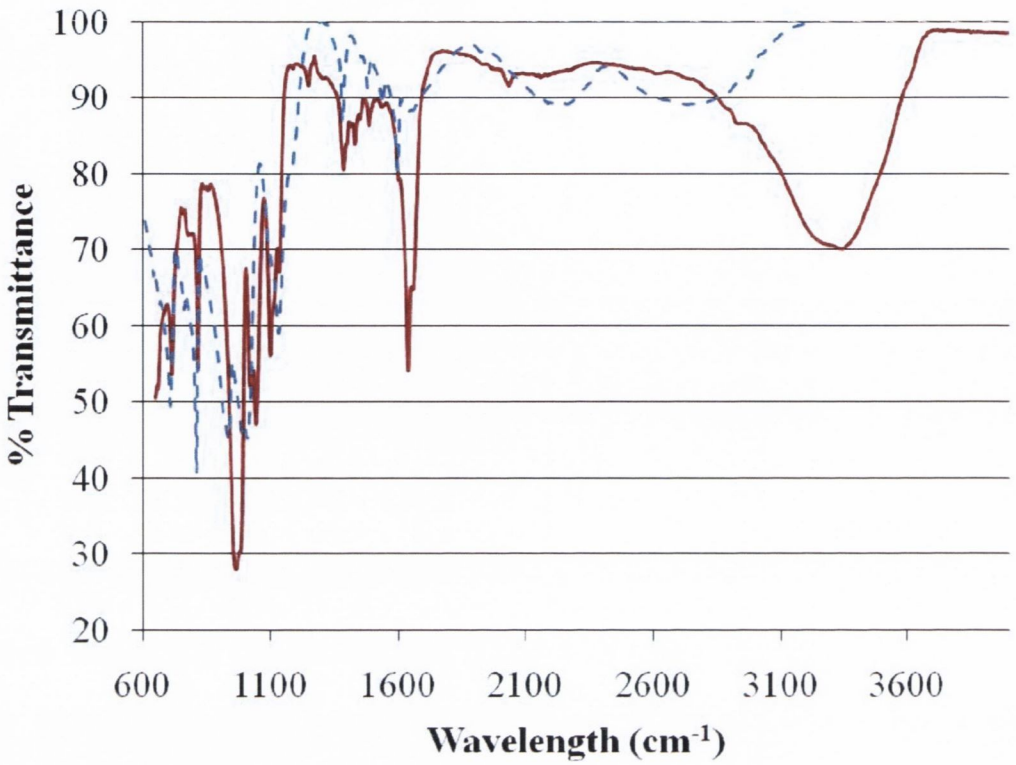

vii) An infrared spectrum of **11a** measured between 600 cm^{-1} and 4000 cm^{-1}

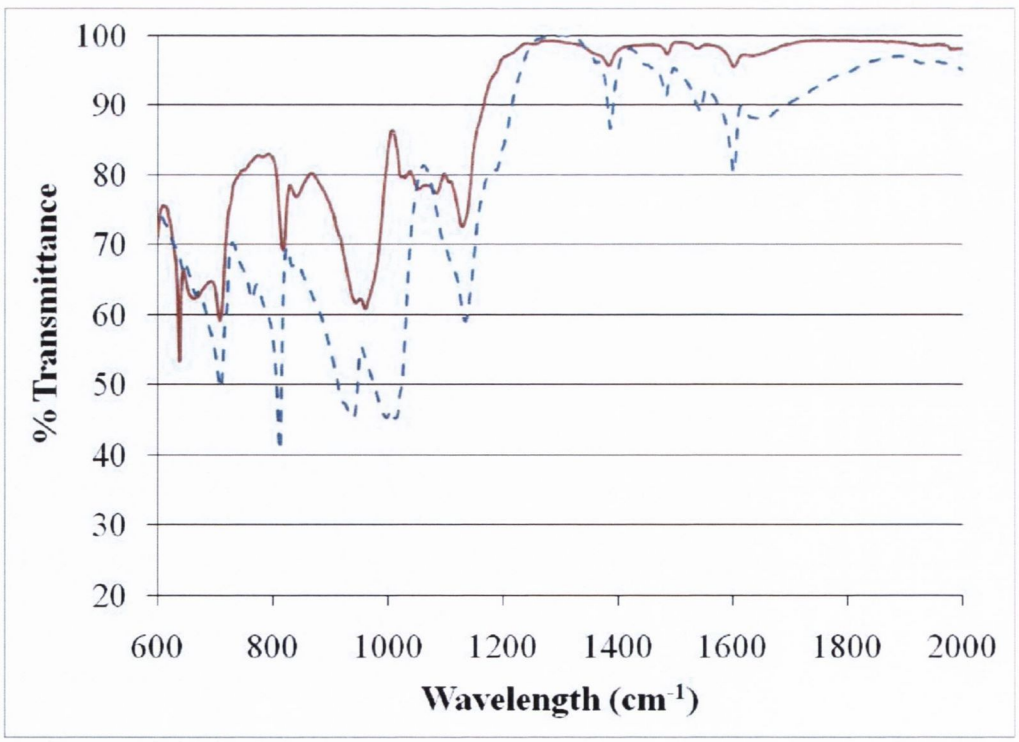

-Preliminary investigations in the removal or exchange of the encapsulated solvent molecules

Compound **11** was prepared without triethylamine or sodium azide and characterised by mass spectrometry. Compound **11** was prepared from a reaction mixture in which DMF was replaced by DMA or NMP. Single crystals that were formed for these two separate reaction mixtures were measured using single crystal X-ray diffraction and confirmed the isolation of anionic cluster comparable to **11**. The synthesis of **11a** was also carried out in an aqueous solution without DMF solvent. The resulting green powder of **11a** was prepared from the evaporation of the aqueous reaction solution and the infrared spectrum was recorded. Due to the evaporation of the reaction mixture there was a sodium azide impurity; future work will investigate the full characterisation of the anionic clusters in **11** without sodium azide or DMF. An infrared spectrum of the dehydrated compound **11a** which was prepared in a purely aqueous solution

viii) An infrared spectrum comparing **11** (DMF inclusive – black dashed line) with **11a** (no DMF – red solid line)

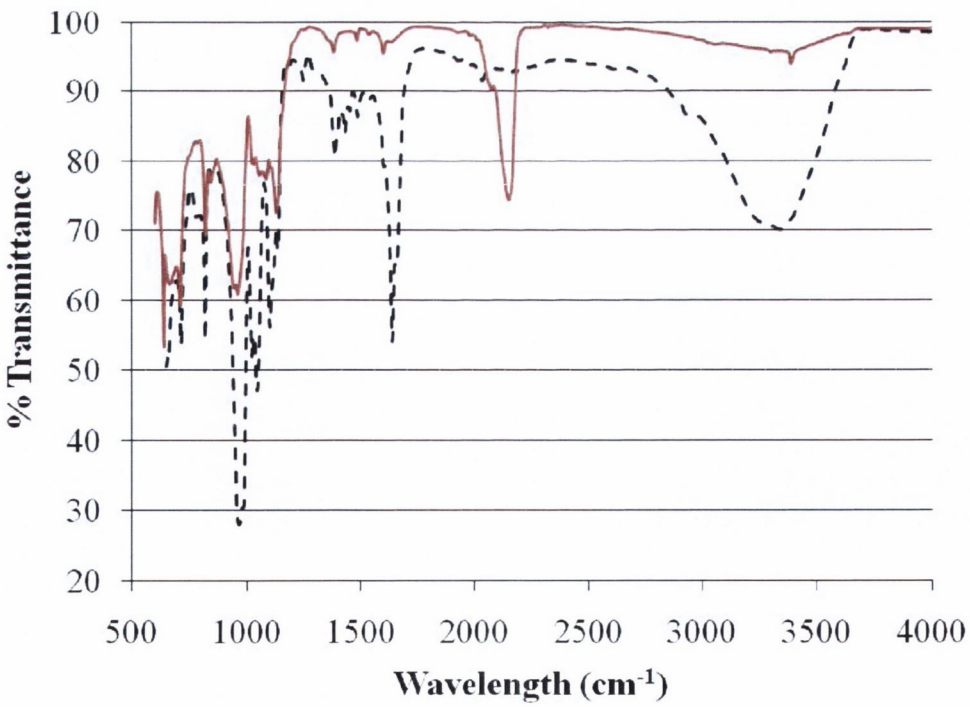

ix) The full range of the mass spectra of **11** recorded in an aqueous solution

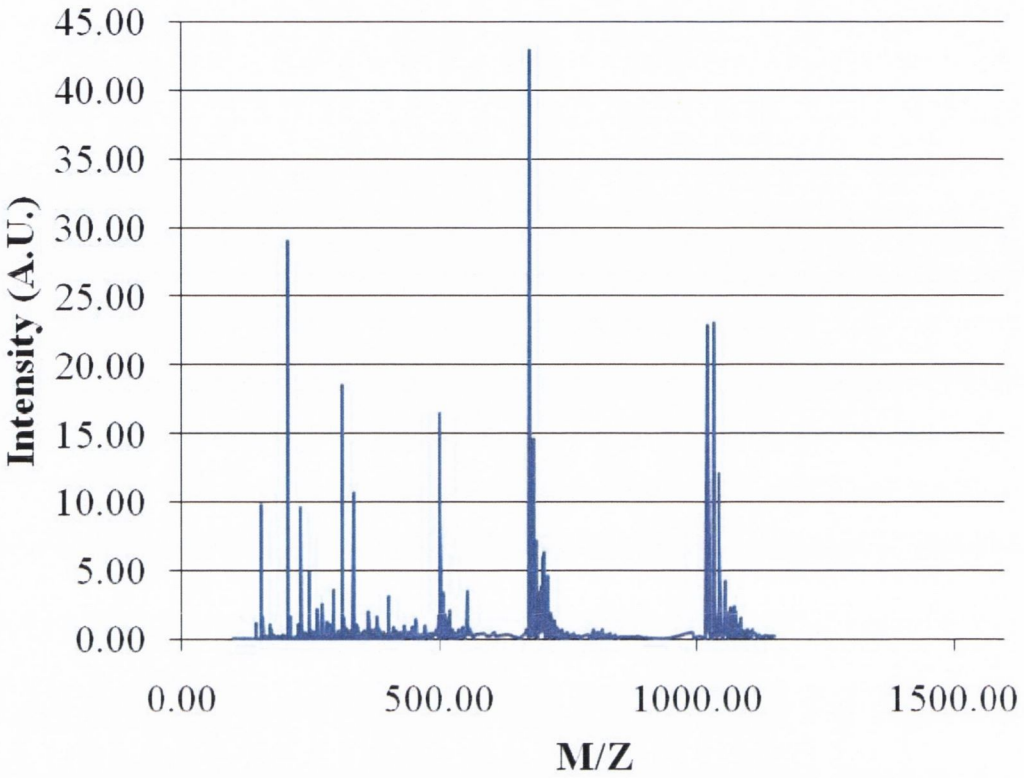

x) Control experiments testing the cell viability of the cancer cells lines against the starting materials of **9** and **11**

a)

b)

c)

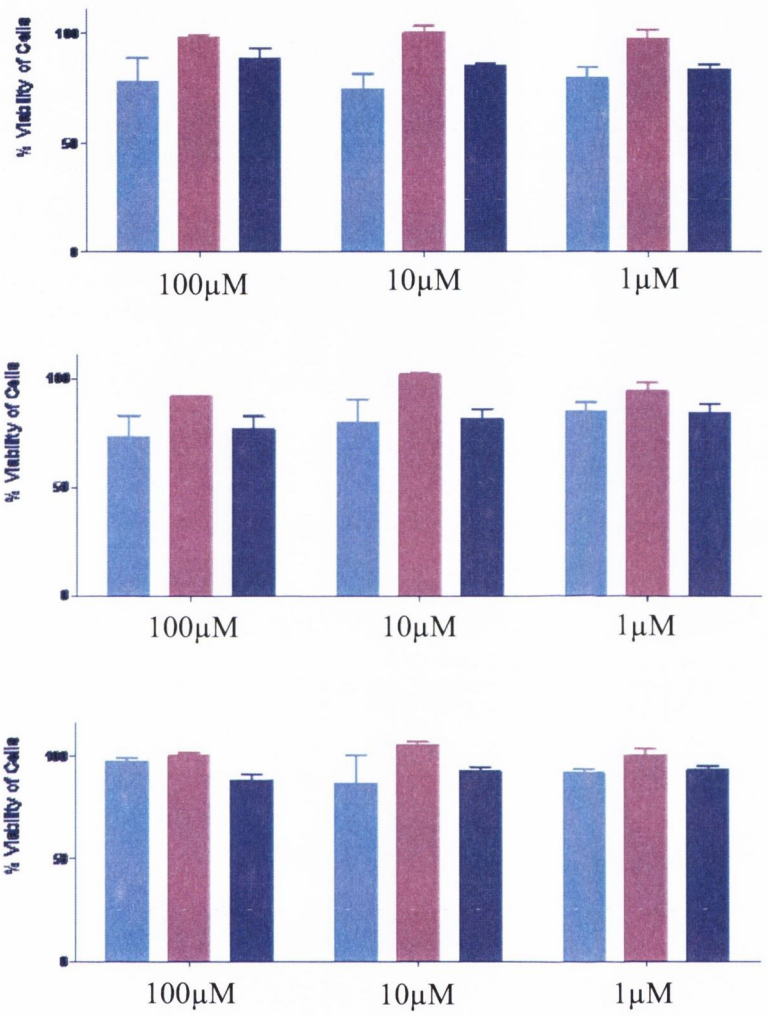

Figure 4.26 – Control tests on cell viability using three dose concentrations of 100 μM, 10 μM and 1 μM for (a) (1,4-benzene)bisphosphonic acid, (b) ([1,1'-biphenyl]-4,4'-diyl)bisphosphonic acid and (c) sodium orthovanadate against the three different cancer cells. Colour code: A549 light blue, Mutu-ls pink, K562 dark blue.